
Mechanism Design

Enumeration of Kinematic Structures According to Function

Mechanical Engineering Series

Frank Kreith - Series Editor

Published Titles

Entropy Generation Minimization

Adrian Bejan

Finite Element Method Using MATLAB

Young W. Kwon & Hyochoong Bang

Fundamentals of Environmental Discharge Modeling

Lorin R. Davis

Intelligent Transportation Systems: New Principles and Architectures

Sumit Ghosh & Tony Lee

Mathematical & Physical Modeling of Materials Processing Operations

Olusegun Johnson Ilegbusi, Manabu Iguchi & Walter E. Wahnsiedler

Mechanics of Composite Materials

Autar K. Kaw

Mechanics of Fatigue

Vladimir V. Bolotin

Mechanism Design: Enumeration of Kinematic Structures According to Function

Lung-Wen Tsai

Nonlinear Analysis of Structures

M. Sathyamoorthy

Practical Inverse Analysis in Engineering

David M. Trujillo & Henry R. Busby

Thermodynamics for Engineers

Kau-Fui Wong

Viscoelastic Solids

Roderic S. Lakes

Forthcoming Titles

Distributed Generation: The Power Paradigm for the New Millennium

Anne-Marie Borbely & Jan F. Kreider

Engineering Experimentation

Euan Somerscales

Energy Audit of Building Systems: An Engineering Approach

Moncef Krarti

Finite Element Method Using MATLAB, 2nd Edition

Young W. Kwon & Hyochoong Bang

Introduction Finite Element Method

Chandrakant S. Desai & Tribikram Kundu

Mechanics of Solids & Shells

Gerald Wempner & Demosthenes Talaslidis

Principles of Solid Mechanics

Rowland Richards, Jr.

Mechanism Design

Enumeration of Kinematic Structures According to Function

Lung-Wen Tsai

Presidential Chair Professor
Department of Mechanical Engineering
Bourns College of Engineering
University of California, Riverside



CRC Press

Boca Raton London New York Washington, D.C.

ON THE COVER:

A 4-speed automatic transmission. (Courtesy of General Motors, Warren, MI.)

Library of Congress Cataloging-in-Publication Data

Tsai, Lung-Wen.

Mechanism design : enumeration of kinematic structures according to function /

Lung-Wen Tsai

p. cm.--(Mechanical engineering series)

Includes bibliographical references and index.

ISBN 0-8493-0901-8

1. Machinery, Kinematics of. 2. Machine design. I. Title. II. Advanced topics in mechanical engineering series.

TJ175 .T78 2000

621.8'11--dc21

00-056415

This book contains information obtained from authentic and highly regarded sources. Reprinted material is quoted with permission, and sources are indicated. A wide variety of references are listed. Reasonable efforts have been made to publish reliable data and information, but the author and the publisher cannot assume responsibility for the validity of all materials or for the consequences of their use.

Neither this book nor any part may be reproduced or transmitted in any form or by any means, electronic or mechanical, including photocopying, microfilming, and recording, or by any information storage or retrieval system, without prior permission in writing from the publisher.

The consent of CRC Press LLC does not extend to copying for general distribution, for promotion, for creating new works, or for resale. Specific permission must be obtained in writing from CRC Press LLC for such copying.

Direct all inquiries to CRC Press LLC, 2000 N.W. Corporate Blvd., Boca Raton, Florida 33431.

Trademark Notice: Product or corporate names may be trademarks or registered trademarks, and are used only for identification and explanation, without intent to infringe.

© 2001 by CRC Press LLC

No claim to original U.S. Government works

International Standard Book Number 0-8493-0901-8

Library of Congress Card Number 00-056415

Printed in the United States of America 1 2 3 4 5 6 7 8 9 0

Printed on acid-free paper

Preface

This textbook has evolved from class notes used for a course in systematic design of mechanisms that the author has taught for over a decade. Although it is written primarily for senior and first-year graduate level students in engineering, it is equally valuable for practicing engineers, particularly for mechanism and machine designers.

Traditionally, mechanisms are created by the designer's intuition, ingenuity, and experience. This ad hoc approach, however, cannot ensure the identification of all feasible design alternatives, nor does it necessarily lead to an optimum design. Two approaches have been developed to alleviate the problem. The first involves the development of atlases of mechanisms grouped according to function for use as a primary source of ideas. The second makes use of a symbolic representation of the kinematic structure and the combinatorial analysis as a tool for enumeration of mechanisms.

This textbook introduces a systematic methodology for the creation and classification of mechanisms. The approach is partly analytical and partly algorithmic. It is based on the idea that, during the conceptual design phase, some of the functional requirements of a desired mechanism can be transformed into structural characteristics that can be employed for systematic enumeration of mechanisms. The kinematic structure of a mechanism contains the essential information about which link is connected to which other link by what type of joint. Using graph theory, combinatorial analysis, and computer algorithms, kinematic structures of the same nature, i.e., the same the number of degrees of freedom, type of motion (planar or spatial), and complexity can be enumerated in an essentially systematic and unbiased manner. Then each mechanism structure is sketched and evaluated with respect to the remaining functional requirements. This results in a class of feasible mechanisms that can be subject to dimensional synthesis, kinematic and dynamic analyses, design optimization, and design detailing.

This textbook is organized as follows:

Chapter 1 provides a brief review of the design process and a systematic methodology for creation of mechanisms. Some terminologies related to the kinematics of mechanism are defined. Mechanisms are classified according to the nature of motion into planar, spherical, and spatial mechanisms.

Chapter 2 is concerned with the basic concepts of graph theory, which is essential for structural analysis and structural synthesis of mechanisms. This material is extremely important since the design methodology employs graphs to represent the mechanism structure and mechanism structures are enumerated with the aid of graph theory.

Chapter 3 introduces several methods of representation of the kinematic structure of mechanisms. The kinematic structure, which contains the essential information about which link is connected to which other links by what types of joint, will be used for enumeration of mechanisms.

Chapter 4 examines the structural characteristics of mechanisms. The correspondence between graph and mechanism is established, from which several important mechanism structural characteristics are derived. The degrees of freedom of a mechanism, the loop-mobility criterion, the concept of structural isomorphism, and various methods of identification of structural isomorphism are described.

Chapter 5 deals with the enumeration of graphs of kinematic chains. Systematic algorithms for the enumeration of contracted and conventional graphs are presented. Atlases of contracted graphs and conventional graphs are developed. Using these atlases, an enormous number of mechanisms can be developed.

Chapter 6 describes a general procedure for the enumeration and classification of mechanisms. Planar bar linkages, geared mechanisms, cam mechanisms, spherical mechanisms, and spatial mechanisms are enumerated and classified according to the number of degrees of freedom, the number of independent loops, etc.

Chapter 7 covers the enumeration and classification of epicyclic gear trains (EGTs). The structural characteristics of EGTs are identified. Various methods of enumeration including Buchsbaum and Freudenstein's method, the genetic graph approach, and the parent bar linkage method are discussed. Furthermore, the theory of fundamental circuits is introduced for the speed-ratio analysis of EGTs.

Chapters 8 and 9 offer several conceptual design examples to demonstrate the power of the methodology. Chapter 8 concentrates on the enumeration of automotive mechanisms, whereas Chapter 9 involves the enumeration of robotic mechanisms. Atlases of parallel manipulators and robotic wrist mechanisms are developed.

Appendix A presents an algorithm for solving a system of m linear equations in n unknowns. A nested do-loops algorithm serves as the basis for systematic enumeration of mechanisms. Appendix B provides an atlas of contracted graphs having two to four independent loops. Appendix C is comprised of an atlas of graphs of kinematic chains having up to three independent loops and eight links. Appendix D offers an atlas of planar linkages with one, two, and three degrees of freedom. Appendix E contains an atlas of spatial one-dof, single-loop kinematic chains. Appendix F includes an atlas of epicyclic gear trains classified according to the number of degrees of freedom, the number of independent loops, and the vertex degree listing. Appendix G furnishes the schematic diagrams and clutching sequences of some commonly used epicyclic transmission gear trains.

Prerequisites for readers of this textbook include the basic concepts of combinatorial analysis, graph theory, matrix theory, and the kinematics of mechanisms that are usually taught at the undergraduate level. Thomas Edison said, "genius is one percent

inspiration and ninety-nine percent perspiration.” Inspiration can occur more readily when perspiration is properly directed and focused. The methodology presented in this book is intended to help designers better organize the perspiration so that the inspiration can take place early in the design process. For those who are willing to try, the rewards should be well worth it.

The author wishes to express his sincere appreciation to Dr. Bernard Roth, his former Ph.D. advisor at Stanford University, and Dr. Ferdinand Freudenstein, Professor Emeritus at Columbia University, for their lifelong advice and encouragement. A major portion of the material presented in this textbook is derived from Dr. Freudenstein and his former students’ research results. Others are taken from the author’s research in collaboration with professional colleagues, Ting Liu and Roland Maki, and with his former students, Sun-Lai Chang, Goutam Chatterjee, Dar-Zen Chen, Hsin-I Hsieh, Chen-Chou Lin, Richard Stamper, and Farhad Tahmasebi. Their efforts are greatly appreciated. Lastly, the author appreciates the patience and sacrifice of his family members, Lung-Chu Tsai, Jule Ann Tsai, and David Jeanchung Tsai, over the past few years while the textbook was being written.

Lung-Wen Tsai
Riverside, California

The Author



Lung-Wen Tsai is a Presidential Chair Professor in the Department of Mechanical Engineering at the University of California in Riverside. He obtained his B.S. degree in mechanical engineering from the National Taiwan University in Taipei, Taiwan; M.S. degree in engineering science from the State University of New York (SUNY) in Buffalo, New York; and Ph.D. in mechanical engineering from Stanford University in Stanford, California.

From 1973 to 1978, Dr. Tsai was a research and development engineer for Hewlett Packard responsible for the design of instrumentation tape recorders and X-Y plotters. From 1978 to 1986 he was a senior staff research engineer for General Motors and led projects in the development of variable-stroke engine mechanisms, variable-valve timing mechanisms, active engine balancing devices, automatic transmission mechanisms, and kinematics of robot manipulators. His most recent position was with the University of Maryland in College Park from 1986 to July 2000 where he established a nationally recognized research and education program in mechanisms and machine theory, automotive engineering, and robot manipulators. Dr. Tsai joined the Department of Mechanical Engineering at the University of California at Riverside in the Fall of 2000.

Dr. Tsai is a registered professional engineer in California, a Fellow of the ASME, and a member of the SAE. He is Chief Editor for the *ASME Journal of Mechanical Design* and Chairman of the 2000 ASME International Design Engineering Technical Conferences and the Computer in Engineering Conference. Dr. Tsai has published one book on robot analysis (*Robot Analysis: The Mechanics of Serial and Parallel Manipulators*, John Wiley & Sons, New York, 1999) and more than 100 journal and

conference proceedings papers. He is the recipient of numerous awards, including the 1984 ASME Mechanism Committee best paper award, 1989 and 1991 AMR Procter & Gamble Awards, 1985 ASME Melville Medal, 1986 GM John Campbell Award, 1988 SAE Arch Colwell Merit Award, and 1993 AMR South-Pointing-Chariot Rotating Trophy.

Contents

1	Introduction	1
1.1	Introduction	1
1.2	A Systematic Design Methodology	2
1.3	Links and Joints	3
1.4	Kinematic Chains, Mechanisms, and Machines	9
1.5	Kinematics of Mechanisms	11
1.6	Planar, Spherical, and Spatial Mechanisms	12
1.7	Kinematic Inversions	15
1.8	Summary	16
	References	17
2	Basic Concepts of Graph Theory	21
2.1	Definitions	21
2.1.1	Degree of a Vertex	21
2.1.2	Walks and Circuits	22
2.1.3	Connected Graphs, Subgraphs, and Components	22
2.1.4	Articulation Points, Bridges, and Blocks	23
2.1.5	Parallel Edges, Slings, and Multigraphs	23
2.1.6	Directed Graph and Rooted Graph	23
2.1.7	Complete Graph and Bipartite	24
2.1.8	Graph Isomorphisms	25
2.2	Tree	26
2.3	Planar Graph	26
2.4	Spanning Trees and Fundamental Circuits	28
2.5	Euler's Equation	30
2.6	Topological Characteristics of Planar Graphs	30
2.7	Matrix Representations of Graph	31
2.7.1	Adjacency Matrix	32
2.7.2	Incidence Matrix	33
2.7.3	Circuit Matrix	35
2.7.4	Path Matrix	36
2.8	Contracted Graphs	38

2.9	Dual Graphs	40
2.10	Summary	43
	References	44
	Exercises	44
3	Structural Representations of Mechanisms	47
3.1	Introduction	47
3.2	Functional Schematic Representation	48
3.3	Structural Representation	51
3.4	Graph Representation	52
3.4.1	Advantages of Using Graph Representation	53
3.5	Matrix Representation	57
3.5.1	Adjacency Matrix	57
3.5.2	Incidence Matrix	58
3.6	Summary	59
	References	60
	Exercises	61
4	Structural Analysis of Mechanisms	65
4.1	Introduction	65
4.2	Correspondence Between Mechanisms and Graphs	65
4.3	Degrees of Freedom	66
4.4	Loop Mobility Criterion	71
4.5	Lower and Upper Bounds on the Number of Joints on a Link	72
4.6	Link Assortments	74
4.7	Partition of Binary Link Chains	76
4.8	Structural Isomorphism	79
4.9	Permutation Group and Group of Automorphisms	81
4.9.1	Group	82
4.9.2	Group of Automorphisms	83
4.10	Identification of Structural Isomorphism	85
4.10.1	Identification by Classification	85
4.10.2	Identification by Characteristic Polynomial	86
4.10.3	Optimum Code	89
4.10.4	Degree Code	90
4.11	Partially Locked Kinematic Chains	92
4.12	Summary	93
	References	94
	Exercises	95
5	Enumeration of Graphs of Kinematic Chains	101
5.1	Introduction	101
5.2	Enumeration of Contracted Graphs	102
5.3	Enumeration of Conventional Graphs	107
5.4	Atlas of Graphs of Kinematic Chains	111

5.5	Summary	112
	References	112
	Exercises	113
6	Classification of Mechanisms	115
6.1	Introduction	115
6.2	Planar Mechanisms	116
6.2.1	Planar Linkages	116
6.2.2	Planar Geared Mechanisms	129
6.2.3	Planar Cam Mechanisms	133
6.3	Spherical Mechanisms	135
6.4	Spatial Mechanisms	136
6.4.1	Spatial One-dof Mechanisms	138
6.4.2	Spatial Multi-dof, Multiple-Loop Mechanisms	140
6.5	Summary	141
	References	141
	Exercises	143
7	Epicyclic Gear Trains	145
7.1	Introduction	145
7.2	Structural Characteristics	146
7.3	Buchsbaum–Freudenstein Method	151
7.4	Genetic Graph Approach	158
7.5	Parent Bar Linkage Method	159
7.6	Mechanism Pseudoisomorphisms	161
7.7	Atlas of Epicyclic Gear Trains	162
7.7.1	One-dof Epicyclic Gear Trains	163
7.7.2	Two-dof Epicyclic Gear Trains	163
7.7.3	Three-dof Epicyclic Gear Trains	164
7.8	Kinematics of Epicyclic Gear Trains	165
7.8.1	Fundamental Circuit Equations	167
7.8.2	Examples	168
7.9	Summary	172
	References	172
	Exercises	174
8	Automotive Mechanisms	179
8.1	Introduction	179
8.2	Variable-Stroke Engine Mechanisms	179
8.2.1	Functional Requirements	180
8.2.2	Structural Characteristics	180
8.2.3	Enumeration of VS-Engine Mechanisms	181
8.3	Constant-Velocity Shaft Couplings	184
8.3.1	Functional Requirement	184
8.3.2	Structural Characteristics	185

8.3.3	Enumeration of C-V Shaft Couplings	186
8.4	Automatic Transmission Mechanisms	189
8.4.1	Functional Requirements	194
8.4.2	Structural Characteristics	197
8.4.3	Enumeration of Epicyclic Gear Mechanisms	198
8.5	Canonical Graph Representation of EGMs	199
8.5.1	Structural Characteristics of Canonical Graphs	201
8.5.2	Enumeration of Canonical Graphs	204
8.5.3	Identification of Fundamental Circuits	209
8.5.4	Detection of Transfer Vertices	214
8.6	Atlas of Epicyclic Gear Transmission Mechanisms	215
8.7	Summary	217
	References	217
	Exercises	219
9	Robotic Mechanisms	221
9.1	Introduction	221
9.2	Parallel Manipulators	221
9.2.1	Functional Requirements	222
9.2.2	Structural Characteristics	222
9.2.3	Enumeration of Planar Parallel Manipulators	225
9.2.4	Enumeration of Spherical Parallel Manipulators	227
9.2.5	Enumeration of Spatial Parallel Manipulators	228
9.3	Robotic Wrist Mechanisms	231
9.3.1	Functional Requirements	234
9.3.2	Structural Characteristics	238
9.3.3	Enumeration of Three-dof Wrist Mechanisms	240
9.4	Summary	243
	References	245
	Exercises	247
A	Solving m Linear Equations in n Unknowns	249
A.1	Solving One Equation in n Unknowns	249
A.2	Solving m Equations in n Unknowns	250
	References	252
B	Atlas of Contracted Graphs	253
C	Atlas of Graphs of Kinematic Chains	255
D	Atlas of Planar Bar Linkages	261
E	Atlas of Spatial One-dof Kinematic Chains	275
F	Atlas of Epicyclic Gear Trains	279

G Atlas of Epicyclic Gear Transmission Mechanisms	291
Index	307

Chapter 1

Introduction

1.1 Introduction

Design is the creation of synthesized solutions in the form of products or systems that satisfy customer's requirements [9, 25, 30, 34]. When we are given a design problem, we try to make the best use of our knowledge and the available information to understand the problem and generate as many feasible solutions as possible. Then, we evaluate these concepts against the customer's requirements and select a most promising concept for design analysis and design optimization. We may think of the design as a mapping of the customer's requirements into a physical embodiment. The better we understand the problem associated with the customer's requirements, the better design we can achieve.

The *design process* can be logically divided into three interrelated phases: (1) *product specification and planning phase*, (2) *conceptual design phase*, and (3) *product design phase*. During the product specification and planning phase, we identify the customer's requirements and translate them into engineering specifications in terms of the functional requirements and the time and money available for the development, and plan the project accordingly. In the conceptual design phase, we generate as many design alternatives as possible, evaluate them against the functional requirements, and select the most promising concept for design detailing. A rough idea of how the product will function and what it will look like is developed. In the product design phase, we perform a thorough design analysis, design optimization, and simulation of the selected concept. Function, shape, material, and production methods are considered. Several prototype machines are constructed and tested to demonstrate the concept. Finally, an engineering documentation is produced and the design goes into the production phase. However, if the concept selected for the product design is shown to be impractical, it may be necessary to go back to the conceptual design phase to select an alternate concept or to generate additional concepts. In this regard, it may be necessary to reevaluate the engineering specifications developed in the product specification and planning phase.

Design is a continuous process of refining customer requirements into a final product. The process is iterative in nature and the solutions are usually not unique. It

involves a process of decision making. A talented and experienced engineer can often make sound engineering decisions to arrive at a fine product. Although the third phase is usually the most time consuming phase, most of the manufacturing cost of a product is committed by the end of conceptual design phase. According to a survey, 75% of the manufacturing cost of a typical product is committed during the first two phases. Decisions made after the conceptual design phase only have 25% influence on the manufacturing cost. Therefore, it is critical that we pay sufficient attention to the product specification and conceptual design phases. One approach for the generation of concepts is to identify the overall function of a device based on the customer's requirements, and decompose it into subfunctions. Then, various concepts that satisfy each of the functions are generated and combined into a complete design. Techniques for generation of concepts include literature and patent search, imitation of natural systems, analysis of competitor products, brainstorming, etc.

In this text, we concentrate on the conceptual design phase of mechanisms. The conceptual design is traditionally accomplished by the designer's intuition, ingenuity, and experience. An alternate approach is to generate an atlas of mechanisms classified according to functional characteristics for use as the sources of ideas for mechanism designers [1, 17, 19, 20, 21, 24]. This approach, however, cannot ensure the identification of all feasible mechanisms, nor does it necessarily lead to an optimum design.

Recently, a new approach based on an abstract representation of the *kinematic structure*, which is somewhat similar to the symbolic representation of chemical compounds, has evolved. The kinematic structure contains the essential information about which link is connected to which other links by what types of joint. It can be conveniently represented by a graph and the graph can be enumerated systematically using combinatorial analysis and computer algorithms [6, 7, 8, 10, 13, 15, 35]. This approach, which appears to be promising, is the basis of this text.

In the following, we briefly introduce the methodology and review some of the fundamentals of the kinematics of mechanisms to facilitate the development of the methodology.

1.2 A Systematic Design Methodology

The methodology is based on the application of graph theory and combinatorial analysis. First, the functional requirements of a class of mechanisms are identified. Then, kinematic structures of the same nature are enumerated systematically using graph theory and combinatorial analysis. Third, each kinematic structure is sketched and qualitatively evaluated according to its potential in meeting the functional requirements. Finally, a promising concept is chosen for dimensional synthesis, design optimization, computer simulation, and prototype demonstration. The process may be iterated several times until a final product is achieved.

We summarize the methodology as follows:

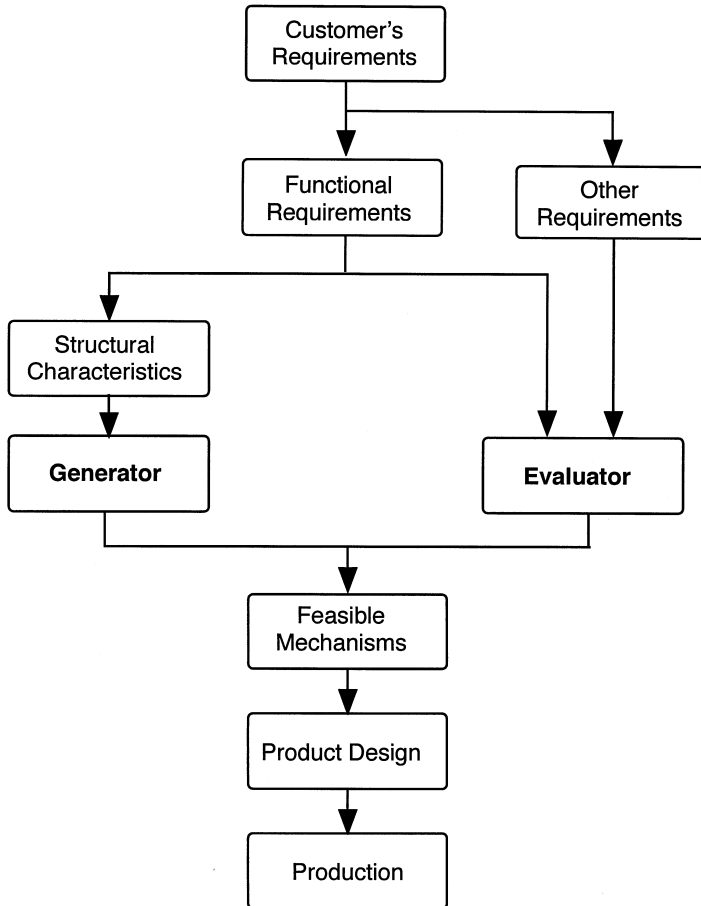
1. Identify the functional requirements, based on customers' requirements, of a class of mechanisms of interest.
2. Determine the nature of motion (i.e., planar, spherical, or spatial mechanism), degrees of freedom (dof), type, and complexity of the mechanisms.
3. Identify the structural characteristics associated with some of the functional requirements.
4. Enumerate all possible kinematic structures that satisfy the structural characteristics using graph theory and combinatorial analysis.
5. Sketch the corresponding mechanisms and evaluate each of them qualitatively in terms of its capability in satisfying the remaining functional requirements. This results in a set of feasible mechanisms.
6. Select a most promising mechanism for dimensional synthesis, design optimization, computer simulation, prototype demonstration, and documentation.
7. Enter the production phase.

We note that the methodology consists of two engines: a *generator* and an *evaluator* as shown in Figure 1.1. Some of the functional requirements are transformed into the structural characteristics and incorporated in the generator as rules of enumeration. The generator enumerates all possible solutions using graph theory and combinatorial analysis. The remaining functional requirements are incorporated in the evaluator as evaluation criteria for the selection of concepts [3]. This results in a class of feasible mechanisms. Finally, a most promising candidate is chosen for the product design. The process may be iterated several times until a final product is achieved. This methodology has been successfully applied in the structure synthesis of planar linkages, epicyclic gear trains, automotive transmission mechanisms, variable-stroke engine mechanisms, robotic wrist mechanisms, etc. [2, 3, 7, 12, 14, 22, 29, 31].

How many of the functional requirements should be incorporated in the generator is a matter of engineering decision. The more functional requirements that are translated into structural characteristics and incorporated in the generator, the less work is needed from the evaluator. However, this may make the generator too complex to develop. Generally, if a functional requirement can be written in a mathematical form, it should be included in the generator. The method presented in this text is similar in a way to that described in [36].

1.3 Links and Joints

We define a material body as a rigid body if the distance between any two points of the body remains constant. In reality, rigid bodies do not exist, since all known

**FIGURE 1.1**

A systematic mechanism design methodology.

materials deform under stress. However, we may consider a body as rigid if its deformation under stress is negligibly small. The use of rigid bodies makes the study of kinematics of mechanisms easier. However, for light-weight and high-speed mechanisms, the elastic effects of a material body may become significant and must be taken into consideration. In this text, unless otherwise stated, we shall treat all bodies as being rigid. A rigid body may be considered as being infinitely large for study of the kinematics of mechanisms.

The individual rigid bodies making up a machine or mechanism are called *members* or *links*. For convenience, certain nonrigid bodies such as chains, cables, or belts, which momentarily serve the same function as rigid bodies, may also be considered

as links. From the kinematics point of view, two or more members connected together such that no relative motion can occur between them will be considered as one link.

The links in a machine or mechanism are connected in pairs. The connection between two links is called a *joint*. A joint physically adds some constraint(s) to the relative motion between the two members. The kind of relative motion permitted by a joint is governed by the form of the surfaces of contact between the two members. The surface of contact of a link is called a *pair element*. Two such paired elements form a *kinematic pair*.

We classify kinematic pairs into *lower pairs* and *higher pairs* according to the contact between the paired elements. A kinematic pair is called a lower pair if one pair of the element not only forms the envelope of the other, but also encloses it. The forms of the lower pair elements are geometrically identical, one being solid while the other is hollow. Lower pairs have surface contact. On the other hand, if the pair elements do not enclose each other, we call the pair a higher pair. Higher pairs have line or point contact between the element surfaces.

There are six lower pairs and two higher pairs that are frequently used in mechanisms as shown in Figure 1.2. We describe each of them briefly as follows.

A *revolute joint*, *R*, permits two paired elements to rotate with respect to one another about an axis that is defined by the geometry of the joint. Therefore, the revolute joint is a one degree-of-freedom (dof) joint; that is, it imposes five constraints on the paired elements. The revolute joint is sometimes called a *turning pair*, a *hinge*, or a *pin joint*.

A *prismatic joint*, *P*, allows two paired elements to slide with respect to each other along an axis defined by the geometry of the joint. Similar to a revolute joint, the prismatic joint is a one-dof joint. It imposes five constraints on the paired elements. The prismatic joint is also called a *sliding pair*.

A *cylindric joint*, *C*, permits a rotation about and an independent translation along an axis defined by the geometry of the joint. Therefore, the cylindric joint is a two-dof joint. It imposes four constraints on the paired elements. A cylindric joint is kinematically equivalent to a revolute joint in series with a prismatic joint with their joint axes parallel to or coincident with each other.

A *helical joint*, *H*, allows two paired elements to rotate about and translate along an axis defined by the geometry of the joint. However, the translation is related to the rotation by the pitch of the joint. Hence, the helical joint is a one-dof joint. It imposes five constraints on the paired elements. The helical joint is sometimes called a *screw pair*.

A *spherical joint*, *S*, allows one element to rotate freely with respect to the other about the center of a sphere. It is a ball-and-socket joint that permits no translations between the paired elements. Hence, the spherical joint is a three-dof joint; that is, it imposes three constraints on the paired elements. A spherical joint is kinematically equivalent to three intersecting revolute joints.

A *plane pair*, *E*, permits two translational degrees of freedom on a plane and a rotational degree of freedom about an axis that is normal to the plane of contact. Hence, the plane pair is a three-dof joint; that is, it imposes three constraints on the paired elements.

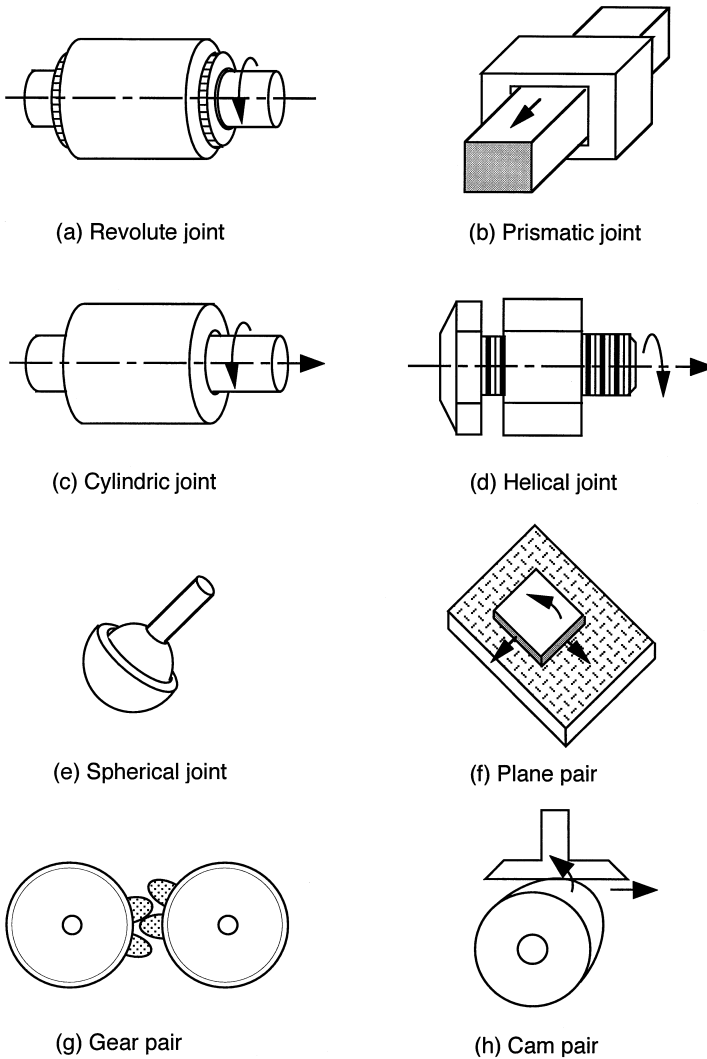


FIGURE 1.2
Eight frequently used kinematic pairs.

A *gear pair*, G , permits one gear to roll and slide with respect to the other at the point of contact between two meshing teeth. In addition, the motion space of each gear is constrained on a plane perpendicular to its central axis of rotation. Therefore, the gear pair is a two-dof joint. It imposes four constraints on the paired elements. The meshing surfaces of a gear pair must satisfy the *law of gearing* and the diametric pitch of a pair of gears must be equal to one another [23]. Figure 1.3 shows a spur gear pair manufactured by Boston Gear. When the pitch diameter of one gear becomes

infinitely large, it becomes a rack-and-pinion gear pair. A bevel gear pair may be employed to change the direction of rotation.

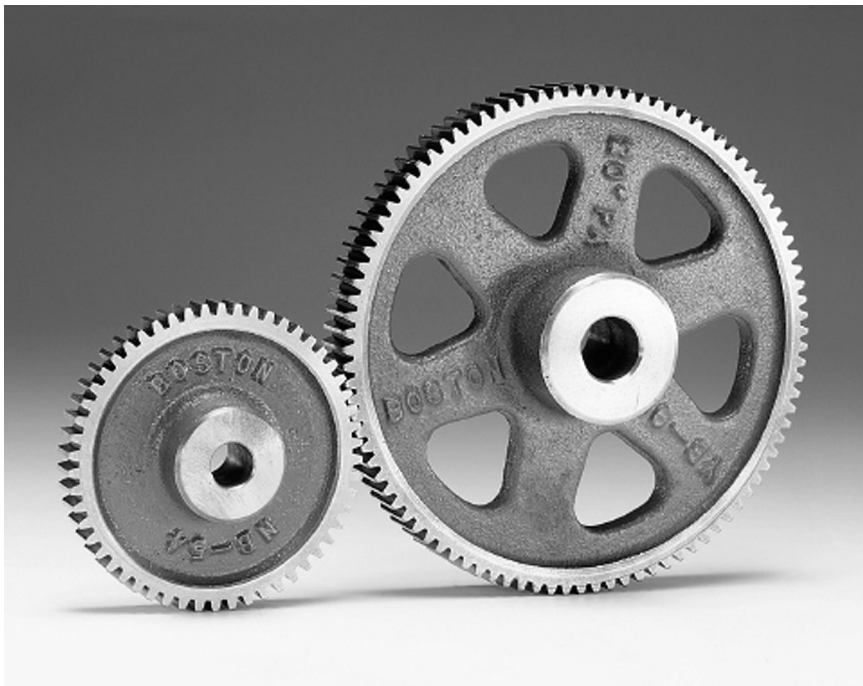


FIGURE 1.3

A spur gear pair. (Courtesy of Boston Gear, Boston, MA.)

Similar to a gear pair, a *cam pair*, C_p , allows a *follower* to roll and slide with respect to the *cam* at the point of contact. However, the two mating surfaces of a cam pair can virtually take any desired form [18]. A spring is incorporated to keep the two paired elements in contact. Hence, the cam pair is also a two-dof joint.

Further, there is a commonly used composite joint called the *universal joint* as shown in Figure 1.4. A universal joint is made up of two intersecting revolute joints. Therefore, it is a two-dof joint. The universal joint is sometimes referred to as the *Hooke joint* or *Cardan joint*. Neither Hooke nor Cardan invented the universal joint. The reason we associate Hooke's name with the joint is that he put it in use in the 17th century.

Revolute, prismatic, cylindric, helical, spherical, and plane pairs are lower pairs. Gear and cam pairs are higher pairs. Table 1.1 summarizes the degrees of freedom and the types of motion associated with each of the kinematic pairs.

A higher pair can often be replaced by a combination of two lower pairs in order to reduce stress concentration and wear at the point of contact. For example, a cylindric rod riding in a rectangular guide as shown in Figure 1.5a is not practical. The same constraint can be achieved by adding an intermediate link and connecting them with



FIGURE 1.4
Universal joint. (Courtesy of Boston Gear, Boston, MA.)

Table 1.1 Eight Frequently Used Kinematic Pairs.

Kinematic Pair	Symbol	Joint DOF	Rotational	Translational
Revolute	R	1	1	0
Prismatic	P	1	0	1
Cylindric	C	2	1	1
Helical	H	1	1	coupled
Spherical	S	3	3	0
Plane	E	3	1	2
Gear Pair	G	2	1	1
Cam Pair	C_p	2	1	1

a combination of revolute and prismatic joints as shown in Figure 1.5b. Hence, the two-dof motion permitted by the higher pair is obtained by two lower pairs.

A link is called a *binary link* if it is connected to only two other links, a *ternary link* if it is connected to three other links, a *quaternary link* if it is connected to four other links, and so on. A joint is called a *binary joint*, if it connects only two links, and a *multiple joint*, if it connects more than two links.



(a) A cylindric rod riding in a rectangular guide (b) Equivalent revolute and prismatic joints

FIGURE 1.5

Substitution of a higher pair with two lower pairs.

1.4 Kinematic Chains, Mechanisms, and Machines

A *kinematic chain* is an assemblage of links, or rigid bodies, that are connected by joints. If every link in a kinematic chain is connected to every other link by one and only one path, it is called an *open-loop chain*. On the other hand, if every link is connected to every other link by at least two distinct paths, the kinematic chain forms one or more closed loops and is called a *closed-loop chain*. Clearly, it is possible for a kinematic chain to contain both closed- and open-loop chains. We call such a kinematic chain a *hybrid kinematic chain*.

When one of the links in a kinematic chain is fixed to the ground or *base*, it is called a *mechanism*. The link that is fixed to the base is called the *fixed link*. As the input link(s) move with respect to the base, all other links perform constrained motions. Thus, a mechanism is a device that transforms motion and/or torque from one or more links to the others. For example, Figure 1.6 shows a crank-and-slider mechanism that transforms a continuous rotation of the crank into a reciprocal motion of the slider and vice versa.

When one or more mechanisms are assembled together with other hydraulic, pneumatic, and electrical components such that mechanical forces of nature can be compelled to do work, we call such an assembly a *machine*. That is, a machine is an assemblage of several components for the purpose of transforming external energy into useful work.

Although the terms mechanism and machine are often used synonymously, in reality there is a definite difference. Figure 1.7 shows a 6-axis milling machine produced by Giddings & Lewis Machine Tools. The basic mechanism of the machine consists of a moving platform, a fixed base, and six supporting limbs. Each limb is made up of two members that are connected to each other by a prismatic joint. The upper end of each limb is connected to the moving platform by a universal joint, whereas the lower end is connected to the base by a spherical joint. The motion of the prismatic joint is controlled by a motor-driven ball screw. Together it forms a parallel manipulator generally known as the *Stewart-Gough manipulator*.

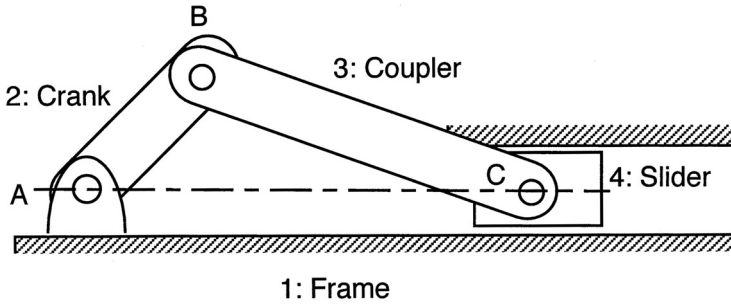


FIGURE 1.6
Crank-and-slider mechanism.

The platform itself is a mechanism and not a machine. When actuators, sensors, spindle, loading/unloading mechanism, and a controller are incorporated, it becomes a machine. We observe that a machine may consist of several mechanisms. However, a mechanism is not necessarily a machine since it may be part of a machine to serve as a motion transformation device.

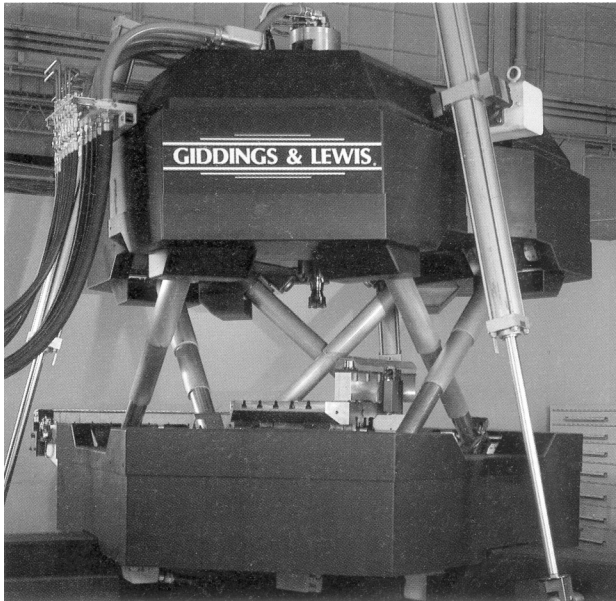


FIGURE 1.7
VARIAX[®] machining center. (Courtesy of Giddings & Lewis Machine Tools, Fond Du Lac, WI.)

1.5 Kinematics of Mechanisms

A rigid body is said to be under motion when it is instantaneously changing its position and/or orientation. Since the change of position can only be observed with respect to another body, the motion of a rigid body is a relative measure. Kinematics of a mechanism is the study of relative motion among the various links of a mechanism or machine by neglecting the inertia effects and the forces that cause the motion. In studying the kinematics of a mechanism, the motion of a link is often measured with respect to a fixed link or a reference frame, which may not necessarily be at rest.

There are two branches of kinematics known as *kinematic analysis* and *kinematic synthesis*.

Kinematic analysis is the study of relative motions associated with the links of a mechanism or machine and is a critical step toward proper design of a mechanism. Specifically, given a mechanism and the motion of its input link(s), the relative displacement, velocity, acceleration, etc., of the other links are to be found. These characteristics can be derived by considering the constraints imposed by the joints. The problem can be formulated by the graphical, vector algebra, matrix, or other mathematical methods [11, 23].

Kinematic synthesis is the reverse problem of kinematic analysis. In this case, the designer is challenged to devise a new mechanism that satisfies certain desired motion characteristics of an output link. The kinematic synthesis problem can be further divided into three interrelated phases:

1. *Type synthesis* refers to the selection of a specific type of mechanism for product development. During the conceptual design phase, the designer considers as many types of mechanism as possible and decides what type has the best potential of meeting the design objectives. The type of mechanism — cam, linkage, gear train, and so on — is determined. The selection depends to a great extent on the functional requirements of a machine and other considerations such as materials, manufacturing processes, and cost.
2. *Number synthesis* deals with the determination of the number of links, type of joint, and number of joints needed to achieve a given number of degrees of freedom of a desired mechanism. During this phase of study, the designer makes sure that a mechanism has the correct number of links that are connected with proper types of joints to ensure mobility. Number synthesis also involves the enumeration of all feasible kinematic structures or linkage topologies for a given number of degrees of freedom, number of links, and type of joints. For this reason it is sometimes called *structure synthesis* or *topological synthesis*. Various methodologies have been developed for systematic enumeration of kinematic structures [13]. A thorough understanding of the structural characteristics of a given type of mechanism is critical for the development of an efficient algorithm.

3. *Dimensional synthesis* deals with the determination of the dimensions or proportions of the links of a mechanism. Laying out a cam profile to meet a desired lift specification is a dimensional synthesis problem. Determination of the center distance between two pivots of a link in a bar-linkage is also a dimensional synthesis problem. Both geometric and analytical methods of synthesis may be used to perform dimensional synthesis. The Burmester theorem can be applied in the dimensional synthesis of planar linkages [16]. Recently, the theorem was extended to that of spatial linkages [4, 5, 26, 27, 28, 32, 33]. Typical problems in dimensional synthesis include function generation, coupler-point curve synthesis, and rigid body guidance.

Type synthesis involves design factors such as materials, manufacturing processes, reliability consideration, and cost issues that are usually determined at the initial phase of the design process. In this text, we are concerned primarily with the structure synthesis of mechanisms.

1.6 Planar, Spherical, and Spatial Mechanisms

Mechanisms can be classified into three types according to their nature of motion. A rigid body is said to be under *planar motion* if the motion of all particles in the rigid body are constrained in parallel planes. A *planar mechanism* is one in which all the moving links perform parallel planar motions. For a planar mechanism, the loci of all points in all links can be conveniently drawn in one plane. Planar mechanisms that utilize only lower-pair joints are called *planar linkages*. Revolute and prismatic joints are the only allowable lower pairs in planar linkages. Furthermore, the axis of a revolute joint must be perpendicular to the plane of motion, whereas the direction of translation of a prismatic joint must be parallel to the plane of motion. For examples, Figures 1.8, 1.9, and 1.10 show a planar four-bar linkage, a planar plate cam-and-follower mechanism, and a planar spur-gear drive, respectively.

A rigid body is said to be performing a *spherical motion* if the motions of all particles in the rigid body are confined on concentric spherical surfaces. When a rigid body performs a spherical motion, one of its points remains stationary. A *spherical mechanism* is one in which all the moving links perform concentric spherical motions about a common stationary point, called the *spherical center*. In a spherical mechanism, the motions of all particles can be conveniently described by their radial projections on the surface of a unit sphere. The revolute joint is the only permissible lower-pair joint for constructing spherical mechanisms. In addition, all the joint axes must intersect at a common point.

Figure 1.11 shows a spherical four-bar linkage known as the *universal joint*. The universal joint is used to transmit motion between two intersecting but non-collinear shafts. However, it is not a constant-velocity coupling device. In rear wheel drive vehicles, two Hooke joints are connected in series to achieve constant-velocity

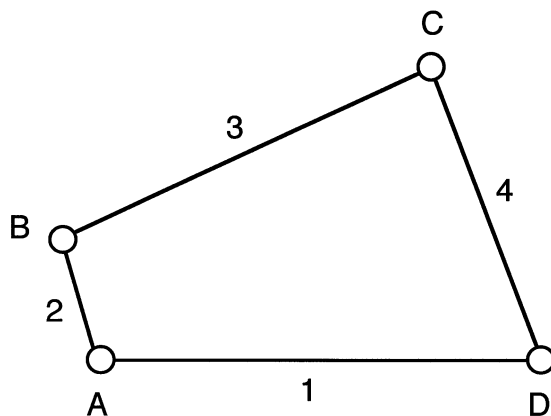


FIGURE 1.8
Four-bar linkage.

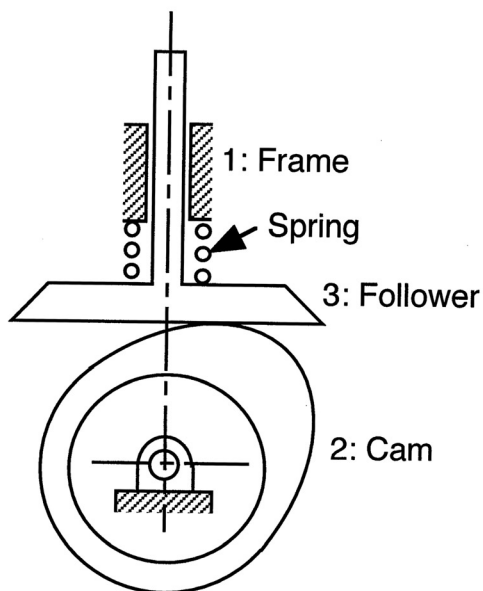


FIGURE 1.9
Cam-and-follower mechanism.

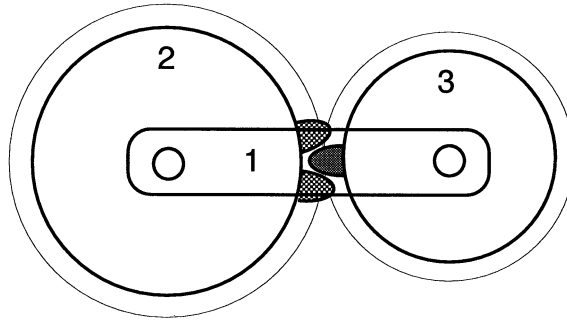


FIGURE 1.10
Spur-gear drive.

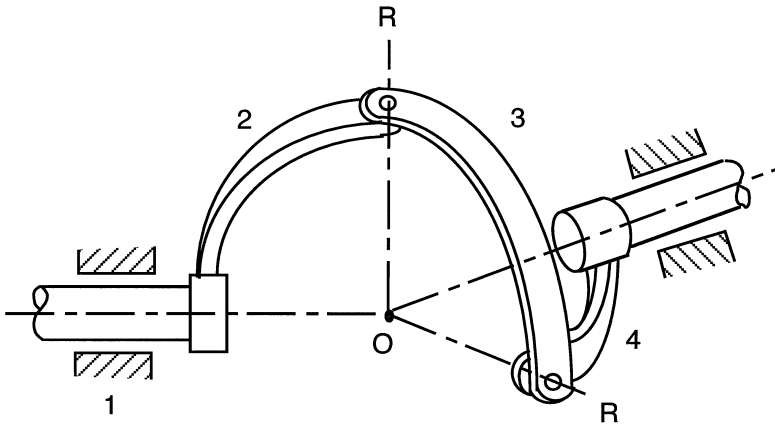


FIGURE 1.11
Spherical four-bar linkage.

coupling between the output shaft of a transmission and the input shaft of a differential gearbox.

The four revolute joints shown in Figure 1.11 intersect at a common point “O.” Link 1 serves as the fixed link, link 2 the input link, link 3 the coupler link, and link 4 the output link. The dimensions of such a spherical four-bar can be defined by the angles between the joint axes. All particles in link 3 move on concentric spherical surfaces centered at the fixed point O. Link 2 rotates about a fixed joint axis. The path of any particle in link 2 lies on a circle perpendicular to the axis of rotation. Since the axis of rotation passes through O, we can think of the particles in link 2 as moving on spheres centered at point O. Similarly, the motion of link 4 can also be considered as spherical. Thus, all moving links in the universal joint possess spherical motions.

A rigid body is said to be undergoing a *spatial motion* if its motion is not planar or spherical. A *spatial mechanism* is a mechanism that cannot be classified as planar or spherical. In this regard, we cannot associate some unique motion characteristics with spatial mechanisms. However, a spatial mechanism may have several links performing planar motions that are not parallel to one another.

Figure 1.12 shows a spatial swash-plate mechanism that can be used as a compressor mechanism. For a compressor, link 1 serves as the fixed link, link 2 the input link, link 3 the coupler, and link 4 the output link. As link 2 rotates about the fixed joint axis, link 4 makes a reciprocating motion about its prismatic joint axis, while link 3 makes a spatial motion. The swash-plate mechanism can also be used as an engine mechanism.

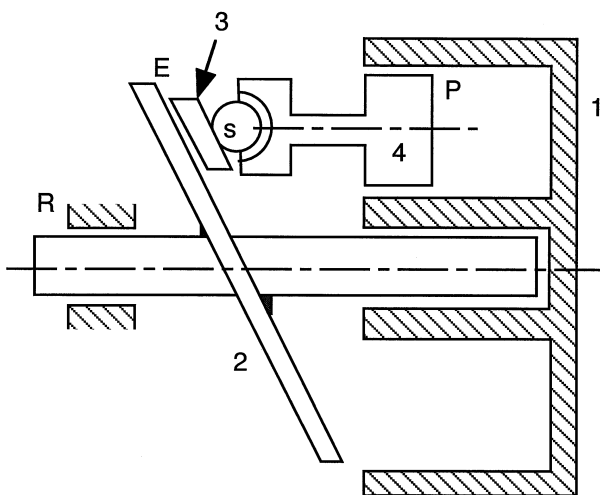


FIGURE 1.12
Swash-plate mechanism.

Planar and spherical mechanisms can be considered as special cases of spatial mechanisms. They occur as a consequence of special geometry in the particular orientations of their joint axes. Because of the special geometry, the kinematic synthesis and analysis problems become relatively simple.

1.7 Kinematic Inversions

As described earlier, a mechanism is defined by fixing one of the links in a kinematic chain to the ground. When different links of a kinematic chain are chosen as the fixed link, the relative motions between all the links are not altered. However, their motions

with respect to the ground may be completely different. The process of selecting various links of a kinematic chain as the fixed link is called *kinematic inversion*.

Applying kinematic inversion, many mechanisms can be derived from a given kinematic chain. However, some of them may be structurally isomorphic with the others. Figure 1.13 shows four inversions of a four-link chain. However, except for the difference in link lengths, the mechanism shown in Figure 1.13a is structurally isomorphic with that of Figure 1.13d; and the mechanism shown in Figure 1.13b is structurally isomorphic with that of Figure 1.13c.

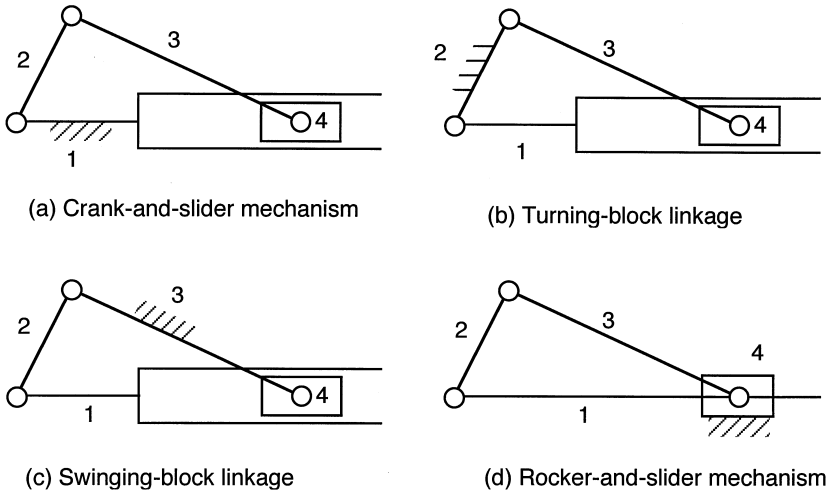


FIGURE 1.13
Four kinematic inversions of a four-bar chain.

1.8 Summary

The term mechanical design and three interrelated phases of the design process were introduced. Then, a systematic design methodology for the enumeration of kinematic structures of mechanisms was outlined. Fundamental terminologies for mechanisms that are essential for the development of the systematic methodology were reviewed, including the definitions of links, joints, kinematic chains, mechanisms, and machines. The classification of mechanisms according to the nature of motion was made and the concept of kinematic inversion was described.

References

- [1] Artobolevsky, I., 1977, *Mechanisms in Modern Engineering Design*, (5 volumes), translated by Weinstein, N., MIR Publishers, Moscow.
- [2] Buchsbaum, F. and Freudenstein, F., 1970, Synthesis of Kinematic Structure of Geared Kinematic Chains and other Mechanisms, *Journal of Mechanisms*, 5, 357–392.
- [3] Chatterjee, G. and Tsai, L.W., 1994, Enumeration of Epicyclic-Type Automatic Transmission Gear Trains, *SAE 1994 Trans., Journal of Passenger Cars*, Sec. 6, 103, 1415–1426.
- [4] Chen, P. and Roth, B., 1969, A Unified Theory for Finitely and Infinitesimally Separated Position Problems of Kinematic Synthesis, *ASME Journal of Engineering for Industry*, Series B, 91, 203–208.
- [5] Chen, P. and Roth, B., 1969, Design Equations for Finitely and Infinitesimally Separated Position Synthesis of Binary Links and Combined Link Chains, *ASME Journal of Engineering for Industry*, Series B, 91, 209–219.
- [6] Crossley, F.R.E., 1964, A Contribution to Grübler's Theory in Number Synthesis of Plane Mechanisms, *ASME Journal of Engineering for Industry*, Series B, 86, 1–8.
- [7] Crossley, F.R.E., 1965, The Permutation of Kinematic Chains of Eight Members or Less from the Graph-Theoretic Viewpoint, in *Developments in Theoretical and Applied Mechanics*, Vol. 2, Pergamon Press, Oxford, 467–486.
- [8] Davies, T.H., 1968, An Extension of Manolescu's Classification of Planar Kinematic Chains and Mechanisms of Mobility $m \geq 1$, Using Graph Theory, *Journal of Mechanisms*, 3, 87–100.
- [9] Dieter, G.E., 1991, *Engineering Design: A Materials and Processing Approach*, McGraw-Hill, New York, NY.
- [10] Dobrjanskyj, L. and Freudenstein, F., 1967, Some Application of Graph Theory to the Structural Analysis of Mechanisms, *ASME Journal of Engineering for Industry*, Series B, 89, 153–158.
- [11] Erdman, A.G. and Sandor, G.N., 1991, *Mechanism Design: Analysis and Synthesis*, Prentice Hall, Upper Saddle River, NJ.
- [12] Freudenstein, F. and Dobrjanskyj, L., 1965, On a Theory for the Type Synthesis of Mechanism, in *Proceedings of the 11th International Congress of Applied Mechanics*, Springer, Berlin 420–428.

- [13] Freudenstein, F. and Maki, E.R., 1979, Creation of Mechanisms According to Kinematic Structure and Function, *Journal of Environmental and Planning B*, 6, 375–391.
- [14] Freudenstein, F. and Maki, E.R., 1983, Development of an Optimum Variable-Stroke Internal-Combustion Engine from the Viewpoint of Kinematic Structure, *ASME Journal of Mechanisms, Transmissions, and Automation in Design*, 105, 2, 259–266.
- [15] Freudenstein, F. and Woo, L.S., 1974, Kinematic Structure of Mechanisms, in *Basic Questions of Design Theory*, North Holland, Amsterdam, 141–164.
- [16] Hartenberg, R.S. and Denavit, J., 1965, *Kinematic Synthesis of Linkages*, McGraw-Hill, New York, NY.
- [17] Horton, H.L., 1951, *Ingenious Mechanisms for Designers and Inventors*, Vol. 3, Industrial Press Inc., New York, NY.
- [18] Jensen, P.W., 1987, *Cam Design and Manufacture*, Marcel Dekker, Inc., New York, NY.
- [19] Jensen, P.W., 1991, *Classical and Modern Mechanisms for Engineers and Inventors*, Marcel Dekker, Inc., New York, NY.
- [20] Jones, F.D., 1930, *Ingenious Mechanisms for Designers and Inventors*, Vol. 1, Industrial Press Inc., New York, NY.
- [21] Jones, F.D., 1936, *Ingenious Mechanisms for Designers and Inventors*, Vol. 2, Industrial Press Inc., New York, NY.
- [22] Lin, C.C. and Tsai, L.W., 1989, The Development of an Atlas of Bevel-Gear Type Spherical Wrist Mechanisms, in *Proceedings of the First National Conference on Applied Mechanisms and Robotics*, Cincinnati, OH, Paper No. 89-AMR-2A-3.
- [23] Martin, G.H., 1982, *Kinematics and Dynamics of Machines*, McGraw-Hill, New York, NY.
- [24] Newell, J.A. and Horton, H.L., 1967, *Ingenious Mechanisms for Designers and Inventors*, Vol. 4, Industrial Press Inc., New York, NY.
- [25] Pahl, G. and Beitz, W., 1992, *Engineering Design: A Systematic Approach*, K. Wallace, Ed., Springer-Verlag, London.
- [26] Roth, B., 1967, On the Screw Axis and Other Special Lines Associated with Spatial Displacements of a Rigid Body, *ASME Journal of Engineering for Industry*, Series B, 89, 102–110.
- [27] Roth, B., 1967, Kinematics of Motion Through Finitely Separately Positions, *ASME Journal of Applied Mechanics*, Series B, 34, 591–598.
- [28] Roth, B., 1967, Finite Position Theory Applied to Mechanism Synthesis, *ASME Journal of Applied Mechanics*, Series B, 34, 599–605.

- [29] Sohn, W. and Freudenstein, F., 1986, An Application of Dual Graphs to the Automatic Generation of the Kinematic Structures of Mechanism, *ASME Journal of Mechanisms, Transmissions, and Automation in Design*, 108, 3, 392–398.
- [30] Suh, N.P., 1990, *The Principles of Design*, Oxford University Press, New York, NY.
- [31] Tsai, L.W. and Lin, C.C., 1989, The Creation of Non-fractionated Two-Degree-of-Freedom Epicyclic Gear Trains, *ASME Journal of Mechanisms, Transmissions, and Automation in Design*, 111, 4, 524–529.
- [32] Tsai, L.W. and Roth, B., 1972, Design of Dyads with Helical, Cylindric, Spherical, Revolute and Prismatic Joints, *Mechanism and Machine Theory*, 7, 85–102.
- [33] Tsai, L.W. and Roth, B., 1973, A Note on the Design of Revolute-Revolute Cranks, *Mechanism and Machine Theory*, 8, 23–31.
- [34] Ullman, D., 1992, *The Mechanical Design Process*, McGraw-Hill, New York, NY.
- [35] Woo, L.S., 1967, Type Synthesis of Plane Linkages, *ASME Journal of Engineering for Industry*, Series B, 89, 159–172.
- [36] Yan, H.S., 1998, *Creative Design of Mechanical Devices*, Springer-Verlag, Singapore.

Chapter 2

Basic Concepts of Graph Theory

In this chapter we introduce some fundamental concepts of graph theory that are essential for structure analysis and structure synthesis of mechanisms. Readers are encouraged to refer to Gibsons [1] and Harary [2] for more detailed descriptions of the theory.

2.1 Definitions

A *graph* consists of a set of vertices (points) together with a set of edges or lines. The set of vertices is connected by the set of edges. Let the graph be denoted by the symbol G , the vertex by set V , and the edge by set E . We call a graph with v vertices and e edges a (v, e) graph. Edges and vertices in a graph should be labeled or colored, otherwise they are indistinguishable.

Each edge of a graph connects two vertices called the *end points*. We specify an edge by its end points; that is, e_{ij} denotes the edge connecting vertices i and j . An edge is said to be *incident* with a vertex, if the vertex is an end point of that edge. The two end points of an edge are said to be *adjacent*. Two edges are adjacent if they are incident to a common vertex. For the $(11, 10)$ graph shown in Figure 2.1a, e_{23} is incident at vertices 2 and 3. Edges e_{12} , e_{23} , and e_{25} are adjacent.

2.1.1 Degree of a Vertex

The *degree of a vertex* is defined as the number of edges incident with that vertex. A vertex of zero degree is called an *isolated vertex*. We call a vertex of degree two a binary vertex, a vertex of degree three a ternary vertex, and so on. For the graph shown in Figure 2.1a, the degree of vertex 2 is three, the degree of vertex 10 is one, and vertex 11 is an isolated vertex.

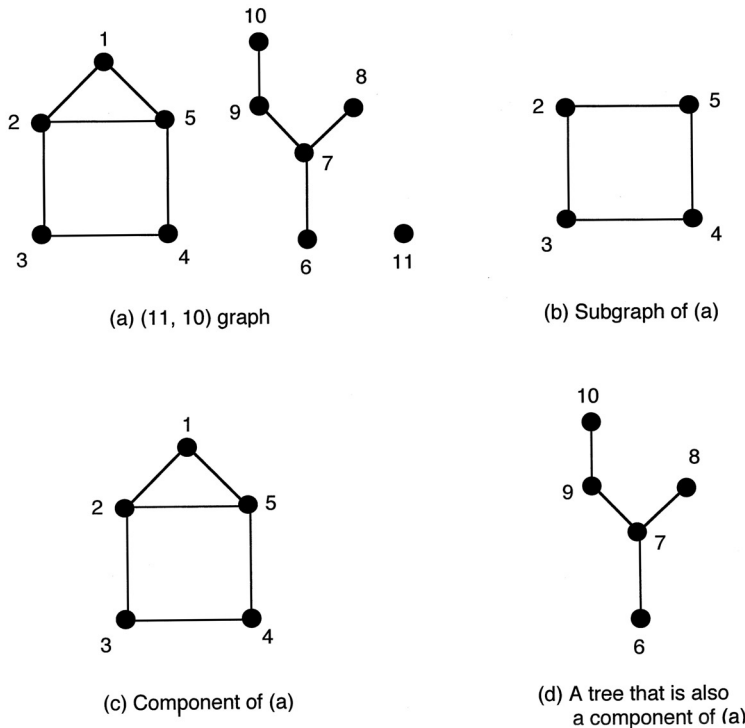


FIGURE 2.1
Graph, subgraph, component, and tree.

2.1.2 Walks and Circuits

A sequence of alternating vertices and edges, beginning and ending with a vertex, is call a *walk*. A walk is called a *trail* if all the edges are distinct and a *path* if all the vertices and, therefore the edges are distinct. In a path, no edge may be traversed more than once. The *length* of a path is defined as the number of edges between the beginning and ending vertices. If each vertex appears once, except that the beginning and ending vertices are the same, the path forms a *circuit* or *cycle*. For the graph shown in Figure 2.1a, the sequence $(2, e_{23}, 3, e_{34}, 4, e_{45}, 5)$ is a path, whereas the sequence $(2, e_{23}, 3, e_{34}, 4, e_{45}, 5, e_{52}, 2)$ is a circuit.

2.1.3 Connected Graphs, Subgraphs, and Components

Two vertices are said to be *connected*, if there exists a path from one vertex to the other. Note that two connected vertices are not necessarily adjacent. A graph G is said to be *connected* if every vertex in G is connected to every other vertex by at least one path. The minimum degree of any vertex in a connected graph is equal to one.

For example, the graph shown in Figure 2.1b is connected, whereas the one shown in Figure 2.1a is not.

A *subgraph* of G is a graph having all the vertices and edges contained in G . In other words, a subgraph of G is a graph obtained by removing a number of edges and/or vertices from G . The removal of a vertex from G implies the removal of all the edges incident at that vertex, whereas the removal of an edge does not necessarily imply the removal of its end points although it may result in one or two isolated vertices.

A graph G may contain several pieces, called *components*, each being a connected subgraph of G . By definition, a connected graph has only one component, otherwise it is disconnected. For example, the graph shown in Figure 2.1a has three components; the graph shown in Figure 2.1b is a subgraph, but not a component of Figure 2.1a; whereas the graphs shown in Figures 2.1c and d are components of Figure 2.1a.

2.1.4 Articulation Points, Bridges, and Blocks

An *articulation point* or *cut point* of a graph is a vertex whose removal results in an increase of the number of components. Similarly, a *bridge* is an edge whose removal results in an increase of the number of components. A graph is called a *block*, if it is connected and has no cut points. The minimal degree of a vertex in a block is equal to two. For the graph shown in Figure 2.1a, vertices 7 and 9 are cut points, whereas e_{67} , e_{78} , e_{79} , and $e_{9,10}$ are bridges.

2.1.5 Parallel Edges, Slings, and Multigraphs

Two edges are said to be *parallel*, if the end points of the two edges are identical. A graph is called a *multigraph* if it contains parallel edges. A *sling* or *self-loop* is an edge that connects a vertex to itself. Figure 2.2a shows a multigraph, whereas Figure 2.2b shows a graph with a sling. A graph that contains no slings or parallel edges is said to be a *simple graph*. In this text, we shall use the term graph to imply a simple graph unless it is otherwise stated.

2.1.6 Directed Graph and Rooted Graph

When a direction is assigned to every edge of a graph, the graph is said to be a *directed graph*. A *rooted graph* is a graph in which one of the vertices is uniquely identified from the others. This unique vertex is called the *root*. The root is commonly used to denote the *fixed link* or *base* of a mechanism, and it is symbolically represented by two small concentric circles. Figure 2.3 shows a directed graph in which vertex 1 is identified as the root.

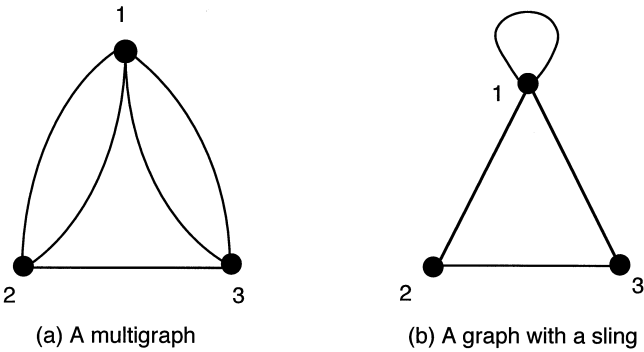


FIGURE 2.2
A multigraph and a graph with a sling.

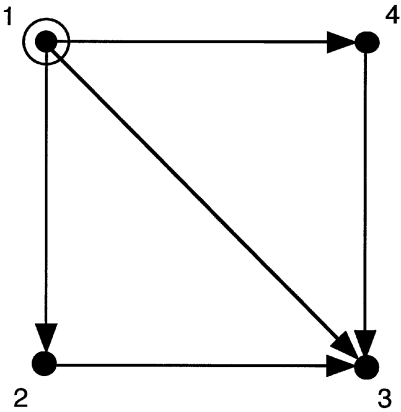


FIGURE 2.3
A directed graph.

2.1.7 Complete Graph and Bipartite

If every pair of distinct vertices in a graph are connected by one edge, the graph is called a *complete graph*. By definition, a complete graph has only one component. A complete graph of n vertices contains $n(n - 1)/2$ edges and it is denoted as a K_n graph. Figure 2.4a shows a K_5 graph.

A graph G is said to be a *bipartite* if its vertices can be partitioned into two subsets, V_1 and V_2 , such that every edge of G connects a vertex in V_1 to a vertex in V_2 . Furthermore, the graph G is said to be a *complete bipartite* if every vertex of V_1 is connected to every vertex of V_2 by one edge. A complete bipartite is denoted by $K_{i,j}$, where i is the number of vertices in V_1 and j the number of vertices in V_2 . Figure 2.4b shows a $K_{3,3}$ complete bipartite.

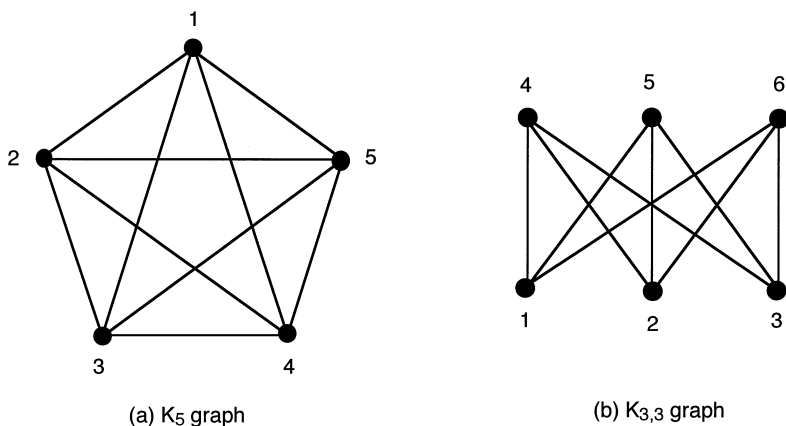


FIGURE 2.4
 K_5 and $K_{3,3}$ graphs.

2.1.8 Graph Isomorphisms

Two graphs, G_1 and G_2 , are said to be *isomorphic* if there exists a one-to-one correspondence between their vertices and edges that preserve the incidence. It follows that two isomorphic graphs must have the same number of vertices and the same number of edges, and the degrees of the corresponding vertices must be equal to one another. Figure 2.5 shows a (6, 9) graph that is isomorphic with the $K_{3,3}$ graph shown in Figure 2.4b.

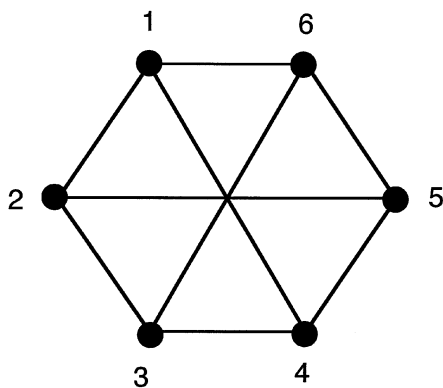


FIGURE 2.5
 A (6, 9) graph.

2.2 Tree

A *tree* is a connected graph that contains no circuits. Let T be a tree with v vertices. T possesses the following properties:

1. Any two vertices of T are connected by one and precisely one path.

Proof: Since T is connected, there exists at least one path between any two vertices, j and k . Assume that two distinct paths, P and Q , exist between vertices j and k . Following these two paths from vertex j to k , let them first diverge at vertex j' and then converge at vertex k' . Then, that section of P from j' to k' and that section of Q from j' to k' form a circuit. This leads to a contradiction since T contains no circuit. Therefore, there exists one and only one path between any two vertices of T .

2. T contains $(v - 1)$ edges.

Proof: We prove this property induction. Clearly $v = e + 1$ holds for a connected graph of one or two vertices. Assume that $v = e + 1$ holds for a tree of fewer than v vertices. If T has v vertices, the removal of any edge disconnects T in exactly two components because of the first property. By the induction hypothesis, each component contains one more vertex than edge. Therefore, the total number of edges in T must be equal to $v - 1$.

3. Connecting any two nonadjacent vertices of a tree with an edge leads to a graph with one and only circuit.

Proof: Since every two nonadjacent vertices are connected by a path, walking from the first vertex to the second along the existing path and returning to the first vertex by the added edge completes a circuit.

Figure 2.6 shows a family of trees with six vertices.

2.3 Planar Graph

A graph is said to be *embedded* in a plane when it is drawn on a plane surface such that all edges are drawn as straight lines and no two edges intersect each other. A graph is *planar* if it can be embedded in a plane. Specifically, if G is a planar graph, there exists an isomorphic graph G' such that G' can be embedded in a plane. G' is said to be the planar representation of G . The graph shown in Figure 2.7a is a planar graph since it can be embedded in a plane as shown in Figure 2.7b. However, the complete graph and the complete bipartite shown in Figure 2.4 are not planar.

Planar representation of a graph divides the plane into several connected regions, called *loops* or *circuits*. Each loop is bounded by several edges of the graph. The

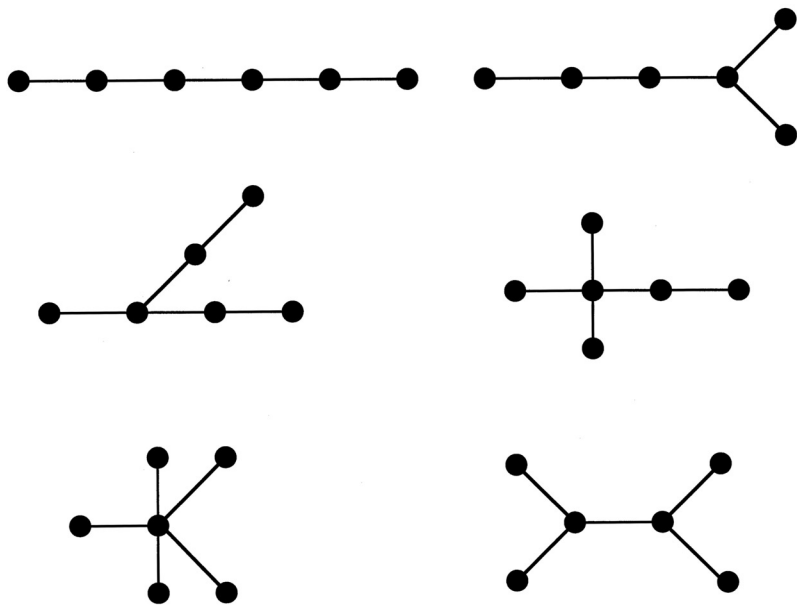


FIGURE 2.6
A family of trees with six vertices.

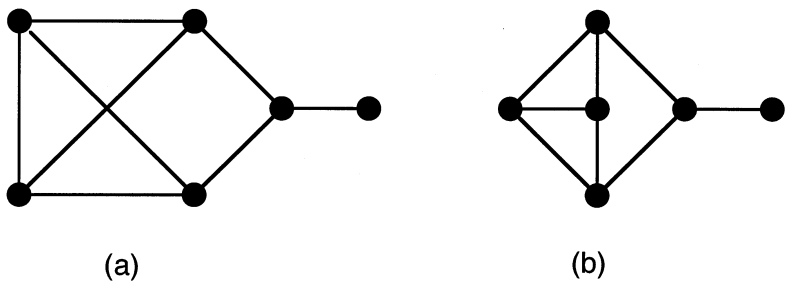


FIGURE 2.7
A graph and its planar embedding.

region external to the graph is called the *external loop* or *peripheral loop*. For example, Figure 2.8 shows a planar graph with four loops (including the peripheral loop).

The following theorem can be proved by using a mapping known as the *stereographic projection*.

THEOREM 2.1

A graph is embeddable in a plane, if and only if it is embeddable on a sphere.

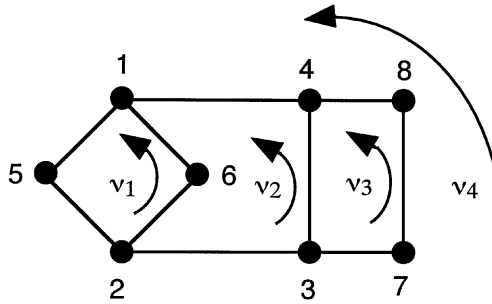


FIGURE 2.8
A planar graph.

COROLLARY 2.1

The planar embedding of a graph can be transformed into a different planar embedding such that any specified loop becomes the external loop.

Obviously, the nature of planarity of a graph is not affected either by dividing an edge into two by the insertion of a vertex, or by the reverse process. Two graphs are said to *homeomorphic* if one can be made isomorphic to the other by applying this process. The following theorem, known as *Kuratowski's theorem*, can be applied for identification of planar graphs [3].

THEOREM 2.2

A graph is planar, if and only if it contains no subgraph homeomorphic to the K_5 or $K_{3,3}$ graph.

2.4 Spanning Trees and Fundamental Circuits

A *spanning tree*, T , is a tree containing all the vertices of a connected graph G . Clearly, T is a subgraph of G . Corresponding to a spanning tree, the edge set E of G can be decomposed into two disjoint subsets, called the *arcs* and *chords*. The arcs of G consist of all the elements of E that form the spanning tree T , whereas the chords consist of all the elements of E that are not in T . The union of the arcs and chords constitutes the edge set E .

In general, the spanning tree of a connected graph is not unique. The addition of a chord to a spanning tree forms one and precisely one circuit. A collection of all the circuits with respect to a spanning tree forms a set of *independent loops* or *fundamental circuits*. The fundamental circuits constitute a basis for the circuit

space. Any arbitrary circuit of the graph can be expressed as a linear combination of the fundamental circuits using the operation of *modulo 2*, i.e., $1 + 1 = 0$.

Figure 2.9a shows a (5, 7) graph G , Figure 2.9b shows a spanning tree T , and Figure 2.9c shows a set of fundamental circuits with respect to the spanning tree T . The arcs of G consist of edges e_{15} , e_{25} , e_{34} , and e_{35} . The chords of G consist of e_{12} , e_{23} , and e_{14} . Figure 2.9d shows a circuit obtained by a linear combination of two fundamental circuits.

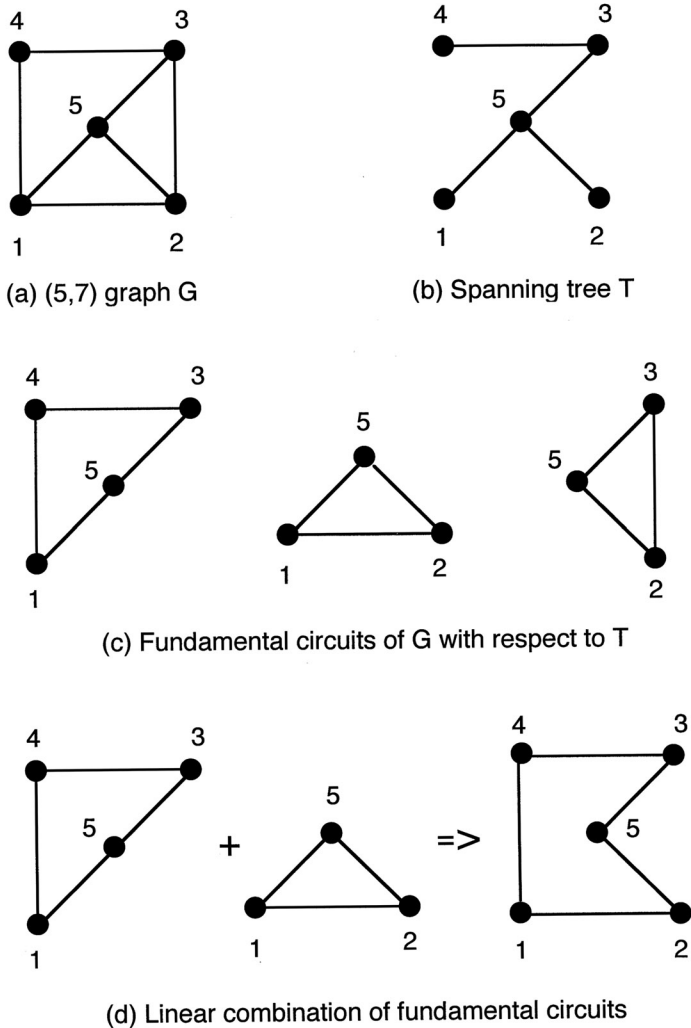


FIGURE 2.9
A spanning tree and the corresponding fundamental circuits.

2.5 Euler's Equation

Let L denote the number of independent loops of a planar connected graph and \tilde{L} represent the total number of loops. Then

$$\tilde{L} = L + 1 . \quad (2.1)$$

Euler's equation, which relates to the number of vertices, the number of edges, and the number of loops of a planar connected graph can be written as

$$\tilde{L} = e - v + 2 . \quad (2.2)$$

In terms of the number of independent loops, we have

$$L = e - v + 1 . \quad (2.3)$$

2.6 Topological Characteristics of Planar Graphs

In this section, we explore some fundamental properties of planar connected graphs that are essential for structure analysis and structure synthesis of mechanisms.

Let d_i denote the degree of a vertex i , and e denote the number of edges in a graph G . Since each edge is incident with two end vertices, it contributes 2 to the sum of the degrees of the vertices. Therefore, the sum of the degrees of all vertices in a graph is equal to twice the number of edges:

$$\sum_i d_i = 2e . \quad (2.4)$$

For the (8, 10) graph shown in Figure 2.8, we have $d_1 = d_2 = d_3 = d_4 = 3$, and $d_5 = d_6 = d_7 = d_8 = 2$. Therefore,

$$\sum_{i=1}^8 d_i = 4 \times 3 + 4 \times 2 = 2 \times 10 .$$

Let the vertices be partitioned into two groups: one consists of even-degree vertices and the other odd-degree vertices. Then, Equation (2.4) can be rearranged as

$$\sum_i d_i \text{ (even-degree vertices)} + \sum_i d_i \text{ (odd-degree vertices)} = 2e . \quad (2.5)$$

Since $\sum_i d_i$ over vertices of even degree and $2e$ are both even numbers, it follows that the number of vertices in a graph with odd degree is even.

Let L_i denote the number of loops with i edges. By definition,

$$\tilde{L} = \sum_i L_i . \quad (2.6)$$

Since each edge serves as a boundary of two loops, it contributes 2 to the sum of the product $i \times L_i$. Hence,

$$\sum_i i L_i = 2e . \quad (2.7)$$

Let v_k denote the number of vertices of degree k , namely, v_2 denotes the number of vertices of degree two, v_3 the number of vertices of degree three, etc. It follows that

$$\sum_i v_i = v_2 + v_3 + v_4 + \cdots + v_m = v , \quad (2.8)$$

where m denotes the maximal degree of a vertex. Since each edge has two end vertices and each of the v_k vertices are incident by k edges, it follows that

$$\sum_i i v_i = 2v_2 + 3v_3 + \cdots + m v_m = 2e . \quad (2.9)$$

Multiplying Equation (2.8) by 3, and subtracting Equation (2.9) from the resulting expression yields

$$3(v_2 + v_3 + v_4 + \cdots + v_m) - (2v_2 + 3v_3 + 4v_4 + \cdots) = 3v - 2e , \quad (2.10)$$

which can be written as

$$v_2 = 3v - 2e + (v_4 + 2v_5 + \cdots + v_m) . \quad (2.11)$$

Equation (2.11) implies that the number of binary vertices is bonded by the following equation,

$$v_2 \geq 3v - 2e . \quad (2.12)$$

2.7 Matrix Representations of Graph

The topological structure of a graph can be conveniently represented in matrix form. In this section, we introduce a few frequently used matrix representations of graph. The matrix representation makes analytical manipulation of graphs on a digital computer feasible. It leads to the development of systematic methodologies for identification and enumeration of graphs.

2.7.1 Adjacency Matrix

To facilitate the study, the vertices of a graph are labeled sequentially from 1 to v . A vertex-to-vertex *adjacency matrix*, A , is defined as follows:

$$a_{i,j} = \begin{cases} 1 & \text{if vertex } i \text{ is adjacent to vertex } j, \\ 0 & \text{otherwise (including } i = j), \end{cases} \quad (2.13)$$

where $a_{i,j}$ denotes the (i, j) element of A . It follows that A is a $v \times v$ symmetric matrix having zero diagonal elements. Each row (or column) sum of A corresponds to the degree of a vertex. Given a graph, the adjacency matrix is uniquely determined. On the other hand, given an adjacency matrix, one can construct the corresponding graph. Hence, the adjacency matrix identifies graphs up to graph isomorphism.

For example, Figure 2.10 shows a graph with both vertices and edges labeled sequentially. Further, vertex 1 is identified as the root. The adjacency matrix is

$$A = \begin{bmatrix} 0 & 1 & 0 & 1 & 1 \\ 1 & 0 & 1 & 0 & 1 \\ 0 & 1 & 0 & 1 & 1 \\ 1 & 0 & 1 & 0 & 0 \\ 1 & 1 & 1 & 0 & 0 \end{bmatrix}. \quad (2.14)$$

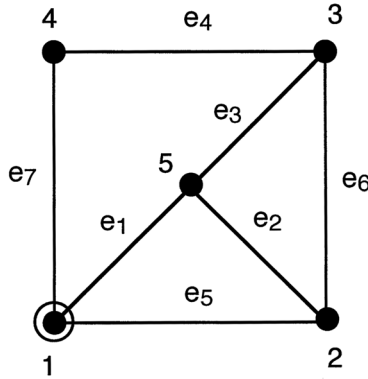


FIGURE 2.10
A labeled graph.

Clearly, the adjacency matrix depends on the labeling of vertices. If A_1 and A_2 are the adjacency matrices of a graph with two different labelings of the vertices, it can be shown that there exists a permutation matrix P such that

$$A_1 = P^{-1} A_2 P. \quad (2.15)$$

However, it should be noted that some properties of A are independent of the labeling of vertices. Let A^n be the n th power of A , and the *length* of a walk be the number of

edges in that walk. The following theorem is useful for identification of the distance between two vertices [2].

THEOREM 2.3

The number of walks of length n from vertex i to vertex j is given by the (i, j) element of A^n .

It follows that the number of walks of length 2 from vertex i to vertex j , $i \neq j$, is given by the (i, j) element of A^2 ; the degree of vertex i is given by the (i, i) element of A^2 ; and the number of triangular loops containing vertex i is given by the (i, i) element of A^3 divided by 2. The distance between vertices i and j , for $i \neq j$, is the least integer n for which the (i, j) element of A^n is nonzero. For example, for the graph shown in Figure 2.10

$$A^2 = \begin{bmatrix} 3 & 1 & 3 & 0 & 1 \\ 1 & 3 & 1 & 2 & 2 \\ 3 & 1 & 3 & 0 & 1 \\ 0 & 2 & 0 & 2 & 2 \\ 1 & 2 & 1 & 2 & 3 \end{bmatrix} \quad \text{and} \quad A^3 = \begin{bmatrix} 2 & 7 & 2 & 6 & 7 \\ 7 & 4 & 7 & 2 & 5 \\ 2 & 7 & 2 & 6 & 7 \\ 6 & 2 & 6 & 0 & 2 \\ 7 & 5 & 7 & 2 & 4 \end{bmatrix}. \quad (2.16)$$

Hence, the number of paths of length 2 are: 1 between vertices 1 and 2, 3 between vertices 1 and 3, 0 between vertices 1 and 4, 1 between vertices 1 and 5, and so on. Similarly, the number of triangular loops containing vertex 2 is 2. The distance between vertices 2 and 4 is 2.

2.7.2 Incidence Matrix

The vertices of a graph are labeled sequentially from 1 to v and the edges are labeled from 1 to e . An *incidence matrix*, B , is defined as a $v \times e$ matrix in which each row corresponds to a vertex and each column corresponds to an edge.

$$B = \begin{matrix} & \begin{matrix} \text{edge } j \\ b_{1,1} & b_{1,2} & \cdots & b_{1,e} \\ b_{2,1} & b_{2,2} & \cdots & b_{2,e} \\ \vdots & \vdots & \vdots & \vdots \\ b_{v,1} & b_{v,2} & \cdots & b_{v,e} \end{matrix} \\ \begin{matrix} \text{vertex } i \end{matrix} & \end{matrix} \quad (2.17)$$

where

$$b_{i,j} = \begin{cases} 1 & \text{if vertex } i \text{ is an end vertex of edge } j, \\ 0 & \text{otherwise.} \end{cases}$$

Since each edge has two end vertices, there are exactly two nonzero elements in each column. Hence, the sum of each column is always equal to 2, whereas the sum of each row is equal to the degree of a vertex. Similar to an adjacency matrix, the

incidence matrix determines a graph up to graph isomorphism. For example, the incidence matrix of the labeled graph shown in Figure 2.10 is given by

$$B = \begin{bmatrix} 1 & 0 & 0 & 0 & 1 & 0 & 1 \\ 0 & 1 & 0 & 0 & 1 & 1 & 0 \\ 0 & 0 & 1 & 1 & 0 & 1 & 0 \\ 0 & 0 & 0 & 1 & 0 & 0 & 1 \\ 1 & 1 & 1 & 0 & 0 & 0 & 0 \end{bmatrix}. \quad (2.18)$$

For a directed graph, the incidence matrix, \bar{B} , is defined as follows:

$$\bar{b}_{i,j} = \begin{cases} +1 & \text{if edge } j \text{ emanates from vertex } i, \\ -1 & \text{if edge } j \text{ terminates at vertex } i, \\ 0 & \text{otherwise.} \end{cases} \quad (2.19)$$

Following the definition above, the sum of each column in \bar{B} is equal to zero and the sum of all the rows is a row of zeros. Hence, the rank of \bar{B} can be at most equal to $v - 1$.

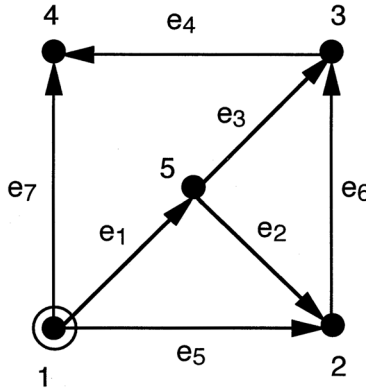


FIGURE 2.11
A directed graph.

For example, Figure 2.11 shows a directed graph obtained by assigning a direction to each edge of the graph shown in Figure 2.10. The incidence matrix is given by

$$\bar{B} = \begin{bmatrix} 1 & 0 & 0 & 0 & 1 & 0 & 1 \\ 0 & -1 & 0 & 0 & -1 & 1 & 0 \\ 0 & 0 & -1 & 1 & 0 & -1 & 0 \\ 0 & 0 & 0 & -1 & 0 & 0 & -1 \\ -1 & 1 & 1 & 0 & 0 & 0 & 0 \end{bmatrix}. \quad (2.20)$$

Let M be a matrix obtained by replacing the i th diagonal elements of $-A$ by the degree of vertex i . It can be shown that

$$\bar{B}\bar{B}^T = M. \quad (2.21)$$

For the graph shown in Figure 2.11,

$$M = \begin{bmatrix} 3 & -1 & 0 & -1 & -1 \\ -1 & 3 & -1 & 0 & -1 \\ 0 & -1 & 3 & -1 & -1 \\ -1 & 0 & -1 & 2 & 0 \\ -1 & -1 & -1 & 0 & 3 \end{bmatrix}. \quad (2.22)$$

The following theorem, known as the *Matrix-Tree Theorem*, is useful for determination of the number of spanning trees in a graph [2].

THEOREM 2.4

Let A be the adjacency matrix of a connected graph G . Then all cofactors of the matrix M are equal, and their common value is equal to the number of spanning trees of G .

A *reduced incidence matrix*, \tilde{B} , is obtained by removing the first row of B , representing the root of a graph. Hence, the reduced incidence matrix is of order $(v-1) \times e$. The i th row denotes the $(i+1)$ th vertex. For example, the reduced incidence matrix for the graph shown in Figure 2.10 is given by

$$\tilde{B} = \begin{bmatrix} 0 & 1 & 0 & 0 & 1 & 1 & 0 \\ 0 & 0 & 1 & 1 & 0 & 1 & 0 \\ 0 & 0 & 0 & 1 & 0 & 0 & 1 \\ 1 & 1 & 1 & 0 & 0 & 0 & 0 \end{bmatrix}. \quad (2.23)$$

2.7.3 Circuit Matrix

The circuits of a graph are labeled sequentially from 1 to ℓ and the edges are labeled from 1 to e . A *circuit matrix*, C , is defined as an $\ell \times e$ matrix in which each row corresponds to a circuit and each column denotes an edge.

$$C = \begin{matrix} & \text{edge } j \\ \begin{bmatrix} c_{1,1} & c_{1,2} & \cdots & c_{1,e} \\ c_{2,1} & c_{2,2} & \cdots & c_{2,e} \\ \vdots & \vdots & \vdots & \vdots \\ c_{\ell,1} & c_{\ell,2} & \cdots & c_{\ell,e} \end{bmatrix} & \text{circuit } i \end{matrix} \quad (2.24)$$

where

$$c_{i,j} = \begin{cases} 1 & \text{if circuit } i \text{ contains edge } j, \\ 0 & \text{otherwise.} \end{cases}$$

Obviously, those edges that do not lie on any circuit do not appear in the circuit matrix. Hence, the circuit matrix does not provide complete information about a graph. Unlike the adjacency and incidence matrices, the circuit matrix does not determine a graph

up to isomorphism. For example, Figure 2.12 shows a graph obtained by labeling the circuits of the graph shown in Figure 2.10. Its circuit matrix is

$$C = \begin{bmatrix} 1 & 1 & 0 & 0 & 1 & 0 & 0 \\ 0 & 1 & 1 & 0 & 0 & 1 & 0 \\ 1 & 0 & 1 & 1 & 0 & 0 & 1 \\ 0 & 0 & 0 & 1 & 1 & 1 & 1 \end{bmatrix}. \quad (2.25)$$

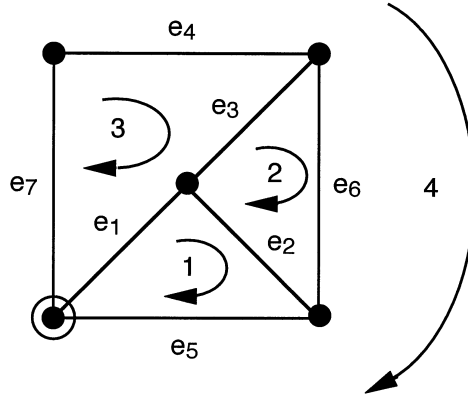


FIGURE 2.12

A graph with labeled circuits.

The row vectors of C are not necessarily independent. For a connected graph G , the number of independent circuits is given by Euler's equation. Corresponding to a given spanning tree, each chord uniquely defines a fundamental circuit. The set of circuits determined from all the chords of G constitutes a basis for the circuit space. Any other circuits can be expressed as a linear combination of the base vectors with the arithmetic of *modulo 2*. For the above example, we observe that the last row of C is equal to the sum of the first three rows.

2.7.4 Path Matrix

A *path matrix*, T , is defined for storing the information about all paths that emanate from the root and terminate at the remaining vertices of a rooted tree. With the root labeled as vertex 1, the remaining vertices are labeled sequentially from 2 to v and the edges are labeled from 1 to $v - 1$. The path matrix is defined as

$$T = \begin{matrix} & \text{vertex } j+1 \\ & \begin{bmatrix} t_{1,1} & t_{1,2} & \cdots & t_{1,v-1} \\ t_{2,1} & t_{2,2} & \cdots & t_{2,v-1} \\ \vdots & \vdots & \vdots & \vdots \\ t_{v-1,1} & t_{v-1,2} & \cdots & t_{v-1,v-1} \end{bmatrix} \\ \text{arc } i & \end{matrix} \quad (2.26)$$

where

$$t_{i,j} = \begin{cases} 1 & \text{if edge } i \text{ lies on the path emanating from the root} \\ & \text{and terminating at vertex } j + 1, \\ 0 & \text{otherwise.} \end{cases}$$

Hence, T is a $(v - 1) \times (v - 1)$ matrix in which each column represents a vertex (excluding the root) and each row corresponds to an arc of the tree. The i th column of T denotes the $(i + 1)$ th vertex. Figure 2.13 shows a spanning tree of the graph shown in Figure 2.10. The path matrix is

$$T = \begin{bmatrix} 1 & 1 & 1 & 1 \\ 1 & 0 & 0 & 0 \\ 0 & 1 & 1 & 0 \\ 0 & 0 & 1 & 0 \end{bmatrix}. \quad (2.27)$$

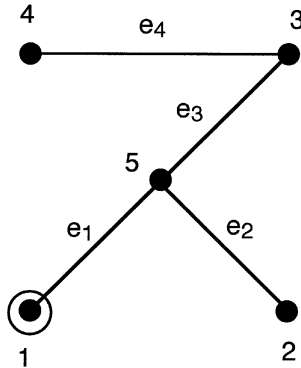


FIGURE 2.13
A rooted spanning tree.

If the reduced incidence matrix of a rooted tree is denoted as \tilde{B}_A , it can be shown that under the arithmetic of *modulo 2*, the product of $T\tilde{B}_A$ is an identity matrix of order $v - 1$,

$$T\tilde{B}_A = I. \quad (2.28)$$

For example, the reduced incidence matrix for the rooted tree shown in Figure 2.13 is

$$\tilde{B}_A = \begin{bmatrix} 0 & 1 & 0 & 0 \\ 0 & 0 & 1 & 1 \\ 0 & 0 & 0 & 1 \\ 1 & 1 & 1 & 0 \end{bmatrix}. \quad (2.29)$$

Substituting Equations (2.27) and (2.29) into Equation (2.28) yields

$$T \tilde{B}_A = \begin{bmatrix} 1 & 0 & 0 & 0 \\ 0 & 1 & 0 & 0 \\ 0 & 0 & 1 & 0 \\ 0 & 0 & 0 & 1 \end{bmatrix}. \quad (2.30)$$

Given a spanning tree, if we partition the edges of a rooted graph into arcs and chords in such a way that the arcs are labeled from 1 to $v - 1$, whereas the chords are labeled from v to e , the incidence matrix can be partitioned in the form

$$\tilde{B} = \left[\tilde{B}_A : \tilde{B}_C \right], \quad (2.31)$$

where \tilde{B}_A denotes the portion of a reduced incidence matrix associated with the arcs and \tilde{B}_C represents the portion associated with the chords of a rooted graph. Let

$$U = T \tilde{B}_C. \quad (2.32)$$

It can be shown that the circuit matrix C is given by

$$C = \left[U^T : I \right]. \quad (2.33)$$

For example, for the graph shown in Figure 2.10 with respect to the spanning tree shown in Figure 2.13,

$$U = \begin{bmatrix} 1 & 0 & 1 \\ 1 & 1 & 0 \\ 0 & 1 & 1 \\ 0 & 0 & 1 \end{bmatrix}. \quad (2.34)$$

Substituting Equation (2.34) into Equation (2.33) yields

$$C = \left[\begin{array}{ccccccc} 1 & 1 & 0 & 0 & 1 & 0 & 0 \\ 0 & 1 & 1 & 0 & 0 & 1 & 0 \\ 1 & 0 & 1 & 1 & 0 & 0 & 1 \end{array} \right]. \quad (2.35)$$

As opposed to Equation (2.25), Equation (2.35) contains only three independent circuits with respect to the spanning tree depicted in Figure 2.13. Equation (2.33) is useful for identification of fundamental circuits of a graph.

2.8 Contracted Graphs

We define a *binary string* of length k as a string of k vertices of degree 2 connected in series by $k + 1$ edges as shown in Figure 2.14. The first and last edges of a binary

string are necessarily incident to nonbinary vertices. For example, the (8, 10) graph shown in Figure 2.8 contains two binary strings of length 1 and a binary string of length 2. The first binary string contains vertex 5, the second contains vertex 6, and the third contains vertices 7 and 8.

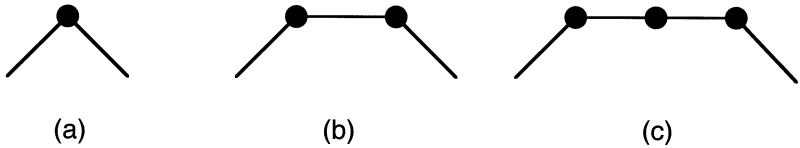


FIGURE 2.14
Binary strings of length one, two, and three.

A *contracted graph* is obtained by replacing every binary string in a graph with a single edge. It follows that a contracted graph has no binary vertices. However, it may contain parallel edges [5]. The process of removing a binary string and replacing it with a single edge is called a *contraction*. Figure 2.15 shows the contracted graph of Figure 2.8 in which there are two parallel edges connecting vertices 1 and 2, and two additional parallel edges connecting vertices 3 and 4.

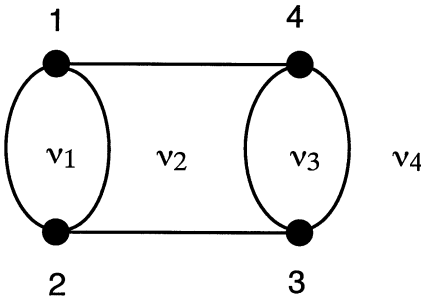


FIGURE 2.15
A contracted graph.

We note that a conventional graph is mapped onto a unique contracted graph. On the other hand, given a contracted graph, many conventional graphs can be constructed from it by replacing the edges with binary strings of certain desired lengths. The process of replacing an edge in a contracted graph with a binary string is called an *expansion*.

From the above discussion, it is clear that the number of vertices in a contracted graph is equal to the number of vertices in the conventional graph diminished by the number of binary vertices; the number of edges in a contracted graph is equal to the number of edges in the conventional graph diminished by the number of binary vertices, whereas the total number of loops remains unchanged. Let v_2 be the number of binary vertices in a conventional graph. Also let v^c be the number of vertices, e^c

the number of edges, and \tilde{L}^c the total number of loops in a contracted graph. Then,

$$v^c = v - v_2, \quad (2.36)$$

$$e^c = e - v_2, \quad (2.37)$$

$$\tilde{L}^c = e^c - v^c + 2 = \tilde{L}. \quad (2.38)$$

Since each binary string of length i contains i binary vertices, it follows that

$$b_1 + 2b_2 + 3b_3 + \cdots + qb_q = v_2, \quad (2.39)$$

where b_i denotes the number of binary strings of length i , and q denotes the longest binary string in a conventional graph. We may consider a binary string of zero length as a special case in which two vertices of degree greater than two are connected directly by an edge. From the definition of a contracted graph, it follows that

$$b_0 + b_1 + b_2 + b_3 + \cdots + b_q = e^c. \quad (2.40)$$

For the conventional graph shown in Figure 2.8, we have $v = 8$, $e = 10$, $\tilde{L} = 4$, $v_2 = 4$, $b_0 = 3$, $b_1 = 2$, and $b_2 = 1$. Equations (2.36), (2.37), and (2.38) predict $v^c = 8 - 4 = 4$, $e^c = 10 - 4 = 6$, and $\tilde{L}^c = 4$, which can be easily verified from the contracted graph shown in Figure 2.15. Obviously, Equations (2.39) and (2.40) are also satisfied.

A contracted graph can also be expressed in matrix form. The vertex-to-vertex *adjacency matrix*, A^c , of a contracted graph is defined as follows:

$$a_{i,j}^c = \begin{cases} k & \text{if vertex } i \text{ is connected to vertex } j \text{ by } k \text{ parallel edges} \\ 0 & \text{otherwise (including } i = j \text{).} \end{cases} \quad (2.41)$$

Following the definition above, the row sum of A^c is equal to the degree of the corresponding vertex. Since a contracted graph has no binary vertex, the minimum degree of a vertex is 3. For example, the adjacency matrix of the contracted graph shown in Figure 2.15 is

$$A^c = \begin{bmatrix} 0 & 2 & 0 & 1 \\ 2 & 0 & 1 & 0 \\ 0 & 1 & 0 & 2 \\ 1 & 0 & 2 & 0 \end{bmatrix}. \quad (2.42)$$

The concept of contracted graphs can be employed for enumeration of planar graphs.

2.9 Dual Graphs

The *dual* of a conventional graph is a graph in which the vertices represent the loops (including the peripheral loop) and the loops represent the vertices of the conventional

graph. Given a conventional graph G , its dual graph G^* is constructed as follows: Place a vertex in each loop of G , and, if two adjacent loops of G share a common edge e , connect the corresponding vertices of G^* by an edge e^* across e . The dual of a simple graph may contain self-loops if the original graph has bridges. It may also become a multigraph if there are binary vertices in the original graph.

For example, Figure 2.16 shows the construction of a dual from the conventional

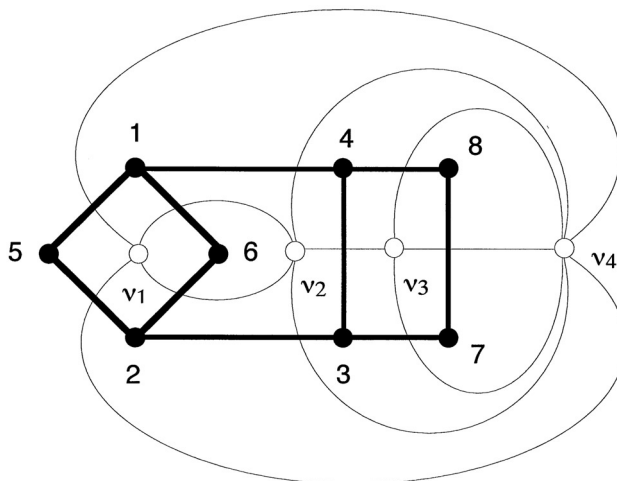


FIGURE 2.16

A graph and its dual.

graph shown in Figure 2.8. To construct the dual graph, we place a vertex, designated as v_1, v_2, v_3 , and v_4 , in each loop of the conventional graph. The edges of the dual graph are sketched as hairlines across every edge of the conventional graph according to the above convention. Since loops 3 and 4 in the conventional graph are divided by three edges, e_{37} , e_{78} , and e_{84} , in the corresponding dual graph v_3 and v_4 are connected by three parallel edges. Similarly, there are two parallel edges connecting v_1 and v_2 , v_1 and v_4 , and v_2 and v_4 .

To further simplify the notation, we replace parallel edges in a dual graph by a single edge and label it with the number of parallel edges. Figure 2.17 shows an edge-labeled dual graph of the graph shown in Figure 2.16. Note that in Figure 2.16 the two parallel edges between v_2 and v_4 are divided by the $v_2 - v_3 - v_4$ vertex chain. In the edge-labeled dual graph shown in Figure 2.17, this information is lost. In this regard, an edge-labeled dual may be transformed into more than one conventional graph. Figure 2.18 shows a second graph, which shares the same edge-labeled dual as that of Figure 2.16.

By definition, the dual of a planar graph G is also a planar graph. It follows that the dual of the dual of G is the original graph G . However, it should be noted that a graph with more than one planar embedding can give rise to more than one dual graph as illustrated in Figure 2.19.

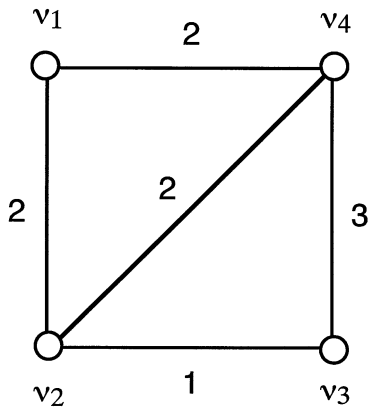


FIGURE 2.17
A labeled dual graph.

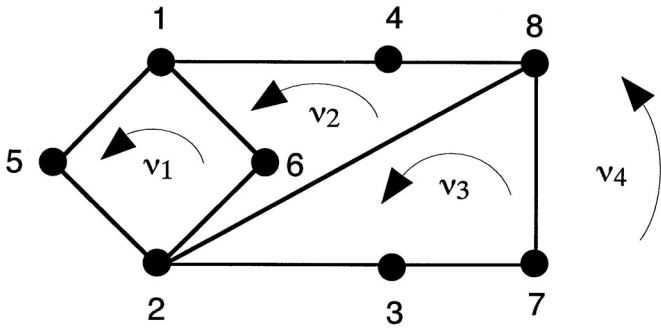


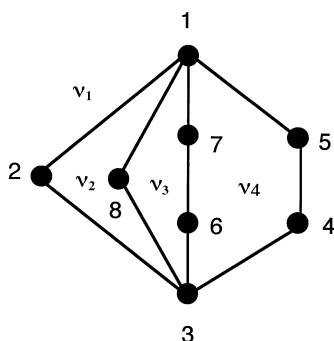
FIGURE 2.18
A graph having the same edge-labeled dual.

We summarize the correspondence between a conventional graph and its dual as follows: (1) the vertices of a dual graph correspond to the loops of a conventional graph, (2) the loops of a dual graph correspond to the vertices of a conventional graph, and (3) degree of a vertex in the dual graph corresponds to the number of edges in a loop of the conventional graph. Let v^d denote the number of vertices, e^d the number of edges, and \tilde{L}^d the total number of loops in a dual graph. The following relations hold:

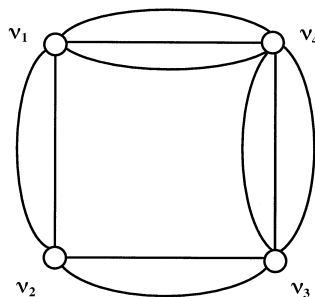
$$v^d = \tilde{L} , \tag{2.43}$$

$$e^d = e , \tag{2.44}$$

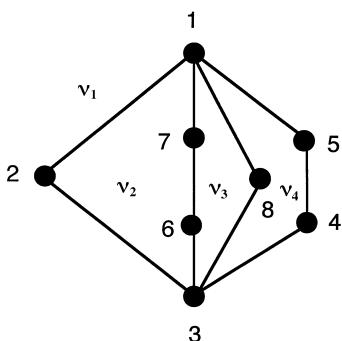
$$\tilde{L}^d = v . \tag{2.45}$$



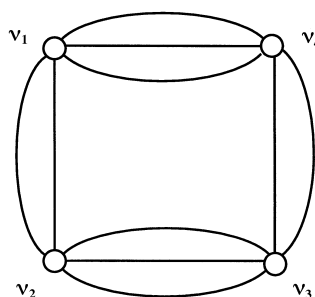
(a) A (7, 10) graph



(b) Dual graph of (a)



(c) Isomorphic graph of (a)



(d) Dual graph of (c)

FIGURE 2.19

Two isomorphic graphs giving rise to two different dual graphs.

Sohn and Freudenstein [4] applied the concept of dual graphs for the development of an automated procedure for the enumeration of the kinematic structures of mechanisms.

2.10 Summary

The basic concepts of graph theory that are essential for structural analysis and structure synthesis of mechanisms were introduced. Graphs, isomorphic graphs, contracted graphs, and dual graphs were defined. The topological characteristics of planar graphs were derived. To facilitate the development of an automated graph enumeration methodology, various matrix representations of graph were introduced.

References

[1] Gibsons, A., 1985, *Algorithmic Graph Theory*, Cambridge University Press, Cambridge, UK.

[2] Harary, F., 1969, *Graph Theory*, Addison-Wesley, Reading, MA.

[3] Kuratowski, K., 1930, Sur le Problème des Courbes Gauches en Topologie, *Fundamental Mathematics*, 15, 271–283.

[4] Sohn, W. and Freudenstein, F., 1986, An Application of Dual Graphs to the Automatic Generation of the Kinematic Structures of Mechanism, *ASME Journal of Mechanisms, Transmissions, and Automation in Design*, 108, 3, 392–398.

[5] Woo, L.S., 1967, Type Synthesis of Plane Linkages, *ASME Journal of Engineering for Industry*, Series B, 89, 159–172.

Exercises

- 2.1 Show that the planar embedding of a graph can be transformed into another planar embedding such that any specified loop becomes the external loop.
- 2.2 Derive the adjacency and incidence matrices for the (6, 7) and (7, 8) graphs shown in Figures 2.20a and b.

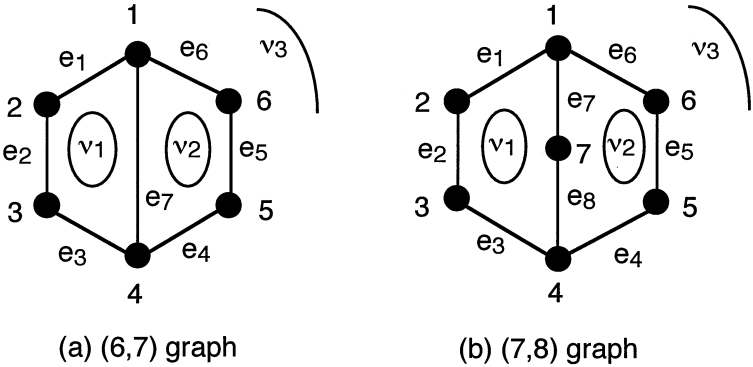


FIGURE 2.20
(6, 7) and (7, 8) graphs with three circuits.

2.3 Derive the adjacency and incidence matrices for the two (8, 10) graphs shown in Figures 2.21a and b.

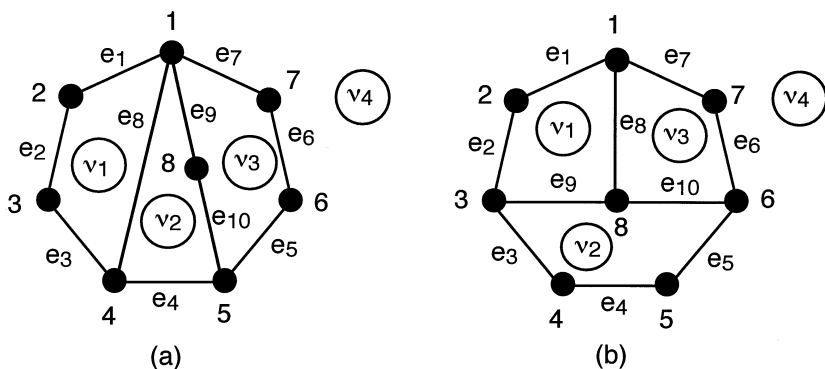


FIGURE 2.21

Two (8, 10) graphs with four circuits.

2.4 Let the thin edges denote the arcs and heavy edges denote the chords. Derive the incidence, path, and circuit matrices for the (6, 8) and (7, 10) rooted graphs shown in Figures 2.22a and b.

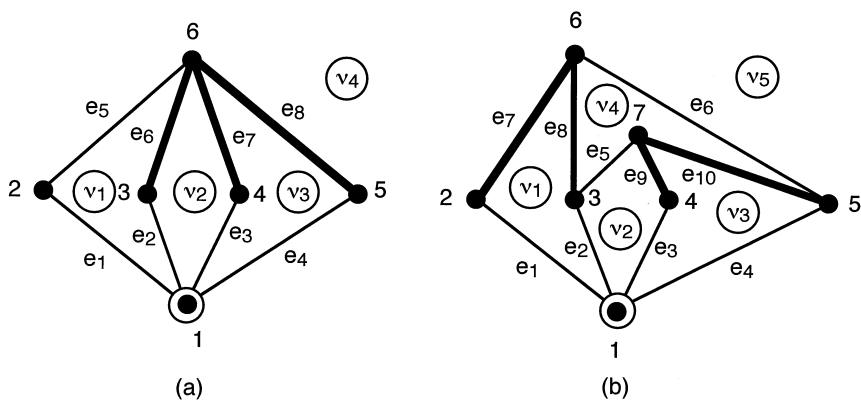


FIGURE 2.22

(6, 8) and (7, 10) rooted graphs.

2.5 Let thin edges denote the arcs and heavy edges denote the chords. Derive the incidence, path, and circuit matrices for the two (7, 10) rooted graphs shown in Figures 2.23a and b.

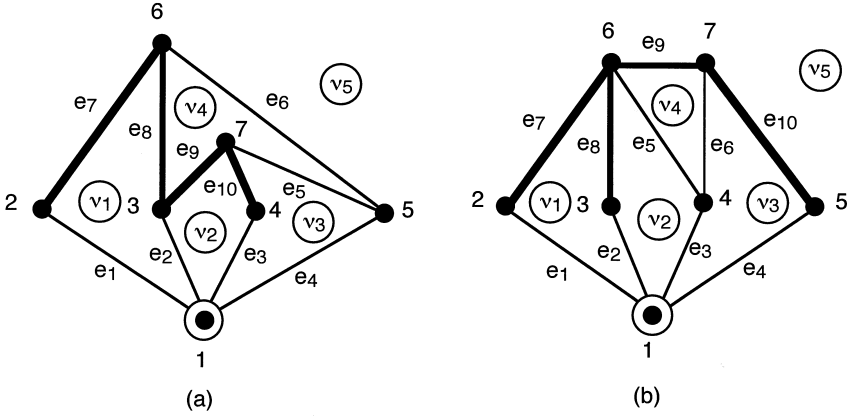


FIGURE 2.23
Two (7, 10) rooted graphs.

2.6 Let thin edges denote the arcs and heavy edges denote the chords. Derive the incidence, path, and circuit matrices for the (7, 9) and (8, 11) rooted graphs shown in Figures 2.24a and b.

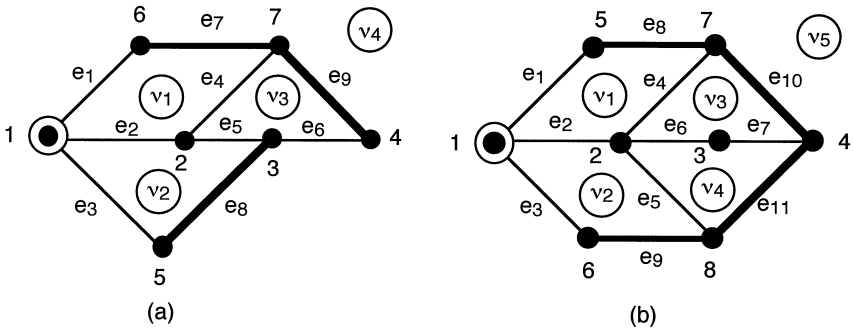


FIGURE 2.24
(7, 9) and (8, 11) rooted graphs.

2.7 Sketch the contracted and dual graphs of the (6, 7) and (7, 8) graphs shown in Figures 2.20a and b.

2.8 Sketch the contracted and dual graphs of the (8, 10) graphs shown in Figures 2.21a and b.

Chapter 3

Structural Representations of Mechanisms

3.1 Introduction

The kinematic structure of a mechanism contains the essential information about which link is connected to which other link by what type of joint. The kinematic structure of a mechanism can be represented in several different ways. Some methods of representation are fairly straightforward, whereas others may be rather abstract and do not necessarily have a one-to-one correspondence. In this chapter various methods of representation of the kinematic structure of a mechanism or kinematic chain are described. For convenience, the following assumptions are made for all methods of representation.

1. For simplicity, all parallel redundant paths in a mechanism will be illustrated by a single path. Parallel paths are usually employed for increasing load capacity and achieving better dynamic balance of a mechanism. For example, Figure 3.1 depicts the components of a basic planetary gear train whose schematic diagram is shown in Figure 3.2a. Although the gear train has four planets, the structural representation is sketched with only one, as illustrated in Figure 3.2b. Similarly, when a link is supported by several coaxial bearings, only one will be shown.
2. All joints are assumed to be binary. A multiple joint will be substituted by a set of equivalent binary joints. In this regard, a ternary joint will be replaced by two coaxial binary joints, a quaternary joint will be replaced by three coaxial binary joints, and so on.
3. Two mechanical components rigidly connected for the ease of manufacturing or assembling will be considered and shown as one link. For example, two gears keyed together on a common shaft to form a compound gear set will be treated as one link.

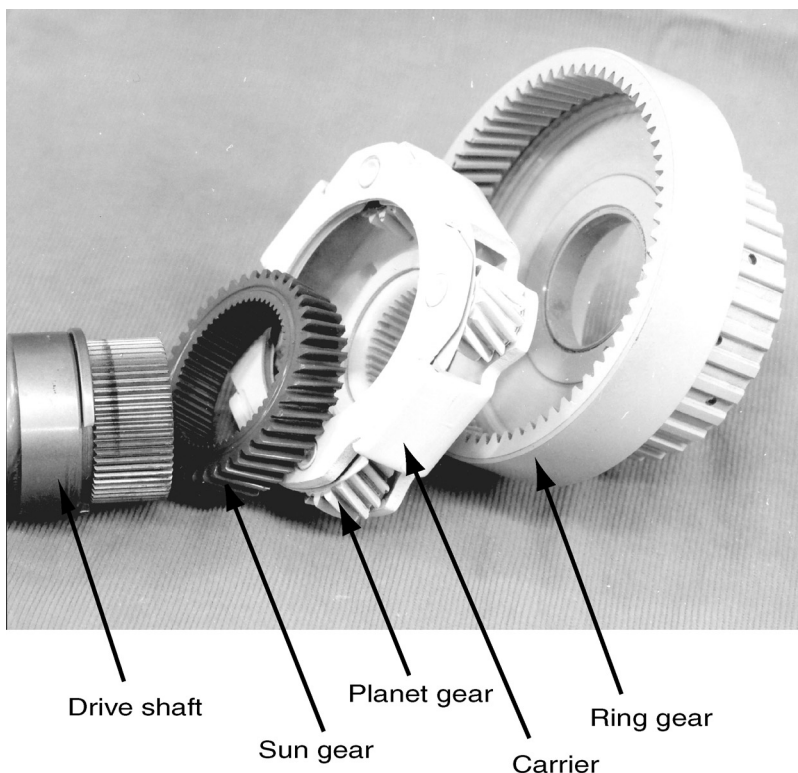
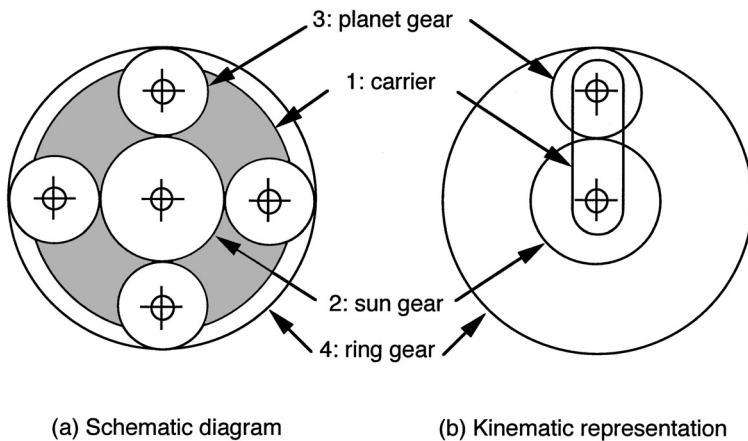


FIGURE 3.1
A basic planetary gear train.

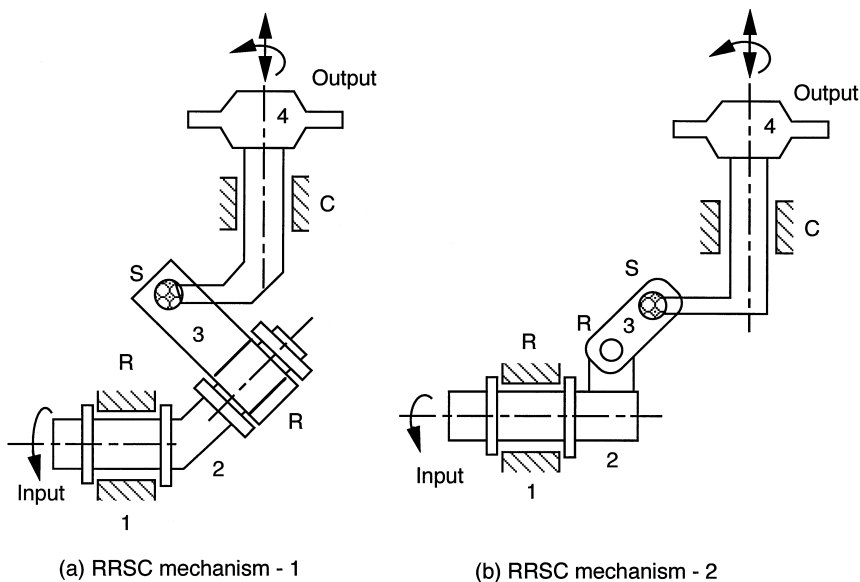
3.2 Functional Schematic Representation

Functional schematic representation refers to the most familiar cross-sectional drawing of a mechanism. Shafts, gears, and other mechanical elements are drawn as such. For clarity and simplicity, only those functional elements that are essential to the structural topology of a mechanism are shown.

Two functional schematics representing different physical embodiments might sometimes share the same structural topology. For example, Figures 3.3a and b show the schematic diagrams of two different mechanisms. Each of the two mechanisms contains four links connected by two revolute, one spherical, and one cylindric joint. The two revolute joint axes in Figure 3.3a intersect at an oblique angle, whereas the two revolute joint axes in Figure 3.3b are perpendicular to each other with an offset distance. Both mechanisms are capable of converting the rotational motion of link 2 into the reciprocating and oscillatory motions of link 4. These two mechanisms are different in physical embodiment, but their structural topologies are identical.

**FIGURE 3.2**

Schematic diagram and kinematic representation.

**FIGURE 3.3**

Functional schematics of two RRSC spatial mechanisms.

Similarly, various planetary gear trains with internal versus external gear mesh may share identical structural topology. Figure 3.4a shows the functional schematic of a spur gear set with an external gear mesh, whereas Figure 3.4b shows the functional schematic of another spur gear set with an internal gear mesh. Each of these two gear sets contains three links. Gear 2 meshes with gear 3, whereas link 1 serves as the carrier. Together, they form a one-dof gear train. In the side view of a gear pair, we use two short parallel lines to indicate the gear mesh. These two gear sets are different in design. However, their structural topologies are identical, to some extent, as will be described in the following section.

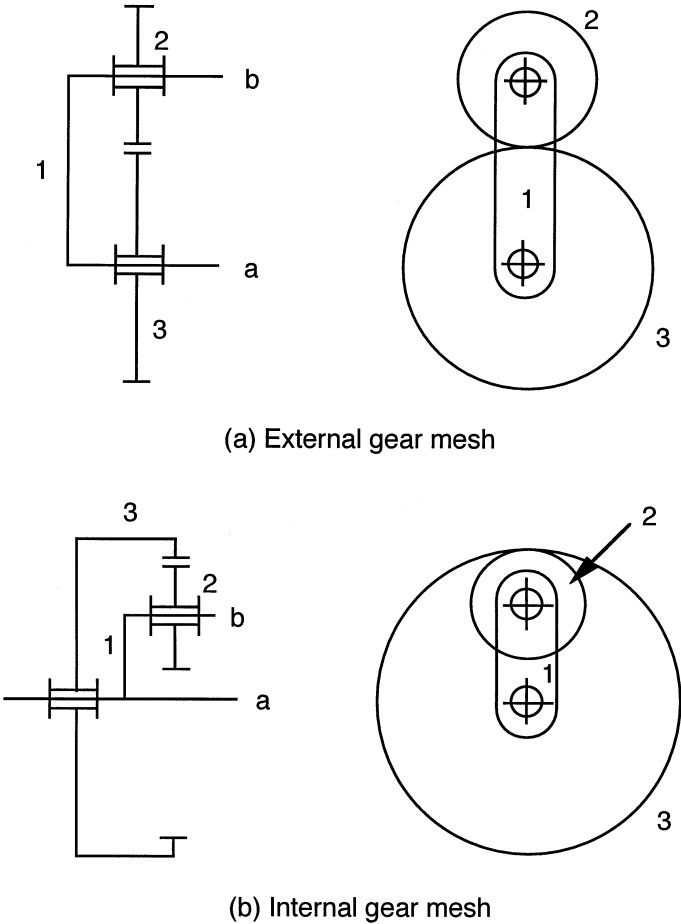


FIGURE 3.4
Functional schematics of two gear sets that share the same structural topology.

3.3 Structural Representation

In a *structural representation*, each link of a mechanism is denoted by a polygon whose vertices represent the kinematic pairs. Specifically, a binary link is represented by a line with two end vertices, a ternary link is represented by a cross-hatched triangle with three vertices, a quaternary link is represented by a cross-hatched quadrilateral with four vertices, and so on. Figure 3.5 shows the structural representation of a binary, ternary, and quaternary link. The vertices of a structural representation can be colored or labeled for the identification of pair connections. For example, *plain vertices* shown in Figure 3.5 denote revolute joints, whereas *solid vertices* denote gear pairs.

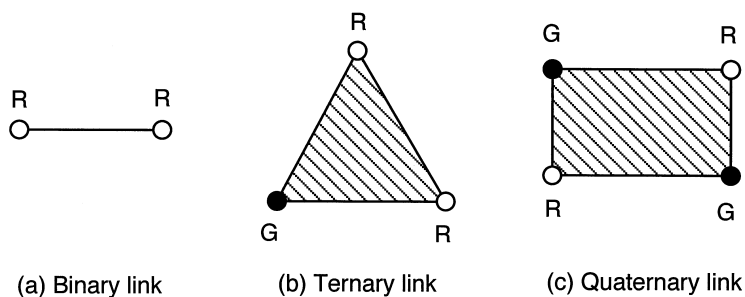
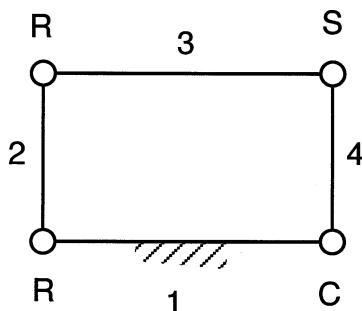


FIGURE 3.5
Structural representation of links.

The structural representation of a mechanism is defined similarly, except that the polygon denoting the fixed link is labeled accordingly. Unlike the functional schematic representation, the dimensions of a mechanism, such as the offset distance and twist angle between two adjacent links, are not shown in the structural representation.

Figure 3.6 shows the structural representation of the two *RRSC* spatial mechanisms depicted in Figure 3.3, where the edge label denotes the link number and the vertex label denotes the joint type. Figure 3.6 shows that the four links are connected in a closed loop by revolute, revolute, spherical, and cylindric joints. We conclude that both mechanisms shown in Figure 3.3 share the same structural topology.

Figure 3.7 depicts the side view of the planetary gear train shown in Figure 3.2 and the corresponding structural representation. We note that, at this level of abstraction, the type of gear mesh is not specified. In this regard, the kinematic structure shown in Figure 3.7 may be sketched in more than one functional schematic. Either gear pair can assume either external or internal gear mesh. Hence, there is no one-to-one correspondence between the functional schematic and the structural representation. To distinguish the difference requires one additional level of abstraction. For example,

**FIGURE 3.6**

Structural representation of the two *RRSC* mechanisms shown in Figure 3.3.

we may use the symbol G_i to represent an internal gear mesh and G_o an external gear mesh.

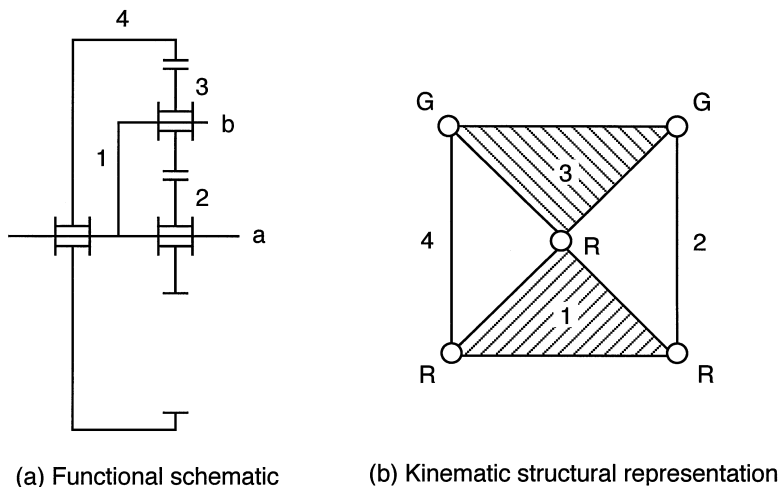
Figure 3.8 shows the schematics and structural representations of some link assortments frequently used in geared kinematic chains.

3.4 Graph Representation

Since a kinematic chain is a collection of links connected by joints, this link and joint assemblage can be represented in a more abstract form called the *graph representation*. In a graph representation, the vertices denote links and the edges denote joints of a mechanism. The edge connection between vertices corresponds to the pair connection between links. To distinguish the differences between various pair connections, the edges can be labeled or colored. For example, the gear pairs in a gear train can be represented by thick edges and the turning pairs (revolute joints) by thin edges. Furthermore, the thin edges can be labeled according to the locations of their axes.

The graph of a mechanism is defined similarly with only one addition; the vertex denoting the fixed link is labeled accordingly, usually with two small concentric circles. For example, Figure 3.9 depicts a graph representation of the *RRSC* mechanism shown in Figure 3.3. The vertices shown in Figure 3.9 are numbered from 1 to 4 representing links 1 to 4, respectively, and the edges are labeled as *R*, *R*, *S*, and *C* according to the pair connections between links.

Similarly, Figure 3.10 illustrates the graph representation of the planetary gear set shown in Figure 3.2. In Figure 3.10, the thick edges denote gear pairs and the thin edges denote turning pairs. Since the type of gear mesh is not specified at this level of abstraction, the graph shown in Figure 3.10 can also represent a gear set with two external gear meshes or two internal meshes.

**FIGURE 3.7**

Functional and structural representations of the planetary gear set shown in Figure 3.2.

The sketching of a graph from a mechanism is very straightforward. However, the inverse process, that is, the sketching of a mechanism from the graph, requires some practice to achieve nice proportions. In general, a single graph can be sketched into several different mechanism embodiments.

Figure 3.11 shows three different kinematic representations of four epicyclic gear trains.

3.4.1 Advantages of Using Graph Representation

The advantages of using the graph representation are:

1. Many network properties of graphs are directly applicable. For example, we can apply Euler's equation to obtain the *loop mobility criterion* of mechanisms directly.
2. The structural topology of a mechanism can be uniquely identified. Using graph representation, the similarity and difference between two different mechanism embodiments can be easily recognized.
3. Graphs may be used as an aid for the development of computer-aided kinematic and dynamic analysis of mechanisms. For example, Freudenstein and Yang [7] applied the *theory of fundamental circuits* for the kinematic and static force analysis of planar spur gear trains. The theory was subsequently extended to the kinematic analysis of bevel-gear robotic mechanisms [12]. Recently,

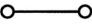
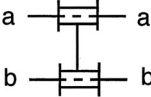

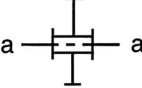
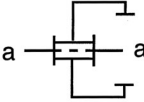

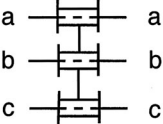

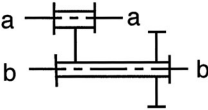

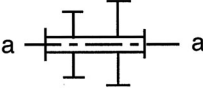
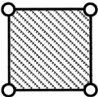
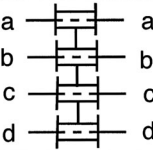
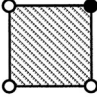
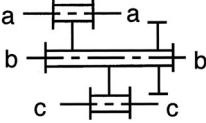
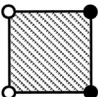
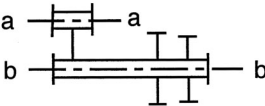
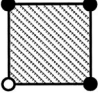
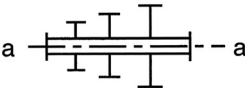
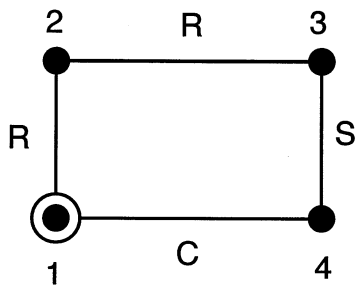
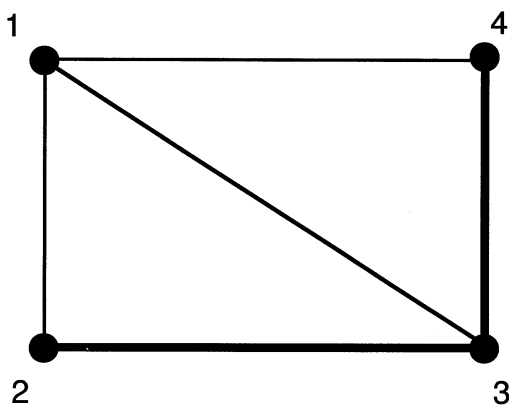
Link type	Functional schematic	
		
		
		
		
		
		
		
		
		

FIGURE 3.8
Link assortments frequently used in geared kinematic chains.

**FIGURE 3.9**

Graph representation of the *RRSC* mechanisms shown in Figure 3.3.

**FIGURE 3.10**

Graph representation of the planetary gear set shown in Figure 3.2.

a systematic methodology for the dynamic analysis of gear coupled robotic mechanisms was developed [13].

4. Graph theory may be employed for systematic enumeration of mechanisms. [1, 2, 4, 6, 8, 10, 11, 14].
5. Graphs can be used for systematic classification of mechanisms. A single atlas of graphs can be used to enumerate an enormous number of mechanisms [5, 6, 9]. This obviates the need for an individual atlas of kinematic chains tailored for each application.
6. Graphs can be used as an aid in automated sketching of mechanisms [3].

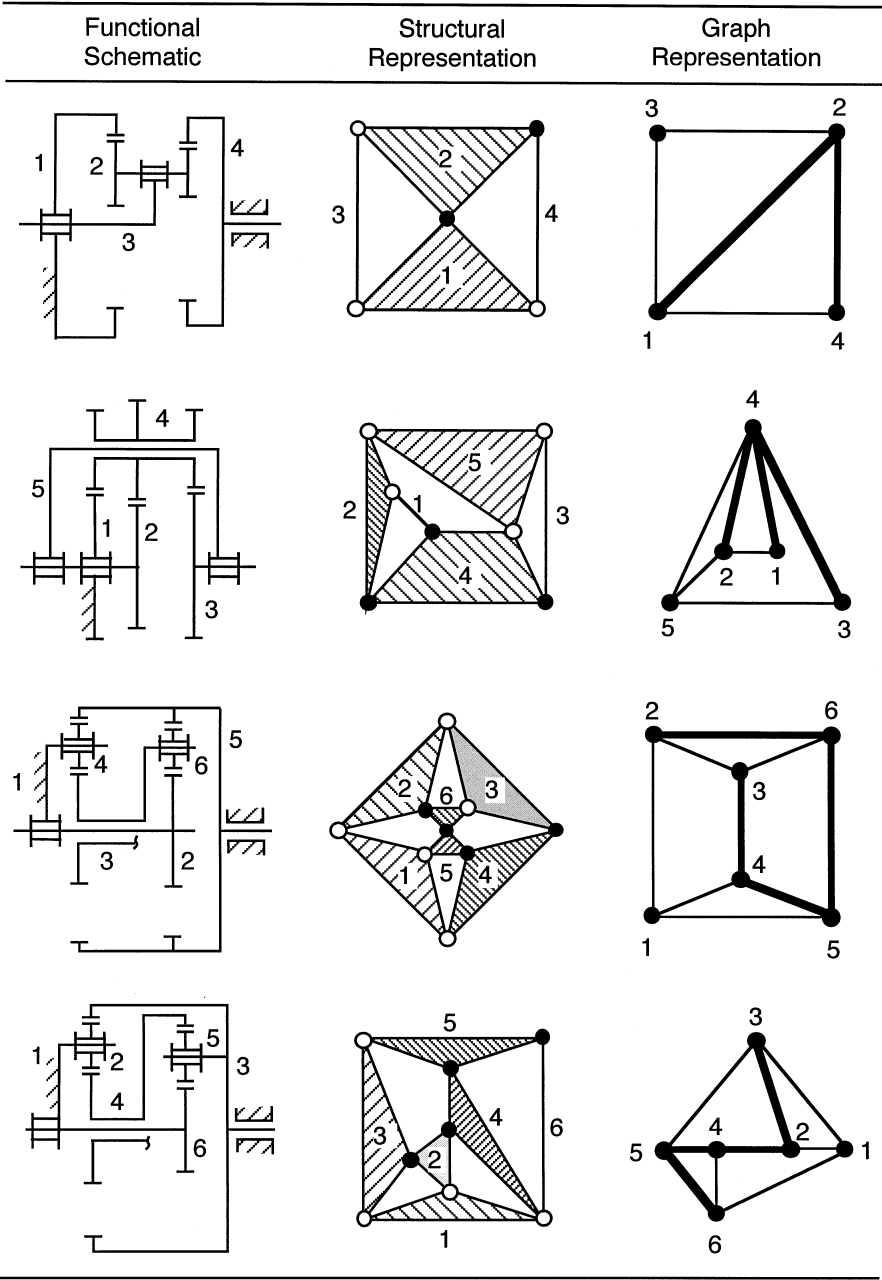


FIGURE 3.11
Kinematic representation of four epicyclic gear trains.

3.5 Matrix Representation

For convenience of computer programming, the kinematic structure of a kinematic chain is represented by a graph and the graph is expressed in matrix form. There are several methods of matrix representation as described in Chapter 2. Perhaps, the most frequently used method is the link-to-link form of adjacency matrix. Other methods of representation, such as the incidence matrix, circuit matrix, and path matrix, are also useful for the identification and classification of mechanisms. Matrix representations are particularly useful for computer aided enumeration of kinematic structures of mechanisms. In the following, we briefly describe the adjacency and incidence matrix representations of kinematic chains.

3.5.1 Adjacency Matrix

The links of a kinematic chain are numbered sequentially from 1 to n . Since in the graph, representation vertices correspond to links and edges correspond to joints, the link-to-link *adjacency matrix*, A , is defined as follows:

$$a_{ij} = \begin{cases} 1 & \text{if link } i \text{ is connected to link } j \text{ by a joint,} \\ 0 & \text{otherwise (including } i = j \text{).} \end{cases} \quad (3.1)$$

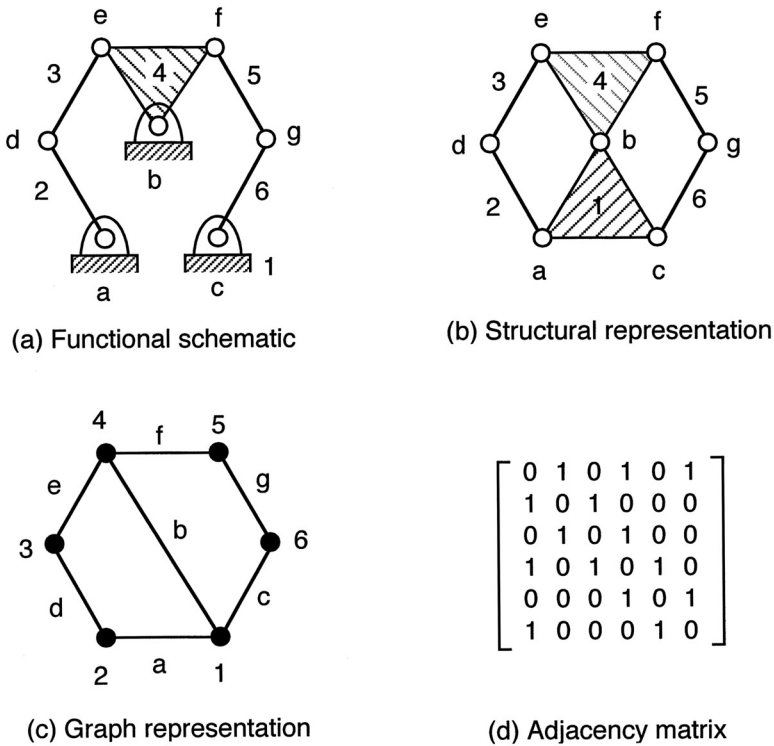
By definition, the adjacency matrix is an $n \times n$ symmetric matrix with zero diagonal elements. The matrix determines the structural topology of a kinematic chain up to structural isomorphism. For example, the link-to-link adjacency matrix of the spur-gear set shown in Figure 3.2 is given by

$$A = \begin{bmatrix} 0 & 1 & 1 & 1 \\ 1 & 0 & 1 & 0 \\ 1 & 1 & 0 & 1 \\ 1 & 0 & 1 & 0 \end{bmatrix}. \quad (3.2)$$

The matrix representation given by Equation (3.2) provides no distinction for the types of joint used in a mechanism. The (2, 3) element in Equation (3.2) simply provides the information that link 2 is connected to link 3 by a joint. It does not give information about the type of joint. To resolve this problem, one additional level of abstraction is needed. We can employ different numerals and/or letters to denote the joint types. For example, we may use the numeral “1” to represent a turning pair and the letter “g” to denote a gear pair. Using this notation, the adjacent matrix of the planetary gear set shown in Figure 3.2 becomes

$$A = \begin{bmatrix} 0 & 1 & 1 & 1 \\ 1 & 0 & g & 0 \\ 1 & g & 0 & g \\ 1 & 0 & g & 0 \end{bmatrix}. \quad (3.3)$$

As a second example, Figure 3.12 shows the functional schematic, kinematic structure, graph, and adjacency matrix representations of a Watt linkage.

**FIGURE 3.12****Watt mechanism and its kinematic representations.**

3.5.2 Incidence Matrix

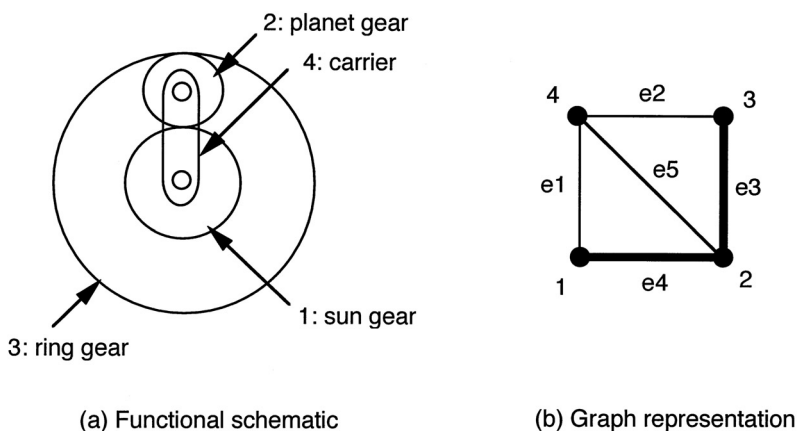
Another useful matrix representation is the *incidence matrix*, B . In addition to labeling the links, the joints are labeled as well. In an incidence matrix each row represents a link, whereas each column denotes a joint as outlined below.

$$B = \begin{matrix} & \text{joint } j \\ \begin{matrix} \text{link } i \\ b_{1,1} & b_{1,2} & \cdots & b_{1,m} \\ b_{2,1} & b_{2,2} & \cdots & b_{2,m} \\ \vdots & \vdots & \vdots & \vdots \\ b_{n,1} & b_{n,2} & \cdots & b_{n,m} \end{matrix} \end{matrix}$$

where

$$b_{ij} = \begin{cases} 1 & \text{if link } i \text{ contains joint } j, \\ 0 & \text{otherwise.} \end{cases} \quad (3.4)$$

The incidence matrix also determines the structural topology of a kinematic chain up to structural isomorphism. Figure 3.13 shows the functional schematic and graph

**FIGURE 3.13**

A planetary gear train and its graph representation.

representation of a planetary gear train with its edges labeled from $e1$ to $e5$. The incidence matrix is given by

$$B = \begin{bmatrix} 1 & 0 & 0 & 1 & 0 \\ 0 & 0 & 1 & 1 & 1 \\ 0 & 1 & 1 & 0 & 0 \\ 1 & 1 & 0 & 0 & 1 \end{bmatrix}. \quad (3.5)$$

3.6 Summary

A kinematic chain is an assemblage of links connected by joints. The study of the nature of connection among various links of a kinematic chain is called the *structural analysis* or *topological analysis*. To facilitate the analysis, several methods of representation of the kinematic structure were described. The study includes the functional schematic representation, structural representation, graph representation, and various matrix representations.

References

- [1] Buchsbaum, F. and Freudenstein, F., 1970, Synthesis of Kinematic Structure of Geared Kinematic Chains and other Mechanisms, *Journal of Mechanisms*, 5, 357–392.
- [2] Chatterjee, G. and Tsai, L.W., 1994, Enumeration of Epicyclic-Type Automatic Transmission Gear Trains, *SAE 1994 Trans., Journal of Passenger Cars*, Sec. 6, 103, 1415–1426.
- [3] Chatterjee, G. and Tsai, L.W., 1996, Computer Aided Sketching of Epicyclic-Type Automatic Transmission Gear Trains, *ASME Journal of Mechanical Design*, 118, 3, 405–411.
- [4] Erdman, A.G. and Bowen, J., 1981, Type and Dimensional Synthesis of Case-ment Window Mechanism, *ASME Mechanical Engineering*, 103, 46–55.
- [5] Fang, W.E. and Freudenstein, F., 1988, The Stratified Representation of Mechanisms, in *Proceedings of the ASME Mechanisms Conference: Trends and Developments in Mechanisms, Machines, and Robotics*, Cambridge, MA, 1, 115–124.
- [6] Freudenstein, F. and Maki, E.R., 1979, Creation of Mechanisms According to Kinematic Structure and Function, *Journal of Environmental and Planning B*, 6, 375–391.
- [7] Freudenstein, F. and Yang, A.T., 1972, Kinematics and Statics of a Coupled Epicyclic Spur-Gear Train, *Mechanisms and Machine Theory*, 7, 263–275.
- [8] Lin, C.C. and Tsai, L.W., 1989, The Development of an Atlas of Bevel-Gear Type Spherical Wrist Mechanisms, in *Proceedings of the First National Conference on Applied Mechanisms and Robotics*, Cincinnati, OH, Paper No. 89-AMR-2A-3.
- [9] Mayourian, M. and Freudenstein, F., 1984, The Development of an Atlas of the Kinematic Structures of Mechanisms, in *Proceedings of the ASME Mechanisms Conference*, Cambridge, MA, Paper No. 84-DET-21.
- [10] Sohn, W., 1987, A Computer-Aided Approach to the Creative Design of Mechanisms, Ph.D. Dissertation, Dept. of Mechanical Engineering, Columbia University, New York, NY.
- [11] Tsai, L.W., 1987, An Application of the Linkage Characteristic Polynomial to the Topological Synthesis of Epicyclic Gear Trains, *ASME Journal of Mechanisms, Transmissions, and Automation in Design*, 109, 3, 329–336.
- [12] Tsai, L.W., 1988, The Kinematics of Spatial Robotic Bevel-Gear Trains, *IEEE Journal of Robotics and Automation*, 4, 2, 150–156.

- [13] Tsai, L.W., Chen, D.Z., and Lin, T.W., 1998, Dynamic Analysis of Geared Robotic Mechanisms Using Graph Theory, *ASME Journal of Mechanical Design*, 120, 2, 240–244.
- [14] Yan, H.S. and Chen, J.J., 1985, Creative Design of a Wheel Damping Mechanism, *Mechanism and Machine Theory*, 20, 6, 597–600.

Exercises

- 3.1 Figure 3.14 shows a Humpage reduction gear train. Sketch the kinematic structure and corresponding graph, and derive the adjacency matrix.

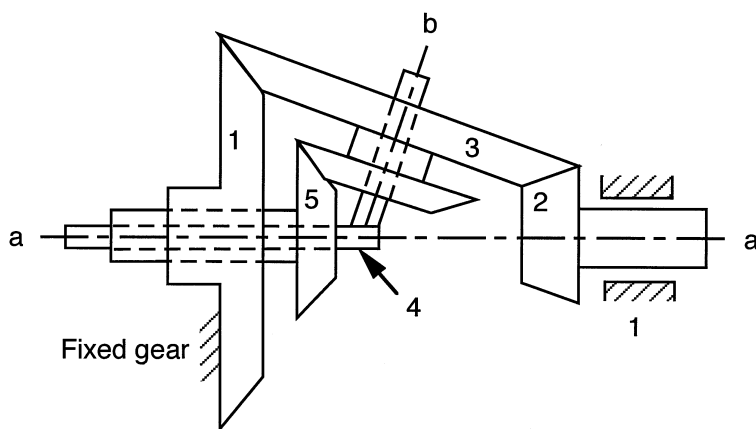


FIGURE 3.14
Humpage reduction gear.

- 3.2 Sketch the kinematic structure and corresponding graph, and derive the adjacency matrix for the wobble-plate mechanism shown in Figure 3.15.
- 3.3 Figure 3.16 shows a z-crank mechanism. Sketch the kinematic structure and corresponding graph, and then derive the incidence matrix.
- 3.4 Sketch the kinematic structure and corresponding graph, and derive the incidence matrix for the mechanism shown in Figure 3.17.
- 3.5 Figure 3.18 shows a $3RPS$ parallel manipulator. Sketch the kinematic structure and corresponding graph, and derive the adjacency matrix.
- 3.6 Sketch the kinematic structure and the corresponding graph, and derive the adjacency matrix for the spur gear train shown in Figure 3.19.

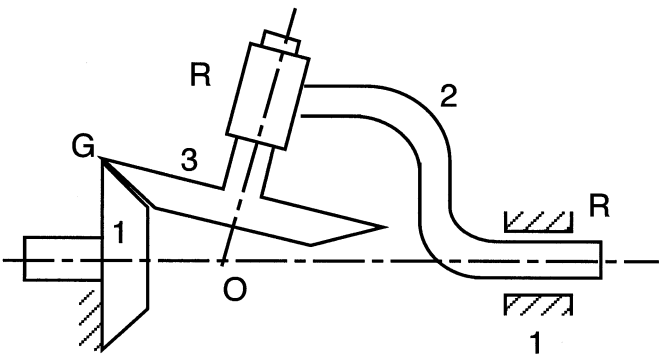


FIGURE 3.15
Wobble-plate mechanism.

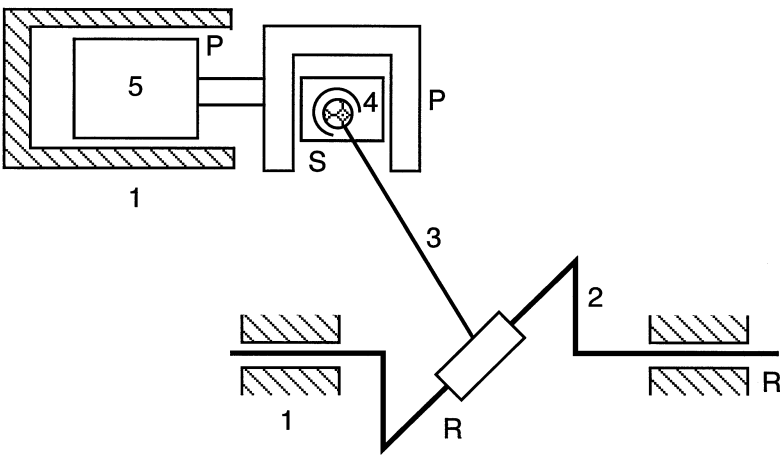


FIGURE 3.16
Z-crank mechanism.

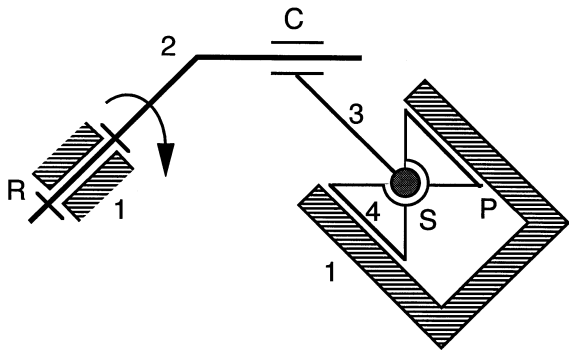


FIGURE 3.17
Spatial RCSP mechanism.

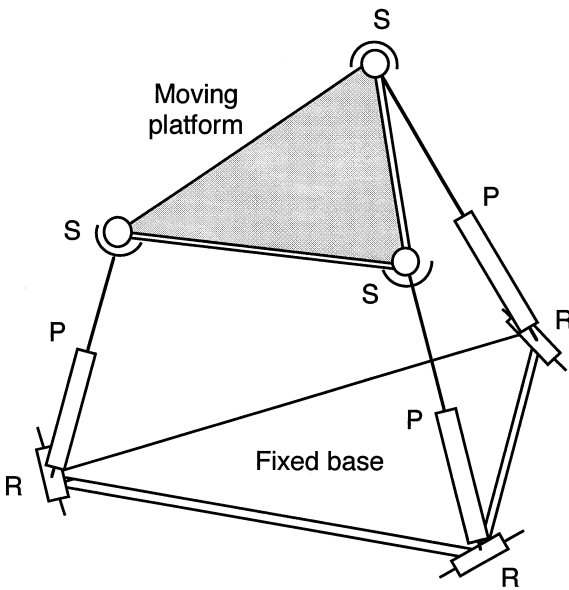


FIGURE 3.18
A 3 RPS parallel manipulator.

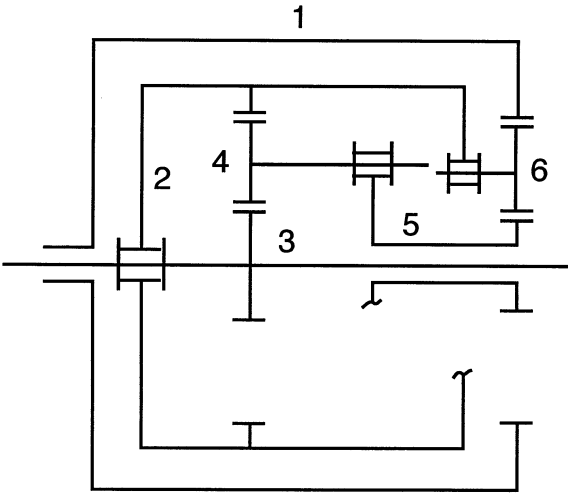


FIGURE 3.19
Six-link spur gear train.

Chapter 4

Structural Analysis of Mechanisms

4.1 Introduction

Structural analysis is the study of the nature of connection among the members of a mechanism and its mobility. It is concerned primarily with the fundamental relationships among the degrees of freedom, the number of links, the number of joints, and the type of joints used in a mechanism. It should be noted that structural analysis only deals with the general functional characteristics of a mechanism and not with the physical dimensions of the links. A thorough understanding of the structural characteristics is very helpful for enumeration of mechanisms.

In this text, graph theory will be used as an aid in the study of the kinematic structure of mechanisms. Except for a few special cases, we limit ourselves to those mechanisms whose corresponding graphs are planar. Although there are a few mechanisms whose corresponding graphs are not planar, these mechanisms usually contain a large number of links. In addition, we also limit ourselves to graphs that contain no articulation points or bridges. A graph with an articulation point or a bridge represents a mechanism that is made up of two mechanisms connected in series with a common link but no common joint, or with a common joint but no common link. These types of mechanisms can be treated as two separate mechanisms and, therefore, are excluded from the study.

A thorough understanding of the structural topology can be helpful in several ways. First of all, mechanisms can be classified into families of similar structural characteristics. Various families of mechanisms can be quickly evaluated during the conceptual design phase. Secondly, a systematic methodology can be developed for enumeration of mechanisms according to certain prescribed structural characteristics.

4.2 Correspondence Between Mechanisms and Graphs

Since the topological structure of a kinematic chain can be represented by a graph, many useful characteristics of graphs can be translated into the corresponding char-

acteristics of a kinematic chain. Table 4.1 describes the correspondence between the elements of a kinematic chain and that of a graph. Table 4.2 summarizes some corresponding characteristics between kinematic chains and graphs.

Table 4.1 Correspondence Between Mechanisms and Graphs.

Graph	Symbol	Mechanism	Symbol
Number of vertices	v	Number of links	n
Number of edges	e	Number of joints	j
Number of vertices of degree i	v_i	Number of links having i joints	n_i
Degree of vertex i	d_i	Number of joints on link i	d_i
Number of independent loops	L	Number of independent loops	L
Total number of loops ($L + 1$)	\tilde{L}	Total number of loops ($L + 1$)	\tilde{L}
Number of loops with i edges	L_i	Number of loops with i joints	L_i

Table 4.2 Structural Characteristics of Mechanisms and Graphs.

Graphs	Mechanisms
$L = e - v + 1$	$L = j - n + 1$
$e - v + 2 \geq d_i \geq 2$	$j - n + 2 \geq d_i \geq 2$
$\sum_i d_i = 2e$	$\sum_i d_i = 2j$
$\sum_i v_i = v$	$\sum_i n_i = n$
$\sum_i i v_i = 2e$	$\sum_i i n_i = 2j$
$v_2 \geq 3v - 2e$	$n_2 \geq 3n - 2j$
$\sum_i L_i = \tilde{L} = L + 1$	$\sum_i L_i = \tilde{L} = L + 1$
$\sum_i i L_i = 2e$	$\sum_i i L_i = 2j$
Isomorphic graphs	Isomorphic mechanisms

4.3 Degrees of Freedom

The *degrees of freedom* of a mechanism is perhaps the first concern in the study of kinematics and dynamics of mechanisms. The degrees of freedom of a mechanism refers to the number of independent parameters required to completely specify the configuration of the mechanism in space. Except for some special cases, it is possible to derive a general expression for the degrees of freedom of a mechanism in terms of the number of links, number of joints, and types of joints incorporated in the mechanism. The following parameters are defined to facilitate the derivation of the degrees of freedom equation.

c_i : degrees of constraint on relative motion imposed by joint i .

F : degrees of freedom of a mechanism.

f_i : degrees of relative motion permitted by joint i .

j : number of joints in a mechanism, assuming that all joints are binary.

j_i : number of joints with i dof; namely, j_1 denotes the number of 1-dof joints, j_2 denotes the number of 2-dof joints, and so on.

L : number of independent loops in a mechanism.

n : number of links in a mechanism, including the fixed link.

λ : degrees of freedom of the space in which a mechanism is intended to function. It is assumed that a single value of λ applies to the motion of all the links of a mechanism. For spatial mechanisms, $\lambda = 6$, and for planar and spherical mechanisms, $\lambda = 3$. We call λ the *motion parameter*.

Intuitively, the degrees of freedom of a mechanism is equal to the degrees of freedom of all the moving links diminished by the degrees of constraint imposed by the joints. If all the links are free from constraint, the degrees of freedom of an n -link mechanism with one link fixed to the ground would be equal to $\lambda(n - 1)$. Since the total number of constraints imposed by the joints are given by $\sum_i c_i$, the net degrees of freedom of a mechanism is

$$F = \lambda(n - 1) - \sum_{i=1}^j c_i . \quad (4.1)$$

The constraints imposed by a joint and the degrees of freedom permitted by the joint are related by

$$c_i = \lambda - f_i . \quad (4.2)$$

Substituting Equation (4.2) into Equation (4.1) yields

$$F = \lambda(n - j - 1) + \sum_{i=1}^j f_i . \quad (4.3)$$

Equation (4.3) is known as the *Grübler* or *Kutzbach* criterion [12]. In reality, the criterion was established much earlier by Ball [4] and probably others. However, unlike earlier researchers, Grübler and Kutzbach developed the equation specifically for mechanisms.

The *Grübler* criterion is valid provided that the constraints imposed by the joints are independent of one another and do not introduce redundant degrees of freedom. A redundant degree of freedom is one that does not have any effect on the transfer of motion from the input to the output link of a mechanism. For example, a binary

link with two end spherical joints possesses a redundant degree of freedom as shown in Figure 4.1. We call this type of freedom a *passive degree of freedom*, because it permits the binary link to rotate freely about a line passing through the centers of the two joints with no torque transferring capability about that line.

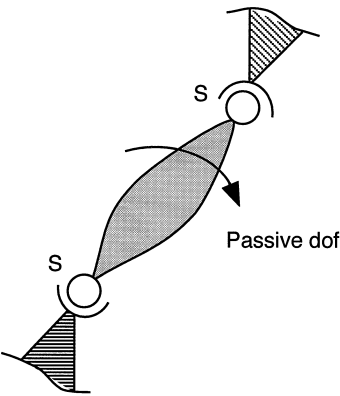


FIGURE 4.1
An S – S binary link.

In general, a binary link with either $S - S$, $S - E$, or $E - E$ pairs as its end joints possesses one passive degree of freedom as outlined in Table 4.3. In addition, a sequence of binary links with $S - S$, $S - E$, or $E - E$ pairs as their terminal joints also possess a passive degree of freedom.

Table 4.3 Binary Links with Passive Degrees of Freedom.

End Joints	Passive Degree of Freedom
$S - S$	Rotation about an axis passing through the centers of the two ball joints.
$S - E$	Rotation about an axis passing through the center of the ball and perpendicular to plane of the plane pair.
$E - E$	Sliding along an axis parallel to the line of intersection of the planes of the two E pairs. If the two planes are parallel, three passive dof exist.

Passive degrees of freedom cannot be used to transmit motion or torque about an axis. When such joint pairs exist, one degree of freedom should be subtracted from the degrees of freedom equation. We exclude the $E - E$ combination as being impractical, because a link (or links) with an $E - E$ pair can slide freely along an axis parallel to the line of intersection of the two E planes. Let f_p be the number of passive degrees of freedom in a mechanism, then Equation (4.3) can be modified as

$$F = \lambda(n - j - 1) + \sum_{i=1}^j f_i - f_p . \tag{4.4}$$

In general, if the Grübler criterion yields $F > 0$, the mechanism has F degrees of freedom. If the criterion yields $F = 0$, the mechanism becomes a structure with zero degrees of freedom. On the other hand, if the criterion yields $F < 0$, the mechanism becomes an overconstrained structure. It should be noted, however, that there are mechanisms that do not obey the degrees of freedom equation. These *overconstrained mechanisms* require special link length proportions to achieve mobility. The Bennett [5] mechanism is a well-known overconstrained spatial $4R$ linkage. It contains four links connected in a loop by four revolute joints. The opposite links have equal link lengths and twist angles, and are related to that of the adjacent link by a special condition. According to Equation (4.3), the degrees of freedom of the Bennett mechanism should be equal to -2 . In reality, the mechanism does possess one degree of freedom. Other well-known overconstrained mechanisms include the Goldberg [10] five-bar and Bricard six-bar linkages. Recently, Mavroidis and Roth [13] developed an excellent methodology for the analysis and synthesis of overconstrained mechanisms. Many previously known and new overconstrained mechanisms can be found in that work. This text is not concerned with overconstrained mechanisms.

Example 4.1 Planar Three-Link Chain

For the planar three-link, $3R$ kinematic chain shown in Figure 4.2, we have $n = 3$ and $j = j_1 = 3$. Equation (4.3) yields $F = 3(3 - 3 - 1) + 3 = 0$. Hence, a planar three-link chain connected by revolute joints is a structure. Three-link structures can be found in many civil engineering applications. \square

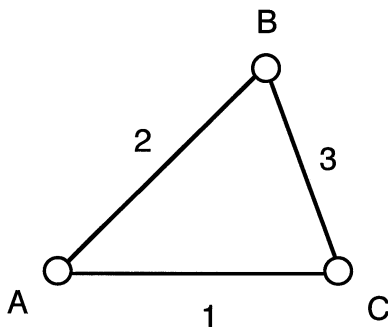


FIGURE 4.2
Three-bar structure.

Example 4.2 Planar Four-Bar Linkage

For the planar four-bar, $4R$ linkage shown in Figure 1.8, we have $n = 4$ and $j = j_1 = 4$. Equation (4.3) yields $F = 3(4 - 4 - 1) + 4 = 1$. Hence, the planar four-bar linkage is a one-dof mechanism. \square

Example 4.3 Planar Five-Bar Linkage

For the planar five-bar, $5R$ linkage shown in Figure 4.3, we have $n = 5$ and $j = j_1 = 5$. Equation (4.3) gives $F = 3(5 - 5 - 1) + 5 = 2$. Hence, the planar five-bar linkage is a two-dof mechanism. \square

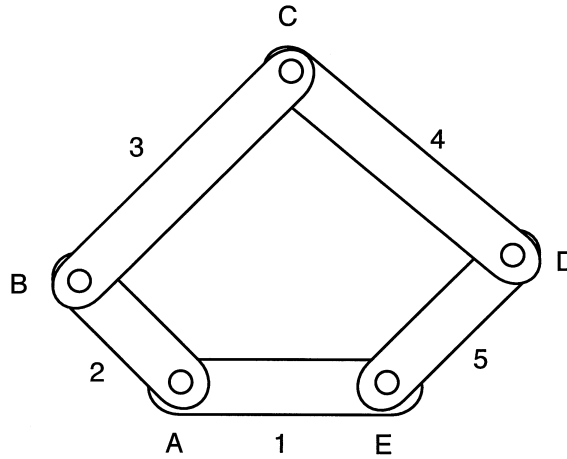


FIGURE 4.3
Five-bar linkage.

Example 4.4 Spur-Gear Drive

For the spur-gear set shown in Figure 1.10, we have $n = 3$ and $j_1 = 2$, $j_2 = 1$. Equation (4.3) gives $F = 3(3 - 3 - 1) + 4 = 1$. Therefore, the spur-gear drive is a one-dof mechanism. \square

Example 4.5 Spatial RCSP Mechanism

For the spatial RCSP mechanism shown in Figure 3.17, we have $n = 4$, $j_1 = 2$, $j_2 = 1$, and $j_3 = 1$. Equation (4.3) yields $F = 6(4 - 4 - 1) + 2 \times 1 + 1 \times 2 + 1 \times 3 = 1$. Hence, the RCSP linkage is a one-dof mechanism. \square

Example 4.6 Swash-Plate Mechanism

For the swash-plate mechanism shown in Figure 1.12, we have $n = 4$, $j_1 = 2$, $j_2 = 0$, $j_3 = 2$, $j = j_1 + j_3 = 4$, and $f_p = 1$. Equation (4.4) gives $F = 6(4 - 4 - 1) + 2 \times 1 + 2 \times 3 - 1 = 1$.

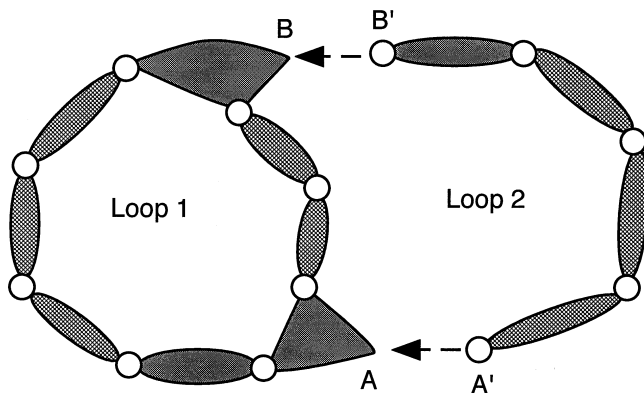
Both the RCSP and swash-plate mechanisms can be designed as a compressor or engine mechanism. \square

4.4 Loop Mobility Criterion

In the previous section, we derive an equation that relates the degrees of freedom of a mechanism to the number of links, number of joints, and type of joints. It is also possible to establish an equation that relates the number of independent loops to the number of links and number of joints in a kinematic chain.

The four-bar linkage shown in Figure 1.8 is a single-loop kinematic chain having four links connected by four joints. The five-bar linkage shown in Figure 4.3 is also a single-loop kinematic chain. It is made up of five links connected by five joints. We observe that for a single-loop kinematic chain (planar, spherical, or spatial), the number of joints is equal to the number of links ($n = j$), and the links are all binary.

We now extend a single-loop chain to a two-loop chain. This can be accomplished by taking an open-loop chain and joining its two ends to members of a single-loop chain by two joints as shown in Figure 4.4. We observe that by extending from a



Note that A and B are two attachment points.

FIGURE 4.4

Formation of a multiloop chain.

one- to two-loop chain, the number of joints added is more than the number of links by one. Similarly, an open-loop chain can be added to a two-loop chain to form a three-loop chain, and so on. By induction, extending a kinematic chain from 1 to L loops, the difference between the number of joints and number of links is increased by $L - 1$. Therefore,

$$L = j - n + 1. \quad (4.5)$$

Or, in terms of the total number of loops, we have

$$\tilde{L} = j - n + 2. \quad (4.6)$$

Equation (4.5) is known as *Euler's equation*. Combining Equation (4.5) with Equation (4.3) yields

$$\sum_{i=1}^j f_i = F + \lambda L . \quad (4.7)$$

Equation (4.7) is known as the *loop mobility criterion*. The loop mobility criterion is useful for determining the number of joint degrees of freedom needed for a kinematic chain to possess a given number of degrees of freedom.

Example 4.7 Four-Bar Linkage

For the planar four-bar linkage shown in Figure 1.8, we have $n = 4$, $j = 4$. Equation (4.5) yields $L = 1$. For $F = 1$, Equation (4.7) yields $\sum f_i = 1 + 3 \times 1 = 4$. Hence, the total number of joint degrees of freedom should be equal to four to achieve a one-dof mechanism. \square

Example 4.8 Humpage Gear Reducer

The Humpage gear reduction unit shown in Figure 3.14 is a five-bar spherical mechanism, in which links 1, 2, and 5 are three coaxial bevel gears, link 3 is a compound planet gear, and link 4 is the carrier. In this mechanism, link 1 is fixed to the ground, link 5 is the input link, and link 2 serves as the output link. The compound planet gear 3 meshes with gears 1, 2, and 5. Overall, the mechanism has four revolute joints and three gear pairs. With $\lambda = 3$, $n = 5$, $j_1 = 4$, $j_2 = 3$, and $F = 1$, Equation (4.5) yields $L = 3$ and Equation (4.7) yields $\sum f_i = 10$. \square

4.5 Lower and Upper Bounds on the Number of Joints on a Link

Since we are interested primarily in nonfractionated closed-loop chains, every link should be connected to at least two other links. Let d_i denote the number of joints on link i . The lower bound on d_i is

$$d_i \geq 2 . \quad (4.8)$$

The upper bound on d_i can be established from graph theory. Using the fact that the number of loops of which a vertex is a part is equal to its degree, and the maximum degree of a vertex is equal to the total number of loops, we have

$$\tilde{L} \geq d_i , \quad (4.9)$$

where $\tilde{L} = L + 1$. Combining Equations (4.8) and (4.9) yields

$$\tilde{L} \geq d_i \geq 2. \quad (4.10)$$

In other words, the minimum number of joints on each link of a closed-loop chain is 2 and the maximum number is limited by the total number of loops.

Example 4.9 Stephenson Six-Bar Linkage

Figure 4.5 shows the kinematic structure and graph representation of the Stephenson six-bar linkage. The number of joints on the links are: $d_1 = d_3 = d_4 = d_6 = 2$, and $d_2 = d_5 = 3$. Since there are six links and seven joints, the number of independent loops is given by $L = j - n + 1 = 7 - 6 + 1 = 2$. Hence, the number of joints on any link is bounded by $3 \geq d_i \geq 2$. \square

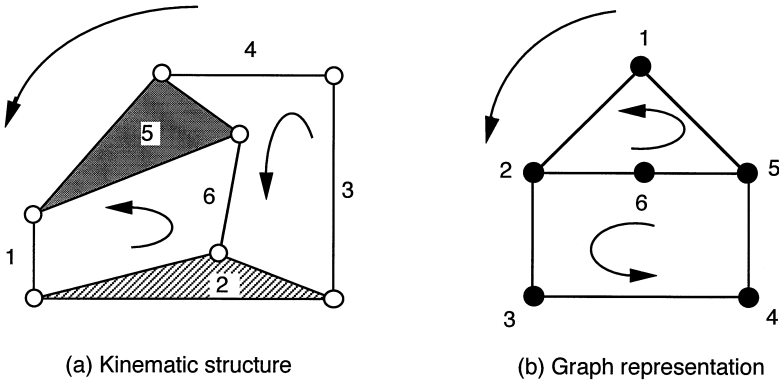


FIGURE 4.5
Stephenson six-bar linkage.

Since each joint connects two links, we have

$$\sum_{i=1}^n d_i = d_1 + d_2 + \cdots + d_n = 2j. \quad (4.11)$$

Equation (4.11) is equivalent to Equation (2.4) derived in Chapter 2. Given the number of joints, Equation (2.4) can be solved for various vertex-degree listings. The solution can be regarded as the number of combinations with repeats permitted of n things taken $2j$ at a time, subject to the constraint imposed by Equation (4.10) [11]. Since $\sum_i d_i$ over vertices of even degree and $2j$ are both even numbers, we conclude that the number of links in a mechanism with an odd number of joints is an even number.

4.6 Link Assortments

Links in a mechanism can be grouped according to the number of joints on them. A link is called a *binary*, *ternary*, or *quaternary* link depending on whether it has two, three, or four joints. Figure 4.6 shows the graph and kinematic structural representations of the above three links.



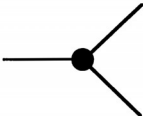
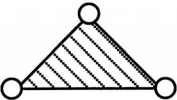
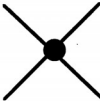
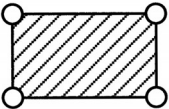
Graph	Kinematic Structure	Comments
		Binary link
		Ternary link
		Quaternary link

FIGURE 4.6
Binary, ternary, and quaternary links.

Let n_i denote the number of links with i joints, that is, n_2 denotes the number of binary links, n_3 the number of ternary links, n_4 the number of quaternary links, and so on. Clearly,

$$n_2 + n_3 + n_4 + \cdots + n_r = n \; , \tag{4.12}$$

where $r = \tilde{L}$ denotes the largest number of joints on a link.

Since each of the n_i links contains i joints and each joint connects exactly two links, the following equation holds.

$$2n_2 + 3n_3 + 4n_4 + \cdots + rn_r = 2j \; . \tag{4.13}$$

Equations (4.12) and (4.13) are equivalent to Equations (2.8) and (2.9) derived in Chapter 2.

Multiplying Equation (4.12) by 3 and subtracting Equation (4.13), we obtain

$$n_2 = 3n - 2j + (n_4 + 2n_5 + \cdots) \; . \tag{4.14}$$

Therefore, the lower bound on the number of binary links is

$$n_2 \geq 3n - 2j. \quad (4.15)$$

Given the number of links and the number of joints, Equations (4.12) and (4.13) can be solved for all possible combinations of n_2, n_3, \dots, n_r . All solutions, however, must be nonnegative integers. The number of solutions can be treated as the number of partitions of the integer $2j$ into parts $2, 3, \dots, r$ with repetition permitted. This is a well-known problem in combinatorial analysis. The solutions can be found by using a *nested-do loops* computer algorithm to vary the values of n_i . See Appendix A for a description of the method. In the following, we study a heuristic algorithm developed by Crossley [8].

1. Given the number of links and the number of joints, find the upper and lower bounds on the number of joints on a link by Equation (4.10), and the minimal number of binary links by Equation (4.15).
2. Find a particular solution to Equations (4.12) and (4.13). This can be done by equating all but two variables, say n_2 and n_3 , to zero and solving the resulting equations for these two variables. This produces one solution called a *link assortment*.
3. For the link assortment obtained in the preceding step, apply *Crossley's operator*, $(1, -2, 1)$ or its negative, wherever possible, to any three consecutive numbers of n_i s. Crossley's operator effectively adds one link with $i - 1$ joints, subtracts two links with i joints, and then adds another link with $i + 1$ joints. The operation does not affect the identities of Equations (4.12) and (4.13). Furthermore, a double application of the operator to any four consecutive n_i s with an offset is equivalent to the application of a $(1, -1, -1, 1)$ operator which, therefore, can be used alternatively.
4. Repeat Step 3 as many times as needed until all the possible assortments are found.

For the purpose of classification, each link assortment is called a *family*. Each family is identified by a *vertex degree listing*. The vertex degree listing is defined as a list of integers representing the number of vertices of the same degree in ascending order. Specifically, in the vertex degree listing, the first digit represents the number of binary links, the second the number of ternary links, the third the number of quaternary links, and so on. For example, a kinematic chain with $n_2 = 4, n_3 = 1, n_4 = 3$, and $n_5 = 2$ (or in terms of a graph there are 4 vertices of degree two, 1 vertex of degree three, 3 vertices of degree four, and 2 vertices of degree five) has a vertex degree listing of "4132."

Example 4.10 Link Assortments of (8, 10) Kinematic Chains

We wish to find all possible link assortments for planar kinematic chains with $n = 8$ and $j = 10$. Applying Equation (4.6), the upper bound on the number of joints on a

link is 4. From Equation (4.15), the lower bound on the number of binary links is 4. Hence, with $n = 8$ and $j = 10$, Equations (4.12) and (4.13) reduce to

$$n_2 + n_3 + n_4 = 8, \quad (4.16)$$

$$2n_2 + 3n_3 + 4n_4 = 20. \quad (4.17)$$

A particular solution to Equations (4.16) and (4.17) is found to be $n_2 = 4$, $n_3 = 4$, and $n_4 = 0$. Applying Crossley's operator, we obtain the following three families of link assortments:

Family	n_2	n_3	n_4
4400	4	4	0
5210	5	2	1
6020	6	0	2

The 4400 family is made up of 4 binary and 4 ternary links; the 5210 family consists of 5 binary, 2 ternary, and 1 quaternary links; and the 6020 family is composed of 6 binary and 2 quaternary links.

The above solutions can also be treated as a problem of solving a system of 2 linear equations in 3 unknowns, subject to the constraints that n_2 , n_3 , and n_4 must be nonnegative integers and that $n_2 \geq 4$. Subtracting $2 \times$ Equation (4.16) from Equation (4.17), we obtain

$$n_3 + 2n_4 = 4. \quad (4.18)$$

Equation (4.18) contains two unknowns. Since both $2n_4$ and 4 are even numbers, n_3 must be an even number. Let n_3 assume the values of 0, 2, and 4, one at a time, then $n_4 = 2$, 1, and 0, respectively. Once n_3 and n_4 are known, we solve Equation (4.16) for n_2 . This leads to the same results. \square

4.7 Partition of Binary Link Chains

Binary links in a mechanism may be connected in series to form a *binary link chain*. The first and last links of a binary link chain are necessarily connected to nonbinary links. We define the length of a binary link chain by the number of binary links in that chain. Furthermore, we consider the special case for which two nonbinary links are connected directly to each other as a binary link chain of zero length. Binary link chains of length 0, 1, 2, and 3 are called the *E*, *Z*, *D*, and *V* chains, respectively, as depicted in Figure 4.7.

Let b_k denote the number of binary link chains of length k , and q denote the maximal length of a binary link chain in a kinematic chain. Applying Equations (2.39)


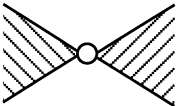
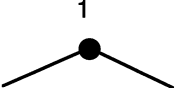
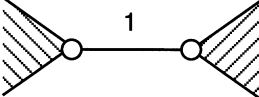
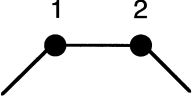
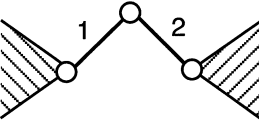
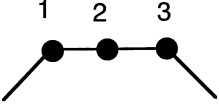
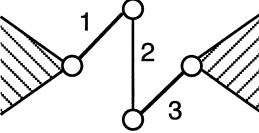
Graph	Kinematic Structure	Comments
		E-chain
		Z-chain
		D-chain
		V-chain

FIGURE 4.7
Various binary link chains.

and (2.40), we obtain

$$b_1 + 2b_2 + 3b_3 + \cdots + qb_q = n_2, \quad (4.19)$$

$$b_0 + b_1 + b_2 + b_3 + \cdots + b_q = j - n_2. \quad (4.20)$$

The length of a binary link chain is limited by the fact that the degrees of freedom associated with a binary link chain must be less than that of the mechanism as a whole. A binary link chain of length k contains k binary links and $k + 1$ joints. If the links and joints of a binary link chain were independently movable with F -dof relative to the rest of the mechanism, Equation (4.7) would lead to

$$\sum_{i=1}^{k+1} f_i = F + \lambda,$$

where $\sum_{i=1}^{k+1} f_i$ denotes the total joint degrees of freedom associated with a binary link chain of length k . It follows that the remaining links and joints of the mechanism

would be overconstrained. Therefore, to avoid such degenerate cases, we impose the condition

$$\sum_{i=1}^{k+1} f_i \leq F + \lambda - 1 . \quad (4.21)$$

The maximum number of joints occurs when all the joints in a binary link chain are one-dof joints. It follows from Equation (4.21) that the length of a binary link chain is limited by

$$q \leq F + \lambda - 2 . \quad (4.22)$$

For each family of link assortment, we can solve Equations (4.19) and (4.20) for various combinations of binary link chains. Since Equation (4.20) contains one more variable than that of Equation (4.19), we can solve Equation (4.19) for b_k for $k = 1, 2, \dots, q$, and then Equation (4.20) for b_0 . The solution to Equation (4.19) can be regarded as the number of partitions of the integer n_2 into parts $1, 2, \dots, q$ with repetition allowed. We can employ a *nested-do loops* computer algorithm to vary the value of each b_k to search for all feasible solutions. We call each solution set of b_k a *branch*. Thus a family of binary link assortment may produce several branches.

Example 4.11 Partition of Binary Links for the (8, 10) Kinematic Chains

We wish to identify all possible partitions of the binary links associated with the (8, 10) planar kinematic chains derived in the preceding section. Assuming $F = 1$, Equation (4.22) gives

$$q \leq 2$$

as the upper bound on the length of a binary link chain.

4400 family: The 4400 family contains 4 binary links. Hence, Equations (4.19) and (4.20) reduce to

$$b_1 + 2b_2 = 4 , \quad (4.23)$$

$$b_0 + b_1 + b_2 = 6 . \quad (4.24)$$

Solving Equation (4.23) for nonnegative integers of b_1 and b_2 , and then Equation (4.24) for b_0 yields

Branch	b_0	b_1	b_2
1	4	0	2
2	3	2	1
3	2	4	0

Hence, there are three branches of binary link chains. The first branch consists of no binary link chains of length 1 and two binary link chains of length 2; the second

consists of two binary link chains of length 1 and one of length 2; and the third consists of four binary link chains of length 1 and none of length 2.

5210 family: The 5210 family contains 5 binary links. Hence, Equations (4.19) and (4.20) reduce to

$$b_1 + 2b_2 = 5, \quad (4.25)$$

$$b_0 + b_1 + b_2 = 5. \quad (4.26)$$

Solving Equation (4.25) for nonnegative integers of b_1 and b_2 , and then Equation (4.26) for b_0 produces

Branch	b_0	b_1	b_2
1	2	1	2
2	1	3	1
3	0	5	0

Therefore, there are three branches of binary link chains. The first branch consists of one binary link chain of length 1 and two binary link chains of length 2; the second consists of three binary link chains of length 1 and one of length 2; and the third consists of five binary link chains of length 1 and none of length 2.

6020 family: The 6020 family contains 6 binary links. Hence, Equations (4.19) and (4.20) reduce to

$$b_1 + 2b_2 = 6, \quad (4.27)$$

$$b_0 + b_1 + b_2 = 4. \quad (4.28)$$

Solving Equation (4.27) for nonnegative integers of b_1 and b_2 , and then Equation (4.28) for b_0 yields

Branch	b_0	b_1	b_2
1	1	0	3
2	0	2	2

The first branch consists of no binary link chains of length 1 and three binary link chains of length 2. The second branch consists of two binary link chains of length 1 and two of length 2. \square

4.8 Structural Isomorphism

Two kinematic chains or mechanisms are said to be *isomorphic* if they share the same topological structure. In terms of graphs, there exists a one-to-one correspondence between their vertices and edges that preserve the incidence. Mathematically,

structural isomorphisms can be identified by their adjacency or incidence matrices. However, the form of an adjacency matrix is dependent on the labeling of links in a kinematic chain.

For example, the graph shown in Figure 3.13 is obtained from a relabeling of the vertices of the graph shown in Figure 3.10. As a result, the adjacency matrix becomes

$$A^* = \begin{bmatrix} 0 & g & 0 & 1 \\ g & 0 & g & 1 \\ 0 & g & 0 & 1 \\ 1 & 1 & 1 & 0 \end{bmatrix}. \quad (4.29)$$

Although the graphs shown in Figures 3.10 and 3.13 represent the same gear train, their adjacency matrices do not assume the same form. The difference comes from the labeling of the links. In fact, the two adjacency matrices, Equations (3.3) and (4.29), are related by a permutation of the rows and the corresponding columns.

Let S be a column matrix whose elements represent the labeling of the links of a kinematic chain and S^* be another column matrix whose elements correspond to a relabeling of the links of the same kinematic chain. Then there exists a permutation matrix, P , such that

$$S^* = PS. \quad (4.30)$$

In this regard, A^* is related to A by a congruence transformation,

$$A^* = P^T A P, \quad (4.31)$$

where P^T denotes the transpose of P . Theoretically, the permutation matrix P can be derived by reordering the columns of an identity matrix. It has a positive or negative unit determinant and the transpose is equal to its inverse [17].

For example, if the column matrix for the graphs shown in Figure 3.10 is

$$S = \begin{bmatrix} 1 \\ 2 \\ 3 \\ 4 \end{bmatrix}, \quad (4.32)$$

then the column matrix for the graph shown in Figure 3.13 is

$$S^* = \begin{bmatrix} 4 \\ 1 \\ 2 \\ 3 \end{bmatrix}. \quad (4.33)$$

Therefore, the permutation matrix is given by

$$P = \begin{bmatrix} 0 & 0 & 0 & 1 \\ 1 & 0 & 0 & 0 \\ 0 & 1 & 0 & 0 \\ 0 & 0 & 1 & 0 \end{bmatrix}. \quad (4.34)$$

Obviously, Equations (4.32), (4.33), and (4.34) satisfy Equation (4.30). Substituting Equations (3.3) and (4.34) into Equation (4.31) yields

$$\begin{aligned}
 A^* &= P^T A P = \begin{bmatrix} 0 & 1 & 0 & 0 \\ 0 & 0 & 1 & 0 \\ 0 & 0 & 0 & 1 \\ 1 & 0 & 0 & 0 \end{bmatrix} \begin{bmatrix} 0 & 1 & 1 & 1 \\ 1 & 0 & g & 0 \\ 1 & g & 0 & g \\ 1 & 0 & g & 0 \end{bmatrix} \begin{bmatrix} 0 & 0 & 0 & 1 \\ 1 & 0 & 0 & 0 \\ 0 & 1 & 0 & 0 \\ 0 & 0 & 1 & 0 \end{bmatrix} \\
 &= \begin{bmatrix} 0 & g & 0 & 1 \\ g & 0 & g & 1 \\ 0 & g & 0 & 1 \\ 1 & 1 & 1 & 0 \end{bmatrix}. \tag{4.35}
 \end{aligned}$$

Equations (4.30) and (4.31) constitute the definition of *structural isomorphism*. In other words, two kinematic structures are said to be isomorphic if there exists a one-to-one correspondence between the links of the two kinematic chains, Equation (4.30), and when the links are consistently renumbered, the adjacency matrices of the two kinematic chains become identical, Equation (4.31).

4.9 Permutation Group and Group of Automorphisms

We observe that the adjacency matrix of a kinematic chain depends on the labeling of the links. An alternate labeling of the links is equivalent to a permutation of n elements or objects. In this section, we introduce the concept of a *permutation group* from which a group of automorphisms of a graph will be described. Automorphic graphs are useful for elimination of isomorphic graphs at the outset.

Consider a set of elements: a, b, c, d, e , and f . These elements may represent the vertices or edges of a graph, or the links or joints of a kinematic chain. Let these elements be arranged in a reference sequence, say (a, b, c, d, e, f) . We call an alternate sequence (b, c, a, d, f, e) a permutation of (a, b, c, d, e, f) , in which $a \rightarrow b$ (element a is mapped into b), $b \rightarrow c$, $c \rightarrow a$, $d \rightarrow d$, $e \rightarrow f$, and $f \rightarrow e$. The reference sequence, (a, b, c, d, e, f) , is called the *identity permutation*.

In a permutation, some elements may map into other elements, whereas others may map into themselves. A mapping of the type $a \rightarrow b \rightarrow c \rightarrow a$, denoted by (abc) , is said to form a *cycle*. We define the *length* of a cycle by the number of elements in that cycle. In particular, a cycle of length 1 maps an element into itself; that is, (d) means that $d \rightarrow d$.

A permutation is said to be represented in cycles if each element occurs exactly once and the mapping of the elements is represented by the cycles. For example, the mapping of (a, b, c, d, e, f) into (b, c, a, d, f, e) has a cyclic representation of $(abc)(d)(ef)$, where the lengths of the 3 cycles are 3, 1, and 2, respectively. In particular, the identity permutation is denoted by $(a)(b)(c)(d)(e)(f)$.

4.9.1 Group

A set of n elements, a_1, a_2, \dots, a_n , is said to form a *group* under a given *group operation*, denoted by the multiplication symbol $a_i \cdot a_j$, if the following axioms are satisfied [7]:

1. *Closure*: If a_i and a_j are two elements of the group, then $a_i \cdot a_j$ is also an element of the group.
2. *Associativity*: For all elements of the group,

$$(a_i \cdot a_j) \cdot a_k = a_i \cdot (a_j \cdot a_k) .$$

In this regard, $(a_i \cdot a_j) \cdot a_k$ is denoted unambiguously by $a_i \cdot a_j \cdot a_k$.

3. *Existence of an identity element*: There exists an element, a_{id} , such that

$$a_{id} \cdot a_j = a_j \cdot a_{id} = a_j$$

for all elements of the group.

4. *Existence of inverses*: For each element, a_j , there exists an *inverse element*, a_j^{-1} , such that

$$a_j \cdot a_j^{-1} = a_{id} .$$

We note that the group operation is not necessarily commutative; that is $a_j \cdot a_k \neq a_k \cdot a_j$.

A *permutation group* is a group whose elements are permutations. The *group operation* for a permutation group is defined as follows. Let permutation a_j map element x_p into x_q , whereas permutation a_k maps element x_q into x_r . Then the product $a_j \cdot a_k$ maps x_p into x_r .

Example 4.12 Symmetric Group of Three Elements

Let three elements, denoted by the integers 1, 2, and 3, be ordered in a reference sequence (1, 2, 3). We show that the following six permutations form a group:

Element	Permutation	Cyclic Representation
a_1	(1, 2, 3) \rightarrow (1, 2, 3)	(1)(2)(3)
a_2	(1, 2, 3) \rightarrow (1, 3, 2)	(1)(23)
a_3	(1, 2, 3) \rightarrow (2, 1, 3)	(12)(3)
a_4	(1, 2, 3) \rightarrow (2, 3, 1)	(123)
a_5	(1, 2, 3) \rightarrow (3, 1, 2)	(132)
a_6	(1, 2, 3) \rightarrow (3, 2, 1)	(13)(2)

Following the definition of group operation, we can construct a multiplication table:

	a_1	a_2	a_3	a_4	a_5	a_6
a_1	a_1	a_2	a_3	a_4	a_5	a_6
a_2	a_2	a_1	a_5	a_6	a_3	a_4
a_3	a_3	a_4	a_1	a_2	a_6	a_5
a_4	a_4	a_3	a_6	a_5	a_1	a_2
a_5	a_5	a_6	a_2	a_1	a_4	a_3
a_6	a_6	a_5	a_4	a_3	a_2	a_1

We conclude that every product is an element of the group; the associative law holds; a_1 is the identity element; a_4 and a_5 are mutually the inverse of each other; and every other element is its own inverse. \square

4.9.2 Group of Automorphisms

We consider a graph as *labeled* when its vertices are labeled by the integers $1, 2, \dots, n$. In this regard, a labeled graph is mapped into another labeled graph when the n integers are permuted. For some permutations, a labeled graph may map into itself. The set of those permutations which map the graph into itself form a group called a *group of automorphisms*. This group of automorphisms is said to be a *vertex-induced* group [9].

Similarly, the edges of a graph may be labeled. We call the group of permutations that maps the graph into itself an *edge-induced* group of automorphisms.

Example 4.13 Stephenson Chain

Consider the Stephenson chain shown in Figure 4.8a, where the six links are labeled from 1 to 6. The corresponding graph is shown in Figure 4.8b. Let this labeling of the graph be the identity permutation, $a_1 = (1)(2)(3)(4)(5)(6)$. Figures 4.8c through e show three permutations of the labeling that can be denoted as $a_2 = (1)(2)(3)(4)(56)$, $a_3 = (14)(23)(5)(6)$, and $a_4 = (14)(23)(56)$, respectively. In the following we show that the above four labeled graphs form a group of automorphisms.

Following the definition of group operation, we can construct a multiplication table:

	a_1	a_2	a_3	a_4
a_1	a_1	a_2	a_3	a_4
a_2	a_2	a_1	a_4	a_3
a_3	a_3	a_4	a_1	a_2
a_4	a_4	a_3	a_2	a_1

We conclude that every product is an element of the group; the associative law holds; a_1 is the identity element; and every element is its own inverse. Therefore, a_1, a_2, a_3 , and a_4 form a group of automorphisms. \square

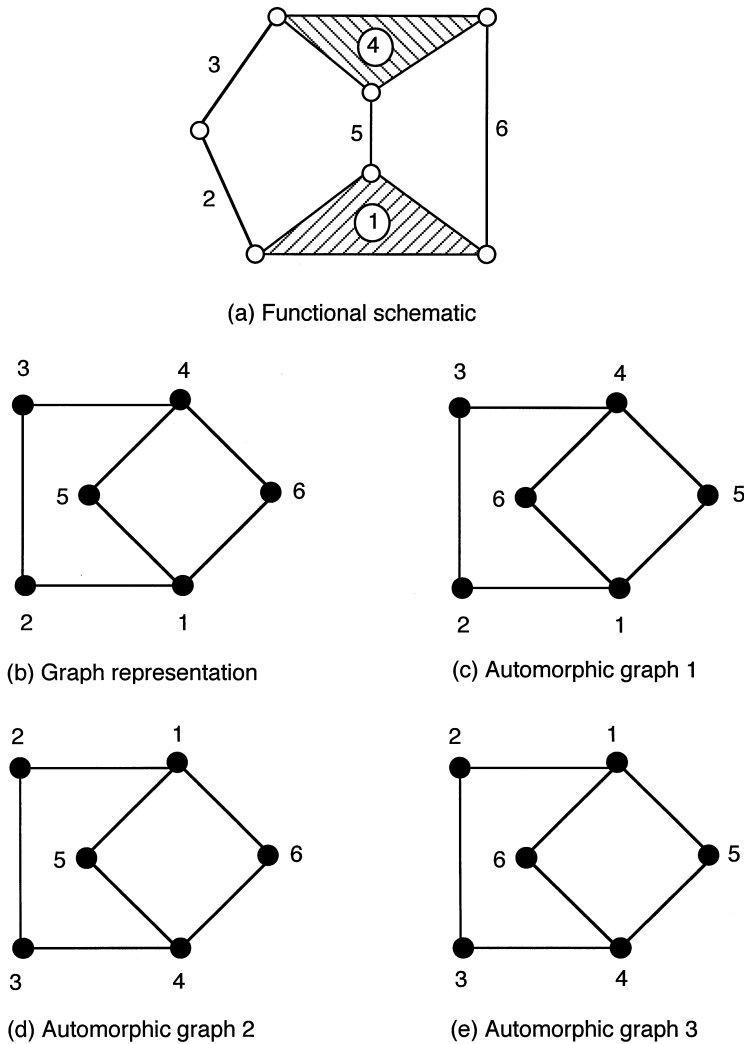


FIGURE 4.8
Stephenson chain, its graph representation, and automorphic graphs.

Two vertices of a graph are said to be *similar* if they are contained in the same cycle of a permutation of a vertex-induced group of automorphisms. In the above example, vertices 1 and 4 are similar. Vertices 5 and 6, and 2 and 3 are also similar. Similar vertices have the same vertex degrees and their adjacent vertices also have the same vertex degrees. In other words, similar vertices possess the same attributes. Automorphic graphs are by definition isomorphic. Analogously, two edges of a graph

are said to be *similar* if they are contained in the same cycle of a permutation of an edge-induced group of automorphisms.

4.10 Identification of Structural Isomorphism

An important step in structure synthesis of kinematic chains or mechanisms is the identification of isomorphic structures. Undetected isomorphic structures lead to duplicate solutions, while falsely identified isomorphisms reduce the number of feasible solutions for new designs. Several methods of identification have been proposed. Some are based on visual approaches while others are based on heuristic approaches. Each method has its own advantages and disadvantages. An ideal algorithm, however, should satisfy the following conditions [15]:

1. *Uniqueness.* There exists a one-to-one correspondence between the kinematic chain and its mathematical representation so that structural isomorphism can be uniquely identified.
2. *Efficiency.* The algorithm for identification of isomorphic mechanisms should be simple and computationally efficient. This is essential for automated identification of structural isomorphisms.
3. *Decodability.* The mathematical representation can be transformed into a unique kinematic chain. This makes it possible for a large number of graphs or mechanisms to be stored in a computer for use by designers.

Both the adjacency and incidence matrices determine the topological structure of a mechanism up to structural isomorphism. They satisfy the uniqueness and decodability conditions. However, they are computationally inefficient. For this reason, other methods of identification have been proposed. The following provides brief descriptions of several of them.

4.10.1 Identification by Classification

Kinematic chains (or graphs) can be classified into families according to the number of links, number of joints, various link assortments, etc. Obviously, kinematic chains of different families cannot be isomorphic with one another. This fact has been used for classification and identification of the topological structures of kinematic chains.

For example, Buchsbaum and Freudenstein [6] classified the graphs of epicyclic gear trains according to their (1) number of vertices, (2) number of edges, and (3) *vertex degree listing*. Yan and Hwang [20, 21] expanded the above classification method to include other attributes such as joint assortments, and so on.

Kinematic chains can also be classified by their corresponding contracted graphs. Obviously, two kinematic chains that belong to two different contracted graphs cannot

be isomorphic. For example, Figure 4.9 shows two (11, 14) graphs. Both graphs contain 11 vertices and 14 edges. In addition, they share the same vertex degree listing of 6410. Hence, up to this level of classification, it appears that they might be isomorphic. However, the contracted graph of the graph shown in Figure 4.9a belongs to the 58-2 graph shown in Table B.1, whereas the one shown in Figure 4.9b belongs to the 58-3 graph. Therefore, they are not isomorphic.

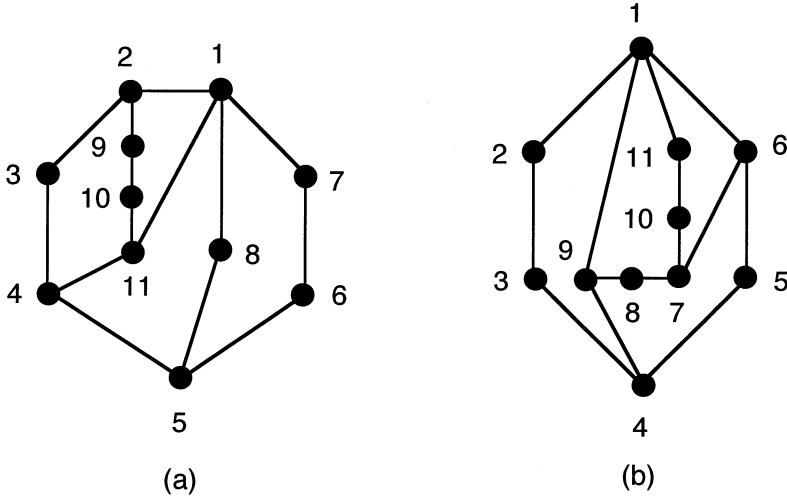


FIGURE 4.9
Two (11, 14) graphs.

4.10.2 Identification by Characteristic Polynomial

In the preceding section, we have shown that the problem of testing structural isomorphism is equivalent to one of determining a permutation matrix P that transforms the A into A^* for the two kinematic chains in question. For an n -link kinematic chain, there are $n!$ possible ways of labeling the links and, therefore, $n!$ possible permutation matrices. Therefore, it is impractical to identify the permutation matrix by trial-and-error. Fortunately, there exists a convenient method for the determination of such a permutation matrix.

A well-known theorem of matrix algebra states that the congruence relation given by Equation (4.31) can exist only if the characteristic polynomials of the two adjacency matrices, A and A^* , are equal to each other; that is,

$$|xI - A| = |xI - A^*| \quad (4.36)$$

holds for all x , where x is a dummy variable and I is an identity matrix of the same order as A . We conclude that

THEOREM 4.1

The adjacency matrices of two isomorphic kinematic chains possess the same characteristic polynomial.

For example, the linkage characteristic polynomial for the graph shown in Figure 3.10 is

$$p(x) = \begin{vmatrix} x & -1 & -1 & -1 \\ -1 & x & -g & 0 \\ -1 & -g & x & -g \\ -1 & 0 & -g & x \end{vmatrix} = x^4 - (3 + 2g^2)x^2 - 4gx, \quad (4.37)$$

and the linkage characteristic polynomial for the graph shown in Figure 3.13 is

$$p^*(x) = \begin{vmatrix} x & -g & 0 & -1 \\ -g & x & -g & -1 \\ 0 & -g & x & -1 \\ -1 & -1 & -1 & x \end{vmatrix} = x^4 - (3 + 2g^2)x^2 - 4gx. \quad (4.38)$$

Since $p(x) = p^*(x)$, the two graphs are most likely isomorphic.

It should be noted that the above theorem is a necessary, but not a sufficient condition for two kinematic chains to be isomorphic. Although this condition is not completely discriminatory, it can successfully distinguish bar linkages with up to eight links. As the number of links increases, however, the probability of failing to detect structural isomorphism increases. Counter examples have been found where two nonisomorphic kinematic chains share the same characteristic polynomial [14].

For example, Figure 4.10 shows two (10, 13) nonisomorphic graphs sharing the characteristic polynomial:

$$p(x) = x^{10} - 13x^8 + 53x^6 - 8x^5 - 82x^4 + 26x^3 + 39x^2 - 16x. \quad (4.39)$$

Similarly, Figure 4.11 shows two (11, 14) nonisomorphic graphs sharing the characteristic polynomial:

$$p(x) = x^{11} - 14x^9 + 65x^7 - 130x^5 + 112x^3 + 32x. \quad (4.40)$$

This method of identification requires the derivation of characteristic polynomials. Uicker and Raicu [17] presented a computer method for derivation of the coefficients numerically. Yan and Hall [18, 19] developed a set of rules for determination of the polynomials by inspection. Tsai [16] suggested the use of the random number technique to improve the computational efficiency. Obviously, we can always use a commercial software such as *Mathematica* or *Matlab* for derivation of characteristic polynomials symbolically.

Because the characteristic polynomial cannot fully identify structural isomorphisms, the method is often augmented by other techniques such as classification of kinematic chains according to their contracted graphs. For example, the graph shown in Figure 4.10a belongs to the 58-2 contracted graph shown in Table B.1, whereas

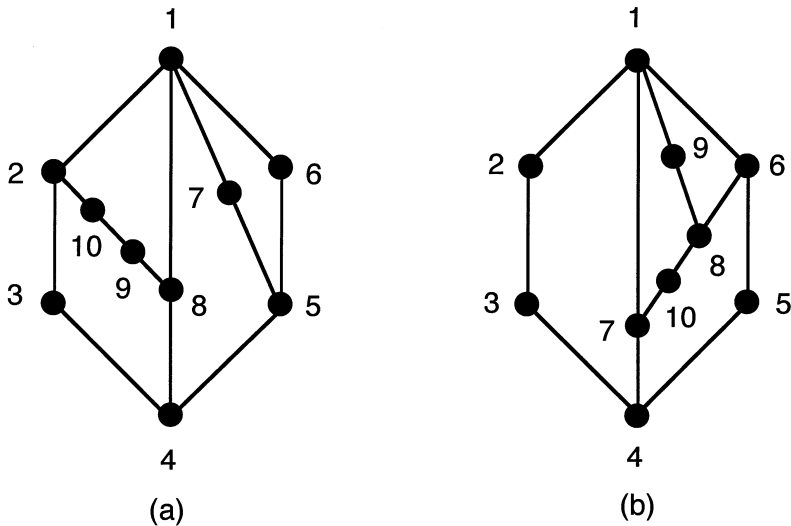


FIGURE 4.10
Two (10, 13) nonisomorphic graphs.

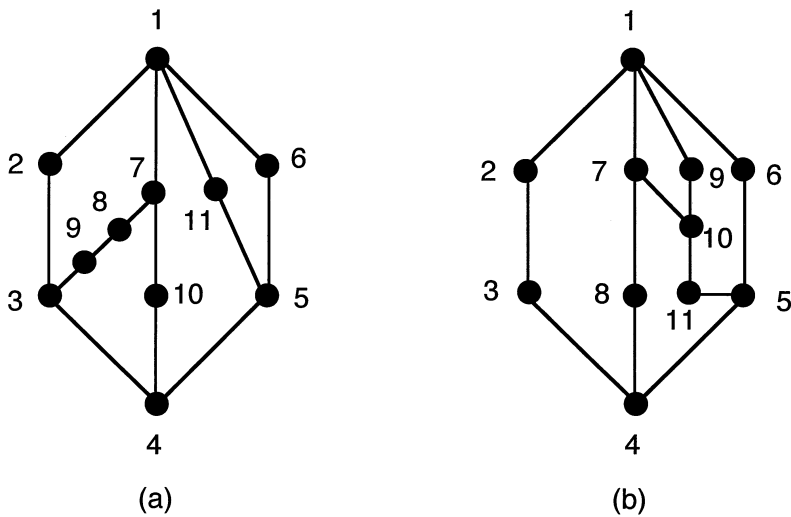


FIGURE 4.11
Two (11, 14) nonisomorphic graphs.

the one shown in Figure 4.10b belongs to the 58-3 contracted graph. Therefore, these two graphs cannot be isomorphic although they share a common characteristic polynomial. Similarly, the graphs shown in Figure 4.11a and b cannot be isomorphic because they belong to two different contracted graphs, 58-2 and 58-3, respectively.

4.10.3 Optimum Code

Despite the extraordinary degree of discrimination, the method of characteristic polynomial encounters difficulties in three respects. (1) The method is not decodable. (2) It is not a sufficient condition for identification of structural isomorphism. (3) The computational efficiency is poor. To overcome these difficulties, Ambekar and Agrawal [1, 2, 3] suggested a method of identification called the *optimum code*. In contrast to the characteristic polynomial method, the optimum code guarantees the decodability and positive identification of structural isomorphism. The method involves a technique for labeling the links of a kinematic chain such that a binary string obtained by concatenating the upper triangular elements of the adjacency matrix row by row, excluding the diagonal elements, is maximized. This is called the *MAX code*.

To illustrate the concept, let us consider the six-link Stephenson chain shown in Figure 4.8a. The corresponding labeled graph is shown in Figure 4.8b. Let the labeling of the vertices shown in Figure 4.8b be denoted by an identity permutation $a_1 = (1)(2)(3)(4)(5)(6)$. Then the adjacency matrix is given by

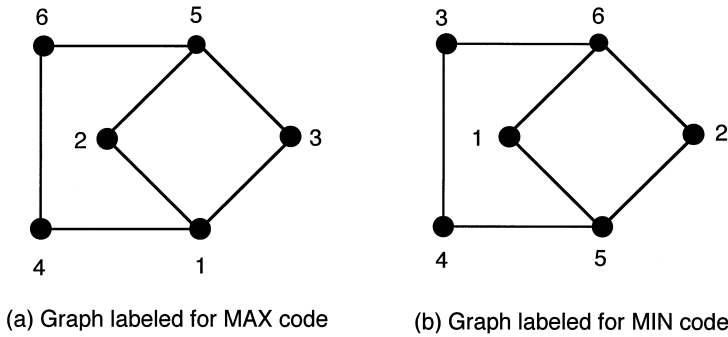
$$A_1 = \begin{bmatrix} 0 & 1 & 0 & 0 & 1 & 1 \\ 1 & 0 & 1 & 0 & 0 & 0 \\ 0 & 1 & 0 & 1 & 0 & 0 \\ 0 & 0 & 1 & 0 & 1 & 1 \\ 1 & 0 & 0 & 1 & 0 & 0 \\ 1 & 0 & 0 & 1 & 0 & 0 \end{bmatrix}. \quad (4.41)$$

Excluding the diagonal elements, there are 15 binary elements in the upper triangular adjacency matrix, namely 10011, 1000, 100, 11, and 0. Writing these elements in sequence we obtain a binary string of 100111000100110, which can be converted into a decimal number as follows.

$$100111000100110_2 = 2^{14} + 2^{11} + 2^{10} + 2^9 + 2^5 + 2^2 + 2^1 = 20006.$$

Figure 4.12a shows a different labeling of the vertices that corresponds to the permutation $a_2 = (1)(245)(36)$. For this labeling, the adjacency matrix becomes

$$A_2 = \begin{bmatrix} 0 & 1 & 1 & 1 & 0 & 0 \\ 1 & 0 & 0 & 0 & 1 & 0 \\ 1 & 0 & 0 & 0 & 1 & 0 \\ 1 & 0 & 0 & 0 & 0 & 1 \\ 0 & 1 & 1 & 0 & 0 & 1 \\ 0 & 0 & 0 & 1 & 1 & 0 \end{bmatrix}. \quad (4.42)$$

**FIGURE 4.12**

Stephenson chain labeled for the MAX and MIN codes.

Therefore, the upper triangular elements of A_2 form a binary string of 111000010010011, which is equal to a decimal number of 28819.

It can be shown that, among all possible labelings of the graph, the labeling shown in Figure 4.12a leads to a maximum number. We call the number 28819 the *MAX code* of the Stephenson chain. We note that several labelings of a graph may lead to the same MAX code due to the existence of graph automorphisms.

Alternately, we can also search for a labeling of the Stephenson chain that minimizes the binary string of the upper triangular elements. We call the resulting decimal number the *MIN code*. Intuitively, for the permutation $a_3 = (15)(3)(246)$ shown in Figure 4.12b, we obtain a minimum binary string of 000110011101100, which gives 3308 as the MIN code.

Using the above method, the problem of testing structural isomorphism is converted into a problem of comparing the optimum codes of two kinematic chains in question. For an n -link kinematic chain, the method requires $n!$ permutations to arrive at the optimum code. Clearly, there is a need to develop a more efficient heuristic algorithm for determination of the optimum code [1]. A poorly developed algorithm may lead to a local optimum and, therefore, may reduce the robustness of the method. From the definition of the MAX code, we observe that the first few rows of the upper triangular adjacency matrix constitute the most significant bits of the code. Furthermore, in each row, the closer an element is to the diagonal of the adjacency matrix, the more contribution it makes to the binary code. Therefore, any efficient algorithm should aim at shifting as many 1s to the most significant bits of the binary code as possible. Further, the concept of a group of automorphisms can be employed to further reduce the number of permutations.

4.10.4 Degree Code

In this section we describe a heuristic algorithm called the *degree code* [15]. Recall that the degree of a vertex is defined as the number of edges incident to it. From the kinematics point of view, the degree of a vertex represents the number of joints on a

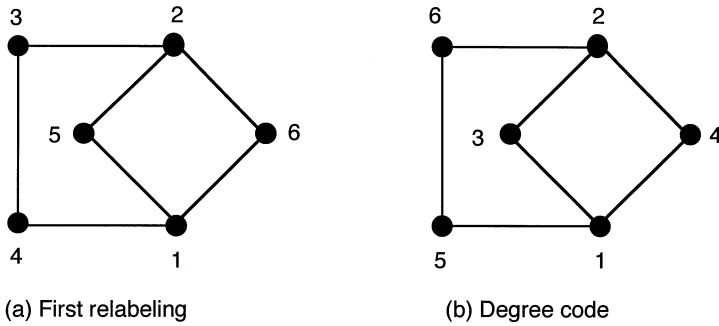
link. Hence, a vertex of degree 2 denotes a binary link, a vertex of degree 3 represents a ternary link, and so on. In the degree code, the vertex degrees are used as a constraint for labeling the links of a kinematic chain. Links of the same degrees are grouped together and the various groups of links are arranged in a descending order according to their vertex degree. While searching for an optimum code, permutation of the links are constrained within each group such that the degrees of all vertices are always kept in a descending order. This method not only preserves the advantages of the optimum code, but also reduces the number of permutations needed for searching the optimum. For example, if the links of an n -link kinematic chain are divided into 3 groups having p , q , and r number of links, respectively, where $n = p + q + r$, the total number of permutations reduces from $n!$ to $p!q!r!$.

The procedure for finding the degree code of a kinematic chain can be summarized as follows:

1. Identify the degree of each vertex in the graph of a kinematic chain and arrange the vertices of the same degree into groups.
2. Renumber the vertices according to the descending order of vertex degrees.
3. Permute the vertices of the same degree to get a new labeling of the graph. Similar vertices, if any, can be arranged in a subgroup to further reduce the number of permutations.
4. For each permutation, calculate the decimal number of the binary string obtained by concatenating, row-by-row, the upper-right triangular elements of the corresponding adjacency matrix.
5. The maximum number obtained from all possible permutations is defined as the degree code.

For example, the degrees of vertices 1 through 6 of the graph shown in Figure 4.8b are 3, 2, 2, 3, 2, and 2, respectively. Since there are two vertices of degree 3 and four vertices of degree 2, the vertices are divided into two groups: (1, 4) and (2, 3, 5, 6). As a first attempt, we relabel the graph as shown in Figure 4.13a where integers 1 and 2 are assigned to the two vertices of degree 3. Under the new labeling, the two groups consist of (1, 2) and (3, 4, 5, 6). We notice that vertices 1 and 2 are similar. Hence, there is no need to permute these two vertices. Similarly, there is no need to permute vertices 5 and 6. Following the above procedure, it can be shown that among all possible permutations, the permutation shown in Figure 4.13b produces a maximum number. The adjacency matrix is

$$A_4 = \begin{bmatrix} 0 & 0 & 1 & 1 & 1 & 0 \\ 0 & 0 & 1 & 1 & 0 & 1 \\ 1 & 1 & 0 & 0 & 0 & 0 \\ 1 & 1 & 0 & 0 & 0 & 0 \\ 1 & 0 & 0 & 0 & 0 & 1 \\ 0 & 1 & 0 & 0 & 1 & 0 \end{bmatrix}. \quad (4.43)$$

**FIGURE 4.13**

Stephenson chain labeled for the degree code.

Therefore, the binary string is 011101101000001, which is equal to a degree code of 15169. We note that the degree code is smaller than the *MAX code*, because permutations of the links for the degree code are confined within each group of vertices of the same degree.

Finally, we note that the degree codes for the graphs shown in Figures 4.10a and b are 28055807549442 and 28055872017416, respectively. Although the two graphs share a common characteristic polynomial, their degree codes are unequivocally different.

4.11 Partially Locked Kinematic Chains

For a multiple loop mechanism, the degrees of freedom associated with any loop can be estimated by Equation (4.3) using the number of links, number of joints, and type of joints making up that loop. The degrees of freedom associated with any loop must be at least equal to one, to ensure that no part of a mechanism is locked. In other words, there must be a sufficient number of links and joints in each loop so that it does not form a rigid structure.

Substituting $F \geq 1$ and $L = 1$ into Equation (4.7) yields

$$\sum_i f_i \geq \lambda + 1. \quad (4.44)$$

Hence, the total joint degrees of freedom in a loop should not be less than four for planar and spherical mechanisms, and seven for spatial mechanisms. For example, no three-link loop is permitted in a planar linkage, since any three-link loop with lower pair joints forms a structure. On the other hand, a three-link loop is permitted in a planar mechanism consisting of a gear or cam pair.

It is also possible for a multiloop chain to form a rigid structure. For example, Figure 4.14b shows a five-bar linkage with zero degrees of freedom. A kinematic

chain containing such a locked chain as its subchain should be discarded from further consideration, since it can always be replaced by an equivalent kinematic chain with fewer numbers of links and joints.

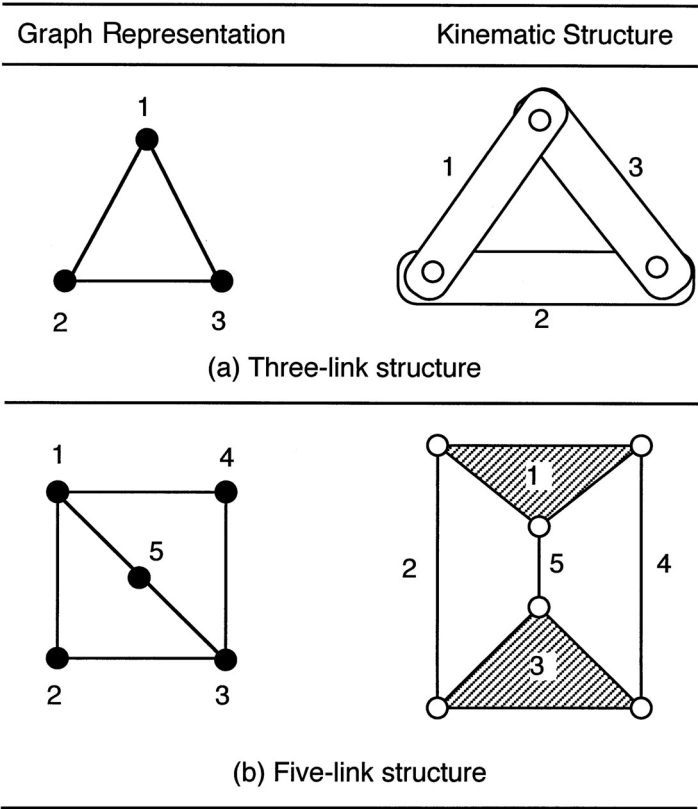


FIGURE 4.14
Two overconstrained kinematic chains.

4.12 Summary

The correspondence between graphs and mechanisms were discussed, from which several important properties of graphs were directly translated into that of mechanisms. The study includes the degrees of freedom equation, loop mobility criterion, upper and lower bounds on the number of joints on a link, link assortments, and the partition of binary links. In addition, the concept of structural isomorphism

was defined. Various methods of identification of structural isomorphism, including the characteristic polynomials, the MAX code, and the degree code, were studied. Finally, the concept of partially locked kinematic chains was introduced. These structural characteristics are extremely useful for the development of computer algorithms for systematic enumeration of mechanisms.

References

- [1] Ambekar, A.G. and Agrawal, V.P., 1986, On Canonical Numbering of Kinematic Chains and Isomorphism Problem: MAX Code, 86-DET-169, in *Proceedings of the ASME Design Engineering Technical Conference*, Columbus, Ohio.
- [2] Ambekar, A.G. and Agrawal, V.P., 1987, Canonical Numbering of Kinematic Chains and Isomorphism Problem: MIN Code, *Mechanisms and Machine Theory*, 22, 5, 453–461.
- [3] Ambekar, A.G. and Agrawal, V.P., 1987, Identification of Kinematic Chains, Mechanisms, Path Generators and Function Generators Using the MIN Code, *Mechanisms and Machine Theory*, 22, 5, 463–471.
- [4] Ball, R.S., 1900, *A Treatise on the Theory of Screws*, Cambridge University Press, Cambridge.
- [5] Bennett, G.T., 1903, A New Mechanism, *Engineering*, 76, 777–778.
- [6] Buchsbaum, F. and Freudenstein, F., 1970, Synthesis of Kinematic Structure of Geared Kinematic Chains and other Mechanisms, *Journal of Mechanisms*, 5, 357–392.
- [7] Cayley, A., 1895, The Theory of Groups, Graphical Representation, in *Mathematical Papers*, Cambridge University Press, Cambridge, 11, 365–367.
- [8] Crossley, F.R.E., 1964, A Contribution to Grübler's Theory in Number Synthesis of Plane Mechanisms, *ASME Journal of Engineering for Industry*, Series B, 86, 1–8.
- [9] Freudenstein, F., 1967, The Basic Concept of Polya's Theory of Enumeration with Application to the Structural Classification of Mechanisms, *Journal of Mechanisms*, 3, 3, 275–290.
- [10] Goldberg, M., 1943, New Five-Bar and Six-Bar Linkages in Three Dimensions, *Trans. of ASME*, 65, 649–661.
- [11] Hall, M., 1986, *Combinatorial Theory*, John Wiley & Sons, New York, NY.

- [12] Kutzbach, K., 1929, Mechanische Leitungsverzweigung, *Maschinenbau, Der Betrieb* 8, 21, 710–716.
- [13] Mavroidis, C. and Roth, B., 1994, Analysis and Synthesis of Over Constrained Mechanisms, *ASME Journal of Mechanical Design*, 117, 1, 69–74.
- [14] Sohn, W. and Freudenstein, F., 1986, An Application of Dual Graphs to the Automatic Generation of the Kinematic Structures of Mechanism, *ASME Journal of Mechanisms, Transmissions, and Automation in Design*, 108, 3, 392–398.
- [15] Tang, C.S. and Liu, T., 1988, The Degree Code-A New Mechanism Identifier, in *Proceedings of the ASME Mechanisms Conference: Trends and Developments in Mechanisms, Machines, and Robotics*, 147–151.
- [16] Tsai, L.W., 1987, An Application of the Linkage Characteristic Polynomial to the Topological Synthesis of Epicyclic Gear Trains, *ASME Journal of Mechanisms, Transmissions, and Automation in Design*, 109, 3, 329–336.
- [17] Uicker, J.J. and Raicu, A., 1975, A Method for the Identification and Recognition of Equivalence of Kinematic Chains, *Mechanisms and Machine Theory*, 10, 375–383.
- [18] Yan, H.S. and Hall, A.S., 1981, Linkage Characteristic Polynomials: Definition, Coefficients by Inspection, *ASME Journal of Mechanical Design*, 103, 578–584.
- [19] Yan, H.S. and Hall, A.S., 1982, Linkage Characteristic Polynomials: Assembly Theorem, Uniqueness, *ASME Journal of Mechanical Design*, 104, 11–20.
- [20] Yan, H.S. and Hwang, W.M., 1983, A Method for Identification of Planar Linkages, *ASME Journal of Mechanisms, Transmissions, and Automation in Design*, 105, 658–662.
- [21] Yan, H.S. and Hwang, W.M., 1984, Linkage Path Code, *Mechanisms and Machine Theory*, 19, 4, 425–529.

Exercises

- 4.1 Find the numbers of degrees of freedom for the mechanism shown in Figure 4.15.
- 4.2 Find the number of degrees of freedom for the mechanism shown in Figure 4.16.
- 4.3 Find the number of degrees of freedom and number of independent loops for the mechanism shown in Figure 3.18.
- 4.4 Find the number of degrees of freedom and number of independent loops for the mechanism shown in Figure 4.17.

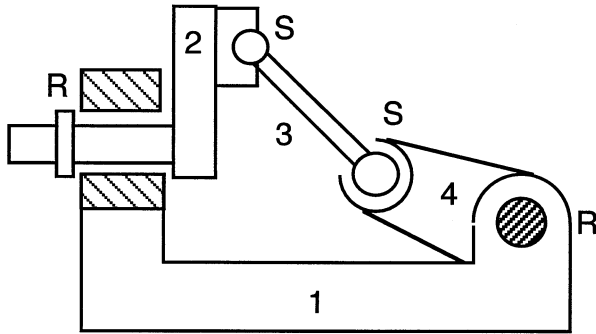


FIGURE 4.15
Spatial *RSSR* linkage.

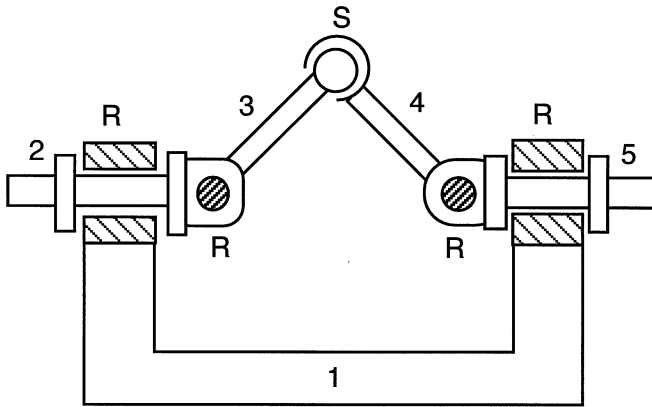


FIGURE 4.16
Spatial five-bar linkage.

- 4.5 Sketch a planar graph with six vertices and ten edges in which the degree of a vertex reaches its maximum.
- 4.6 For planar one-dof linkages with turning pairs, show that the maximum number of ternary links cannot exceed $n - F - 3$.
- 4.7 Show that planar two-dof, seven-link linkages must be made up of two independent loops.
- 4.8 What is the maximum number of joints a link can have in a planar epicyclic gear train?
- 4.9 Do the intermittent motion mechanisms, such as the Geneva mechanism shown in Figure 4.18, have defined degrees of freedom and are they constant, variable, or indeterminate?

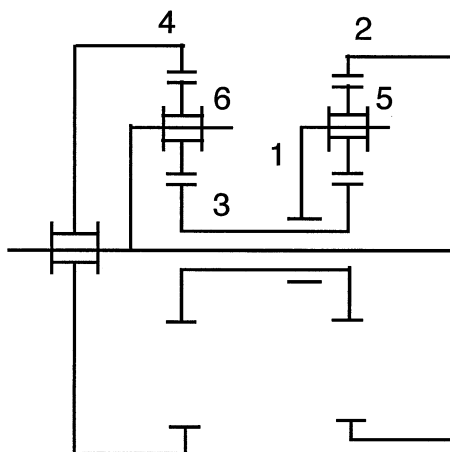


FIGURE 4.17
Six-link epicyclic gear train.

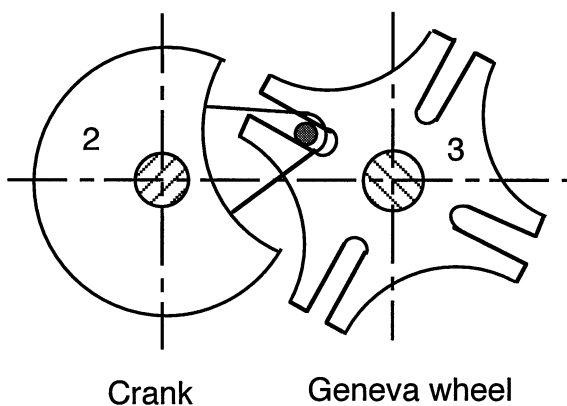


FIGURE 4.18
Geneva mechanism with a pin-in-slot joint.

- 4.10 Single degree-of-freedom gear trains with four links must have three revolute and two gear pairs. Sketch all the possible nonisomorphic graphs and the corresponding mechanisms, if they exist.
- 4.11 Prove that if there exists a planar linkage with n members consisting of n_2 binary links, n_3 ternary links, \dots , n_p polygonal links, and with F degrees of freedom, then there exists another linkage having F degrees of freedom and $n + 2$ members that contain $n_3 + 2$ ternary links, although the number of all other polygonal links remains unchanged.

- 4.12 Prove that any planar F -dof linkage must have at least $F + 3$ binary links.
- 4.13 Prove that the maximum number of ternary links in a planar one-dof linkage cannot exceed $n - 4$.
- 4.14 Find the various link assortments associated with planar, 2-dof, 9-bar linkages. Partition the binary links obtained for each link assortment into as many combinations of binary link chains as possible.
- 4.15 Derive the characteristic polynomials for the two (5, 6) graphs shown in Figure 4.19 using Matlab.

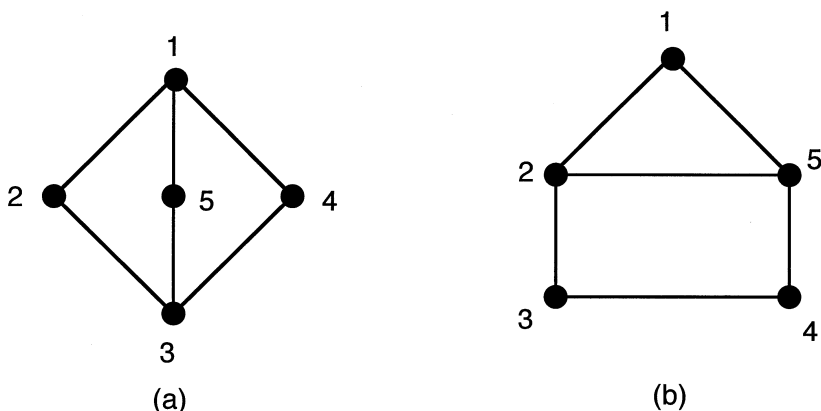


FIGURE 4.19
(5, 6) graph.

- 4.16 Derive the characteristic polynomials for the two graphs shown in Figure 4.9.
- 4.17 Derive the characteristic polynomials and prove that the two linkages shown in Figure 4.20 are isomorphic.
- 4.18 Show that the two linkages shown in Figure 4.21 are isomorphic using the characteristic polynomial method.
- 4.19 Derive the MAX code for the two (5, 6) graphs shown in Figure 4.19.
- 4.20 Show that the two linkages shown in Figure 4.20 are isomorphic using the degree code.
- 4.21 Show that the two linkages shown in Figure 4.21 are isomorphic using the degree code.

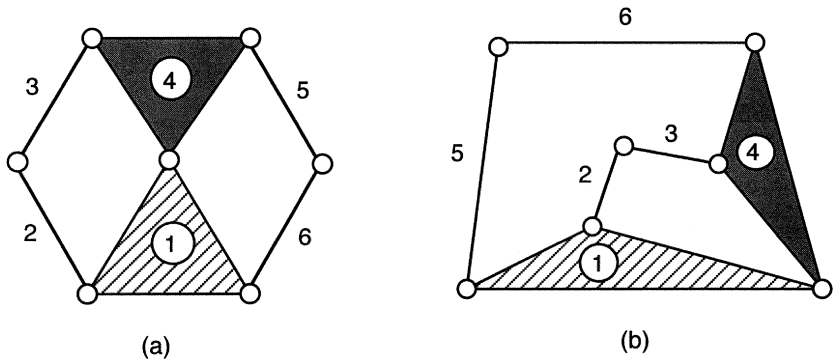


FIGURE 4.20
Watt six-link chains.

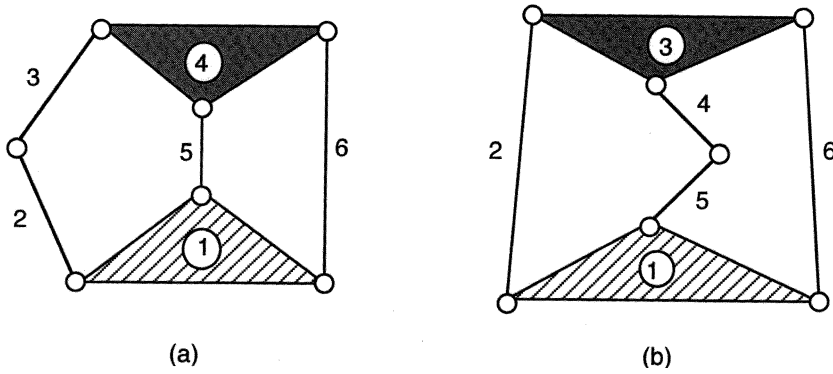


FIGURE 4.21
Stephenson six-link chains.

Chapter 5

Enumeration of Graphs of Kinematic Chains

5.1 Introduction

In Chapter 3 we have shown that the topological structures of kinematic chains can be represented by graphs. Several useful structural characteristics of graphs of kinematic chains were derived. In this chapter we show that graphs of kinematic chains can be enumerated systematically by using graph theory and combinatorial analysis.

There are enormous graphs. Obviously, not all of them are suitable for construction of kinematic chains. Only those graphs that satisfy the structural characteristics described in Chapter 4 along with some other special conditions, if any, are said to be *feasible solutions*. The following guidelines are designed to further reduce the complexity of enumeration:

1. Since we are primarily interested in closed-loop kinematic chains, all graphs should be connected with a minimal vertex degree of 2.
2. All graphs should have no articulation points or bridges. A mechanism that is made up of two kinematic chains connected by a common link but no common joint, or by a common joint but no common link is called a *fractionated mechanism*. Fractionated mechanisms are useful for some applications. However, the analysis and synthesis of such mechanisms can be accomplished easily by considering each nonfractionated submechanism. Therefore, this type of mechanism is excluded from the study.
3. Unless otherwise stated, nonplanar graphs will be excluded. Although this is somewhat arbitrary, in view of the complexity of such mechanisms, it is reasonable to exclude them. It has been shown that for the graph of a planar one-dof linkage to be nonplanar, it must have at least 10 links.

Perhaps, Cayley, Redfield, and Pólya are among the first few pioneers in the development of graphical enumeration theory. Pólya's enumeration theorem provides a powerful tool for counting the number of graphs with a given number of vertices

and edges [7]. A tutorial paper on Pólya's theorem can be found in Freudenstein [6]. Although there is no general theory for enumeration of graphs at this time, various algorithms have been developed [1, 2, 3, 4, 5, 14]. Woo [13] presented an algorithm based on contraction of graphs. Sohn and Freudenstein [10] employed the concept of dual graphs to reduce the complexity of enumeration (See also [9]). Tuttle et al. [11, 12] applied group theory.

In this chapter we introduce several methods for the enumeration of contracted graphs and graphs of kinematic chains.

5.2 Enumeration of Contracted Graphs

In Chapter 2 we have shown that a conventional graph can be transformed into a contracted graph by a process known as *contraction*. In a contracted graph, the number of vertices is equal to that of the conventional graph diminished by the number of binary vertices, $v^c = v - v_2$; the number of edges is also equal to that of the conventional graph diminished by the number of binary vertices, $e^c = e - v_2$; whereas the total number of loops remains unchanged, $L^c = L$. Since there are fewer vertices and edges in a contracted graph, enumeration of conventional graphs can be greatly simplified by enumerating an atlas of contracted graphs followed by an expansion of the graphs. In this section we describe a systematic procedure for enumeration of contracted graphs.

The *adjacency matrix*, A^c , of a contracted graph is a $v^c \times v^c$ symmetric matrix with all the diagonal elements equal to zero and the off-diagonal elements equal to the number of parallel edges connecting the two corresponding vertices. From this definition, we observe that the sum of all elements in each row of A^c is equal to the degree of the vertex. Let $a_{i,j}$ denote the (i, j) element of A^c . It follows that

$$\begin{aligned}
 0 + a_{1,2} + a_{1,3} + \cdots + a_{1,\ell} &= d_1, \\
 a_{2,1} + 0 + a_{2,3} + \cdots + a_{2,\ell} &= d_2, \\
 a_{3,1} + a_{3,2} + 0 + \cdots + a_{3,\ell} &= d_3, \\
 &\vdots \\
 a_{\ell,1} + a_{\ell,2} + \cdots + a_{\ell,\ell-1} + 0 &= d_\ell,
 \end{aligned} \tag{5.1}$$

where $\ell = v^c$ denotes the number of vertices in a contracted graph and d_i represents the degree of vertex i . Since the adjacency matrix is symmetric, $a_{i,j} = a_{j,i}$. To eliminate articulation points, every vertex must be connected to at least two other vertices. Hence, there must be at least two nonzero elements in each equation above. Hence,

$$d_i - 1 \geq a_{i,j} \geq 0. \tag{5.2}$$

For a contracted graph, Equation (4.11) can be written as

$$d_1 + d_2 + \cdots + d_\ell = 2e^c . \quad (5.3)$$

Since there are no binary vertices, Equation (4.10) reduces to

$$\tilde{L} \geq d_i \geq 3 . \quad (5.4)$$

Given v^c and e^c , the adjacency matrix of a contracted graph can be derived by solving Equations (5.1) and (5.3) subject to the constraints imposed by Equations (5.2) and (5.4).

First, we solve Equation (5.3) for the d_i s. Without loss of generality, we assume that $d_1 \leq d_2 \leq \cdots \leq d_\ell$. The solution to Equation (5.3) can be regarded as the number of partitions of $2e^c$ objects into ℓ places with repetition allowed. The solutions can be obtained by the *nested-do loops* computer program outlined in Appendix A.

For each set of d_i , $i = 1, 2, \dots, \ell$, we solve Equation (5.1) for $a_{i,j}$. Due to symmetry and the zero diagonal elements of the matrix, there are only $\ell(\ell - 1)/2$ unknowns. It is obvious that for $\ell = 2$, the contracted graph is obtained by connecting all the edges from one vertex to the other. For $\ell = 3$, Equation (5.1) leads to 3 linear equations in 3 unknowns. Hence, a unique solution of A^c is obtained. It turns out that, for $\ell \geq 4$, the system of equations in Equation (5.1) can be solved one at a time by the following procedure.

- S1. For $i = 1$, we solve the first equation of Equation (5.1) for $a_{1,j}$ for $j = 2, 3, \dots, \ell$ using the *nested-do loops* computer program described in Appendix A. Increment i from $i = 1$ to $i = 2$.
- S2. Substitute $a_{j,i} = a_{i,j}$, for $j = 1, 2, \dots, i - 1$, obtained from the previous step into the i th equation and solve the resulting equation for $a_{i,j}$ for $j = i + 1, i + 2, \dots, \ell$.
- S3. Repeat step 2 for $i = 3, 4, \dots$ until $i = \ell - 3$.
- S4. Substitute all the known $a_{i,j}$ into the last three equations of Equation (5.1) and solve for the remaining three unknowns. The value of each $a_{i,j}$ must be a nonnegative integer. Otherwise, it is not feasible.
- S5. Check for graph isomorphisms.
- S6. Repeat S1 to S5 until all the solution sets of d_i are executed.

In the following, we illustrate the procedure by a few examples.

Example 5.1 Enumeration of (2, 4) Contracted Graphs

We wish to enumerate all feasible contracted graphs with 2 vertices and 4 edges. For $v^c = 2$ and $e^c = 4$, $\tilde{L} = e^c - v^c + 2 = 4$. Equation (5.3) reduces to

$$d_1 + d_2 = 8 ,$$

where $4 \geq d_i \geq 3$. There is only one feasible solution: $d_1 = d_2 = 4$. Since there are only 2 vertices, all edges emanating from 1 vertex must terminate at the other. The resulting contracted graph is shown in Figure 5.1. \square

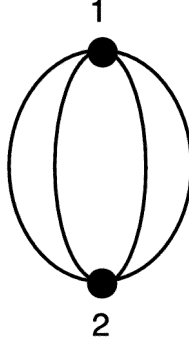


FIGURE 5.1
A (2, 4) contracted graph.

Example 5.2 Enumeration of (3, 5) Contracted Graphs

We wish to enumerate all feasible contracted graphs having 3 vertices and 5 edges. For $v^c = 3$ and $e^c = 5$, $\tilde{L} = e^c - v^c + 2 = 4$. Equation (5.3) reduces to

$$d_1 + d_2 + d_3 = 10 ,$$

where $4 \geq d_i \geq 3$. Solving the above equation by the procedure outlined in Appendix A yields $d_1 = d_2 = 3$ and $d_3 = 4$ as the only solution.

Substituting $d_1 = d_2 = 3$ and $d_3 = 4$ into Equation (5.1) results in a system of 3 equations in 3 unknowns:

$$\begin{aligned} a_{1,2} + a_{1,3} &= 3 , \\ a_{1,2} + a_{2,3} &= 3 , \\ a_{1,3} + a_{2,3} &= 4 , \end{aligned} \tag{5.5}$$

where $2 \geq a_{i,j} \geq 0$. Solving Equation (5.5) yields $a_{1,2} = 1$ and $a_{1,3} = a_{2,3} = 2$. Hence, the adjacency matrix of the contracted graph is

$$A^c = \begin{bmatrix} 0 & 1 & 2 \\ 1 & 0 & 2 \\ 2 & 2 & 0 \end{bmatrix} .$$

The corresponding graph is shown in Figure 5.2. \square

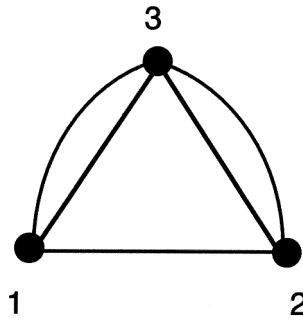


FIGURE 5.2
A (3, 5) contracted graph.

Example 5.3 Enumeration of (4, 6) Contracted Graphs

We wish to enumerate all feasible contracted graphs with 4 vertices and 6 edges. For $v^c = 4$ and $e^c = 6$, $\tilde{L} = e^c - v^c + 2 = 4$. Hence, Equation (5.3) reduces to

$$d_1 + d_2 + d_3 + d_4 = 12, \quad (5.6)$$

where $4 \geq d_i \geq 3$. Solving Equation (5.6) by the procedure outlined in Appendix A yields $d_1 = d_2 = d_3 = d_4 = 3$ as the only solution.

Substituting $d_1 = d_2 = d_3 = d_4 = 3$ into Equation (5.1) leads to a system of 4 equations in 6 unknowns:

$$a_{1,2} + a_{1,3} + a_{1,4} = 3, \quad (5.7)$$

$$a_{1,2} + a_{2,3} + a_{2,4} = 3, \quad (5.8)$$

$$a_{1,3} + a_{2,3} + a_{3,4} = 3, \quad (5.9)$$

$$a_{1,4} + a_{2,4} + a_{3,4} = 3, \quad (5.10)$$

where $2 \geq a_{i,j} \geq 0$. Equation (5.7) contains 3 unknowns: $a_{1,2}$, $a_{1,3}$, and $a_{1,4}$. At this point, no distinction can be made among the 4 vertices. Without loss of generality, we assume that $a_{1,2} \leq a_{1,3} \leq a_{1,4}$. Note that solutions obtained in any other order will simply lead to isomorphic graphs. Solving Equation (5.7) for $a_{1,2}$, $a_{1,3}$, and $a_{1,4}$ yields the following two solutions:

Solution	$a_{1,2}$	$a_{1,3}$	$a_{1,4}$
1	0	1	2
2	1	1	1

Solution 1: Substituting $a_{1,2} = 0$, $a_{1,3} = 1$, and $a_{1,4} = 2$ into Equations (5.8),

(5.9), and (5.10) yields

$$a_{2,3} + a_{2,4} = 3, \quad (5.11)$$

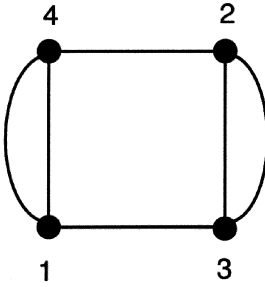
$$a_{2,3} + a_{3,4} = 2, \quad (5.12)$$

$$a_{2,4} + a_{3,4} = 1. \quad (5.13)$$

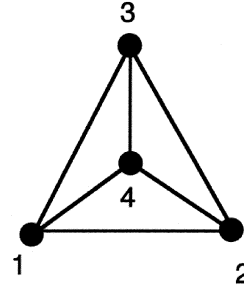
Solving Equations (5.11), (5.12), and (5.13), we obtain $a_{2,3} = 2$, $a_{2,4} = 1$, and $a_{3,4} = 0$. Thus, the adjacency matrix of the contracted graph is

$$A^c = \begin{bmatrix} 0 & 0 & 1 & 2 \\ 0 & 0 & 2 & 1 \\ 1 & 2 & 0 & 0 \\ 2 & 1 & 0 & 0 \end{bmatrix}.$$

The corresponding contracted graph is shown in Figure 5.3a.



(a) (4, 6) contracted graph-1



(b) (4, 6) contracted graph-2

FIGURE 5.3

Two (4, 6) contracted graphs.

Solution 2: Substituting $a_{1,2} = a_{1,3} = a_{1,4} = 1$ into Equations (5.8), (5.9), and (5.10) yields

$$a_{2,3} + a_{2,4} = 2, \quad (5.14)$$

$$a_{2,3} + a_{3,4} = 2, \quad (5.15)$$

$$a_{2,4} + a_{3,4} = 2. \quad (5.16)$$

Solving Equations (5.14), (5.15), and (5.16), yields $a_{2,3} = a_{2,4} = a_{3,4} = 1$. Hence, the adjacency matrix of the contracted graph is

$$A^c = \begin{bmatrix} 0 & 1 & 1 & 1 \\ 1 & 0 & 1 & 1 \\ 1 & 1 & 0 & 1 \\ 1 & 1 & 1 & 0 \end{bmatrix}.$$

The corresponding contracted graph is shown in Figure 5.3b. \square

The above procedure can be employed to enumerate contracted graphs having several vertices and edges. An atlas of contracted graphs with up to four independent loops and six vertices is given in Appendix B.

5.3 Enumeration of Conventional Graphs

Various algorithms for enumeration of conventional graphs have been developed. Obviously the procedure described in the preceding section for enumeration of contracted graphs can also be applied. However, direct enumeration of the adjacency matrices becomes more involved with a larger number of vertices and edges. In this section, we outline a systematic enumeration methodology developed by Woo [13]. The method is based on the concept of *expansion* from contracted graphs. The procedure involves the following steps:

- S1. Given the number of links and the number of joints, solve Equations (4.12) and (4.13) for all possible *link assortments*. We call each link assortment a *family*.
- S2. For each family, identify the corresponding contracted graphs from Appendix B.
- S3. Solve Equations (4.19) and (4.20) for all possible combinations of *binary link chains*. We call each combination of binary link chains a *branch*.
- S4. Permute the edges of each contracted graph with each combination of binary link chains obtained in S3 in as many arrangements as possible. This is equivalent to the problem of coloring the edges of a graph. Here, the concept of similar edges can be employed to reduce the number of permutations.
- S5. Eliminate those graphs that contain either parallel edges or partially locked subchains.
- S6. Check for graph isomorphisms. Note that only those graphs that belong to the same family and same branch can possibly be isomorphic to one another.

In the following, we illustrate the procedure with an example.

Example 5.4 Enumeration of (6,8) Graphs

We wish to enumerate all possible (6, 8) graphs of planar one-dof kinematic chains. For $n = 6$ and $j = 8$, we have $\tilde{L} = 8 - 6 + 2 = 4$. Equations (4.12) and (4.13)

reduce to

$$n_2 + n_3 + n_4 = 6, \quad (5.17)$$

$$2n_2 + 3n_3 + 4n_4 = 16. \quad (5.18)$$

The minimal number of binary links is given by Equation (4.15),

$$n_2 \geq 2.$$

Solving Equations (5.17) and (5.18) for nonnegative integers of n_i by using Crossley's operator yields three families of link assortments:

Family	n_2	n_3	n_4
2400	2	4	0
3210	3	2	1
4020	4	0	2

Next, we find the corresponding contracted graphs and solve Equations (4.19) and (4.20) for all possible partitions of binary links. Since we are interested in $F = 1$ kinematic chains, the length of any binary link chain is bounded by Equation (4.22),

$$q \leq 2.$$

2400 family: For the 2400 family, the corresponding contracted graphs have $v^c = 6 - 2 = 4$ vertices and $e^c = 8 - 2 = 6$ edges. There are two contracted graphs with 4 vertices and 6 edges as shown in Figure 5.3.

With $n_2 = 2$, $e_c = 6$, and $q = 2$, Equations (4.19) and (4.20) reduce to

$$b_1 + 2b_2 = 2, \quad (5.19)$$

$$b_0 + b_1 + b_2 = 6. \quad (5.20)$$

Solving Equation (5.19) for nonnegative integers b_1 and b_2 , and then Equation (5.20) for b_0 yields two branches of binary link chains:

Branch	b_0	b_1	b_2
1	5	0	1
2	4	2	0

For the first branch, we replace one of the six edges in each contracted graph shown in Figure 5.3 with a binary link chain of length two. This is equivalent to a problem of labeling one edge in one color and the remaining edges in another color. There are six possible ways of labeling each contracted graph. Due to the existence of similar edges, only two labelings of the graph shown in Figure 5.3a are nonisomorphic. However, both labelings lead to a graph with parallel edges and, therefore, are not

feasible. Since all edges in Figure 5.3b are similar, there is only one nonisomorphic labeling of the graph as shown in Figure 5.4a.

Similarly, for the second branch, we replace two of the six edges with a binary link chain of length one. This is equivalent to a problem of labeling two edges in one color and the remaining edges in another color. There are 15 possible ways of labeling each contracted graph. After eliminating those graphs that are isomorphic or contain parallel edges, we obtain three labeled nonisomorphic graphs as shown in Figure 5.4b.

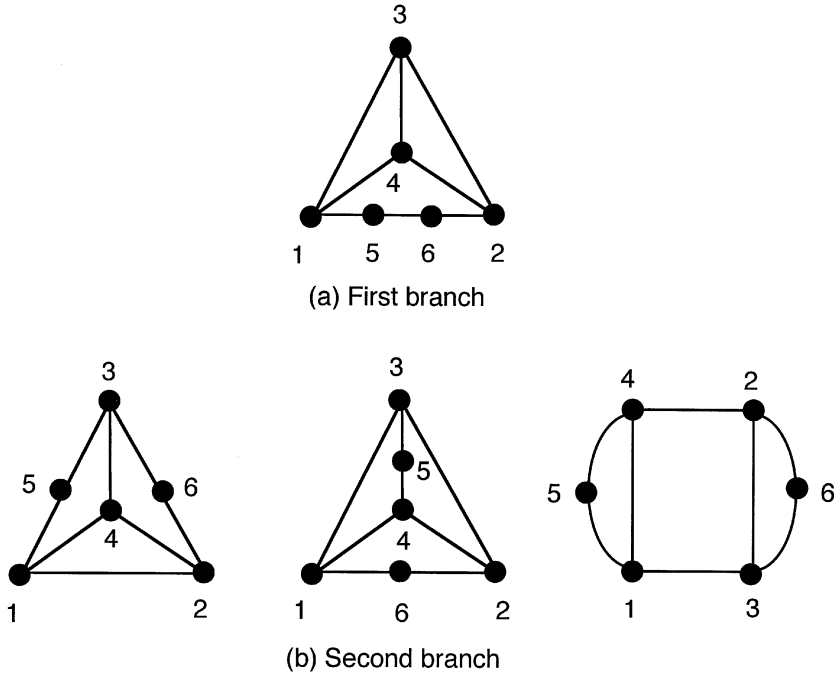


FIGURE 5.4

Four nonisomorphic graphs derived from the 2400 family.

3210 family: For the 3210 family, the corresponding contracted graphs have $v^c = 6 - 3 = 3$ vertices and $e^c = 8 - 3 = 5$ edges. There is only one contracted graph with 3 vertices and 5 edges as shown in Figure 5.2.

With $n_2 = 3$, $e_c = 5$, and $q = 2$, Equations (4.19) and (4.20) reduce to

$$b_1 + 2b_2 = 3, \quad (5.21)$$

$$b_0 + b_1 + b_2 = 5. \quad (5.22)$$

Solving Equation (5.21) for nonnegative integers b_1 and b_2 , and then Equation (5.22) for b_0 yields two families of binary link chains:

Branch	b_0	b_1	b_2
1	3	1	1
2	2	3	0

For the first branch, we replace one of the edges in the contracted graph shown in Figure 5.2 by a binary link chain of length one and another by a binary link chain of length two. Note that there are two sets of two parallel edges. To avoid parallel edges in the conventional graph, one in each set of two parallel edges must be replaced by a binary link chain. In addition, the two sets of parallel edges are similar. Hence, we obtain only one labeled nonisomorphic graph as shown in Figure 5.5a. For the second branch, we replace three edges of the contracted graph each with a binary link chain of length one. Again, at least one in each set of two parallel edges must be replaced by a binary link chain. Thus, there are three possible ways of labeling the edges. Due to similar edges, only two are nonisomorphic as shown in Figure 5.5b.

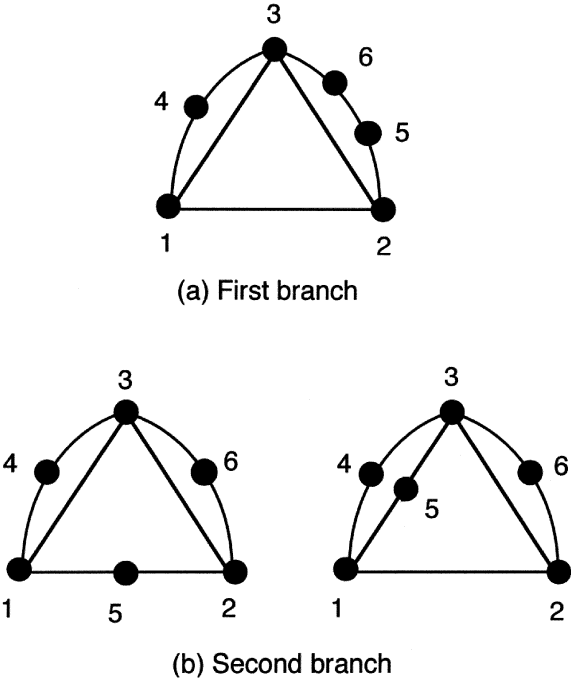


FIGURE 5.5
Three nonisomorphic graphs derived from the 3210 family.

4020 family: For the 4020 family, the corresponding contracted graphs have $v^c = 6 - 4 = 2$ vertices and $e^c = 8 - 4 = 4$ edges. There is only one contracted graph with 2 vertices and 4 edges as shown in Figure 5.1.

With $n_2 = 4$, $e_c = 4$, and $q = 2$, Equations (4.19) and (4.20) reduce to

$$b_1 + 2b_2 = 4, \tag{5.23}$$

$$b_0 + b_1 + b_2 = 4. \tag{5.24}$$

Solving Equation (5.23) for nonnegative integers b_1 and b_2 , and then Equation (5.24) for b_0 yields three families of binary link chains:

Branch	b_0	b_1	b_2
1	2	0	2
2	1	2	1
3	0	4	0

For the first branch, we replace two of the four parallel edges of the contracted graph shown in Figure 5.1 each with a binary link chain of length two. This produces no feasible solutions because the resulting graphs always contain two parallel edges. For the second branch, we replace two of the four edges of the contracted graph each with a binary link chain of length one and one with a binary link chain of length two. For the third branch, we replace all four edges of the contracted graph each with a binary link chain of length one. As a result, we obtain two nonisomorphic graphs as shown in Figure 5.6. \square

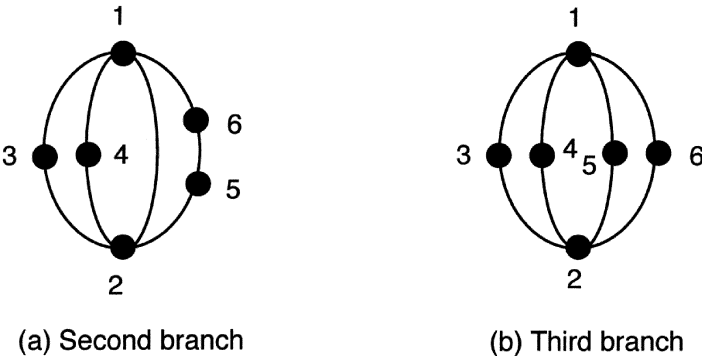


FIGURE 5.6
Two nonisomorphic graphs derived from the 4020 family.

5.4 Atlas of Graphs of Kinematic Chains

Using the enumeration procedure described in the preceding section, graphs with a given number of vertices and edges can be enumerated systematically. Appendix C provides an atlas of graphs of kinematic chains with up to three independent loops

and eight vertices. All graphs given in Appendix C are sketched in such a way that the longest circuit forms the peripheral loop and the vertex of highest degree appears on the top (or upper-left corner), provided that it does not cause crossing of the edges. These graphs are arranged in the order of complexity according to the number of loops, number of vertices, and length of peripheral loop. An atlas of all kinds of graphs can be found in Read and Wilson [8].

5.5 Summary

We have shown that systematic algorithms using graph theory and combinatorial analysis can be developed for enumeration of graphs of kinematic chains. Contracted graphs with up to four loops and six vertices are provided in Appendix B. Based on the concept of expansion from contracted graphs, an algorithm for enumeration of conventional graphs is described. Conventional graphs with up to three independent loops and eight vertices are tabulated in Appendix C. Using these atlases, an enormous number of mechanisms can be developed by labeling the edges of the graphs according to the available joint types and the choice of fixed links. This is the subject of the following chapters.

References

- [1] Chang, S.L. and Tsai, L.W., 1990, Topological Synthesis of Articulated Gear Mechanisms, *IEEE Journal of Robotics and Automation*, 6, 1, 97–103.
- [2] Chatterjee, G. and Tsai, L.W., 1994, Enumeration of Epicyclic-Type Automatic Transmission Gear Trains, *SAE 1994 Trans., Journal of Passenger Cars*, Sec. 6, 103, 1415–1426.
- [3] Crossley, F.R.E., 1964, A Contribution to Grübler's Theory in Number Synthesis of Plane Mechanisms, *ASME Journal of Engineering for Industry*, Series B, 86, 1–8.
- [4] Crossley, F.R.E., 1965, The Permutation of Kinematic Chains of Eight Members or Less from the Graph-Theoretic Viewpoint, in *Developments in Theoretical and Applied Mechanics*, Vol. 2, Pergamon Press, Oxford, 467–486.
- [5] Davies, T.H., 1968, An Extension of Manolescu's Classification of Planar Kinematic Chains and Mechanisms of Mobility $m \geq 1$, Using Graph Theory, *Journal of Mechanisms and Machine Theory*, 4, 87–100.

- [6] Freudenstein, F., 1967, The Basic Concept of Polya's Theory of Enumeration with Application to the Structural Classification of Mechanisms, *Journal of Mechanisms*, 3, 275–290.
- [7] Pólya, G., 1938, Kombinatorische Anzahlbestimmungen für Gruppen, Graphen und Chemische Verbindungen, *Acta Math.*, 68, 145–254.
- [8] Read, R.C. and Wilson, R.J., 1998, *An Atlas of Graphs*, Oxford University Press, New York.
- [9] Sohn, W. 1987, A Computer-Aided Approach to the Creative Design of Mechanisms, Ph.D. Dissertation, Dept. of Mechanical Engineering, Columbia University, New York, NY.
- [10] Sohn, W. and Freudenstein, F., 1986, An Application of Dual Graphs to the Automatic Generation of the Kinematic Structures of Mechanism, *ASME Journal of Mechanisms, Transmissions, and Automation in Design*, 108, 3, 392–398.
- [11] Tuttle, E.R., Peterson, S.W., and Titus, J.E., 1989, Enumeration of Basic Kinematic Chains Using the Theory of Finite Groups, *ASME Journal of Mechanisms, Transmissions, and Automation in Design*, 111, 4, 498–503.
- [12] Tuttle, E.R., Peterson, S.W., and Titus, J.E., 1989, Further Application of Group Theory to the Enumeration and Structural Analysis of Basic Kinematic Chains, *ASME Journal of Mechanisms, Transmissions, and Automation in Design*, 111, 4, 494–497.
- [13] Woo, L.S., 1967, Type Synthesis of Plane Linkages, *ASME Journal of Engineering for Industry*, Series B, 89, 159–172.
- [14] Yan, H.S., 1998, *Creative Design of Mechanical Devices*, Springer-Verlag, Singapore.

Exercises

- 5.1 Enumerate all the feasible (3, 6) contracted graphs.
- 5.2 Enumerate all the feasible (4, 7) contracted graphs.
- 5.3 Enumerate all the feasible (5, 7) conventional graphs of planar kinematic chains using Woo's method.
- 5.4 Enumerate all the feasible (6, 8) conventional graphs of planar kinematic chains using Woo's method.
- 5.5 Enumerate all the feasible (7, 9) conventional graphs of planar kinematic chains using Woo's method.

Chapter 6

Classification of Mechanisms

6.1 Introduction

Using graph representation, mechanism structures can be conveniently represented by graphs. The classification problem can be transformed into an enumeration of nonisomorphic graphs for a prescribed number of degrees of freedom, number of loops, number of vertices, and number of edges.

The degrees of freedom of a mechanism are governed by Equation (4.3). The number of loops, number of links, and number of joints in a mechanism are related by Euler's equation, Equation (4.5). The loop mobility criterion is given by Equation (4.7). Since we are primarily interested in nonfractionated closed-loop mechanisms, the vertex degree in the corresponding graphs should be at least equal to two and not more than the total number of loops; that is, Equation (4.10) should be satisfied. Furthermore, there should be no articulation points or bridges, and the mechanism should not contain any partially locked kinematic chain as a subchain.

In this chapter, we classify mechanisms in accordance with the type of motion followed by the number of degrees of freedom, the number of loops, the number of links, the number of joints, and the vertex degree listing. The general procedure for enumeration and classification of mechanisms is as follows. Given the number of degrees of freedom, F , and the number of independent loops, L ,

1. Solve Equations (4.3), (4.5), and (4.7) for the number of links and the number of joints.
2. Solve Equations (4.12) and (4.13) for various link assortments, n_2, n_3, n_4, \dots
3. Identify feasible graphs and their corresponding contracted graphs from the atlases of graphs listed in Appendices C and B or any other available resources such as Read and Wilson [14].
4. Label the edges of each feasible graph with a given set of desired joint types. This problem may be regarded as a partition of the edges into several parts. Each part represents one type of joint. Two permutations are said to be *equivalent*, if their corresponding labeled graphs are isomorphic. Therefore, we

need to find the number of nonequivalent permutation sequences. For simple kinematic chains, the enumeration of labeled graphs can be accomplished by inspection. For more complicated kinematic chains, a computer algorithm employing partitioning and combinatorial schemes may be needed.

5. Identify the fixed, input, and output links as needed.
6. Check for mechanism isomorphisms and evaluate functional feasibility.

In the following, we illustrate the above procedure with several examples in order of increasing complexity.

6.2 Planar Mechanisms

First, we study planar mechanisms. We shall limit the investigation to the following types of joint: revolute (R), prismatic (P), gear pair (G), and cam pair (C_p). The *pin-in-slot* joint can be replaced by prismatic and revolute joints with an intermediate link. Both revolute and prismatic joints are one-dof joints, while gear and cam pairs are two-dof joints. A mechanism is called a *linkage* if it is made up of only lower pairs; that is, R and P joints. It is called a *geared mechanism* if it contains gear pairs, a *cam mechanism* if it contains cam pairs, and a *gear-cam mechanism* if it contains both gear and cam pairs.

6.2.1 Planar Linkages

Since revolute and prismatic joints are one-dof joints, the total joint degrees of freedom in a planar linkage is equal to the number of joints; that is,

$$\sum_{i=1}^j f_i = j . \quad (6.1)$$

Substituting $\lambda = 3$ and Equation (6.1) into Equations (4.3) and (4.7) yields

$$F = 3n - 2j - 3 , \quad (6.2)$$

$$j = F + 3L . \quad (6.3)$$

Eliminating j between Equations (4.5) and (6.3) gives

$$n = F + 2L + 1 . \quad (6.4)$$

Equations (6.3) and (6.4) imply that given the number of degrees of freedom, each time we increase the number of loops by one, it is necessary to increase the number of links by two and the number of joints by three.

Solving Equations (6.4) for L and then substituting the resulting expression into Equation (4.10), we obtain

$$\frac{n - F + 1}{2} \geq d_i \geq 2. \quad (6.5)$$

In particular, for planar one-dof linkages, Equation (6.5) further reduces to

$$\frac{n}{2} \geq d_i \geq 2.$$

Since we are interested in mechanisms with positive mobility, only those kinematic chains that satisfy Equations (6.3) and (6.4) are said to be feasible. Furthermore, those kinematic chains with partially locked subchains such as the three- and five-link chains shown in Figure 4.14 should be excluded from consideration.

We note that if a link has only two prismatic joints, they should not be parallel otherwise the link will possess a passive degree of freedom. Except for the three-link wedge shown in Figure 6.1, two links, each containing two prismatic joints, cannot

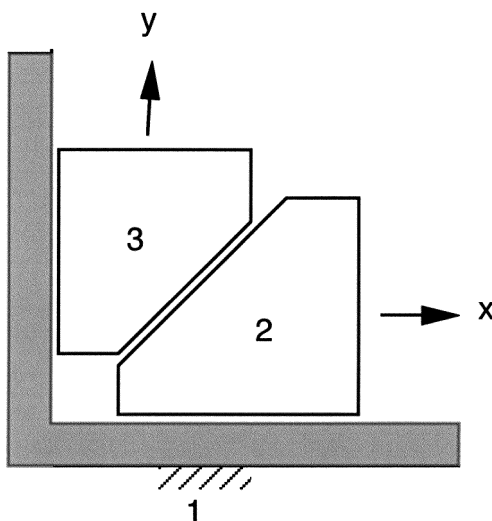


FIGURE 6.1
A three-link wedge.

be connected to each other. In general, there are no three-link planar mechanisms that are composed exclusively of revolute and prismatic joints. The three-link wedge mechanism shown in Figure 6.1 is an exception. Every link in the three-link wedge mechanism performs planar translation without rotation. Hence, the motion parameter is equal to 2, i.e., $\lambda = 2$.

Planar One-dof Linkages

For planar one-dof linkages, Franke [4] showed that the number of nonisomorphic kinematic structures having three independent loops is sixteen. Woo [28] showed

that there are 230 nonisomorphic kinematic structures with four independent loops. Table 6.1 summarizes the number of solutions for planar one-dof linkages with up to four independent loops. In Table 6.1, the classification is made in accordance with the number of independent loops followed by the number of links and then the various link assortments.

Table 6.1 Classification of Planar One-dof Linkages.

Class							No. of	Total
L	n	j	n_2	n_3	n_4	n_5	Solutions	Number
1	4	4	4	0	0	0	1	1
2	6	7	4	2	0	0	2	2
3	8	10	4	4	0	0	9	16
			5	2	1	0	5	
			6	0	2	0	2	
4	10	13	4	6	0	0	50	230
			5	4	1	0	95	
			6	3	0	1	15	
			6	2	2	0	57	
			7	1	1	1	8	
			7	0	3	0	3	
			8	0	0	2	2	

Four-Bar Linkages. For $F = 1$ and $L = 1$, Equations (6.3) and (6.4) give $n = j = 4$. An examination of the atlas of graphs listed in Appendix C reveals that there is only one (4, 4) graph with one independent loop. The corresponding kinematic chain is given in Table D.1, Appendix D. Hence, the number of joints is equal to the number of links and all the links are necessarily binary. Labeling the four edges of the (4, 4) graph with as many combinations of R and P joints as possible yields the following feasible kinematic chains:

$$RRRR, RRRP, RRPP, \text{ and } RPRP.$$

Note that we have excluded the $RPPP$ chain as a feasible solution, because it has two adjacent links with only sliding pairs.

By assigning various links as the fixed link, we obtain seven basic four-bar mechanisms as shown in Figure 6.2 [6]. These mechanisms can often be found in the heart of industrial machinery. Note that we have essentially enumerated the kinematic chains as combinations of four objects. Then we perform the kinematic inversion by alternating the fixed link to obtain different mechanisms. Finally, we note that for a given application, the input and output links should also be identified.

As shown in Figure 6.2, structure number 1 is the well-known planar four-bar linkage. A four-bar linkage can be designed as a drag-link, crank-and-rocker, double-rocker, or a change-point mechanism depending on the link length ratios [5, 7, 11, 20, 21]. Each of the number 2 and 3 structures contains one prismatic joint. In

No.	Graph	Mechanism	Comments
1			Four-bar linkage
2		(a) (b)	(a) Turning-block linkage (b) Swinging-block linkage
3			Crank-slider mechanism
4			Scotch yoke
5			Cardanic motion
6		(a) (b)	(a) Inverse Cardanic (b) Oldham Coupling
7			Rapson slide

FIGURE 6.2
Seven basic four-bar linkages.

sketching a prismatic joint, we can arbitrarily choose one link as the sliding block and the other as the slotted guide. For this reason, structure number 2 can be sketched into a turning-block linkage or a swinging-block linkage, depending on the choice of pair representation. The turning-block linkage is often used to transform a constant rotational speed of the crankshaft, link 1, into a nonuniform rotational speed or cyclic oscillation of the follower, link 3. The swinging-block linkage can be designed as an oscillating-cylinder engine mechanism as shown in Figure 6.3b. Structure number 3 is the well-known crank-and-slider mechanism, which can be used as an engine or compressor mechanism as shown in Figure 6.3a. Structure number 4 is known as the Scotch yoke mechanism, which has been developed as a compressor in an automotive air conditioning system. Structure number 5 is called the Cardanic motion mechanism. Any point on link 2 of the Cardanic motion mechanism traces an elliptical curve. In particular, the midpoint of link 2 generates a circular path centered about the point defined by the intersection of the two prismatic joint axes.

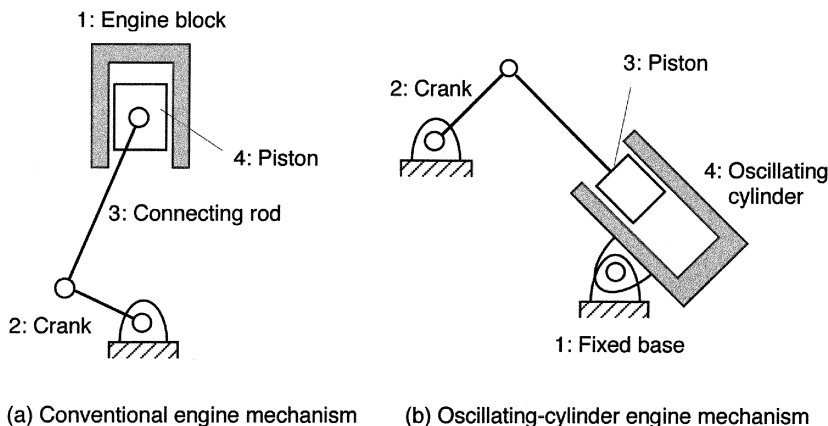


FIGURE 6.3

Two engine mechanisms.

The sketching of a mechanism depends on the experience and skill of a designer. This is best illustrated in structure number 6 (see Figure 6.2). A straightforward sketch yields the inverse Cardanic motion mechanism. However, it would be difficult to conceive the Oldham coupling, if we are not aware of the design to begin with. In this regard, creativity and ingenuity play an important role. The Oldham coupling is used as a constant velocity coupling to allow for small misalignment between two parallel shafts. Because of the kinematic inversion, the center point of link 4 revolves in a circular path at twice the input shaft frequency. Two counterrotating Oldham couplings can be arranged side by side at the midplane of an in-line four-cylinder engine to generate a second harmonic balancing force ([22], [23], [27]). Two such couplings can also be arranged along an axis parallel to the crankshaft of a 90° V-6 engine to generate primary and secondary rotating couples ([25], [26]). Similarly, by

enlarging the two intermediate revolute joints of a drag-link mechanism, a generalized Oldham coupling is obtained [8].

Six-Bar Linkages. For $F = 1$ and $L = 2$, Equations (6.3) and (6.4) yield $n = 6$ and $j = 7$. Hence, planar one-dof linkages with two independent loops contain six links and seven joints. An examination of the atlas of graphs listed in Appendix C reveals that there are three (6, 7) graphs. Excluding the (6, 7)(a) graph, which contains a three-vertex loop as a subgraph, we obtain two unlabeled graphs as shown in Table D.2, Appendix D. Also shown in the table are the vertex degree listing, the corresponding contracted graph, and typical structure representations of the kinematic chains.

The first kinematic structure, listed in Table D.2, Appendix D, is known as the *Watt chain* and the second the *Stephenson chain*. Each of the seven joints in these kinematic chains can be assigned as a revolute or prismatic joint. Furthermore, any of the six links can be chosen as the fixed link. The search for all feasible six-link mechanisms becomes a more complicated task. However, for certain applications, we might prefer one type of joint over the other. Then the task can be reduced to a more manageable size. For example, if we limit ourselves to those mechanisms with all revolute joints and ground-connected input and output links, then the number of feasible six-bar linkages reduces to five as shown in Figure 6.4. The logic behind the choice of fixed, input, and output link for the mechanisms shown in Figure 6.4 is as follows.

Excluding the external loop, the Watt chain consists of two four-bar loops with two common links and one common joint. To construct a mechanism with ground-connected input and output links, one of the two ternary links must be grounded. Any other choice of the fixed link will lead to one active four-bar loop, whereas the other four-bar loop functions as an idler loop. Since the idler loop carries no loads, the resulting mechanism is equivalent to a four-bar linkage. Once the fixed link is chosen, the input and output links must be located on two different loops. Due to symmetry, there is one such choice. Hence, there is only one possible arrangement of the fixed, input, and output links.

The Stephenson chain consists of one four-bar loop and one five-bar loop with three common links and two common joints. The two binary links in the four-bar loop cannot be chosen as the fixed link. Otherwise, it will lead to one active four-bar loop and one passive five-bar loop. Any other links can be chosen as the fixed link. In addition, when one of the two ternary links is chosen as the fixed link, the input and output links cannot be simultaneously located on the four-bar loop.

Figure 6.5b shows a six-bar linkage designed as a quick-return shaper mechanism. The output link 6, which carries a cutting tool, slides back and forth in a fixed guide designated as link 1. The input link 2 rotates about a fixed pivot A . The turning block 3, which slides with respect to an oscillating arm 4, is connected to the input crank by a turning pair at point C . The arm 4 oscillates about a fixed pivot B . The output link 6 is connected to the oscillating arm by a coupler link 5 with two revolute joints. As can be clearly seen from the corresponding graph depicted in Figure 6.5a, the shaper mechanism belongs to the Watt chain with five revolute and two

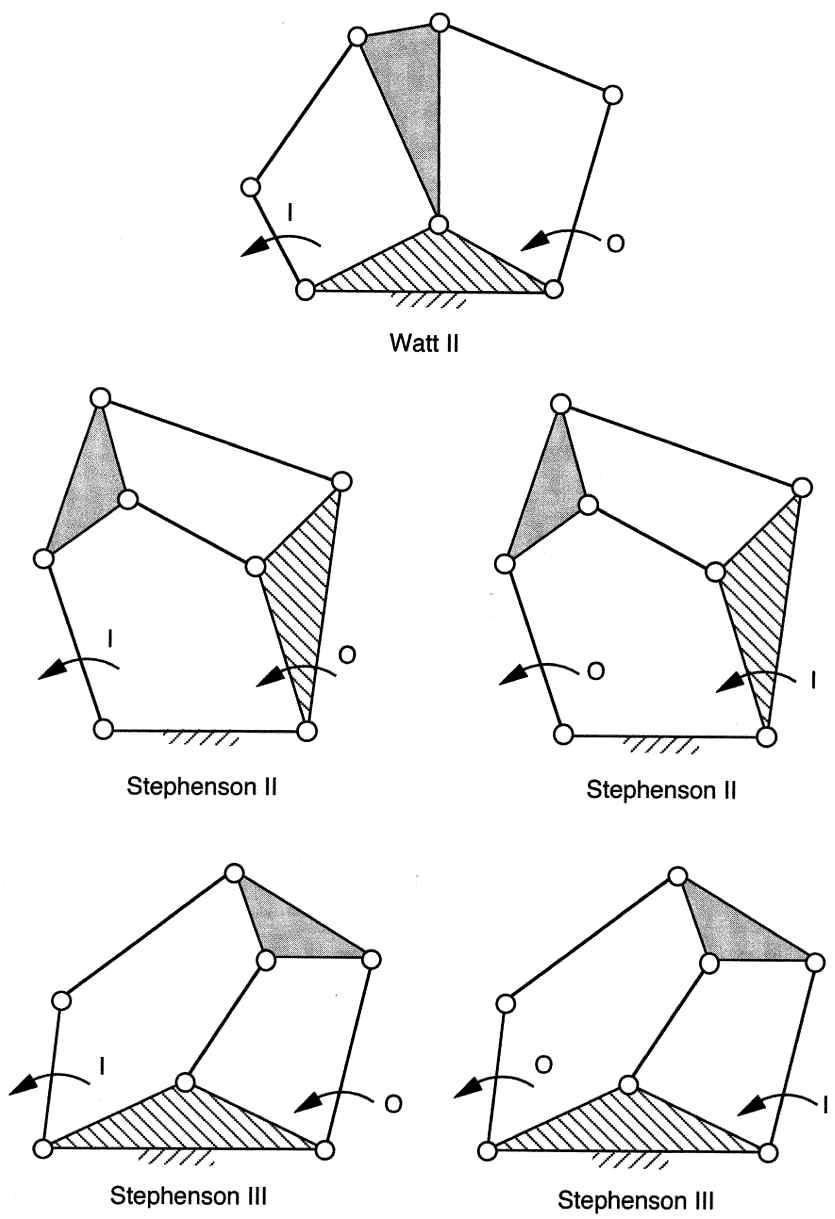


FIGURE 6.4
Planar one-dof six-bar linkages with all revolute joints and ground-connected input and output links.

prismatic joints. As the input crank rotates, the quick return motion is achieved by the turning-block linkage, links 1-2-3-4 as shown in the lower half of the mechanism. Specifically, the ratio of the time period during which the working stroke takes place to the time period required in returning 6 to its initial position to start the next cycle, is equal to the ratio of the angles through which the input crank turns during these respective motions. It can be shown that this ratio depends only on the two link lengths AC and AB . The six-bar construction helps minimize the reaction force between the output link and the fixed guide.

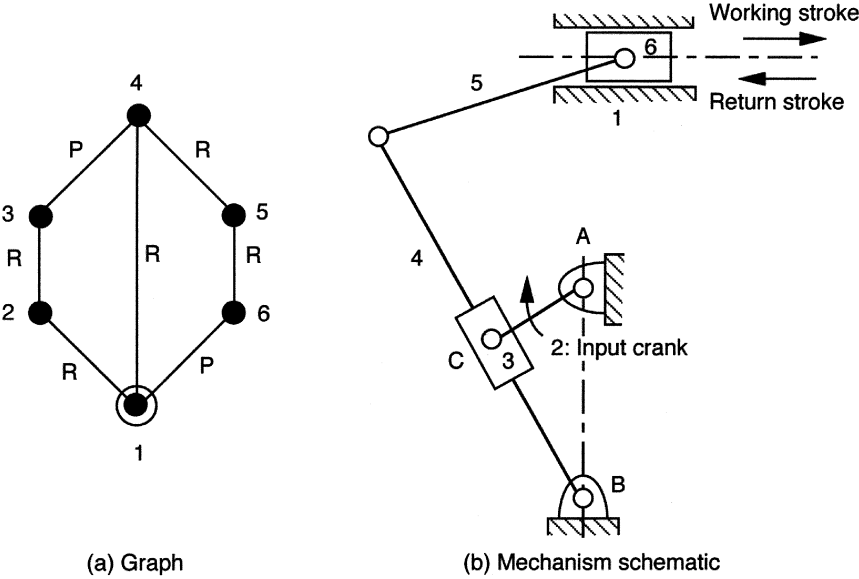


FIGURE 6.5
Shaper mechanism.

Figure 6.6b shows a six-bar linkage developed as a variable valve-timing (VVT) device [1]. This mechanism is made up of two turning-block linkages connected in series. The first turning block linkage consists of links 1, 2, 3, and 4, whereas the second contains links 1, 4, 5, and 6. The two turning block linkages share two common links, 1 and 4. Link 1 is the fixed link. Both the input link 2 and the output link 6 rotate about a common stationary axis B . The intermediate member 4 rotates about an axis A whose location can be altered with respect to the stationary axis B . The other two revolute joints are designated as C and D . The input link 2 takes power from an engine crankshaft by a 2:1 reduction drive. An overhead cam (not shown in the figure) is attached to the output shaft 6. This arrangement converts a constant time scale associated with the crankshaft rotation into a variable time scale associated with valve lift. The change of valve timing is achieved by rotating pivot A about the fixed pivot B . Figure 6.6a shows the corresponding graph representation. This is a Watt chain with five revolute and two prismatic joints.

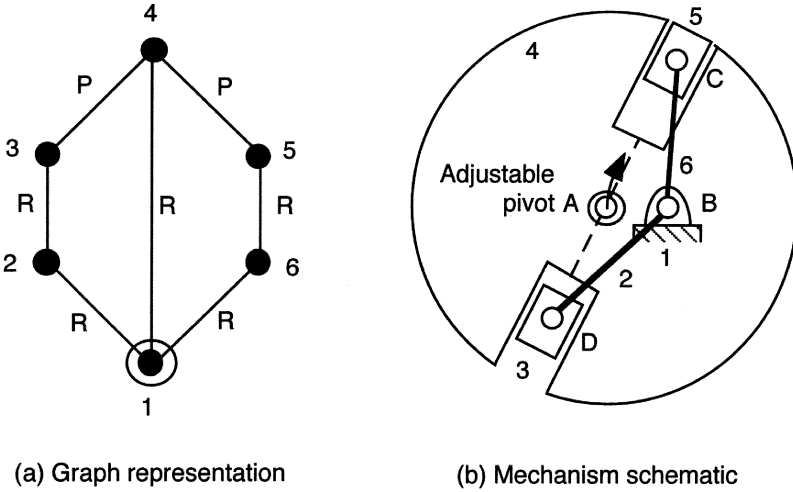


FIGURE 6.6
Variable-valve-timing mechanism.

Eight-Bar Linkages. For $F = 1$ and $L = 3$, Equations (6.3) and (6.4) reduce to $n = 8$ and $j = 10$. Hence, planar one-dof linkages with three independent loops contain eight links and ten joints. Eliminating those graphs containing the three- or five-link structure as a subgraph from the atlas of (8, 10) graphs listed in Appendix C results in 16 nonisomorphic unlabeled graphs as shown in Tables D.3 through D.6, Appendix D. Each of the ten joints can be assigned as a revolute or prismatic joint and any of the ten links can be chosen as the fixed link. We see that the number of possible combinations grows exponentially as the number of links increases.

Planar Two-dof Linkages

For planar two-dof linkages, Crossley [3] showed that there are 32 nonisomorphic kinematic structures with 3 independent loops. Recently, Sohn and Freudenstein [17] proved that the correct number is 35. Furthermore, they found that there are 726 nonisomorphic structures with 4 independent loops. Table 6.2 summarizes the number of solutions in terms of the number of independent loops, the number of links, and the various link assortments for planar two-dof linkages with up to 4 independent loops.

Five-Bar Linkages. For $F = 2$ and $L = 1$, Equations (6.3) and (6.4) yield $n = j = 5$. There is only one (5, 5) graph with one independent loop. The corresponding kinematic structure is given in Table D.7, Appendix D. Labeling the five edges of the graph with as many combinations of R and P joints as possible, yields four nonisomorphic kinematic chains:

$$RRRRR, RRRRP, RRRPP, \text{ and } RRPRP.$$

Here we have limited ourselves to those kinematic chains with no more than two

Table 6.2 Classification of Planar Two-dof Linkages.

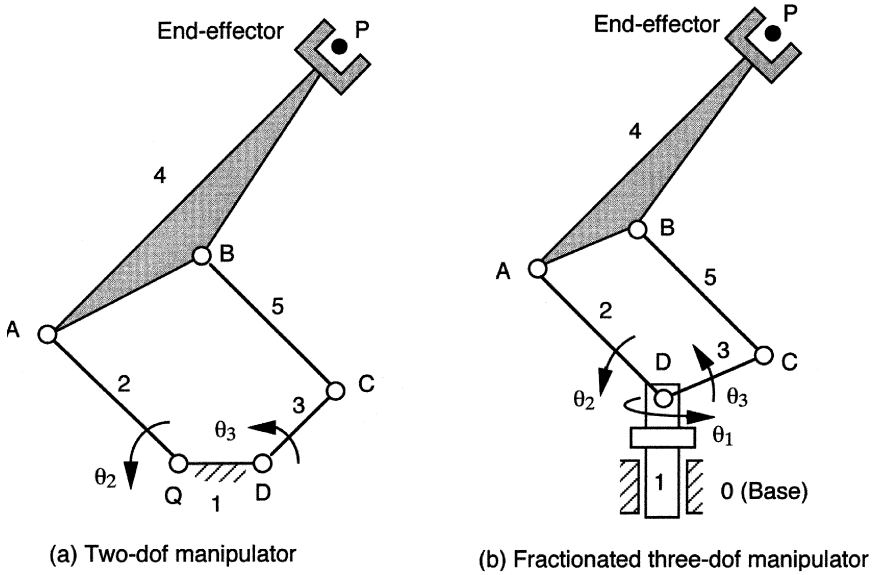
Class							No. of	Total
L	n	j	n_2	n_3	n_4	n_5	Solutions	Number
1	5	5	5	0	0	0	1	1
2	7	8	5	2	0	0	3	3
3	9	11	5	4	0	0	19	35
			6	2	1	0	13	
			7	0	2	0	3	
4	11	14	5	6	0	0		726
			6	4	1	0		
			7	3	0	1		
			7	2	2	0		
			8	1	1	1		
			8	0	3	0		
			9	0	0	2		

prismatic joints. A mechanism that is made up of too many prismatic joints may experience excessive friction.

Many mechanisms can be developed by assigning a different link as the fixed link. However, if we prefer both input links to be ground connected, the output link must necessarily be a floating link. Figure 6.7a shows a planar two-dof 5- R linkage in which links 2 and 3 are assigned as the input links and link 4 as the output link. The position of the end-point P on link 4 can be manipulated anywhere within a 2-dimensional workspace of the manipulator. A parallelogram linkage results when the link lengths are sized according to the conditions: $QA = BC$, $AB = CD$, and $QD = 0$ (i.e., pivots Q and D coincide). Furthermore, if link 1 is allowed to rotate about a fixed axis as shown in Figure 6.7b, the mechanism becomes a fractionated three-dof spatial manipulator.

Seven-Bar Linkages. For $F = 2$ and $L = 2$, Equations (6.3) and (6.4) reduce to $n = 7$ and $j = 8$. Eliminating those graphs containing a three-link structure as a subgraph from the atlas of (7, 8) graphs listed in Appendix C, results in three nonisomorphic unlabeled graphs as shown in Table D.8, Appendix D.

Theoretically, any of the seven links can be assigned as the fixed link. We note that, excluding the external loop, the first kinematic chain consists of a four- and a five-bar loop; the second consists of two five-bar loops; and the third is made up of a four- and a six-bar loop. Since a four-bar loop possesses only one degree of freedom, none of the binary links in the loop can be chosen as the fixed link. Otherwise, it would be impossible to arrange two ground-connected input links. Furthermore if the output link is also to be connected to the ground, the fixed link must be a ternary link. When one of the ternary links in the first or third kinematic chain is fixed, due to the presence of a four-bar loop, a ground-connected output link is impossible. In this regard, the second kinematic chain becomes the only feasible candidate to

**FIGURE 6.7****Two- and three-dof manipulators.**

have ground-connected input and output links. Alternatively, the output link can be a floating link. For example, Figure 6.8 shows a planar two-dof manipulator constructed from the second kinematic chains given in Table D.8, Appendix D. Obviously, each joint shown in Table D.8 can be a revolute or a prismatic joint.

Nine-Bar Linkages. For $F = 2$ and $L = 3$, Equations (6.3) and (6.4) reduce to $n = 9$ and $j = 11$. Eliminating those graphs containing the three- or five-link structure as a subgraph from the atlas of (9, 11) graphs listed in Appendix C leads to 35 nonisomorphic graphs as shown in Tables D.9 through D.14, Appendix D.

Planar Three-dof Linkages

For planar three-dof linkages, Sohn and Freudenstein [17] showed that there are 5 nonisomorphic kinematic structures with 2 independent loops and 74 with 3 independent loops. Table 6.3 summarizes the number of solutions in terms of the number of independent loops, the number of links, and the various link assortments for planar three-dof linkages having up to four independent loops.

Planar three-dof linkages are not as well understood as their planar one- and two-dof counterparts. For a single-loop mechanism, one of the actuators must be installed on the moving links. In this regard, the mass of the floating actuator becomes the load of the others. To reduce the inertia and to increase the stiffness, parallel kinematics machines have been investigated recently. A parallel kinematics machine allows all

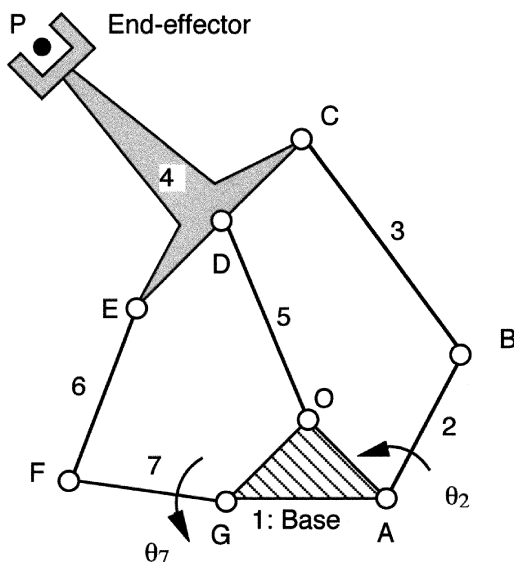


FIGURE 6.8
Planar two-dof parallel manipulator.

actuators to be mounted on the ground. Hence, low inertia, high stiffness, and high speed capabilities can be achieved.

Six-Bar Linkages. For $F = 3$ and $L = 1$, Equations (6.3) and (6.4) yield $n = j = 6$. There is only one (6, 6) graph with one independent loop. The corresponding kinematic structure is shown in Table D.15, Appendix D. One major disadvantage of using this kinematic chain as a three-dof device is that one of the input links cannot be ground connected. Hence, the mass of a floating actuator becomes the load of the grounded actuators.

Eight-Bar Linkages. For $F = 3$ and $L = 2$, Equations (6.3) and (6.4) reduce to $n = 8$ and $j = 9$. Eliminating those graphs containing the three-link structure as a subgraph from the atlas of (8, 9) graphs listed in Appendix C, we obtain five nonisomorphic graphs shown in Table D.15, Appendix D, where the joint type is not assigned.

We note that if the input links are to be ground connected, one of the ternary links must be selected as the fixed link. A careful examination of the kinematic structures reveals that the first and fourth kinematic chains should be excluded from further consideration due to the existence of a four-bar loop. The second kinematic chain should also be excluded because none of its links possesses full three degrees-of-freedom motion. Hence, the third and fifth kinematic chains are the only two feasible solutions. For the fifth kinematic chain to function as a three-dof device, the floating ternary link serves as the output link. For the third kinematic chain, the binary link that lies on the six-bar loop and is immediately adjacent to the floating ternary link,

Table 6.3 Classification of Planar Three-dof Linkages.

Class							No. of	Total
L	n	j	n_2	n_3	n_4	n_5	Solutions	Number
1	6	6	6	0	0	0	1	1
2	8	9	6	2	0	0	5	5
3	10	12	6	4	0	0	43	74
			7	2	1	0	25	
			8	0	2	0	6	
4	12	15	6	6	0	0		1898
			7	4	1	0		
			8	3	0	1		
			8	2	2	0		
			9	1	1	1		
			9	0	3	0		
			10	0	0	2		

serves as the output link. Figure 6.9 shows a planar three-dof parallel manipulator constructed from the fifth graph with all revolute joints.

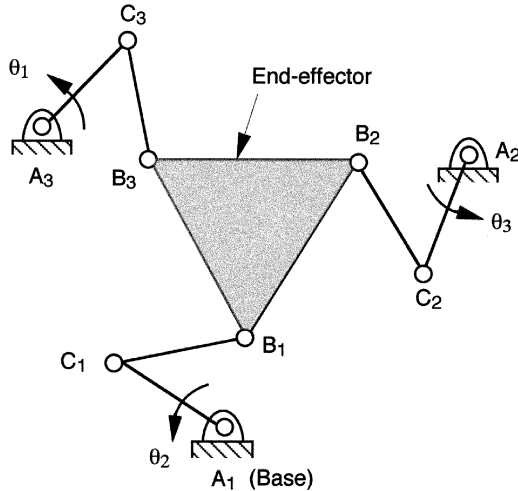


FIGURE 6.9
Planar three-dof parallel manipulator.

Ten-Bar Linkages. For $F = 3$ and $L = 3$, Equations (6.3) and (6.4) give $n = 10$ and $j = 12$. Sohn and Freudenstein [17] showed that there are 74 such kinematic chains — too many to list here. See Sohn [16] for the results.

6.2.2 Planar Geared Mechanisms

Planar geared mechanisms are connected by revolute, R , prismatic, P , and gear, G , pairs. Let j_i denote the number of i -dof joints. By definition,

$$j = j_1 + j_2 . \quad (6.6)$$

Since the revolute and prismatic joints are one-dof joints and the gear pair is a two-dof joint, the sum of the degrees of freedom in all joints can be written as

$$\sum_{i=1}^j f_i = j_1 + 2j_2 . \quad (6.7)$$

Eliminating j_1 between Equations (6.6) and (6.7), and substituting the resulting equation and $\lambda = 3$ into Equation (4.7) yields

$$j + j_2 = F + 3L . \quad (6.8)$$

Hence, the number of joints and the number of links in a geared mechanism depend not only on the degrees of freedom and the number of loops, but also on the number of gear pairs. It has been shown that the number of gear pairs in a geared mechanism cannot exceed the number of independent loops [13]; that is,

$$j_2 \leq L . \quad (6.9)$$

Applying Equations (4.5), (6.8), and (6.9), geared mechanisms can be enumerated and classified according to the number of degrees of freedom, the number of independent loops, and the number of links. Table 6.4 shows the possible joint combinations in terms of the number of independent loops and the number of links for planar one-dof geared mechanisms having up to four independent loops.

We note that some of the mechanisms formed by the joint combinations listed in Table 6.4 will lead to unlimited rotation of all links. We call these types of mechanisms *gear trains*. Gear trains can be classified further into *ordinary gear trains* and *planetary gear trains*. The structural characteristics and the enumeration of epicyclic gear trains will be studied in more detail in the following chapter.

One Independent Loop

The only single-loop graph suitable for a geared mechanism is the (3, 3) graph given in Appendix C. One of the three edges in the graph must be labeled as a gear pair, whereas the other two can be a combination of revolute and prismatic joints; that is, RR , RP , or PP joint pairs. Making all combinations of the one-dof joint pairs with a gear pair yields three feasible kinematic chains:

$$RRG, \text{ } RPG, \text{ and } PPG .$$

The PPG chain is judged to be impractical and is excluded from further consideration. By performing kinematic inversion, we obtain five nonisomorphic mechanisms as

Table 6.4 Classification of One-dof Geared Mechanisms.

Class	No. of Links	No. of Joints	No. of Gear Pairs	No. of Revolute Joints
L	n	j	j_2	j_1
1	3	3	1	2
2	4	5	2	3
	5	6	1	5
3	5	7	3	4
	6	8	2	6
	7	9	1	8
4	6	9	4	5
	7	10	3	7
	8	11	2	9
	9	12	1	11

shown in Figure 6.10. We note that grounding the carrier of the *RRG* chain results in a simple gear set. On the other hand, the kinematic chain becomes a simple planetary gear set when one of the gears is grounded. Similarly, the *RPG* chain produces a simple rack-and-pinion motion, an involute motion, or an inverse rack-and-pinion motion depending on which link is grounded. Obviously, it is also possible to replace the gear pair shown in Figure 6.10 by a noncircular gear pair.

Two Independent Loops

An inspection of Table 6.4 reveals that both (4, 5) and (5, 6) graphs are suitable for construction of one-dof geared mechanisms having two independent loops.

(4, 5) Geared Mechanisms. For the (4, 5) graph, there must be two gear pairs and three one-dof joints. For the purpose of illustration, let us assume that only revolute and gear pairs are used. Then, the problem becomes a determination of labeling the edges with two *G* pairs and three *R* joints. This is equivalent to a 2-coloring problem in graph theory. To prevent the creation of a partially locked kinematic chain, at least one of the three edges in each triangular loop must be labeled as a *G*-edge. For this simple case, however, the problem can be solved by inspection. Figure 6.11 shows three nonisomorphic labeled graphs and the corresponding gear trains sketched by using external gear pairs. Many different geared mechanisms can be derived by performing the kinematic inversion. For example, if link 1 of the first geared mechanism shown in Figure 6.11 is chosen as the fixed link, the resulting mechanism is an ordinary gear train. However, if link 4 is chosen as the fixed link, the mechanism becomes a planetary gear train.

Note that if we allow the gear pairs to assume various combinations of internal and external meshes, the number of possible geared mechanisms will be more than tripled.

No.	Structure	Mechanism	Comments
1			Simple gear set
2			Simple planetary gear set
3			Rack and pinion
4			Involute motion
5			Inverse rack and pinion

FIGURE 6.10
Geared three-link mechanisms.

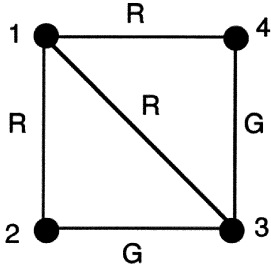
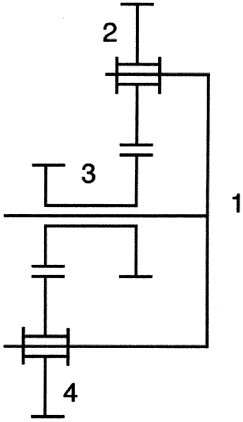
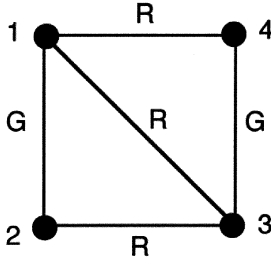
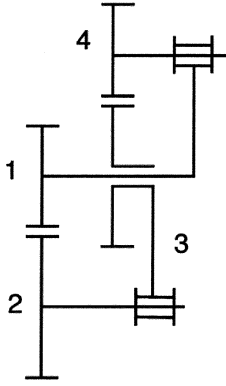
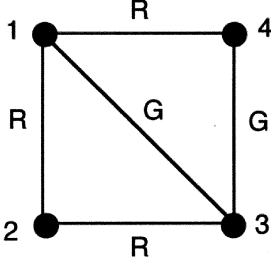
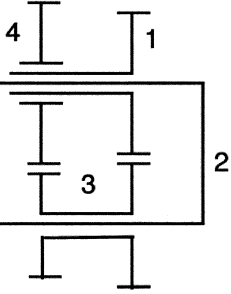
No.	Labeled graphs	Gear trains
1		
2		
3		

FIGURE 6.11
Four-link gear trains.

(5, 6) Geared Mechanisms. Next, we consider the (5, 6)-*a* graph listed in Appendix C. As can be seen from Table 6.4, there must be one gear pair, whereas the remaining joints can be revolute or prismatic. To prevent the formation of a partially locked structure, one of the joints in the three-link loop must be a gear pair. Assuming that only a revolute pair is employed for the one-dof joints, there exist two nonisomorphic labeled graphs as shown in Figure 6.12. The first kinematic chain shown in Figure 6.12 consists of a simple gear pair and a four-bar linkage. The second kinematic chain shown in Figure 6.12 is the well-known geared five-bar mechanism.

No.	Graph	Geared Kinematic Chains
1		
2		

FIGURE 6.12
Geared five-bar chains.

6.2.3 Planar Cam Mechanisms

The enumeration of cam mechanisms is similar to that of geared mechanisms. Since the degrees of freedom associated with a cam pair is identical to that of a gear pair, we can practically replace any gear pair in a geared mechanism by a cam pair without affecting its mobility. For three-link cam mechanisms, we also include the PPC_p labeling. Hence, we have

$$RRC_p, \text{ } RPC_p, \text{ and } PPC_p.$$

Figure 6.13 shows seven nonisomorphic three-link cam mechanisms obtained by assigning different fixed links. In practice, a spring is incorporated in a cam

No.	Graph	Mechanism	Comments
1			Cam-Lever
2			Differential Cam
3			Cam-and-Follower
4			Differential Cam-and-Follower
5			Differential Cam-and-Follower
6			Double Slot-and-Cam Mechanism
7			Inverted Double Slot-and-Cam Mechanism

FIGURE 6.13
Three-link cam mechanisms.

mechanism to keep the cam pair in contact. Finally, we note that more complicated cam mechanisms can be enumerated.

6.3 Spherical Mechanisms

The only available joint type for construction of spherical linkages is the revolute joint. Furthermore, all joint axes must intersect at a common point called the *spherical center*. Since the motion parameter, λ , of spherical mechanisms is identical to that of planar mechanisms, the classification of spherical linkages can be accomplished along the same line as planar bar-linkages. In the following, we simply point out a few known spherical linkages.

The universal joint shown in Figure 1.11 is a spherical four-bar linkage. The four revolute joint axes intersect at a common point, O . The universal joint is used for connecting two intersecting nonparallel shafts.

Another type of spherical linkage is the three-dof orientation mechanism shown in Figure 6.14 [9, 10]. The mechanism consists of a moving platform, link 7, that is connected to a fixed base, link 0, by three kinematically identical limbs. All the revolute joint axes intersect at a common point, O . The orientation of the moving platform is controlled by actuating the three input links 1, 2, and 3.

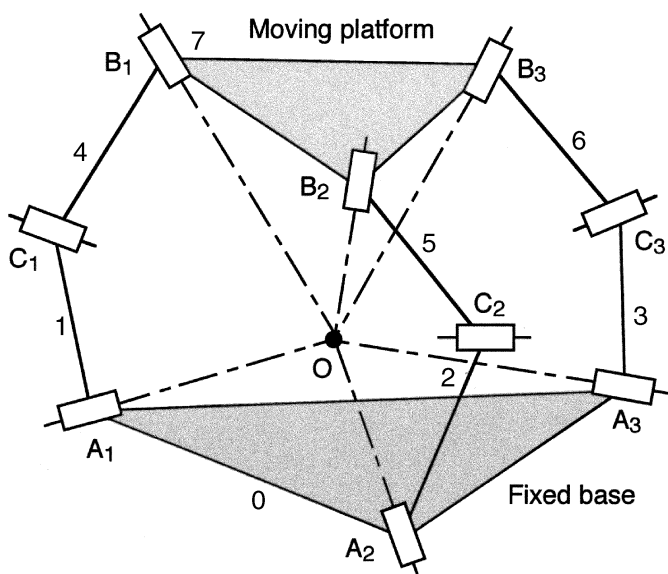


FIGURE 6.14
Spherical parallel manipulator.

Most robotic wrists are geared spherical mechanisms [2, 15, 18, 19, 24]. For the mechanism shown in Figure 6.15, link 1 is the base link; links 2, 5, and 6 are three coaxial input links; and link 4 is the output link, which is called the *end-effector*. The end-effector is free to rotate about three intersecting joint axes, *a*, *b*, and *c*. Rotations of the three input links are transmitted to the end-effector by three bevel-gear pairs, (5, 3), (6, 7), and (7, 4). Together, it forms a three-dof spherical wrist mechanism. The enumeration of spherical wrist mechanisms will be discussed in more details in a chapter to follow.

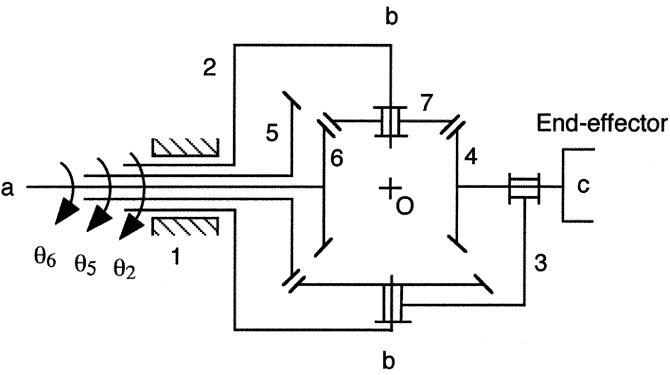


FIGURE 6.15
Geared spherical wrist mechanism.

6.4 Spatial Mechanisms

For spatial mechanisms, we limit ourselves to the following kinematic pairs: revolute (*R*), prismatic (*P*), helical (*H*), cylindric (*C*), spherical (*S*), and plane (*E*) pairs. These kinematic pairs can be grouped according to their joint degrees of freedom as shown in Table 6.5.

Table 6.5 Classification of Kinematic Pairs.	
Joint Degrees of Freedom	Available Joint Types
1	R, P, H
2	C
3	S, E

Other more complicated kinematic pairs are excluded from the following discussions. If such joints are considered, they can be replaced by a combination of two

lower-pair joints with an intermediate link to achieve compactness and good surface contact. For example, Figure 6.16a shows a washing machine agitator mechanism that is made up of three links connected by a revolute, R , sphere-in-cylinder, S_c , and cylindric, C , joint. As the input link 2 rotates, the output link 3 will oscillate and reciprocate simultaneously to generate a washing action. The sphere-in-cylinder joint can be replaced by a revolute and a spherical joint with an intermediate link 4 as shown in Figure 6.16b.

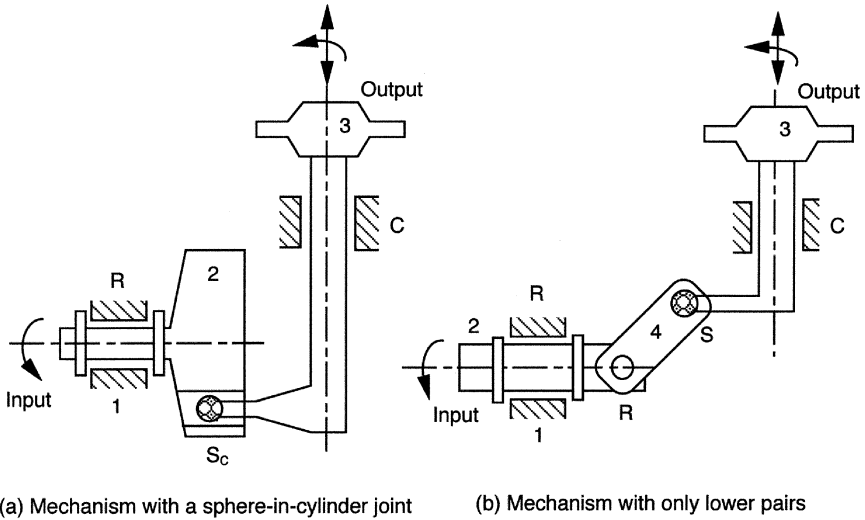


FIGURE 6.16
Washing machine agitator mechanisms.

Under the above assumption, the total number of joints can be written as

$$j = j_1 + j_2 + j_3 . \quad (6.10)$$

The total number of degrees of freedom in all joints is given by

$$\sum_{i=1}^j f_i = j_1 + 2j_2 + 3j_3 . \quad (6.11)$$

Substituting $\lambda = 6$ and Equation (6.11) into Equation (4.7) yields

$$j_1 + 2j_2 + 3j_3 = F + 6L . \quad (6.12)$$

Equation (6.12) is useful for determination of the number of joints for each type of kinematic pair. Given the number of degrees of freedom, the number of loops, and the number of links, we solve Equations (4.5) for the number of joints, and then Equations (6.10) and (6.12) for all possible combinations of joint types.

6.4.1 Spatial One-dof Mechanisms

For spatial one-dof mechanisms, we first solve Equation (4.5) for the number of joints in terms of the number of independent loops and the number of links. Then, we solve Equations (6.10) and (6.12) for all possible combinations of the joint types. We do this by applying the *nested-do loops* algorithm described in Appendix A. The results are summarized in Table 6.6. Note that we have restricted the number of three-dof joints to one in single-loop chains and two in double-loop chains to avoid the possibility of forming passive degrees of freedom.

Table 6.6 Classification of Spatial One-dof Mechanisms.

Class	Type	No. of Links	No. of Joints	No. of 1-dof Joints	No. of 2-dof Joints	No. of 3-dof Joints
L		n	j	j_1	j_2	j_3
1	021	3	3	0	2	1
	211	4	4	2	1	1
	130	4	4	1	3	0
	401	5	5	4	0	1
	320	5	5	3	2	0
	510	6	6	5	1	0
	700	7	7	7	0	0
2	132	5	6	1	3	2
	051	5	6	0	5	1
	322	6	7	3	2	2
	241	6	7	2	4	1
	160	6	7	1	6	0
	512	7	8	5	1	2
	431	7	8	4	3	1
	350	7	8	3	5	0

Each *type* listed in Table 6.6 is denoted by a three-digit number representing the number of one-, two-, and three-dof joints, respectively [12]. For example, the type 211 chain contains 2 one-dof, 1 two-dof, and 1 three-dof joints.

Since each joint of a given type can assume several different kinematic pairs, we can further divide each type by the kind of joints incorporated in the kinematic chain. Such a listing is called a *kind*. For example, the type 211 chain can be further classified into the following kinds: *RRCS*, *RPCS*, *RHCS*, *PPCS*, *PHCS*, *HHCS*, *RRCE*, *RPCE*, *RHCE*, *PPCE*, *PHCE*, and *HHCE*. The above symbolic notations can also be written as *2RCS*, *RPCS*, *RHCS*, *2PCS*, etc. In what follows, we limit the number of prismatic joints to no more than two since mechanisms having more than two prismatic joints are not very practical.

The joints in each *kind* are used to label the edges of a graph. Two labelings are said to be *equivalent* if their corresponding labeled graphs are isomorphic. Therefore, we need to enumerate nonisomorphic labeled graphs of a given kind. For simple kinematic chains, the enumeration can be accomplished by inspection. For complicated

kinematic chains, a computer algorithm employing partitioning and combinatorial schemes is necessary.

Various mechanisms are obtained by selecting a different member of a kinematic chain as the fixed link. This procedure is fairly straightforward. However, some of the inverted mechanisms may be kinematically isomorphic to each other, whereas others may be impractical for applications.

Single-Loop Mechanisms

For single-loop mechanisms, the number of joints is equal to the number of links and all the links are necessarily binary. Furthermore, the joint degrees of freedom should sum up to seven,

$$\sum_{i=1}^j f_i = 7. \quad (6.13)$$

Three-Link Chains. There exists only one type of three-link chain, type 021, which can be classified into two kinds: *CCS* and *CCE*. Note that in constructing a link with two cylindric joints, the two joint axes should not be parallel to each other, otherwise a passive degree of freedom will be introduced. Similarly, in constructing a pair of *C-E* joints, the axis of the cylindric joint should not be parallel to the plane of the *E* pair. Lastly, we note that a mechanism having an input link connected to the ground by a cylindric or spherical joint is not practical, since it is difficult to control the motion of such a joint. Therefore, spatial three-link chains are not very practical.

Four-Link Chains. There are two types of four-link chains: types 211 and 130. Type 211 can be classified into 12 kinds: *RRCS*, *RPCS*, *RHCS*, *PPCS*, *PHCS*, *HHCS*, *RRCE*, *RPCE*, *RHCE*, *PPCE*, *PHCE*, and *HHCE*; whereas type 130 can be classified into three kinds: *RCCC*, *PCCC*, and *HCCC*. Making all possible permutations of the joints yields 33 nonisomorphic labeled graphs of four-link chains as shown in Table E.1, Appendix E.

Five-Link Chains. There are two types of five-link chains: types 401 and 320. To further simplify the problem, let the helical joint be excluded from consideration. Then, type 401 can be classified into six kinds: *RRRRS*, *RRRPS*, *RRPPS*, *RRRRE*, *RRRPE*, and *RRPPE*; whereas type 320 can be classified into three kinds: *RRRCC*, *RRPCC*, and *RPPCC*. Table E.2 in Appendix E shows 24 nonisomorphic labeled graphs of five-link chains.

Six-Link Chains. There exists only one type of six-link chain: type 510. Excluding the helical joint, this type of kinematic chain can be classified into three kinds: *RRRRRC*, *RRRRPC*, and *RRRPPC*. Table E.3 in Appendix E shows ten nonisomorphic labeled graphs of six-link chains.

Seven-Link Chains. There exists only one type of seven-link chain: type 700. Excluding the helical joint, this type of kinematic chain can be classified into three

kinds: $RRRRRRR$, $RRRRRRP$, and $RRRRRPP$. Table E.4 in Appendix E shows five nonisomorphic labeled graphs of seven-link chains.

By assigning different links as the fixed link, numerous mechanisms can be constructed from the kinematic chains given above. Some of the mechanisms constructed may be mechanically complex and, therefore, have limited applications. The four- and five-link mechanisms are of practical interest because they are relatively simple. We conclude this section by pointing out a few sample mechanisms. Figure 6.17 shows a spatial $RCCC$ mechanism, which converts a continuous rotation of link 2 to a reciprocating and oscillating motion of link 4. Figure 3.16 shows a spatial $RRSP$ Z-crank mechanism, which can be used as an engine or compressor mechanism. Figure 4.15 shows a spatial $RSSR$ mechanism with a passive degree-of-freedom. Figure 4.16 shows a spatial $RRSRR$ constant-velocity shaft coupling. Similarly, one-dof, two-loop spatial mechanisms can be enumerated and classified according to the type and kind of joint arrangements.

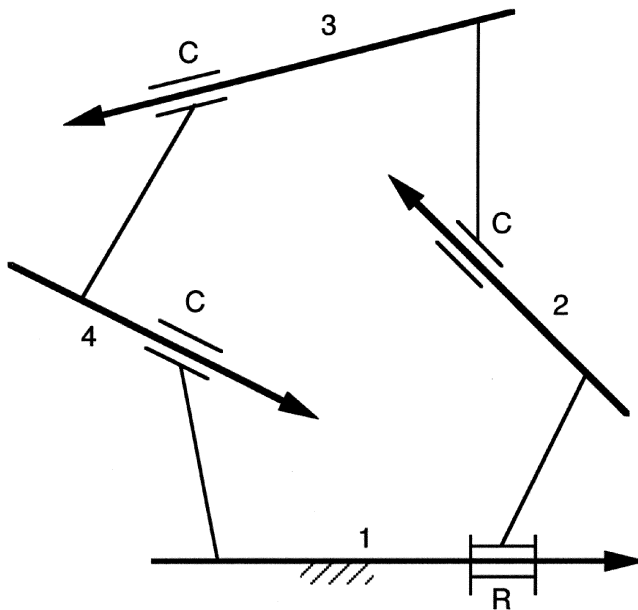


FIGURE 6.17
RCCC spatial four-bar linkage.

6.4.2 Spatial Multi-dof, Multiple-Loop Mechanisms

Spatial multi-dof, multiloop mechanisms can be found in relatively few applications. One commonly known example is the automobile suspension mechanism. Recently, however, there has been an increasing interest in the study of multi-dof spatial mechanisms, particularly the robotics and machine tools industry. An

entirely new class of mechanisms known as *parallel kinematics machines* or *parallel manipulators* will be studied in Chapter 9.

6.5 Summary

In this chapter, we classified mechanisms according to their nature of motion into planar, spherical, and spatial mechanisms. Then we further classified these mechanisms by their degrees of freedom, number of loops, number of links, and types of joints. An atlas of planar linkages with one, two, and three degrees of freedom is developed in Appendix D. In addition, geared mechanisms, cam mechanisms, spherical mechanisms, and spatial one-dof mechanisms are also classified.

References

- [1] Anonymous, 1973, Variable Camshaft Boosts Engine Efficiency, *Automotive Engineering*, 81, 12, 11–13.
- [2] Anonymous, 1982, Bevel Gears Make Robot's Wrist More Flexible, *Machine Design*, 54, 18, 55.
- [3] Crossley, F.R.E., 1964, A Contribution to Grübler's Theory in Number Synthesis of Plane Mechanisms, *ASME Journal of Engineering for Industry*, Series B, 86, 1–8.
- [4] Franke, R., 1951, *Vom Aufbau der Getriebe*, Vols. I-II, Doesseldorf, VDI-Verlag (and 1985).
- [5] Freudenstein, F., 1978, Designing Crank and Rocker Linkages with Optimum Force Transmission, *Product Engineering*, 45–47.
- [6] Freudenstein, F. and Maki, E.R., 1979, Creation of Mechanisms According to Kinematic Structure and Function, *Journal of Environmental and Planning B*, 6, 375–391.
- [7] Freudenstein, F. and Primrose, E.J.F., 1973, The Classical Transmission Angle Problem, in *Proceedings of the Mechanisms Conference*, Institution of Mechanical Engineers, London, 105–110.
- [8] Freudenstein, F., Tsai, L.W., and Maki, E.R., 1984, The Generalized Oldham Coupling, *ASME Journal of Mechanisms, Transmissions, and Automation in Design*, 106, 4, 475–481.

- [9] Gosselin, C. and Angeles, J., 1989, The Optimum Kinematic Design of a Spherical Three-Degree-of-Freedom Parallel Manipulator, *ASME Journal of Mechanisms, Transmissions, and Automation in Design*, 111, 202–207.
- [10] Gosselin, C. and Hamel, J., 1994, The Agile Eye: A High-Performance Three-Degree-of-Freedom Camera-Orienting Device, *IEEE International Conference on Robotics and Automation*, San Diego, CA, 781–786.
- [11] Gupta, K.C., 1977, Design of Four-bar Function Generators with Mini-Max Transmission Angle, *ASME Journal of Engineering for Industry*, Series B, 99, 2, 360–366.
- [12] Harrisberger, L., 1965, A Number Synthesis Survey of Three-Dimensional Mechanisms, *ASME Journal of Engineering for Industry*, Series B, 213–220.
- [13] Mayourian, M. and Freudenstein, F., 1984, The Development of an Atlas of the Kinematic Structures of Mechanisms, *ASME Journal of Mechanisms, Transmissions, and Automation in Design*, 106, 458–461.
- [14] Read, R.C. and Wilson, R.J., 1998, *An Atlas of Graphs*, Oxford University Press, New York, NY.
- [15] Rosheim, M.E., 1989, *Robot Wrist Actuators*, John Wiley & Sons, New York, NY.
- [16] Sohn, W., 1987, A Computer-Aided Approach to the Creative Design of Mechanisms, Ph.D. Dissertation, Dept. of Mechanical Engineering, Columbia University, New York, NY.
- [17] Sohn, W. and Freudenstein, F., 1986, An Application of Dual Graphs to the Automatic Generation of the Kinematic Structures of Mechanism, *ASME Journal of Mechanisms, Transmissions, and Automation in Design*, 108, 3, 392–398.
- [18] Stackhouse, T., 1979, A New Concept in Wrist Flexibility, in *Proceedings of the 9th International Symposium on Industrial Robots*, Washington, D.C., 589–599.
- [19] Trevelyan, J.P., Kovesi, P.D., Ong, M., and Elford, D., 1986, ET: A Wrist Mechanism without Singular Positions, *The International Journal of Robotics Research*, 4, 4, 71–85.
- [20] Tsai, L.W., 1983, Design of Drag-Link Mechanisms with Optimum Transmission Angle, *ASME Journal of Mechanisms, Transmissions, and Automation in Design*, 105, 2, 254–258.
- [21] Tsai, L.W., 1983, Design of Drag-Link Mechanisms with Minimax Transmission Angle Deviation, *ASME Journal of Mechanisms, Transmissions, and Automation in Design*, 105, 4, 686–691.
- [22] Tsai, L.W., 1984, Oldham Coupling Second-Harmonic Balancer, *ASME Journal of Mechanisms, Transmissions, and Automation in Design*, 106, 3, 285–290.

- [23] Tsai, L.W., 1984, Half Speed Balancer, U.S. Patent 4,440,123.
 - [24] Tsai, L.W., 1999, *Robot Analysis: The Mechanics of Serial and Parallel Manipulators*, John Wiley & Sons, New York, NY.
 - [25] Tsai, L.W. and Jacques, R.L., 1984, Balancer for 90 Degree V6 Engines and the Like, U.S. Patent 4,480,607.
 - [26] Tsai, L.W., Maki, E.R., and Jacques, R.C., 1988, Evaluation of the Oldham-Coupling-Type Balancer on a 90-degree V-6 Engine, *SAE Transactions*, 96, 4.10–4.15.
 - [27] Tsai, L.W. and Walter, R., 1984, Evaluation of the Oldham-Coupling-Type Balancer on a 2.5 Liter In-line Four-Cylinder Engine, *SAE 1984 Transactions*, 93, 3.378–3.382.
 - [28] Woo, L.S., 1967, Type Synthesis of Plane Linkages, *ASME Journal of Engineering for Industry*, Series B, 89, 159–172.
-

Exercises

- 6.1 For planar mechanisms made up of only sliding pairs, the motion parameter is $\lambda = 2$. Enumerate this type of one-dof mechanism having four links. Identify the fixed link.
- 6.2 Enumerate all feasible planar, one-dof, six-bar linkages with ground-connected rotatory input and sliding output. Assume that all other joints are revolute.
- 6.3 Enumerate all feasible planar, two-dof, seven-bar linkages with two ground-connected rotatory inputs and one floating output. Assume that all other joints are revolute.
- 6.4 Enumerate the graphs of planar three-dof, ten-bar linkages having a vertex degree listing of $n_2 = 8$, $n_3 = 0$, $n_4 = 2$, and $n_5 = 0$.
- 6.5 Enumerate the graphs of planar three-dof, ten-bar linkages having a vertex degree listing of $n_2 = 6$, $n_3 = 4$, $n_4 = 0$, and $n_5 = 0$.
- 6.6 Enumerate all feasible planar, three-dof, eight-bar linkages with three ground-connected input sliders and one floating output, assuming that all other joints are revolute. Draw the functional schematics illustrating how the input sliders can be arranged geometrically.
- 6.7 Using only revolute joints and gear pairs, enumerate two-dof planar geared mechanisms with four and five links.

- 6.8 Why are the bevel-gear and revolute joints suitable for spherical motion? Enumerate all the feasible spherical mechanisms with four and five links.

Chapter 7

Epicyclic Gear Trains

7.1 Introduction

Gear trains are used to transmit motion and/or power from one rotating shaft to another. An enormous number of gear trains are used in machinery such as automobile transmissions, machine tool gear boxes, robot manipulators, and so on. Perhaps, the earliest known application of gear trains is the *South Pointing Chariot* invented by the Chinese around 2600 B.C. The chariot employed an ingenious differential gear train such that a figure mounted on top of the chariot always pointed to the south as the chariot was towed from one place to another. It is believed that the ancient Chinese used this device to help them navigate in the Gobi desert. Other early applications include clocks, cord winding and rope laying machines, steam engines, etc. A historical review of gear trains, from 3000 B.C. to the 1960s, can be found in Dudley [3].

A gear train is called an *ordinary gear train* if all the rotating shafts are mounted on a common stationary frame, and a *planetary gear train* (PGT) or *epicyclic gear train* (EGT) if some gears not only rotate about their own joint axes, but also revolve around some other gears. A gear that rotates about a central stationary axis is called the *sun* or *ring* gear depending on whether it is an external or internal gear, and those gears whose joint axes revolve about the central axis are called the *planet gears*. Each meshing gear pair has a supporting link, called the *carrier* or *arm*, which keeps the center distance between the two meshing gears constant.

Figure 7.1 shows a compound planetary gear train commonly known as the *Simpson gear set*. The Simpson gear set consists of two basic PGTs, each having a sun gear, a ring gear, a carrier, and four planets. The two sun gears are connected to each other by a common shaft, whereas the carrier of one basic PGT is connected to the ring gear of the other PGT by a spline shaft. Overall, it forms a one-dof mechanism. This gear set is used in most three-speed automotive automatic transmissions.

In this chapter, we describe a systematic methodology for enumeration of epicyclic gear trains with no specific applications in mind. Since the main emphasis is on enumeration, readers should consult other books for more detailed descriptions of the gear geometry, gear types, and other design considerations.

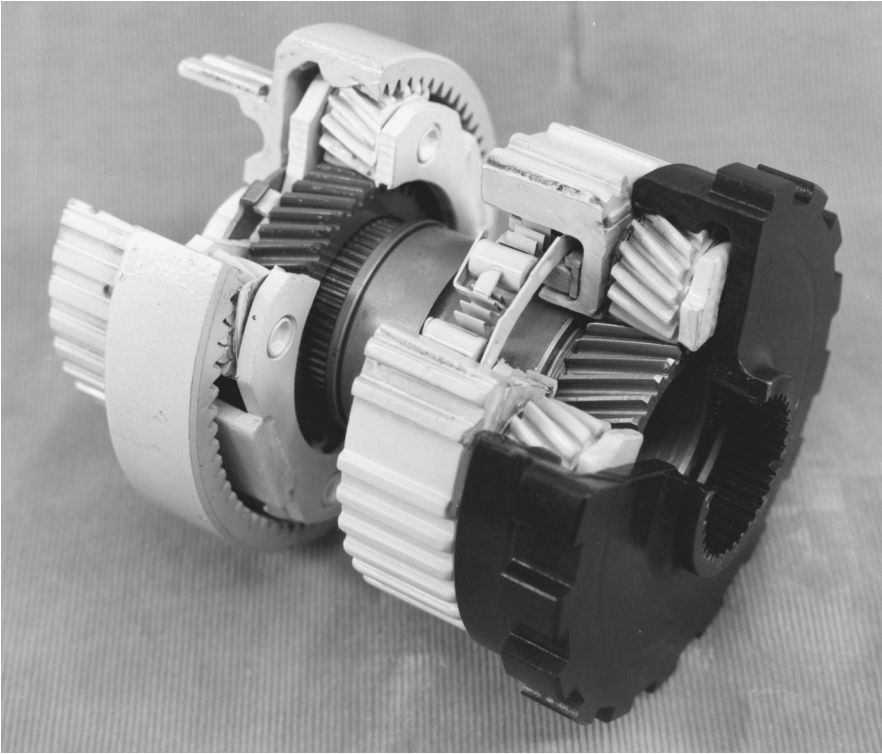


FIGURE 7.1
Compound planetary gear train.

7.2 Structural Characteristics

Epicyclic gear trains belong to a special class of geared kinematic chains. In addition to satisfying the general structural characteristics outlined in Chapters 4 and 6, the following constraints are imposed [2]:

1. All links of an epicyclic gear train are capable of unlimited rotation.
2. For each gear pair, there exists a carrier, which keeps the center distance between the two meshing gears constant.

Based on the above two constraints, the geared five-bar mechanism discussed in Chapter 6 is not an epicyclic gear train. In what follows, we study the effects of these two constraints on the structural characteristics of epicyclic gear trains.

For all links to possess unlimited rotation, the prismatic joint is excluded from design consideration. Hence only revolute joints and gear pairs are allowed for

structure synthesis of EGTs. For convenience, we use a *thin edge* to represent a revolute joint (or turning pair) and a *thick edge* to stand for a gear pair. For this reason, thin edges are sometimes called *turning-pair edges* and thick edges are called *geared edges*.

Let j_g denote the number of gear pairs and j_t represent the number of revolute joints. It is clear that the total number of joints is given by

$$j = j_t + j_g . \quad (7.1)$$

Substituting Equations (6.7) and (7.1) into Equation (4.3), we obtain

$$F = 3(n - 1) - 2j_t - j_g . \quad (7.2)$$

The first constraint implies that there should not be any circuit formed exclusively by turning pairs. Otherwise, either the circuit will be locked or rotation of the links will be limited. The second constraint implies that all vertices should have at least one incident edge that represents a turning pair. Hence, we have

THEOREM 7.1

The subgraph obtained by removing all geared edges from the graph of an EGT is a tree.

Since a tree of v vertices contains $v - 1$ edges, we further conclude that

$$j_t = n - 1 . \quad (7.3)$$

Substituting Equations (7.1) and (7.3) into Equation (4.5), we obtain

$$j_g = L . \quad (7.4)$$

Substituting Equations (7.3) and (7.4) into Equation (7.2) yields

$$L = n - 1 - F = j_t - F . \quad (7.5)$$

Eliminating j_t and j_g from Equations (7.1), (7.4), and (7.5) yields

$$j = F + 2L , \quad (7.6)$$

Summarizing Equations (7.3), (7.4), and (7.5) in words, we have

THEOREM 7.2

In epicyclic gear trains, the number of gear pairs is equal to the number of independent loops; the number of turning pairs is equal to the number of links diminished by one; and the number of degrees of freedom is equal to the difference between the number of turning pairs and the number of gear pairs.

In Chapter 4, we have shown that the degree of a vertex is bounded by Equation (4.10). In terms of kinematic chains,

$$L + 1 \geq d_i \geq 2. \quad (7.7)$$

In words, we have:

THEOREM 7.3

The degree of any vertex in the graph of an EGT lies between 2 and $L + 1$.

In general, the graph of an EGT should not contain any circuit that is made up of only geared edges. Otherwise, the gear train may rely on special link length proportions to achieve mobility. In the case where geared edges form a loop, the number of edges must be even. For example, Figure 7.2 shows a two-dof differential gear train in which gears 3, 4, 5, and 6 form a loop. The four gears are sized such that the pitch diameter of gear 3 is equal to that of gear 5, and the pitch diameter of gear 4 is equal to that of gear 6. Otherwise, the mechanism will not function properly. In fact, we may consider either gear 4 or 6 as a redundant link. That is, removing either gear 4 or 6 from the mechanism does not affect the mobility of the mechanism. This is a typical *fractionated mechanism* in that links 2, 3, 4, 5, and 6 form a one-dof gear train and the second degree of freedom comes from the fact that the gear train itself can rotate as a rigid body about the “a–a” axis.

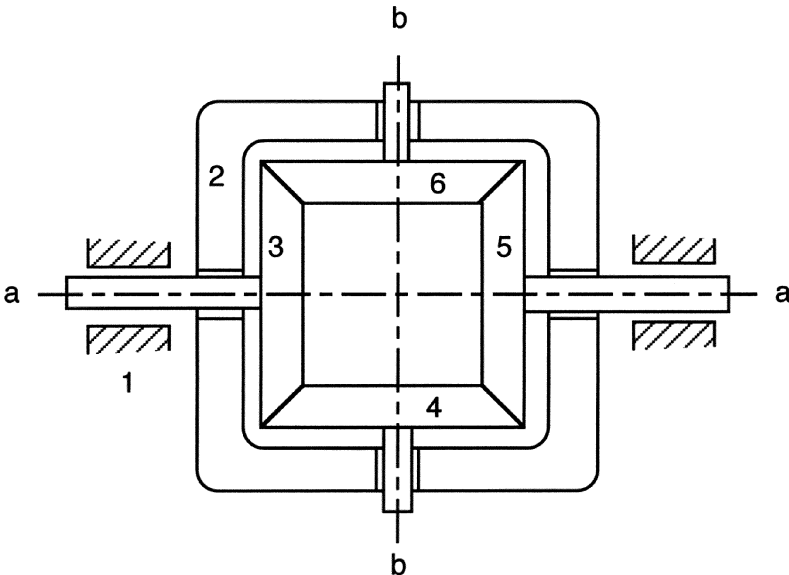


FIGURE 7.2

A differential gear train.

Recall that the subgraph obtained by removing all geared edges from the graph of an EGT is a tree. Any geared edge added onto the tree forms a unique circuit called the *fundamental circuit*. In other words, each fundamental circuit is made up of one geared edge and several turning-pair edges. These turning pairs are responsible for maintaining a constant center distance between the two gears paired by the geared edge. Therefore, the axes of all turning pairs in a fundamental circuit can be associated with two distinct lines in space, one passing through the axis of one gear and the other passing through the axis of the second gear.

Let each turning-pair edge be labeled by a *letter* called the *level*. In this manner, each label or level denotes an axis of a turning pair in space. We define the turning-pair edges that are adjacent to the geared edge of a fundamental circuit as the *terminal edges*. Then, the requirement for constant center distance between two meshing gears can be stated as:

THEOREM 7.4

In an EGT, there are two and only two edge levels between the terminal edges of a fundamental circuit. In other words, there exists one and only one vertex, called the transfer vertex, in each fundamental circuit such that all the turning-pair edges lying on one side of the transfer vertex share one edge level and all the other turning-pair edges lying on the opposite side of the transfer vertex share a different level.

The transfer vertex of a fundamental circuit corresponds to the *carrier* or *arm* of a gear pair. We note that a vertex in the graph of an EGT may serve as the transfer vertex for more than one fundamental circuit. From a mechanical point of view, any vertex having only two incident turning-pair edges must serve as the transfer vertex of a fundamental circuit.

A graph having several turning-pair edges of the same level implies that there are several coaxial links in the corresponding kinematic chain. Hence,

COROLLARY 7.1

All edges of the same level in the graph of an EGT together with their end vertices form a tree.

For example, Figure 7.3a depicts the schematic diagram of the Simpson gear set shown in Figure 7.1. The corresponding graph with its turning pair edges labeled according to their axis locations is shown in Figure 7.3b. Readers can easily verify that Equations (7.3) through (7.5) are satisfied. Removing all the geared edges from the graph leads to a spanning tree as shown Figure 7.3c. Putting the geared edges back on the tree one at a time results in four fundamental circuits as shown in Figures 7.3d through g. From the above corollary, we see that the transfer vertices of these four fundamental circuits are 1, 1, 2, and 2, respectively.

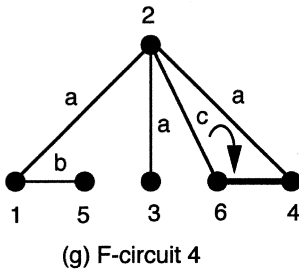
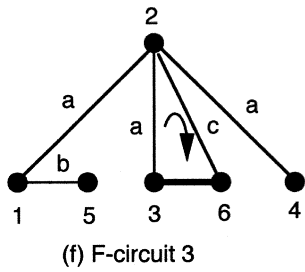
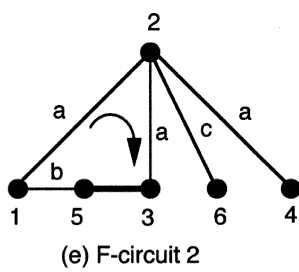
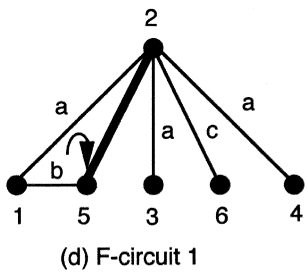
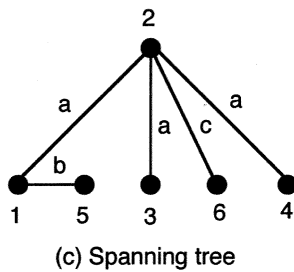
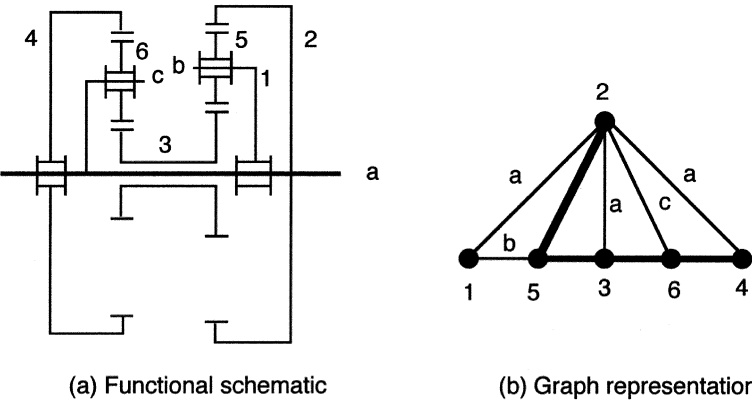


FIGURE 7.3
Graph, spanning tree, and fundamental circuits of an EGT.

We summarize the structural characteristics for the graphs of EGTs as follows:

- C1. The graph of an F -dof, n -link EGT contains $(n - 1)$ turning-pair edges and $n - 1 - F$ geared edges.
- C2. The subgraph obtained by removing all geared edges from the graph of an EGT is a tree.
- C3. Any geared edge added onto the tree forms one unique circuit, called the *fundamental circuit* having one geared edge and several turning-pair edges. Consequently, the number of fundamental circuits is equal to the number of geared edges.
- C4. Each turning-pair edge can be characterized by a *level* that identifies the axis location in space.
- C5. There exists a vertex, called the *transfer vertex*, in each fundamental circuit such that all turning-pair edges lying on one side of the transfer vertex have the same edge level and all turning-pair edges on the opposite side of the transfer vertex share a different edge level.
- C6. Any vertex that has only thin edges incident to it must serve as a transfer vertex of at least one fundamental circuit. In other words, no vertex can have all its incident edges on the same level.
- C7. Turning-pair edges of the same level and their end vertices form a tree.
- C8. The graph of an EGT should not contain any circuit that is made up of only geared edges.

7.3 Buchsbaum–Freudenstein Method

The structural characteristics discussed in the previous section are applicable for both spur and bevel gear trains. Any graph that satisfies the criteria represents a feasible solution. Several heuristic methods of enumeration have been developed by researchers. Perhaps, the first methodology was due to Buchsbaum and Freudenstein [2]. The method involves the following steps:

- S1. Determination of nonisomorphic unlabeled graphs (no distinction between turning and gear pairs).

Given the number of degrees of freedom and the number of links, we search for those unlabeled graphs that satisfy the first structural characteristic, C1, from the atlas of graphs listed in Appendix C. These graphs are classified in accordance with the number of degrees of freedom, number of independent loops, and

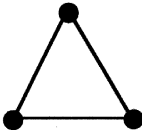
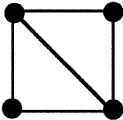
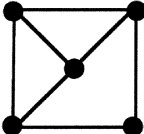
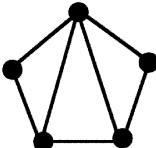
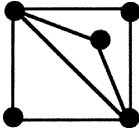
L	v	e	Vertex-degree Listing	Graph
1	3	3	3 0 0 0	
2	4	5	2 2 0 0	
3	5	7	1 4 0 0	
			2 2 1 0	
			3 0 2 0	

FIGURE 7.4
Unlabeled graphs of one-dof EGTs.

vertex-degree listing. Figures 7.4 and 7.5 provide all the feasible unlabeled graphs for one- and two-dof gear trains having one to three independent loops.

S2. Determination of nonisomorphic bicolored graphs.

For each graph obtained in S1, we need to find structurally distinct ways of coloring the edges, one color for the gear pairs and the other for the turning pairs. Specifically, j_g edges of the unlabeled graph are to be assigned as the gear pairs and the remaining edges as the turning pairs. The solution to this problem can be regarded as the number of combinations of j elements taken j_g at a time without repetition. From combinatorial analysis, it can be shown

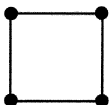
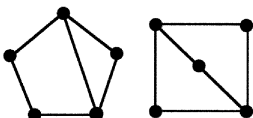
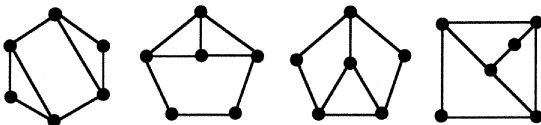
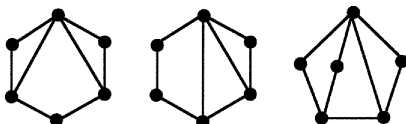
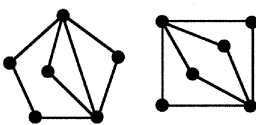
L	v	e	Vertex-degree Listing	Graph
1	4	4	4 0 0 0	
2	5	6	3 2 0 0	
			2 4 0 0	
3	6	8	3 2 1 0	
			4 0 2 0	

FIGURE 7.5

Unlabeled graphs of two-dof EGTs.

that there are

$$C_{j_g}^j = \frac{j!}{j_g!(j - j_g)!} \quad (7.8)$$

possible ways of coloring the edges. A computer program employing a *nested-loops* algorithm can be written to find all possible combinations. For example, we may treat the edges as x_1, x_2, \dots, x_j variables and solve Equation (7.9) for all possible solutions of x_1, x_2, \dots, x_j in ones and zeros, where the “1” represents a gear pair and the “0” a turning pair.

$$x_1 + x_2 + \dots + x_j = j_g. \quad (7.9)$$

We note that some of the graphs obtained by this process may be isomorphic, others may violate the second structural characteristic, C2, and still others may result in partially locked kinematic chains. Hence, the total number of

structurally distinct bicolored graphs would be fewer than the number predicted by Equation (7.8).

For example, the 2210 graph shown in Figure 7.4 has five vertices and seven edges. From the structural characteristic C1, we know that three of the seven edges are to be assigned as gear pairs and the remaining edges as turning pairs. Equation (7.8) predicts $7!/(3!4!) = 35$ possible combinations. After screening out those graphs that do not obey the second structural characteristic, and after eliminating isomorphic graphs, we obtain 12 structurally distinct bicolored graphs as shown in Figure 7.6.

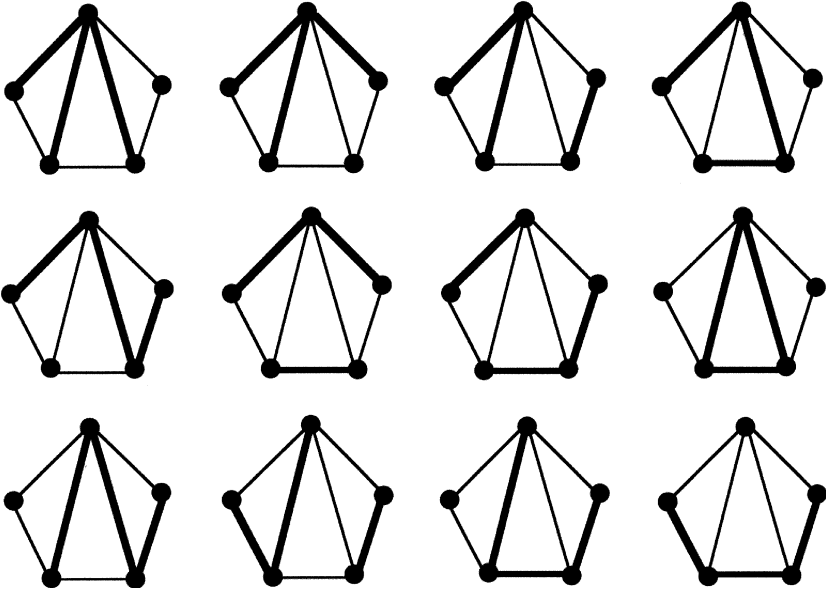


FIGURE 7.6
Bicolored graphs derived from the 2210 graph.

S3. Determination of edge levels.

In this step, the fundamental circuits associated with each bicolored graph derived in the preceding step are identified by applying the third structural characteristic, C3. Then, the turning-pair edges within each fundamental circuit are labeled according to the remaining structural characteristics, C4 through C8. In labeling the turning-pair edges, it is more convenient to start with those fundamental circuits that have fewer numbers of turning-pair edges. In this way, the edge levels can be easily determined by observation. In addition, the number of possible assignments of edge levels for the subsequent circuits is reduced by the fact that some of the edges have already been determined from the preceding circuits. The procedure is continued until all the possible assignments of edge levels are exhausted or the graph is judged to be infeasible.

Consider the graph shown in Figure 7.7a. We start the labeling with the fundamental circuit formed by vertices 1–4–5–1 as shown in Figure 7.7b. Since there are only two turning-pair edges, we can arbitrarily assign a level “a” to the 4–5 edge and a different level “b” to the 1–4 edge. In this regard, vertex 4 serves as the transfer vertex for the circuit. Next, we consider the fundamental circuit defined by the vertices 1–3–4–1. Again, there are only two turning-pair edges associated with the circuit. However, the 1–4 edge level has already been assigned from the previous circuit. Thus, we only need to determine the level of the 3–4 edge. We can assign a new level “c,” or use an existing level “a” for the 3–4 edge as shown in Figures 7.7c and d without violating the structural characteristics C4 through C8. Finally, we consider the fundamental circuit formed by vertices 1–4–3–2–1. Although there are three turning-pair edges associated with the circuit, two of them have already been determined from the other two circuits. Thus, the third edge can be easily determined by observing the fifth structural characteristic, C5. The labeled graphs are shown in Figures 7.7g and h.

As another example, consider the graph shown in Figure 7.8. There are three fundamental circuits. We start the labeling with the circuit formed by vertices 1–4–5–1. Since there are only two turning-pair edges, we can arbitrarily assign a level “a” to the 4–5 edge and a different level “b” to the 1–5 edge. Next, we consider the fundamental circuit defined by the vertices 1–2–3–1. There are only two turning-pair edges associated with this circuit. None of them have been defined from the preceding circuit. Hence, we can arbitrarily assign a new level “c” to the 1–2 edge and another level “d” to the 2–3 edge. This completes the assignment of the second circuit. Finally, we consider the fundamental circuit defined by the vertices 3–2–1–5–4–3. We notice that all the turning-pair edges have already been determined from the other two circuits. A careful examination of the labeling reveals that this circuit contains too many levels, violating the fifth structural characteristic, C5. Hence, we conclude that this graph is not feasible. In fact, this graph should be excluded from the outset since it contains a circuit 1–3–4–1 formed exclusively by geared edges.

S4. Determination of the type of gear meshes.

The two gears paired by each geared edge can assume an external-to-external, external-to-internal, or internal-to-external gear mesh. Therefore, there are 3^{j_g} possible gear mesh arrangements for each labeled graph obtained in S3. Again, some of the arrangements may result in isomorphic mechanisms and should be screened out.

S5. Sketching of the corresponding functional schematics.

In this step, we sketch the functional schematic of each labeled graph. Here we treat an edge of a graph as defining the connection between two links and the thin edge level as defining the axis location of a turning pair. The functional schematic of a labeled graph can be sketched by adhering to the following guidelines.

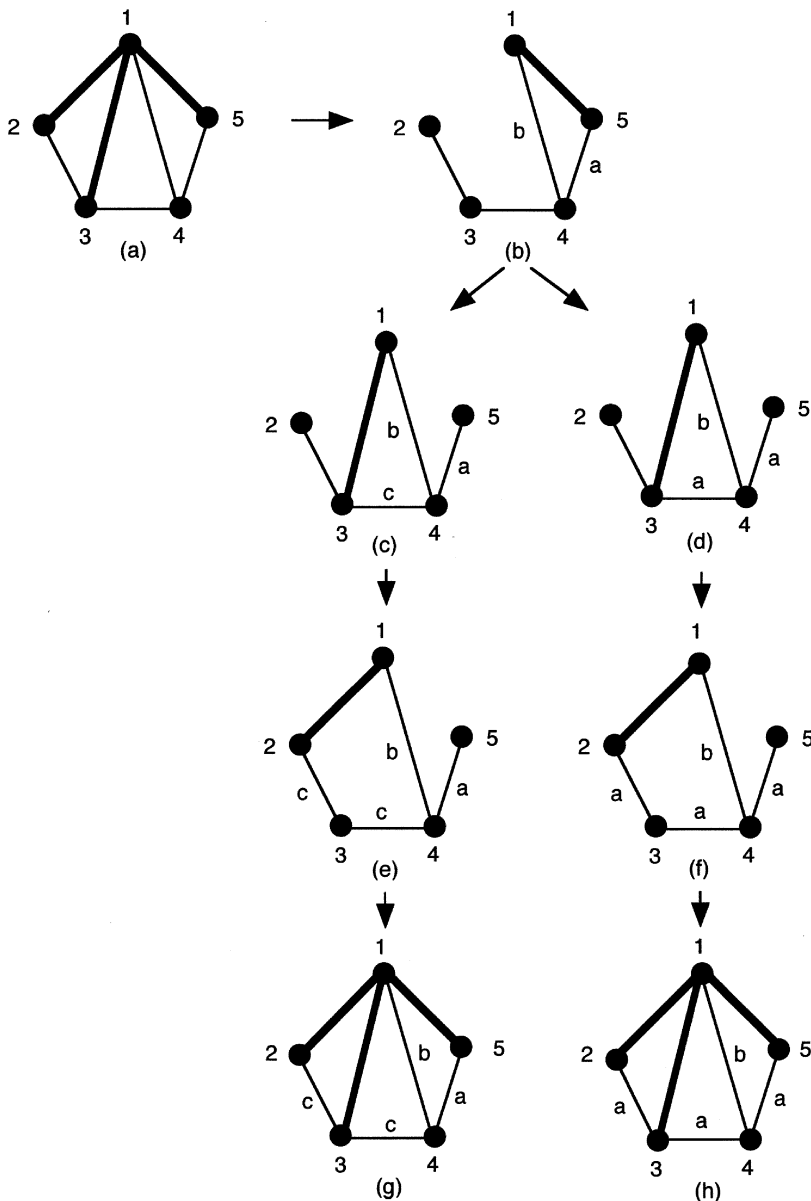
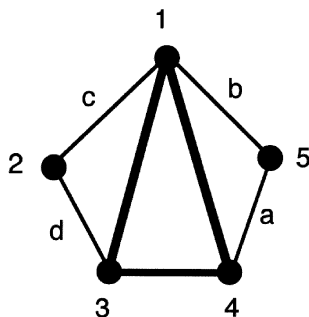


FIGURE 7.7
Two different labelings of turning-pair edges.

**FIGURE 7.8**

A labeled graph that violates the structural characteristics.

1. Sketch a line for each thin edge level. We note that these lines should be drawn parallel to one another for planar epicyclic gear trains, and intersecting at a common point for bevel gear trains. The arrangement of these lines is rather arbitrary and it may occasionally require a rearrangement in order to produce a nice-looking functional mechanism.
2. For each fundamental circuit, draw a pair of gears with their axes of rotation passing through the corresponding center lines defined by the levels of the terminal edges. Connect all gears of the same link number.
3. Draw the remaining links, if any, with their joint axes located on the appropriate center lines in accordance with the edge levels.
4. Complete the remaining turning-pair connections according to the levels of the graph.

For example, Figure 7.9a shows a labeled graph with three fundamental circuits. In sketching the functional schematic of the gear train, we first draw three parallel lines “a,” “b,” and “c” as shown in Figure 7.9b. Then, for the 2–1–3–2 fundamental circuit, we draw a pair of gears (2 and 3) with their axes of rotation passing through the two center lines “a” and “b;” for the 3–1–4–3 fundamental circuit, we draw a second pair of gears (3 and 4) with their rotation axes passing through the center lines “b” and “a;” and for the 4–1–5–4 fundamental circuit, we sketch a third pair of gears (4 and 5) with their axes passing through the center lines “a” and “c,” respectively. We note that link 3 appears in the first and second fundamental circuits. Hence, these two gears are connected as one link. Similarly, link 4 appears in the second and third circuits and, therefore, these two gears are also connected as one link. Finally, we draw link 1, which is the transfer vertex for all fundamental circuits, with its axes of rotation passing through the center lines “a,” “b,” and “c,” and complete all the turning-pair connections in accordance with the edge levels shown in Figure 7.9a. This procedure can be automated by a computer program with a graphical input-output feature.

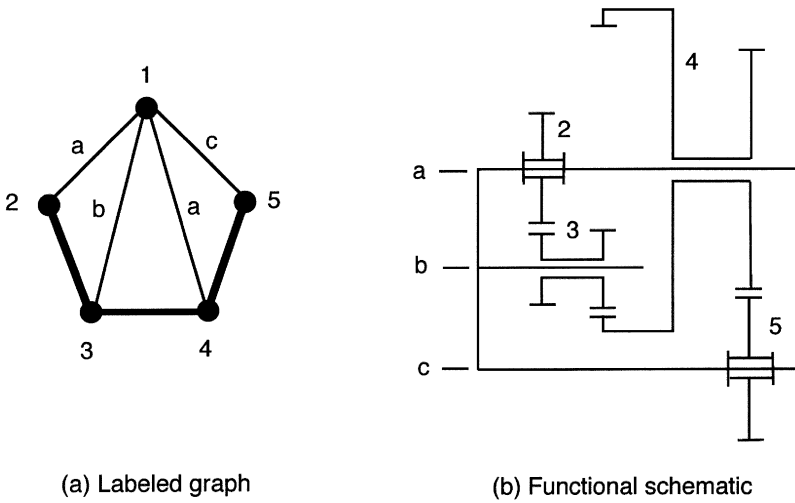


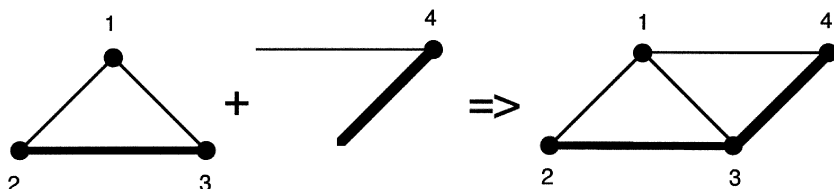
FIGURE 7.9
Sketching of an EGT.

7.4 Genetic Graph Approach

Buchsbaum and Freudenstein's method is a powerful tool for enumeration of EGTs in a systematic and unbiased manner. However, the process becomes more involved as the number of links increases. In this section, we introduce an alternative method called the *genetic graph approach* to improve the efficiency [14].

This approach uses the graph of a basic gear train, called the *genetic graph*, as a building block. In view of the first structural characteristic, each time we increase the number of vertices by one, we also increase the number of loops, the number of turning-pair edges, and the number of geared edges by one. The new vertex can be connected to any vertex of the genetic graph by a turning-pair edge, and to any other vertex by a geared edge, as shown in Figure 7.10a. In this way, $n(n - 1)$ new unlabeled graphs are generated from a genetic graph of n vertices. However, some of the graphs may be rejected due to violation of the structural characteristics, whereas others may be isomorphic to one another. Hence, the total number of nonisomorphic unlabeled graphs is usually fewer than $n(n - 1)$.

The procedure can be automated by a computer program using the adjacency matrix notation and a *nested-do loops* algorithm. Specifically, we start with a given adjacency matrix of order n . Each time we increase the number of vertices by one, we add a row and a corresponding column to the matrix. We first initialize all elements of the new row and the corresponding column to zero. Then we assign a "1" to one element (excluding the diagonal element) in the newly added row (and the corresponding column) for a turning pair, and a "g" to another element for a gear pair. This results



(a) Graph representation

$$A = \begin{bmatrix} 0 & 1 & 1 & : & \# \\ & & & & \vdots \\ 1 & 0 & g & : & \# \\ & & & & \vdots \\ 1 & g & 0 & : & \# \\ \cdots & \cdots & \cdots & & \cdots \\ \# & \# & \# & : & 0 \end{bmatrix}$$

(b) Matrix representation

FIGURE 7.10**Enumeration of EGTs.**

in a matrix of order $n + 1$, representing a new gear train having $n + 1$ links. The process is repeated until all the possible arrangements are exhausted. Finally, graph isomorphisms are checked. Figure 7.10b illustrates the concept of extending a 3×3 matrix to a 4×4 matrix. The upper-left 3×3 submatrix represents the genetic graph shown in Figure 7.10a, and the elements with a pound sign in the fourth row and fourth column are to be filled with a “1” and a “g.” Using this methodology, the first three structural characteristics are automatically satisfied. The process is similar to the conventional method of designing gear trains. A designer starts with a simple gear train and increases the complexity of the design by adding one gear at a time. When a new gear is added, a journal bearing is also incorporated to support the gear.

The approach has been successfully employed for the enumeration of one-dof EGTs with up to five independent loops [9, 14], and the enumeration of two-dof EGTs [16].

7.5 Parent Bar Linkage Method

In this section we introduce another approach called the *parent bar linkage* technique [13]. The parent of a mechanism is defined as that bar linkage that is generated by replacing each q -dof joint in the mechanism with a binary-link chain of length $q - 1$. For example, Figures 7.11a and c show the functional schematic and graph representations of an EGT with two gear pairs. The parent bar linkage is obtained

by replacing each gear pair by two turning pairs and one intermediate binary link as shown in Figures 7.11b and d. We note that the process of joint substitution has no effect on the mobility of a mechanism. The above process can also be reversed; that is, a mechanism with multi-dof joints can be generated by replacing a binary-link chain of length $q - 1$ in a parent bar linkage by a q -dof joint.

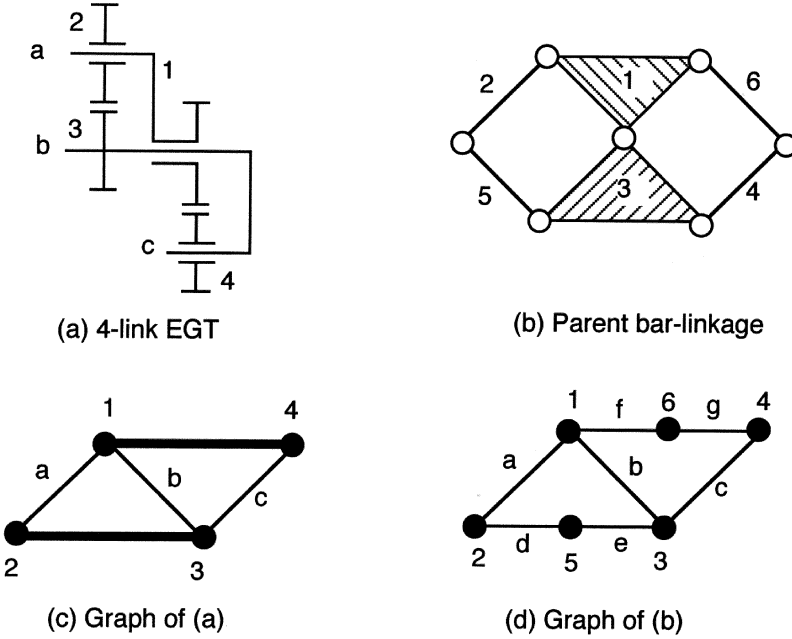


FIGURE 7.11

An epicyclic gear train and its parent bar linkage.

By definition, parent bar linkages have the same number of loops and number of degrees of freedom as the mechanisms generated. Hence, the atlas of bar linkages listed in Appendix D can be used as a basis for generating epicyclic gear trains of the same nature, i.e., same number of degrees of freedom, F , and number of independent loops, L . In general, an n -link bar linkage can be used to construct a gear train, provided that there are at least L number of binary links in the parent bar linkage. The method can summarized as follows.

1. Identify planar bar linkages with the desired number of degrees of freedom, F , and number of independent loops, L , from the atlas of graphs listed in Appendix D. Those parent bar linkages should contain at least one binary vertex in each loop.
2. Replace one binary vertex in each loop along with its incident edges by a geared edge.

3. Eliminate those graphs that do not obey the first and second structural characteristics.
4. Assign a level to each thin edge in accordance with the remaining structural characteristics. This results in a family of EGTs that have the same number of degrees of freedom and number of independent loops as that of the parent bar linkages.
5. Sketch the corresponding functional schematics.

This method can be very efficient, provided that an atlas of parent bar linkages already exists [8, 13].

7.6 Mechanism Pseudoisomorphisms

Since the edges of a graph represent the joints of a kinematic chain, multiple joints cannot be properly represented. For this reason, a ternary joint is represented by two coaxial binary joints, a quaternary joint by three coaxial binary joints, and so on. This notation, however, creates a problem in uniquely representing a mechanism with multiple joints.

When there are several links in a mechanism sharing a common joint axis, it is possible to reconfigure the pair connections among these coaxial links without affecting the functionality of the mechanism. For the mechanism shown in Figure 7.12a, links 1, 2, 3, and 4 share a common joint axis, “a.” Therefore, the revolute joints connecting these four coaxial links can be reconfigured in several different ways. Figure 7.12c shows a rearrangement of the revolute joints. The corresponding graphs are shown in Figures 7.12b and d, respectively. Although these two mechanisms are structurally nonisomorphic, they are kinematically equivalent. From the functional point of view, they are considered to be isomorphic. Such kinematically equivalent mechanisms and their corresponding graphs are called *pseudoisomorphic mechanisms* and *pseudoisomorphic graphs*, respectively [4, 15].

Specifically, the graph shown in Figure 7.12d is obtained from the graph shown in Figure 7.12b by replacing the 1–2 turning-pair edge with a 1–3 turning-pair edge of the same level. The process of replacing a turning-pair edge with another of the same level is called a *vertex selection* [4]. The number of possible vertex selections increases with the number of coaxial links in a mechanism. This creates a need for identification of pseudoisomorphisms. Alternatively, we can identify a unique graph among all the possible pseudoisomorphic graphs as the *canonical graph* to represent all the possible pseudoisomorphic graphs. The canonical graph representation is defined for epicyclic gear trains with the fixed link clearly identified as the root. In

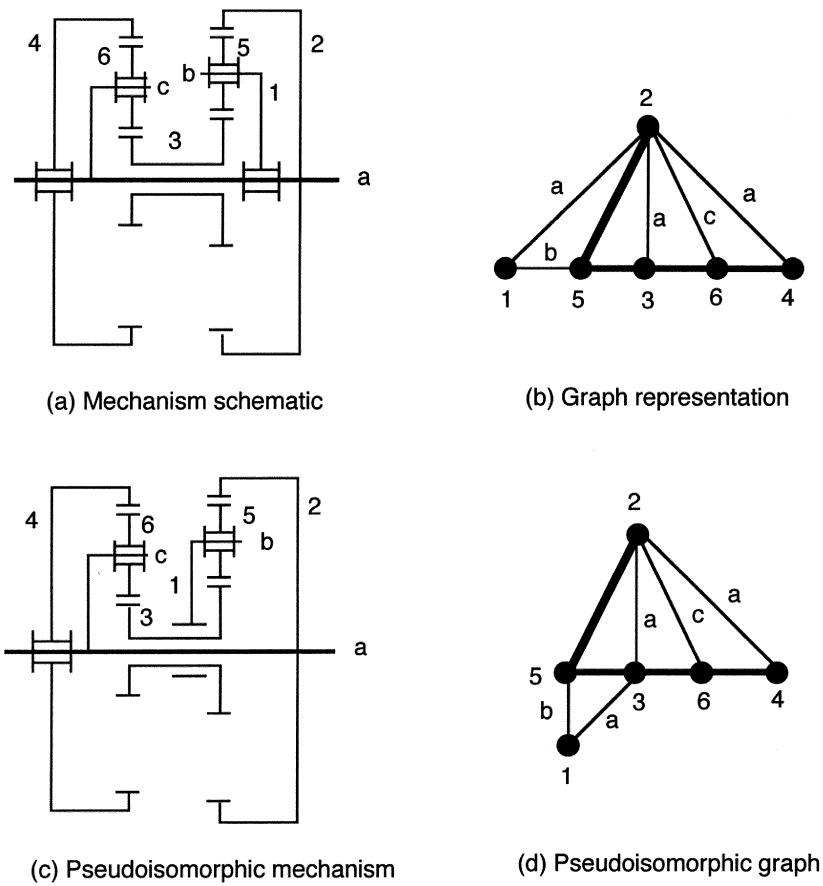


FIGURE 7.12
Pseudoisomorphic mechanisms and their graph representations.

canonical graph representation, all thin-edged paths that emanate from the root and terminate at any other vertex have distinct edge levels. See Chapter 8 for more details.

7.7 Atlas of Epicyclic Gear Trains

Using the methods described in the preceding sections, epicyclic gear trains with one, two, and three degrees of freedom and with up to four independent loops (four gear pairs) have been enumerated by various researchers [2, 4, 13, 14, 16, 8]. Table 7.1 summarizes the number of labeled nonisomorphic graphs in terms of the number of degrees of freedom and the number of independent loops. Appendix F provides an atlas of labeled graphs and typical functional schematics of nonfractionated epicyclic

gear trains classified according to the number of degrees of freedom, number of independent loops, and vertex degree listing.

Table 7.1 Classification of Epicyclic Gear Trains.

Degrees of Freedom F	No. of Loops L	No. of Links n	No. of Joints j	No. of Solutions
1	1	3	3	1
	2	4	5	3
	3	5	7	13
	4	6	9	80
2	1	4	4	0
	2	5	6	0
	3	6	8	3
	4	7	10	50
3	1	5	5	0
	2	6	7	0
	3	7	9	0
	4	8	11	8

7.7.1 One-dof Epicyclic Gear Trains

For one-dof epicyclic gear trains, there are 1 single-loop, 2 two-loop, 6 three-loop, and 26 four-loop, unlabeled nonisomorphic graphs as shown in Figures 7.13 and 7.14. These graphs can be labeled into 1 three-link, 3 four-link, 13 five-link, and 80 six-link, labeled nonisomorphic graphs as shown in Tables F.1 through F.8, Appendix F.

One-dof EGTs are widely used as simple speed reducers, automotive transmission mechanisms, and other power transmission mechanisms. Note that there exists a graph that contains a circuit made up of only geared edges as shown in Figure 7.15. Although this gear train violates the structural characteristic, C8, it does not require special link length proportions to achieve mobility.

7.7.2 Two-dof Epicyclic Gear Trains

For two-dof epicyclic gear trains, there are no nonfractionated EGTs with one or two independent loops. There are 3 labeled nonisomorphic graphs with three independent loops as shown in Table F.9, Appendix F, and 50 labeled nonisomorphic graphs with four independent loops. A skillful engineer can sketch a mechanism from graph number 1 listed in Table F.9 into a two-dof robotic wrist as shown in Figure 7.16. Graphs of two-dof EGTs with four independent loops can be found in Tsai and Lin [16].

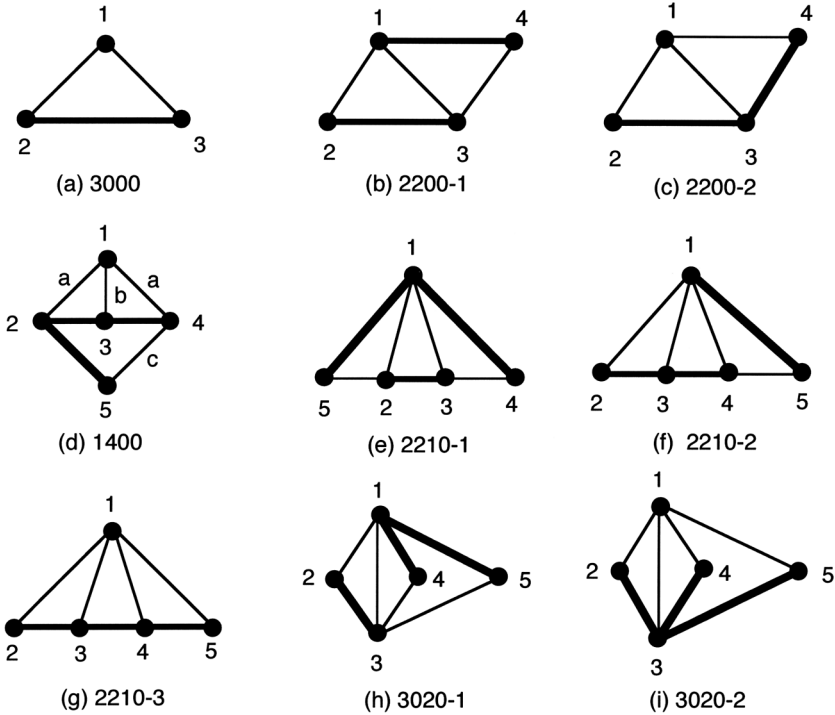


FIGURE 7.13
Unlabeled graphs of 3- to 5-link EGTs.

A two-dof coupling that maintains a constant velocity ratio between the input and output shafts is shown in Figure 7.17. The coupling consists of two hinged frames, links 1 and 2, that house three differential gear trains. The first differential, consisting of bevel gears 3, 4, 5, and 6, determines the speed ratio between the input and output shafts; the second differential, consisting of spur gears 2, 7, and 8, detects relative rotation of the two frames; and the third differential, consisting of bevel gears 8, 9, and 4, picks up the motion of the spur-gear differential to compensate for the velocity fluctuation due to relative rotation of the two frames. The spur gears remain stationary except when the two frames are changing their relative angular orientation. As one frame rotates with respect to the other, the spur-gear train provides an input to the third differential, which in turn either retards or advances the rotation of the first differential keeping the velocity ratio constant at all times.

7.7.3 Three-dof Epicyclic Gear Trains

For three-dof epicyclic gear trains, there are no nonfractionated EGTs with one, two, or three independent loops. Table F.10 in Appendix F gives 8 labeled graphs of three-dof EGTs having four independent loops.

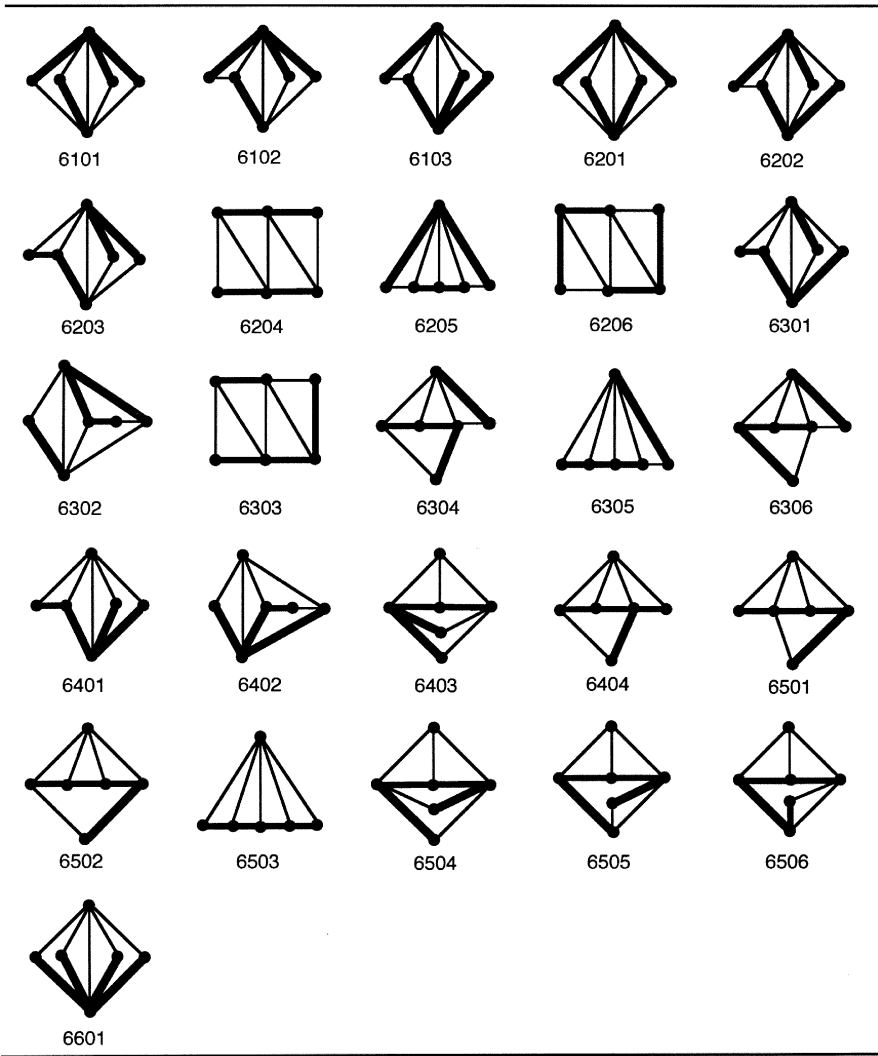


FIGURE 7.14
Unlabeled graphs of 6-link EGTs.

7.8 Kinematics of Epicyclic Gear Trains

Numerous methods for kinematic analysis of EGTs have been proposed by several researchers [1, 6, 7, 10, 11, 12, 17]. The most straightforward approach makes use of the theory of fundamental circuits introduced by Freudenstein and Yang [5]. The

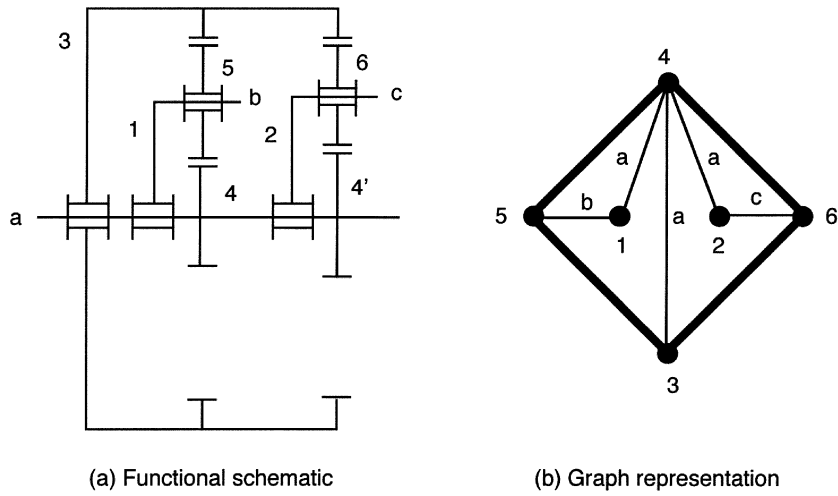


FIGURE 7.15
An EGT having a circuit consisting of only geared edges.

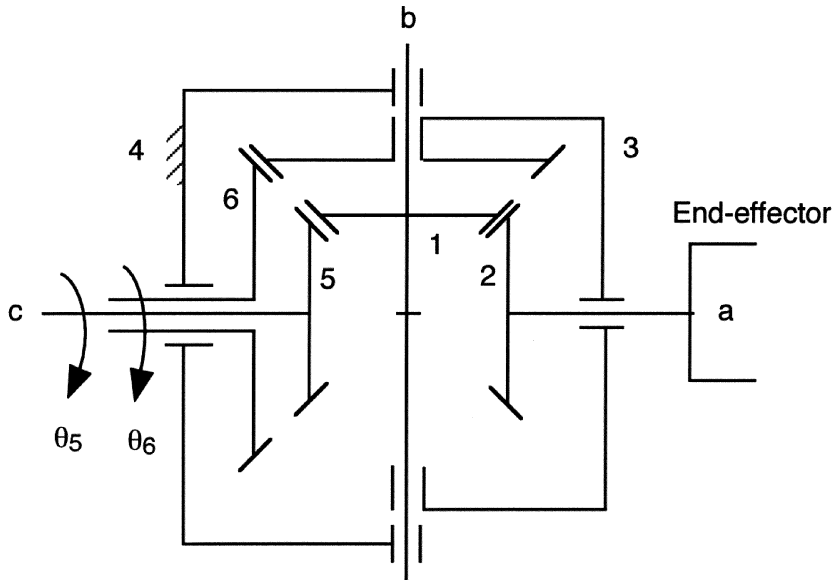


FIGURE 7.16
A two-dof wrist mechanism.

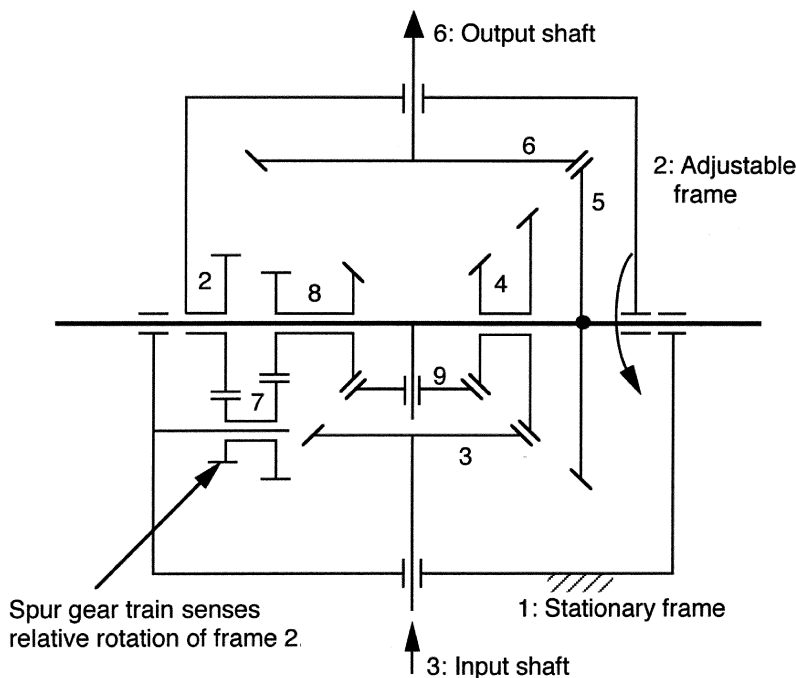


FIGURE 7.17
Constant velocity-ratio drive.

method was subsequently modified by Tsai [15] for the kinematic analysis of bevel-gear robotic mechanisms. This method can be easily implemented on a computer for automated analysis of EGTs.

7.8.1 Fundamental Circuit Equations

In the previous sections, we have shown that when all geared edges are taken off the graph of an EGT, the remaining subgraph is a tree. When a geared edge is put back onto the tree, it forms precisely one circuit called the *fundamental circuit* and the number of fundamental circuits is equal to the number of gear pairs in the gear train. In what follows, we show that a basic kinematic equation can be derived for each fundamental circuit.

Let i and j be a gear pair and k be the carrier. Then links i , j , and k constitute a simple gear train as illustrated in Figure 7.18. Since the tangential velocities at the meshing point of the two gears with respect to the carrier are equal to one another, a *fundamental circuit equation* can be written as

$$\omega_i - \omega_k = \pm N_{j,i} (\omega_j - \omega_k) , \quad (7.10)$$

where ω_i denotes the angular speed of link i , and $N_{ji} = D_j/D_i = T_j/T_i$ represents

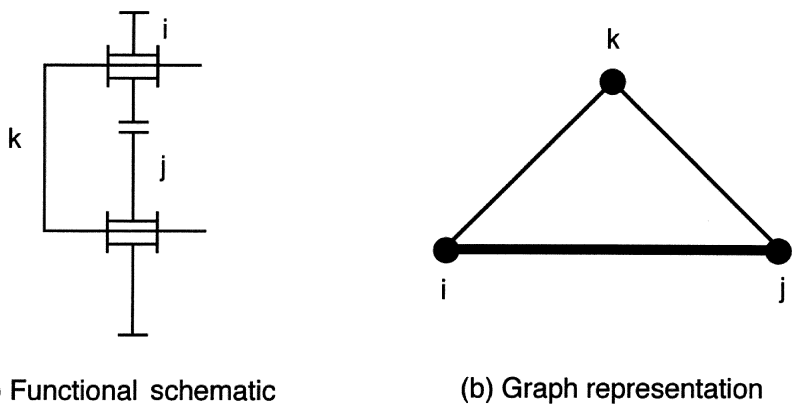


FIGURE 7.18
A gear pair and its fundamental circuit.

the gear ratio, where D_i and T_i are the pitch diameter and the number of teeth on gear i . The sign in Equation (7.10) is positive if a positive rotation of gear i relative to the carrier k produces a positive rotation of gear j , otherwise it is negative. By definition, we have

$$N_{ik} = \frac{1}{N_{ki}}. \quad (7.11)$$

Equation (7.10) is valid whether the gear train is a planar or bevel gear type and whether the carrier is stationary or not. To facilitate the analysis, a positive direction of rotation, z_i -axis, is assigned to each joint axis of an epicyclic gear train. For planar gear trains, it is most convenient to define the positive direction of rotation of all gears to be pointing out of the paper. In this way, we have a positive sign for an internal gear pair and a negative sign for an external gear pair. For bevel gear trains, we simply assign a positive direction of rotation to each joint axis, and obtain the sign of Equation (7.10) by following the above definition. Writing Equation (7.10) once for each fundamental circuit of an epicyclic gear train results in j_g fundamental circuit equations that can be solved for the speed ratios of any two gears.

7.8.2 Examples

Example 7.1 Minuteman Cover Drive

Refer to Figure 7.19 for the functional schematic and graph representation of the Minuteman cover drive. In this mechanism, the first ring gear, link 1, is held stationary; the sun gear, link 2, serves as the input link; and the other ring gear, link 5, is the output link. The compound planet, link 4, meshes with the sun gear 2 and the two ring gears and is supported by the carrier, link 3, by a revolute joint. Link 2 is connected

to links 1, 3, and 5 by revolute joints. Overall, it forms a one-dof compound planetary gear train. We wish to find the speed reduction ratio for this mechanism.

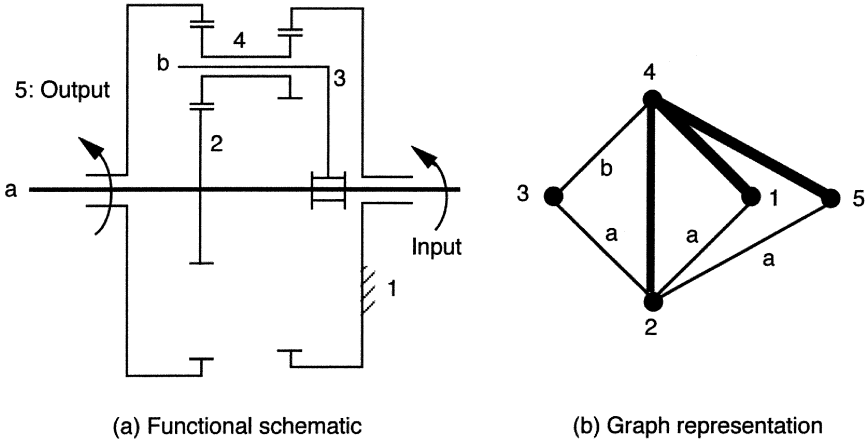


FIGURE 7.19

Minuteman cover drive and its graph representation.

Since there are three gear pairs in the mechanism, the number of fundamental circuits is equal to three. From the graph representation, we can easily identify the three fundamental circuits as $(2, 4)(3)$, $(1, 4)(3)$, and $(4, 5)(3)$. In this notation, the first two numbers in the parentheses denote the gear pair and the third number denotes the carrier. The fundamental circuit equations can be written as

$$\omega_2 - \omega_3 = -N_{42} (\omega_4 - \omega_3) , \quad (7.12)$$

$$\omega_1 - \omega_3 = N_{41} (\omega_4 - \omega_3) , \quad (7.13)$$

$$\omega_4 - \omega_3 = N_{54} (\omega_5 - \omega_3) . \quad (7.14)$$

Since link 1 is fixed, $\omega_1 = 0$, identically. We treat ω_2 as the input and ω_5 as the output of the gear train. Hence, we have three linear equations in three unknowns, ω_3 , ω_4 , and ω_5 . Substituting Equation (7.14) into Equations (7.12) and (7.13) yields

$$\omega_2 - \omega_3 = -N_{42} N_{54} (\omega_5 - \omega_3) , \quad (7.15)$$

$$\omega_3 = -N_{41} N_{54} (\omega_5 - \omega_3) , \quad (7.16)$$

Solving Equation (7.16) for ω_3 and substituting the resulting expression into Equation (7.15) yields

$$\omega_5 = \frac{(N_{41} N_{54} - 1)}{N_{54} (N_{41} + N_{42})} \omega_2 . \quad (7.17)$$

Equation (7.17) gives the overall speed ratio of the gear train. For example, let

$N_{41} = \frac{32}{74}$, $N_{42} = \frac{33}{9}$, and $N_{54} = \frac{75}{33}$, then

$$\frac{\omega_2}{\omega_5} = \frac{\frac{75}{33} \left(\frac{32}{74} + \frac{33}{9} \right)}{\frac{32}{74} \cdot \frac{75}{33} - 1} = -542 .$$

We observe that a very large gear ratio can be obtained from a relatively simple and compact gear train. \square

Example 7.2 Simpson Gear Train

Figure 7.20 shows a schematic diagram of the Simpson gear set, where link 1 is grounded, link 4 serves as the input, and link 2 is the output. We wish to find the speed ratio of the gear train.

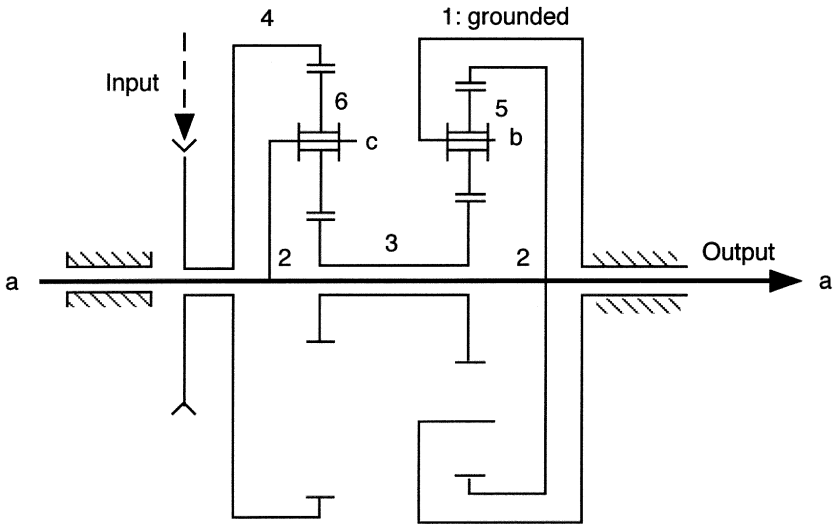


FIGURE 7.20
Simpson gear train.

The graph representation of the gear train is shown in Figure 7.3. There are four fundamental circuits: (5, 2)(1), (5, 3)(1), (6, 4)(2), and (6, 3)(2), and the fundamental circuit equations are

$$\omega_5 - \omega_1 = +N_{25} (\omega_2 - \omega_1) , \quad (7.18)$$

$$\omega_5 - \omega_1 = -N_{35} (\omega_3 - \omega_1) , \quad (7.19)$$

$$\omega_6 - \omega_2 = +N_{46} (\omega_4 - \omega_2) , \quad (7.20)$$

$$\omega_6 - \omega_2 = -N_{36} (\omega_3 - \omega_2) . \quad (7.21)$$

Since link 1 is fixed, $\omega_1 = 0$, identically. We treat ω_4 as the input and ω_2 as the output of the gear train. Hence, we have four linear equations in four unknowns, ω_2 , ω_3 , ω_5 , and ω_6 . We need to eliminate ω_3 , ω_5 , and ω_6 from these four equations.

Equating Equations (7.20) and (7.21) yields

$$N_{36} (\omega_3 - \omega_2) + N_{46} (\omega_4 - \omega_2) = 0 . \quad (7.22)$$

Similarly, equating Equations (7.18) and (7.19) yields

$$N_{35}\omega_3 + N_{25}\omega_2 = 0 . \quad (7.23)$$

Eliminating ω_3 from Equations (7.22) and (7.23) yields the speed ratio as

$$\frac{\omega_4}{\omega_2} = 1 + \frac{N_{36}}{N_{46}} \left(1 + \frac{N_{25}}{N_{35}} \right) . \quad (7.24)$$

Let the gear sizes of the input planetary gear set be $T_4 = 70$, $T_6 = 14$, and $T_3 = 42$; and that of the output planetary gear set be $T'_3 = 30$, $T_5 = 16$, and $T_2 = 62$. Then we have $N_{46} = 5$, $N_{36} = 3$, $N_{25} = 3.875$, and $N_{35} = 1.875$. Substituting these values into Equation (7.24), we obtain

$$\frac{\omega_4}{\omega_2} = 2.84 .$$

This is a typical reduction for the first gear of an automotive automatic transmission mechanism. \square

Example 7.3 Constant Velocity-Ratio Drive

We wish to derive the speed ratio between the input and output shafts of the two-dof differential gear train shown in Figure 7.17.

There are six fundamental circuits: (7, 2)(1); (8, 7)(1); (8, 9)(5); (9, 4)(5); (4, 3)(1); and (5, 6)(2). The fundamental circuit equations are

$$\omega_7 - \omega_1 = -N_{27} (\omega_2 - \omega_1) , \quad (7.25)$$

$$\omega_8 - \omega_1 = -N_{78} (\omega_7 - \omega_1) , \quad (7.26)$$

$$\omega_8 - \omega_5 = -N_{98} (\omega_9 - \omega_5) , \quad (7.27)$$

$$\omega_9 - \omega_5 = +N_{49} (\omega_4 - \omega_5) , \quad (7.28)$$

$$\omega_4 - \omega_1 = +N_{34} (\omega_3 - \omega_1) , \quad (7.29)$$

$$\omega_5 - \omega_2 = -N_{65} (\omega_6 - \omega_2) . \quad (7.30)$$

We now consider the mechanism as a two input device and solve the above six equations for ω_6 in terms of ω_3 and ω_2 . In view of the bevel gear construction, $N_{98}N_{49} = 1$. Since link 1 is fixed, $\omega_1 = 0$ identically. Substituting Equation (7.25) into Equation (7.26), yields

$$\omega_8 = N_{78}N_{27}\omega_2 , \quad (7.31)$$

Substituting Equations (7.28) and (7.31) into Equation (7.27) and making use of the fact that $N_{98}N_{49} = 1$, yields

$$N_{78}N_{27}\omega_2 = -\omega_4 + 2\omega_5 \quad (7.32)$$

Solving Equations (7.29) and (7.30) for ω_4 and ω_5 , respectively, and substituting the results in Equation (7.32), we obtain

$$\omega_6 = -\frac{N_{34}}{2N_{65}}\omega_3 + \frac{2(1 + N_{65}) - N_{27}N_{78}}{2N_{65}}\omega_2. \quad (7.33)$$

By selecting the gear ratios such that $2(1 + N_{65}) = N_{27}N_{78}$, Equation (7.33) reduces to

$$\omega_6 = -\frac{N_{34}}{2N_{65}}\omega_3. \quad (7.34)$$

Therefore, a constant angular speed ratio between the input and output shaft is maintained regardless of whether link 2 is rotating or not. \square

7.9 Summary

The structural characteristics of EGTs were identified. It was shown that an n -link EGT contains $(n - 1)$ turning pairs and $n - 1 - F$ gear pairs. The subgraph formed by deleting all the geared edges from the graph of an EGT is a tree. Any geared edge added onto the tree forms a fundamental circuit, and the number of fundamental circuits is equal to the number of gear pairs. In each fundamental circuit there exists a transfer vertex, which corresponds to the carrier of a gear pair. Using these structural characteristics, various methods of enumeration were presented. An atlas of EGTs with one, two, and three-dof and with up to four independent loops is developed in Appendix F. This atlas can be very helpful for the design of mechanical power transmission mechanisms. Furthermore, a simple and straightforward approach for speed-ratio analysis of EGTs is introduced. The method utilizes the theory of fundamental circuits. Several examples are given to illustrate the method of analysis.

References

- [1] Allen, R.R., 1979, Multiport Model for the Kinematic and Dynamic Analysis of Gear Power Transmissions, *ASME Journal of Mechanical Design*, 101, 248–267.

- [2] Buchsbaum, F. and Freudenstein, F., 1970, Synthesis of Kinematic Structure of Geared Kinematic Chains and other Mechanisms, *Journal of Mechanisms*, 5, 357–392.
- [3] Dudley, D.W., 1969, *The Evolution of the Gear Art*, American Gear Manufacturers Association, Alexandria, VA.
- [4] Freudenstein, F., 1971, An Application of Boolean Algebra to the Motion of Epicyclic Drives, *ASME Journal of Engineering for Industry*, Series B, 93, 176–182.
- [5] Freudenstein, F. and Yang, A.T., 1972, Kinematics and Statics of a Coupled Epicyclic Spur-Gear Train, *Mechanisms and Machine Theory*, 7, 263–275.
- [6] Glover, J.H., 1965, Planetary Gear Systems, *Product Engineering*, September, 72–79.
- [7] Hedman, A., 1993, Transmission Analysis—Automatic Derivation of Relationships, *ASME Journal of Mechanical Design*, 115, 4, 1031–1037.
- [8] Hsu, C.H., 1992, An Application of Generalized Kinematic Chains to the Structural Synthesis of Non-Fractionated Epicyclic Gear Trains, in *Proceedings of the 22nd ASME Mechanisms Conference*, Scottsdale, AZ, DE-Vol. 46, 451–458.
- [9] Kim, J.T. and Kwak, B.M., 1990, Application of Edge Permutation Group to Structural Synthesis of Epicyclic Gear Trains, *Mechanisms and Machine Theory*, 25, 5, 563–574.
- [10] Levai, Z., 1968, Structure and Analysis of Planetary Gear Trains, *Journal of Mechanisms*, 3, 131–148.
- [11] Martin, G.H., 1982, *Kinematics and Dynamics of Machines*, McGraw-Hill Book Co., New York, NY.
- [12] Smith, D., 1979, Analysis of Epicyclic Gear Trains via the Vector Loop Approach, in *Proceedings of the Sixth Applied Mechanisms Conference*, Denver, CO, Paper No. 10.
- [13] Sohn, W., 1987, A Computer-Aided Approach to the Creative Design of Mechanisms, Ph.D. Dissertation, Dept. of Mechanical Engineering, Columbia University, New York, NY.
- [14] Tsai, L.W., 1987, An Application of the Linkage Characteristic Polynomial to the Topological Synthesis of Epicyclic Gear Trains, *ASME Journal of Mechanisms, Transmissions, and Automation in Design*, 109, 3, 329–336.
- [15] Tsai, L.W., 1988, The Kinematics of Spatial Robotic Bevel-Gear Trains, *IEEE Journal of Robotics and Automation*, 4, 2, 150–156.
- [16] Tsai, L.W. and Lin, C.C., 1989, The Creation of Non-fractionated Two-Degree-of-Freedom Epicyclic Gear Trains, *ASME Journal of Mechanisms, Transmissions, and Automation in Design*, 111, 4, 524–529.

- [17] Willis, R.J., 1982, On the Kinematics of the Closed Epicyclic Differential Gears, *ASME Journal of Mechanical Design*, 104, 712–723.

Exercises

- 7.1 Sketch the graph representation for the gear train shown in Figure 7.21 and identify the transfer vertices.

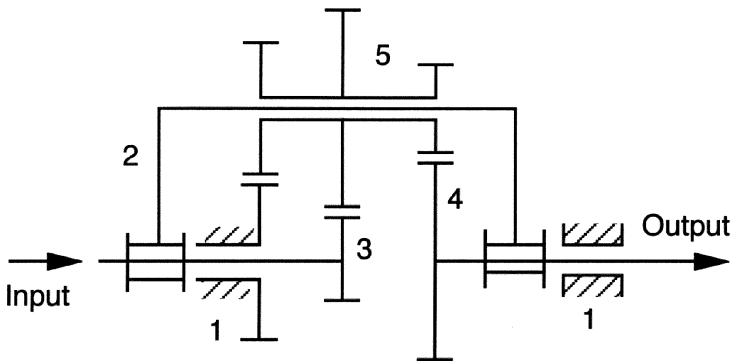
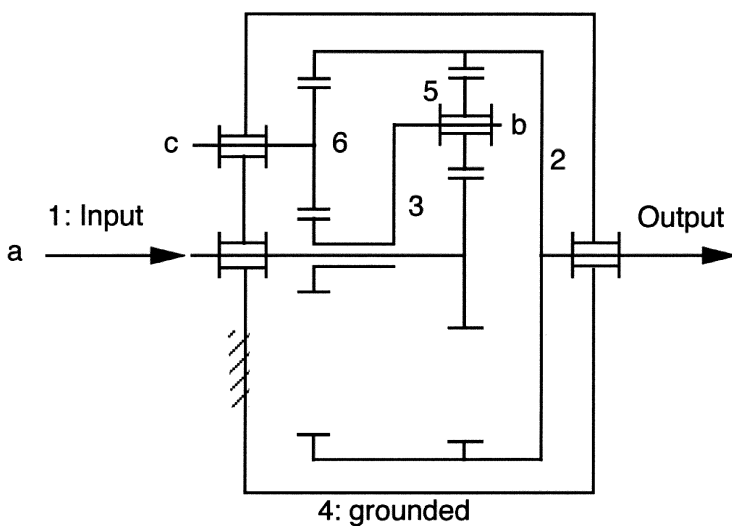
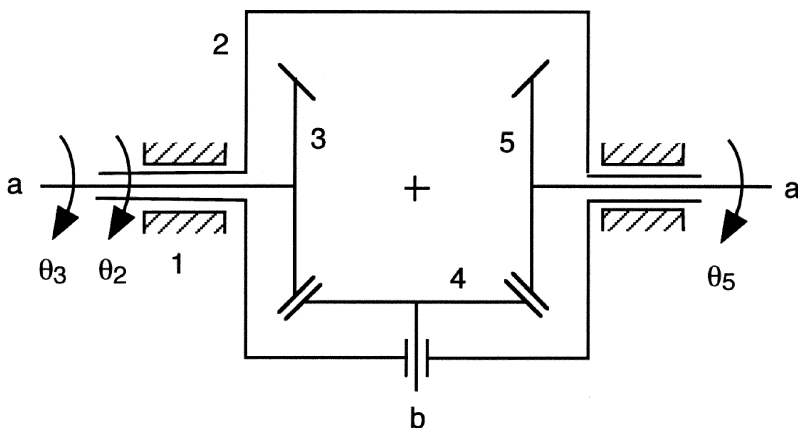


FIGURE 7.21
Triple-planet EGT.

- 7.2 Sketch the graph representation for the gear train shown in Figure 7.22, and identify the transfer vertices.
- 7.3 Label the 1400 (vertex-degree listing) graph shown in Figure 7.4 into as many one-dof EGTs as possible. Sketch one representative EGT using external gears.
- 7.4 Label the 3020 (vertex-degree listing) graph shown in Figure 7.4 into as many one-dof EGTs as possible. Sketch one representative EGT for each labeled graph using external gears.
- 7.5 Label the 4000 (vertex-degree listing) graph shown in Figure 7.5 into as many two-dof EGTs as possible. Sketch one representative EGT and show that, by proper vertex section, the labeled graph can be reconfigured into one with an articulation point.
- 7.6 Label the 3200 (vertex-degree listing) graphs shown in Figure 7.5 into as many two-dof EGTs as possible. Sketch one representative EGT and show that, by proper vertex section, the labeled graphs can be reconfigured into one with an articulation point.

**FIGURE 7.22****Compound planetary gear set - 1.**

- 7.7 Prove that the differential gear train shown in Figure 7.23 is a two-dof EGT. Using the vertex selection technique, show that it can be reconfigured into a mechanism with an articulation point.

**FIGURE 7.23****A differential gear set.**

- 7.8 Enumerate the graphs of one-dof EGTs with two loops by using the parent bar linkage technique. Sketch one representative EGT for each labeled graph using external gears.

- 7.9 Enumerate the graphs of one-dof EGTs with three loops by using the parent bar linkage technique. Sketch one representative EGT for each labeled graph using external gears.
- 7.10 Sketch a three-dof EGT for each of the graphs shown in Table F.10, Appendix F, using external gear meshes.

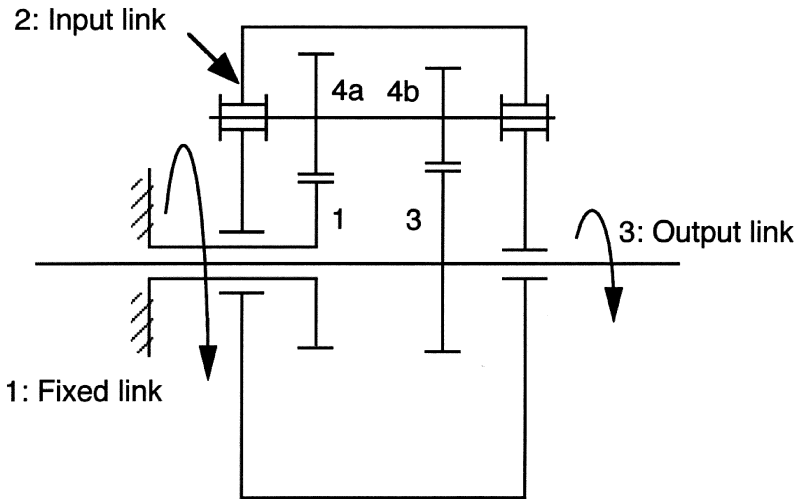


FIGURE 7.24
Robotic speed reducer.

- 7.11 Figure 7.24 shows the schematic diagram of a speed reducer for which the smaller sun gear (link 1) is fixed to the ground, the carrier (link 2) is the input link, and the larger sun gear (link 3) serves as the output link. The compound planet, link 4, meshes with both sun gears. Find the speed reduction ratio and show that a 100:1 speed reduction can be achieved.
- 7.12 Find the speed reduction ratio for the planetary gear train shown in Figure 7.25.

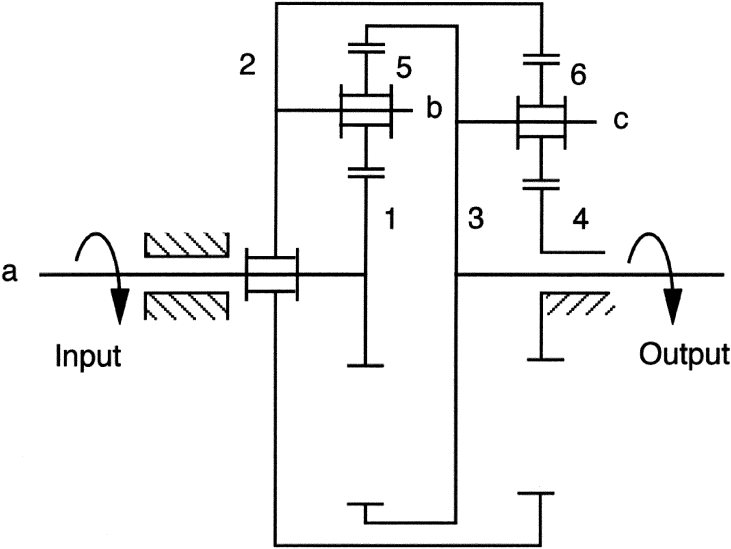


FIGURE 7.25
Compound planetary gear set - 2.

Chapter 8

Automotive Mechanisms

8.1 Introduction

In this chapter, we illustrate the usefulness of the systematic design methodology by enumerating a few automotive related mechanisms, including variable-stroke engine mechanisms, constant-velocity shaft couplings, and automatic transmission mechanisms.

For each case, we first identify the functional requirements. Then, we translate some of the requirements into structural characteristics for the purpose of enumeration of the kinematic structures. Lastly, we apply the remaining functional requirements along with other requirements, if any, for qualitative evaluation of the kinematic structures. This results in a class of feasible mechanisms or design alternatives. Since we are primarily concerned with the enumeration and qualitative evaluation of various design alternatives, other phases of design such as dimensional synthesis, design optimization, and design detailing will not be considered.

8.2 Variable-Stroke Engine Mechanisms

Most automobiles employ internal combustion engines as the source of power. Such a vehicle is typically equipped with an engine that is large enough to meet desired performance criteria such as maximum acceleration and hill climbing capability. On the other hand, only a fraction of the engine power is needed for highway cruising. To meet various load requirements, it is necessary to incorporate some kind of engine load control mechanism. Most internal combustion engines employ the crank-and-slider mechanism with a constant stroke length as the engine mechanism. Load control is achieved by throttling the inlet. Throttling, however, introduces pumping losses. It becomes clear that engine efficiency can be improved if the throttling can be eliminated or reduced.

One approach is to employ a mechanism to vary the valve lift, and the valve opening and closing points, with respect to the engine *top-dead-center*, as a function

of vehicle load requirements. Another approach is to vary the piston stroke length and, therefore, the displacement of the engine. More specifically, under light-load operations, the engine runs at short stroke such that the air-fuel mixture induced in the cylinder is only sufficient to meet the load requirement. For high-load operations, the engine runs at long stroke to increase the output power. According to a computer simulation, an automobile equipped with a variable-stroke engine can potentially improve its fuel economy by 20% with a concurrent reduction in NO_x emission [14]. The improvement in fuel economy comes primarily from a reduction of pumping loss due to the elimination of inlet throttling. Another reason is due to reduction in engine friction under short stroke operations [17, 18].

In this section, we study the enumeration of a class of variable-stroke engine mechanisms.

8.2.1 Functional Requirements

For a variable-stroke engine mechanism to function properly, the mechanism should be able to maintain a nearly constant compression ratio as the stroke length changes. It is also desirable to maintain a constant phase angle relation between the top-dead-center position of the piston and the crankshaft angle. In addition, the time required to change the stroke length from short to long should be within a few tenths of a second to meet the acceleration performance requirement. Finally, the mechanism should be relatively simple and economic to produce. In this regard, the design of a variable-stroke engine presents a very challenging problem to automotive engineers. We summarize the functional requirements of a variable-stroke engine mechanism as follows:

- F1. The mechanism should have the capability to change the stroke length as a function of engine load requirements.
- F2. The compression ratio should remain approximately constant for all stroke lengths.
- F3. The top-dead-center position of the piston with respect to the crankshaft angle should remain approximately constant for all stroke lengths.
- F4. The time required to change the stroke from short to long should be within a few tenths of a second.
- F5. The mechanism can be manufactured economically.

8.2.2 Structural Characteristics

There are three types of engine configurations: axial, in-line, and rotary configurations. In an *axial configuration*, such as the *swash-plate* and *wobble-plate* engine mechanisms, the cylinders are arranged in a circumference with their axes parallel to the crankshaft. In an *in-line configuration*, such as the crank-and-slider engine

mechanism, the cylinders are arranged longitudinally with their axes perpendicular to the axis of the crankshaft to form an in-line or *V* configuration. A *rotary configuration*, such as the *Wankel engine*, consists of two rotating parts: a triangular shaped rotor and an eccentric output shaft. The rotor revolves directly on the eccentric shaft. It uses an internal gear that meshes a fixed gear on the engine block to maintain a correct phase relationship between the rotor and eccentric shaft rotations. The axial type involves spatial motion and the rotary type requires higher kinematic pairs. In what follows, we concentrate on the in-line configuration.

Theoretically, a variable-stroke engine mechanism should possess two degrees of freedom: one for converting reciprocating motion of the piston into rotary motion of the crankshaft and the other for adjusting the stroke length. To simplify the problem, we temporarily exclude the degree of freedom associated with the control of stroke length. Since it is undesirable to incorporate a stroke length controller on a floating link, the change of stroke length will be accomplished by adjusting the location of a “fixed pivot.” That is, the second degree of freedom is obtained by moving a chosen “fixed pivot” of a one-dof mechanism along either a straight or curved guide. Hence, the engine block should be a ternary link such that, in addition to the adjustable pivot, there are two permanently fixed joints: one for connecting the crankshaft and the other for connecting the piston to the engine block. This simplification reduces the search domain from two-dof to one-dof planar linkages. We assume that only revolute and prismatic joints are permitted. To reduce friction, we further limit the number of prismatic joints to one, which will be used for connecting the piston to the engine block. From the above discussion, we summarize the engine specific structural characteristics as follows:

1. Mechanism type: planar linkages
2. Degree of freedom: $F = 1$ (Change of stroke length will be accomplished by adjusting the location of a fixed pivot.)
3. Joint types: revolute (R) and prismatic (P)
4. Number of prismatic joints: one (ground-connected)
5. Fixed link: ternary link

Note that we have incorporated only the first functional requirement into the structural characteristics. The remaining functional requirements are difficult to translate in mathematical form and, therefore, will be included in the *evaluator* for selection of feasible mechanisms. As a matter of fact, some of the requirements may not be judged properly without more detailed dimensional synthesis and design optimization.

8.2.3 Enumeration of VS-Engine Mechanisms

We begin our search with one-dof six-bar linkages. There are two kinematic structures: Watt and Stephenson types as shown in Table D.2, Appendix D. Both kinematic chains have two ternary links. Following the structural characteristics described

above, we assign one of the ternary links as the fixed link and one of the ground-connected joints as the prismatic joint. As a result, we obtain four nonisomorphic kinematic structures as shown in Figure 8.1. The following notations apply to all the schematic diagrams shown in Figure 8.1. Link 1 is the fixed link (engine block), link 2 is the crank, link 4 is connected to the fixed link by an adjustable pivot, link 5 is the connecting rod (attached to the piston), and link 6 is the piston.

We observe that the piston and the crankshaft of the second mechanism shown in Figure 8.1 belong to a four-bar loop. A change in the location of the adjustable pivot does not have any effect on the stroke length. Consequently, this mechanism is excluded from further consideration. The other three mechanisms remain as feasible solutions. Next, we evaluate these mechanisms against the second functional requirement. At this point, it is unclear whether these mechanisms can provide an approximately constant compression ratio. More detailed dimensional synthesis and design optimization are needed. The selection of a promising candidate for detailed analysis and synthesis is dependent on the designer's experience and creativity. We now check against the third and fourth functional requirements. It appears to be impossible for any of these mechanisms to maintain a constant top-dead-center position with respect to the crankshaft angle. A phase compensation mechanism or a computer-controlled spark ignition system will be needed if any of the above candidates are to be developed as a viable variable-stroke engine. Whether the change of stroke length can be accomplished within a few tenths of a second depends on the selected actuating system and the controller. Finally, we point out that these mechanisms potentially can be manufactured economically.

Note that if we allow the maximum number of prismatic joints to be two with the condition that no link can contain more than one prismatic joint, the number of nonisomorphic mechanism structures increases to 16 [3].

It is interesting to note that structure number 4 shown in Figure 8.1 was developed as a variable-stroke engine by the Sandia National Laboratories [13]. A cross-sectional view of the variable-stroke engine mechanism is shown in Figure 8.2. We note that the adjustable pivot, the lower end of link 4, is connected to the engine block by an additional link and its location is controlled by a linear ball screw. A phase changing device was incorporated in this prototype engine to compensate for the change in phase angle due to stroke length variation.

To overcome the disadvantages associated with six-link variable-stroke engine mechanisms, Freudenstein and Maki [3] developed an eight-link variable-stroke engine mechanism. In their study, a maximum of two prismatic joints were allowed with the condition that no link can contain more than one prismatic joint. Figure 8.3 shows a paired-cylinder variable-stroke engine mechanism developed by Freudenstein and Maki. A sliding block, link 9, is added between link 5 and the engine block for the purpose of adjusting the stroke length. Because of the ingenious design, the top-dead-center position of the pistons with respect to the crank angle remains constant as sliding block 9 moves up and down. The compression ratio has also been optimized to a nearly constant value. Readers are referred to the above reference for more details of the development.

No.	Graph	Functional Schematic	Comment
(1)	<p>A graph with 6 vertices labeled 1 through 6. Vertex 1 is at the bottom, connected to 2 and 6. Vertex 2 is connected to 1 and 3. Vertex 3 is connected to 2 and 4. Vertex 4 is connected to 3 and 5. Vertex 5 is connected to 4 and 6. Vertex 6 is connected to 5 and 1. All edges are labeled 'R' (revolute). There is a prismatic joint 'P' between vertex 1 and vertex 6.</p>	<p>A schematic of a Watt chain mechanism. It consists of two parallel vertical guides (1 and 2) and two horizontal guides (3 and 4). A central link (5) connects the two horizontal guides. A vertical link (6) connects the two vertical guides. The mechanism is shown in a specific configuration with arrows indicating motion.</p>	Watt chain
(2)	<p>A graph with 6 vertices labeled 1 through 6. Vertex 1 is at the bottom, connected to 2 and 4. Vertex 2 is connected to 1 and 3. Vertex 3 is connected to 2 and 5. Vertex 5 is connected to 3 and 6. Vertex 6 is connected to 5 and 4. Vertex 4 is connected to 6 and 1. All edges are labeled 'R' (revolute). There is a prismatic joint 'P' between vertex 1 and vertex 4.</p>	<p>A schematic of a Watt chain mechanism. It consists of two parallel vertical guides (1 and 2) and two horizontal guides (3 and 4). A central link (5) connects the two horizontal guides. A vertical link (6) connects the two vertical guides. The mechanism is shown in a specific configuration with arrows indicating motion.</p>	Watt chain (Not feasible)
(3)	<p>A graph with 6 vertices labeled 1 through 6. Vertex 1 is at the bottom, connected to 2 and 4. Vertex 2 is connected to 1 and 3. Vertex 3 is connected to 2 and 5. Vertex 5 is connected to 3 and 6. Vertex 6 is connected to 5 and 4. Vertex 4 is connected to 6 and 1. All edges are labeled 'R' (revolute). There is a prismatic joint 'P' between vertex 1 and vertex 4.</p>	<p>A schematic of a Stephenson chain mechanism. It consists of two parallel vertical guides (1 and 2) and two horizontal guides (3 and 4). A central link (5) connects the two horizontal guides. A vertical link (6) connects the two vertical guides. The mechanism is shown in a specific configuration with arrows indicating motion.</p>	Stephenson chain
(4)	<p>A graph with 6 vertices labeled 1 through 6. Vertex 1 is at the bottom, connected to 2 and 4. Vertex 2 is connected to 1 and 3. Vertex 3 is connected to 2 and 5. Vertex 5 is connected to 3 and 6. Vertex 6 is connected to 5 and 4. Vertex 4 is connected to 6 and 1. All edges are labeled 'R' (revolute). There is a prismatic joint 'P' between vertex 1 and vertex 4.</p>	<p>A schematic of a Stephenson chain mechanism. It consists of two parallel vertical guides (1 and 2) and two horizontal guides (3 and 4). A central link (5) connects the two horizontal guides. A vertical link (6) connects the two vertical guides. The mechanism is shown in a specific configuration with arrows indicating motion.</p>	Stephenson chain

FIGURE 8.1
Six-link VS-engine mechanisms with only one prismatic joint.

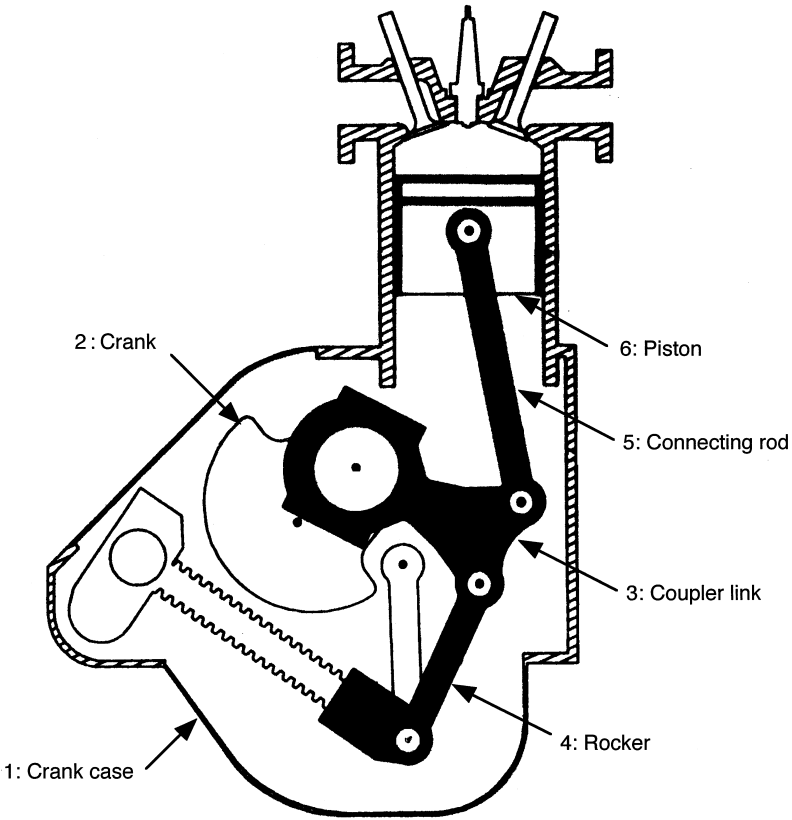


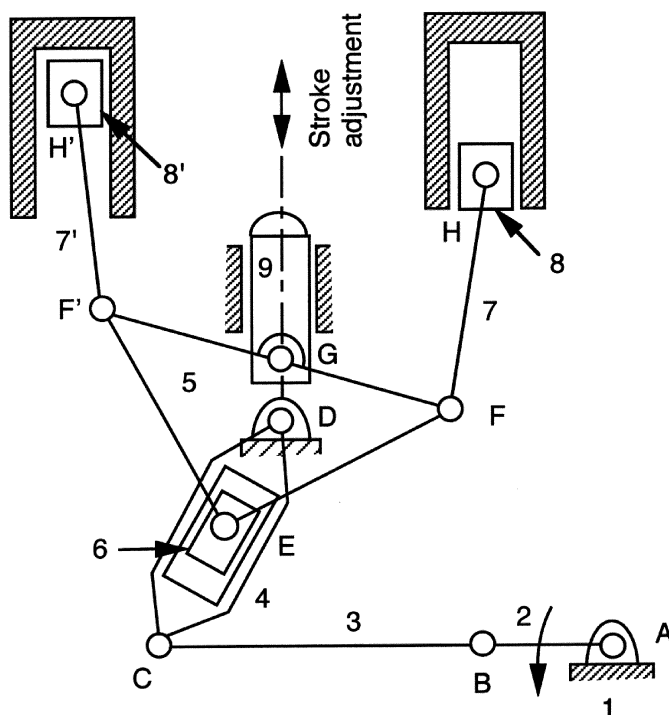
FIGURE 8.2
Sandia Laboratory's VS-engine mechanism.

8.3 Constant-Velocity Shaft Couplings

Constant-velocity (C-V) shaft couplings are widely used in automobiles and other machinery for transmitting power from one shaft to another to allow for small misalignments or relative motion between the two shafts. In this section, a class of C-V shaft couplings will be enumerated.

8.3.1 Functional Requirement

The functional requirement of a C-V shaft coupling can be simply stated as a mechanism for transmitting a one-to-one angular velocity ratio between two nonparallel intersecting shafts.

**FIGURE 8.3****General Motors paired-cylinder VS-engine mechanism.**

8.3.2 Structural Characteristics

Although several different types of C-V shaft couplings exist, the principle of operation is common to all couplings. Namely, they are one-dof mechanisms and the one-to-one angular velocity ratio between the input and output shaft is associated with a symmetry of the coupling about a plane called the *homokinetic plane*, which bisects the two shaft axes perpendicularly [8]. Perhaps, the most elementary form of C-V coupling is the bend-shaft coupling shown in Figure 8.4, where the axes of two identical shafts intersect at a point O . The homokinetic plane is the plane passing through O , perpendicular to the paper, and bisecting the angle between the two shaft axes. As the shafts rotate, the contact point Q lies in the homokinetic plane for all phases. Since the perpendicular distances from the contact point Q to the two shaft axes, r_1 and r_2 , are always equal to each other, the angular velocity ratio of the two shafts remains constant at all times. This mechanism is not very practical because it involves a five-dof higher pair.

Although it is conceivable that a single-loop C-V shaft coupling that violates the above general principle may exist, we will not be concerned with such a possibility. We note that the Hook joint is not a C-V shaft coupling. Although two Hook joints can

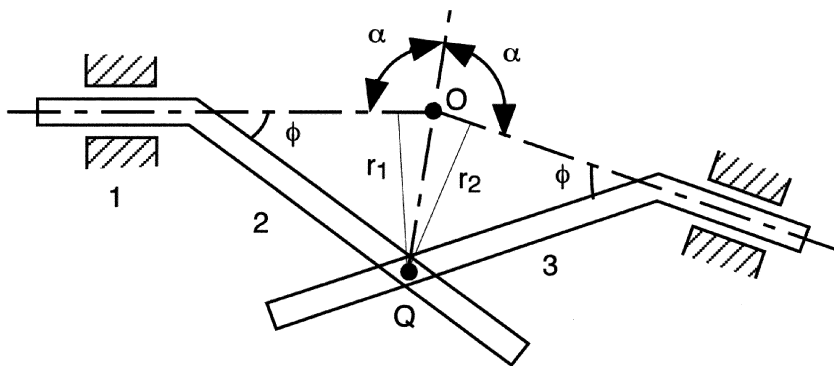


FIGURE 8.4
Bend-shaft C-V coupling.

be arranged to achieve a constant-velocity coupling effect, the resulting mechanism does not obey the general degree-of-freedom equation.

There are two basic types of C-V shaft couplings: *ball type* and *linkage type* [10]. The ball type is characterized by point contact between the balls and their races in the yokes of the shafts, whereas the linkage type is characterized by surface contact between the links. In the following, we limit ourselves to the linkage type. Further, we concentrate on the single-loop spatial mechanisms. We assume that revolute, prismatic, cylindric, spherical, and plane pairs are the available joint types. We summarize the structural characteristics of C-V shaft couplings as follows:

1. Type of mechanism: spatial single-loop linkages.
2. Degree-of-freedom: $F = 1$.
3. Mechanism structure is symmetrical about a homokinetic plane.
4. Available joint types: R, P, C, S, and E.

8.3.3 Enumeration of C-V Shaft Couplings

Figure 8.5a shows the general configuration of a C-V shaft coupling [2], where the fixed link is denoted as link 1, the input link as link 2, and the output link as link 3. Both the input and output links are connected to the fixed link by revolute joints. The connection between the input link and the output link is abstractly represented by a rectangular box. The homokinetic plane intersects perpendicularly at the axis of symmetry. The rest of the mechanism remains to be determined.

Since we are interested in single-loop C-V shaft couplings, the number of links is equal to the number of joints and all the links are necessarily binary. The loop

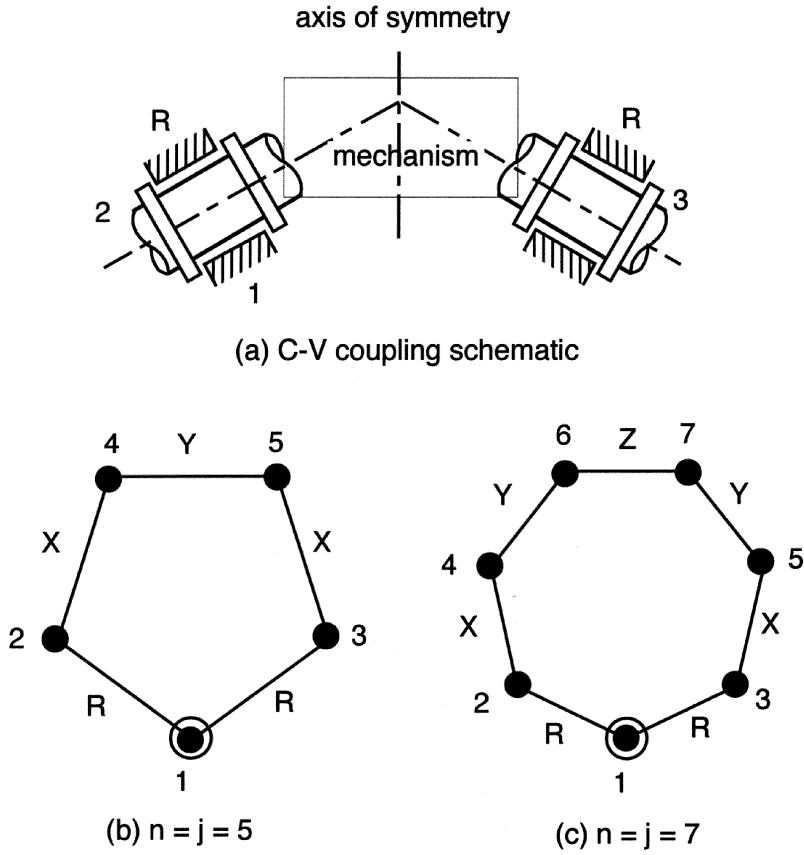


FIGURE 8.5
General configuration of a C-V shaft coupling.

mobility criterion, Equation (4.7), requires that

$$\sum_i f_i = 7. \tag{8.1}$$

Since the minimum degrees of freedom in any joint is one, the number of joints and, therefore, the number of links should not exceed seven; that is,

$$n = j \leq 7. \tag{8.2}$$

Since the first and last joints are preassigned as revolute joints and the mechanism is symmetrical about the homokinetic plane, the number of links (and joints) should be odd; that is

$$n = j = 3, 5, \text{ or } 7. \tag{8.3}$$

The case $n = j = 3$ requires a five-dof joint as shown in Figure 8.4, which is judged to be impractical. Hence,

$$n = j = 5 \text{ or } 7.$$

The graph representations of these two families of mechanisms are sketched in Figures 8.5b and c, where vertex 1 denotes the ground-connected link, vertex 2 the input link, and vertex 3 the output shaft. The two ground-connected joints are prelabeled as revolute. The other joint types are labeled symmetrically with respect to the fixed link as X and Y for the five-link chain, and X , Y , and Z for the seven-link chain.

Let the degrees of freedom associated with the X , Y , and Z joints be denoted by f_x , f_y , and f_z , respectively. We now discuss the enumeration of each family of C-V shaft couplings as follows.

Five-Link C-V Shaft Couplings. Figure 8.5b indicates that there are two prelabeled revolute joints, two unknown X joints, and one Y joint. Substituting this information into Equation (8.1) yields

$$2f_x + f_y = 5. \quad (8.4)$$

We have one equation in two unknowns and both unknowns are restricted to positive integers. Solving Equation (8.4) yields the following two solutions:

$$f_x = 1, \quad f_y = 3;$$

and

$$f_x = 2, \quad f_y = 1.$$

The first solution implies that the X joint can be either a revolute or prismatic joint, while the Y joint can be a spherical or plane pair. The second solution implies that the X joint is a cylindric joint, while the Y joint can be a revolute or prismatic joint. Labeling the graph shown in Figure 8.5b with these joint distributions results in six distinct mechanisms, with the names of some known C-V couplings given in parentheses below:

RRERR (Tracta coupling),
 RRSRR (Clements coupling),
 RPEPR,
 RPSPR (Altmann coupling),
 RCRCR (Myard coupling),
 RCPCR.

Seven-Link C-V Shaft Couplings. Figure 8.5c shows the graph of a seven-link chain with two prelabeled revolute joints and two unknown X , two unknown Y , and one unknown Z joints. Substituting this information into Equation (8.1) yields

$$2f_x + 2f_y + f_z = 5. \quad (8.5)$$

Hence, we have one equation in three unknowns and they must be all positive integers. The only solution to Equation (8.5) is

$$f_x = f_y = f_z = 1 .$$

That is, all the X , Y , and Z joints must be either revolute or prismatic. Labeling the graph shown in Figure 8.5c with this joint distribution results in six distinct kinematic structures as given below:

RRRRRRR (Myard, Voss, Wachter and Reiger),
 RRRPRRR,
 RRPRPRR (Derby, S.W. Industries),
 RPRRRPR,
 RRPPPRR,
 RPRPRPR.

Overall, a total of 12 kinematic structures of C-V shaft couplings are found. For convenience, functional schematic diagrams of the six well-known C-V shaft couplings are sketched in Figure 8.6.

8.4 Automatic Transmission Mechanisms

Automotive transmissions can be generally classified as *manual* and *automatic transmissions*. This section deals with the enumeration of automatic transmission mechanisms. A commercial automotive automatic transmission is shown in Figure 8.7. As can be seen from the figure, an automatic transmission typically consists of a torque converter, a gear train, a set of clutches, and a clutch controller. In front wheel drive vehicles, the *final reduction unit* and the *differential* are also located in the transmission housing.

The torque converter has three purposes. First of all, it serves as a fluid coupling to provide a smooth transmission of torque from the engine to the wheels. It also allows a vehicle to stop without stalling the engine. Second, it multiplies the engine torque for additional vehicle performance. Third, with the use of a torque converter clutch, it provides a direct mechanical link between the engine and the gear train to further improve fuel economy. The torque converter consists of an impeller, a turbine, a stator, and a converter clutch. The impeller is mechanically connected to the engine crankshaft. It receives power from the engine and imparts motion to the transmission fluid. The fluid escapes through the outer circumference of the impeller and enters the turbine. The turbine is mechanically connected to the gear train. The fluid leaves the turbine at the inner circumference of the turbine blades and reenters the impeller through the stator blades. The purpose of the stator blades is to redirect the fluid flow from the turbine to the impeller, providing a torque multiplication to the transmission. The torque amplification factor is a function of the difference in speeds between the impeller and the turbine, typically 2:1 at the start. As the vehicle speed increases and torque multiplication is no longer needed, centrifugal force changes the direction

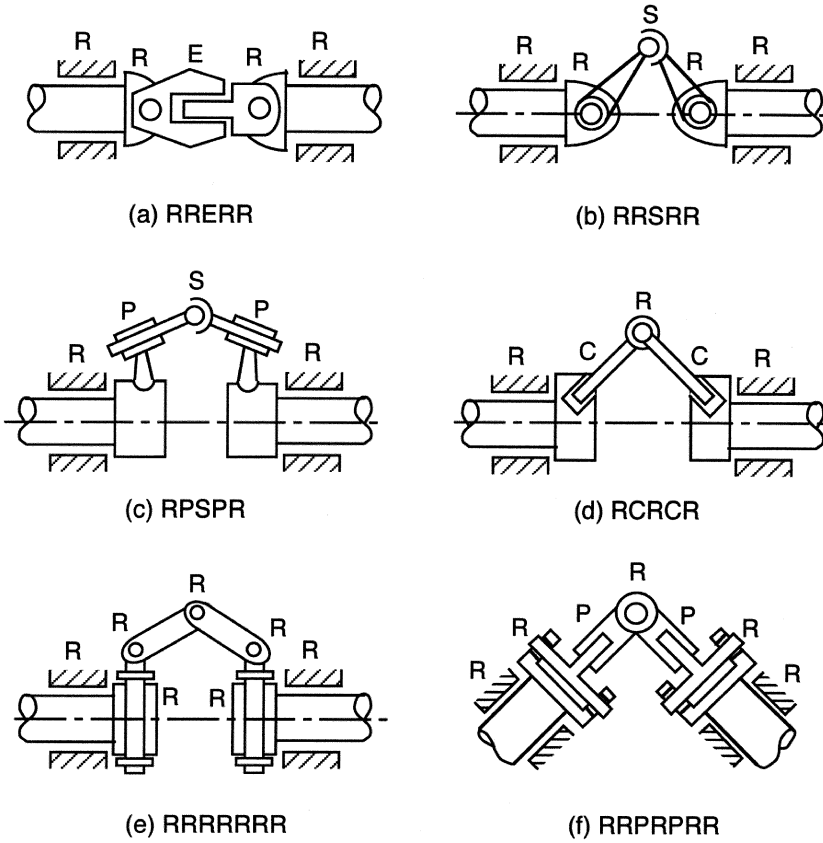
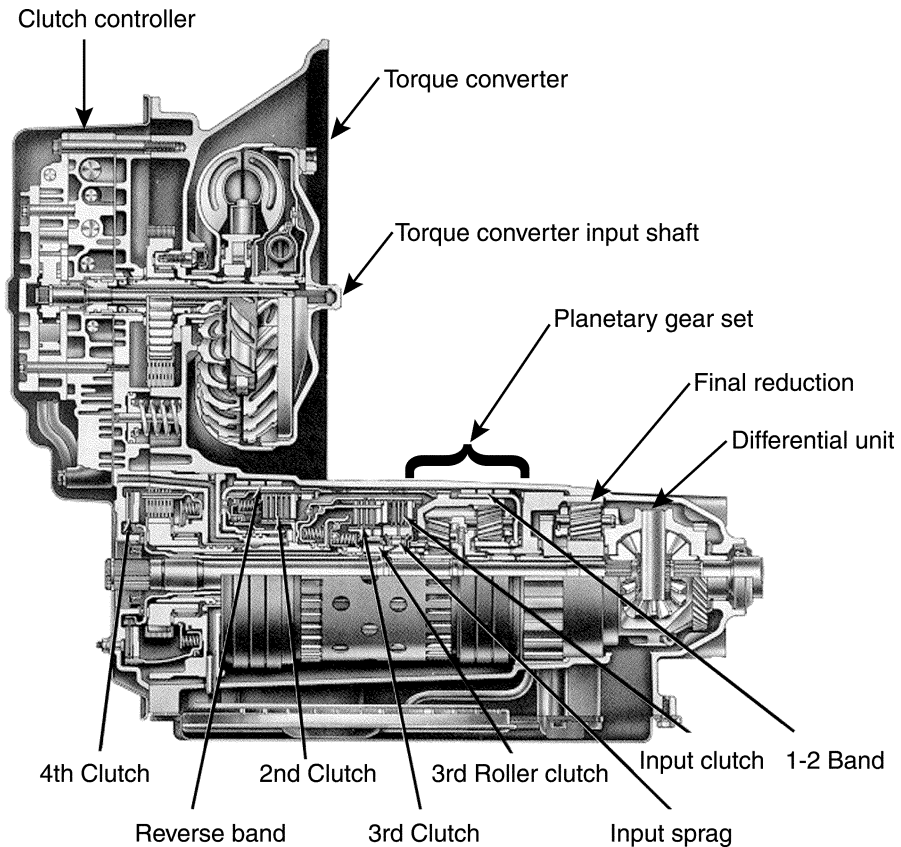


FIGURE 8.6

Functional schematic diagrams of six C-V shaft couplings.

of fluid flow and the reaction force on the stator, forcing the stator to rotate freely. Under this condition, the torque converter functions as a fluid coupling. On highway cruising, the converter clutch mechanically locks up the impeller and turbine together to further improve fuel economy.

Figure 8.8a shows a schematic diagram of the ratio change gear train where the *rotating* and *band clutches* are designated as C_i and B_i , respectively. The input shaft of the gear train is connected to the output shaft of the torque converter by a chain-and-sprocket. The output ring gear, link 2, can be clutched either to the input shaft by a rotating clutch, C_2 , or to the housing of the transmission by a band clutch, B_3 . Similarly, the input sun gear, link 1, can be clutched either to the input shaft by a rotating clutch, C_1 , or to the housing by a band clutch, B_2 . The output sun gear, link 4, can be clutched to the housing by a band clutch, B_1 . The input ring gear/output carrier, which is permanently attached to the final reduction unit, is designated as the output of the gear train.

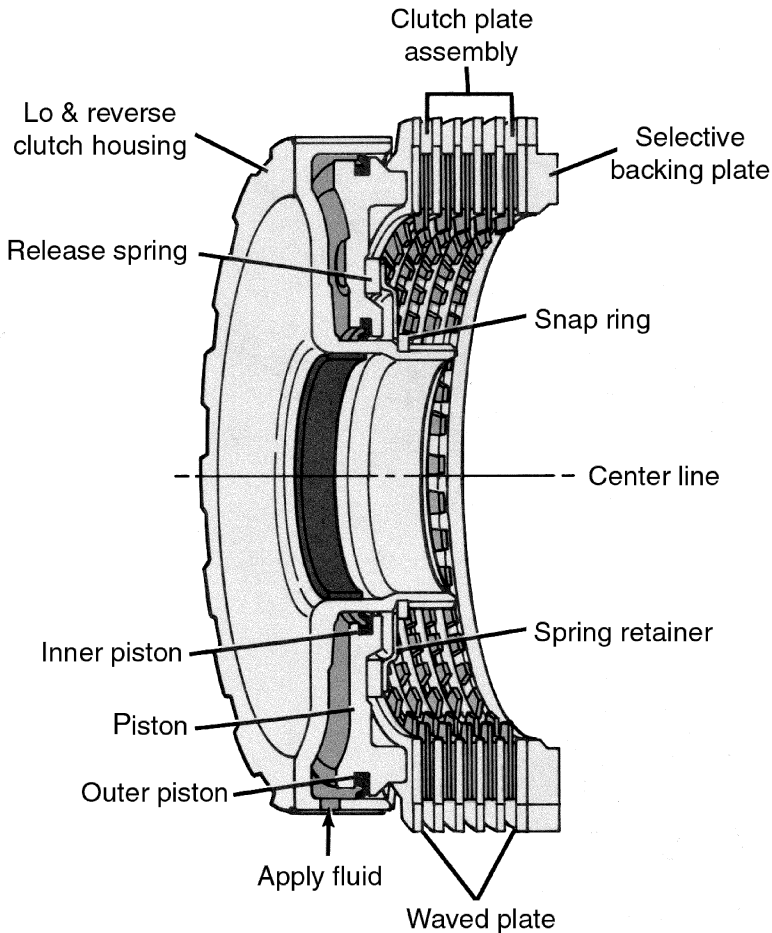
**FIGURE 8.7**

A 4-speed automatic transmission. (Courtesy of General Motors, Warren, MI.)

In a transmission, *one-way clutches* (OWC) are often used to smooth out the transient responses during the change of speed ratios. For brevity, one-way clutches are not sketched in the diagram. Figures 8.9 through 8.11 show a typical rotating clutch, band clutch, and one-way clutch, respectively.

The final reduction unit is connected to the output shaft of the gear train and operates in reduction at all times. It is designed to better match the engine power to vehicle performance requirements under various operating conditions. The inclusion of a final reduction unit also permits the same transmission to be used in different vehicles by changing the reduction ratio. The final reduction unit shown in Figure 8.7 is a planetary gear train. Other types of final reduction units, such as a simple gear pair, have also been used.

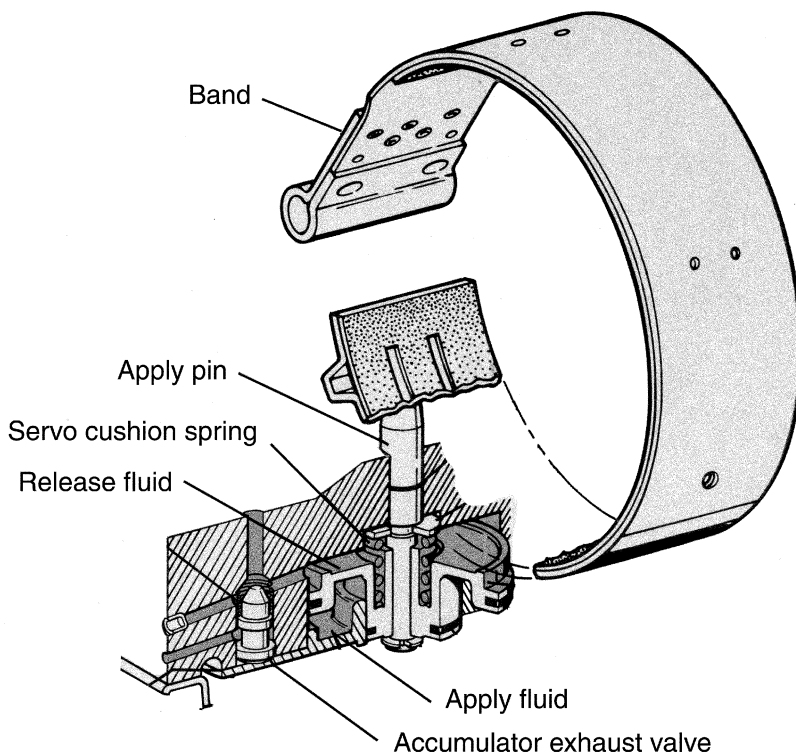
The bevel-gear differential is a two-dof mechanism that provides a mechanical means for one wheel to travel faster than the other when the vehicle is going around

**FIGURE 8.9**

Typical rotating clutch. (Courtesy of General Motors, Warren, MI.)

an intermediate idler gear, 8. The two main shafts rotate in opposite directions when the transmission is in the drive mode. For this reason, this type of transmission is called a *countershaft* or *layshaft* transmission. In addition, a short shaft is added to support the intermediate idler gear for the reverse drive. In Figure 8.12, C_4 denotes a dog clutch. The dog clutch is engaged either on the drive side (D) or on the reverse side (R). Hence, it changes the engagement only from the drive mode to the reverse mode and vice versa.

The main difference between countershaft and epicyclic gear type transmissions is that the former employs two counter-rotating shafts, whereas the latter uses an epicyclic gear train. Other types of automatic transmissions such as the continuous-variable transmission and hydraulic transmission also exist. The countershaft type

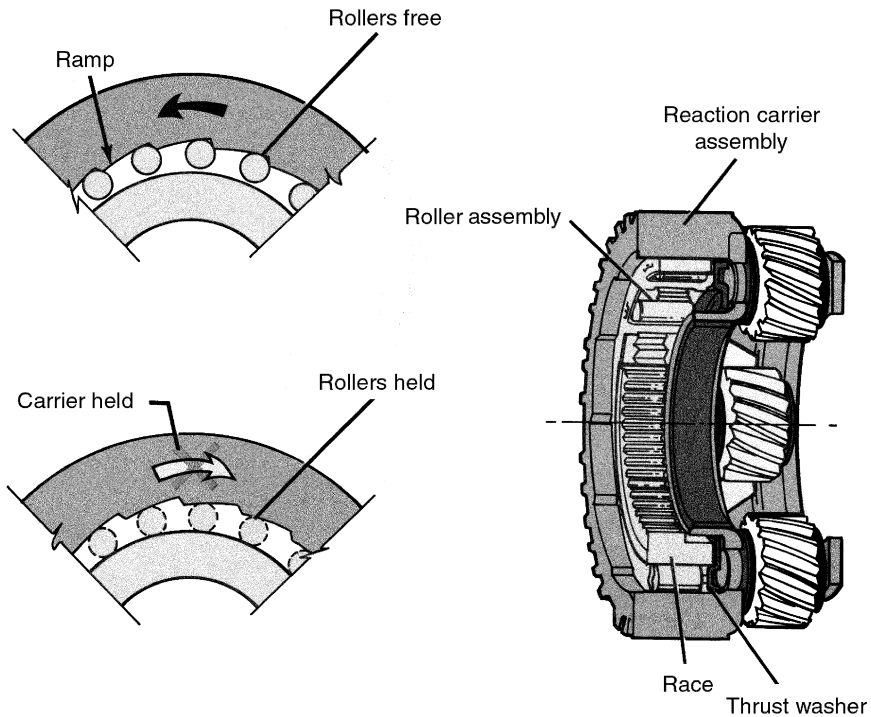
**FIGURE 8.10**

Typical band clutch. (Courtesy of General Motors, Warren, MI.)

has been used by the Honda and Saturn corporations. However, the most widely used automotive automatic transmission mechanism is the epicyclic gear type. In what follows, we concentrate our study on the epicyclic gear type transmission mechanisms.

8.4.1 Functional Requirements

In a transmission mechanism, the term *speed ratio* is defined as the ratio of the input shaft speed to the output shaft speed of the gear train. Various speed ratios are obtained by engaging and disengaging clutches. The speed ratios of an automotive transmission are tailored for vehicle performance and fuel economy. It should provide a vehicle with several forward speeds, typically including a first gear for starting, a second and/or third gear for passing, an overdrive for fuel economy at road speeds, and a reverse. A table showing a sequence of speed ratios and the corresponding clutching conditions is called a *clutching sequence*. Figure 8.8b shows the clutching sequence of the epicyclic gear transmission depicted in Figure 8.8a, where an *X* indicates that the corresponding clutch is engaged. We note that during speed ratio changes, only one clutch is engaged while another is simultaneously disengaged. We

**FIGURE 8.11**

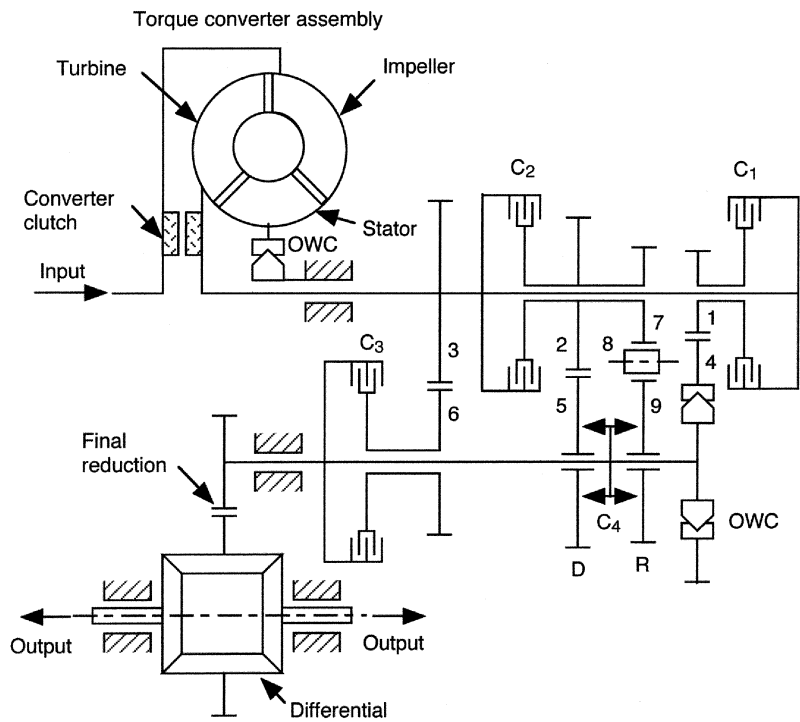
Typical one-way clutch. (Courtesy of General Motors, Warren, MI.)

call this kind of operation a single *clutch-to-clutch shift*. This is an important feature for a transmission to shift smoothly from one speed to another. The *direct drive* (third range) is obtained by simultaneously engaging two coaxial links of the gear train to the input shaft.

Change of speed ratios should be kept sufficiently small to achieve smooth transition. On the other hand, the overall *ratio range* between the first and the last speed should be as large as possible to better match the engine power to vehicle performance and fuel economy requirements. The ratio of two speed ratios from one speed to the next is called the *step ratio*. For the transmission shown in Figure 8.8, the step ratios are: 1.86 ($2.921/1.567$) from the first to the second speed, 1.57 ($1.567/1.00$) from the second to the third speed, and 1.42 ($1.000/0.705$) from the third to the fourth speed, and the overall ratio range is 4.14 ($2.921/0.705$). Obviously, with a given number of design parameters, there is a compromise between the choice of step ratios and the overall ratio range.

From the above discussion, we summarize the functional requirements of an automatic transmission mechanism as follows:

- F1. The mechanism should be capable of providing several speed ratios, including



(a) Functional schematic

Range	Ratio	C ₁	C ₂	C ₃	C ₄	OWC	Shift Transient
Drive 1	2.38	X			D	X	OWC to C ₂
Drive 2	1.50	X	X		D		
Drive 3	0.91	X		X	D		C ₂ to C ₃
Reverse	-1.95		X		R		

C₄: dog clutch OWC: One Way Clutch

(b) Clutching sequence

FIGURE 8.12
Functional schematic and clutching sequence of a countershaft transmission.

a reverse, by engaging different links to the power source and the housing of a transmission mechanism.

- F2. The overall speed ratio range should be sufficiently large to cover both high and low load operations.
- F3. The step ratios should be sufficiently small and follow a geometric progression; that is, the speed ratio changes by an approximately constant percentage from one speed to the next.
- F4. A single clutch-to-clutch shift in speeds is preferred.

8.4.2 Structural Characteristics

From the structure synthesis point of view, the torque converter, clutch controller, final reduction, and differential can be temporarily ignored. This simplifies the problem to the synthesis of an epicyclic gear train along with a set of properly arranged clutching sequences.

An examination of existing transmission mechanisms reveals that when all clutches are disengaged, most of the ratio-change mechanisms are fractionated epicyclic gear mechanisms (EGMs). That is, they are made up of a one-dof epicyclic gear train with its central axis supported by the housing of a transmission mechanism. The second degree of freedom comes from a rotation of the entire gear set about its central axis. Although there also exist fractionated three-dof EGMs, in what follows we will not be concerned with such possibilities [16].

Further examination of the EGMs indicates that only coaxial links of an EGM are used as the input shaft, output shaft, and reaction member. Thus, for a one-dof EGT with n_c coaxial links, the number of possible choices of the input, output, and reaction member is equal to $n_c(n_c - 1)(n_c - 2)$. Adding a direct drive, which can always be obtained by simultaneously clutching two coaxial links to the power source, yields a total number of possible speed ratios of

$$m = n_c (n_c - 1) (n_c - 2) + 1 . \quad (8.6)$$

If one of the coaxial links is permanently selected as the output link, the number of possible speed ratios reduces to

$$m = (n_c - 1) (n_c - 2) + 1 . \quad (8.7)$$

Hence, for a transmission mechanism to provide n_r desired speed ratios, including a reverse gear, the number of coaxial links, n_c , should satisfy

$$(n_c - 1) (n_c - 2) + 1 \geq n_r . \quad (8.8)$$

We note that an EGM should not contain any *redundant links*. A link is considered to be redundant if it is never used as an input, output, or reaction member, and the removal of the link does not affect the mobility of the mechanism. Such a link will

never carry any power in any phase of operation. For example, Figure 8.13 shows an EGT with a redundant link. If line a is the central axis, then link 3 is a revolving planet that cannot physically serve as an input, output, or reaction member. It will not carry any load but free spinning.

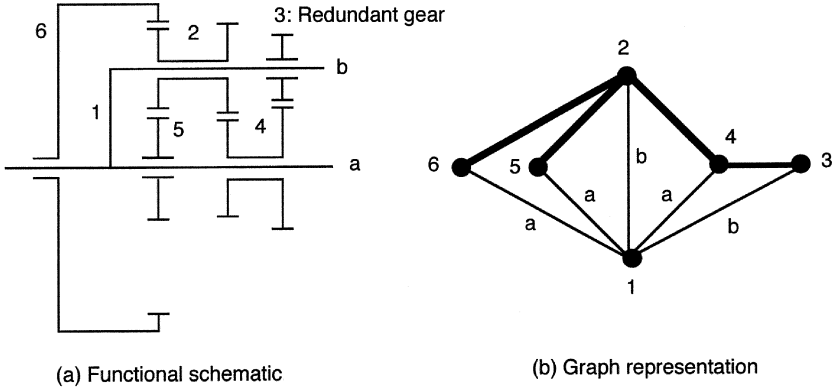


FIGURE 8.13
An EGT with a redundant link.

From the above discussion, we summarize the structural characteristics of EGMs as follows:

- C1. An EGM is a fractionated two-DOF mechanism. Specifically, it is made up of a one-dof EGT supported by the housing of a transmission mechanism on a central axis. Therefore, an EGM should obey all the structural characteristics described in Chapter 7.
- C2. If n_r is the number of desired speed ratios, the number of coaxial links, n_c , should satisfy Equation (8.8).
- C3. There shall be no redundant links or partially locked subchains.

8.4.3 Enumeration of Epicyclic Gear Mechanisms

From the above discussion, we conclude that the design of a transmission gear train can be naturally divided into four interrelated steps. First, a feasible one-dof EGT is identified. Second, the EGT is integrated with the housing of a transmission to form a fractionated two-dof EGM. Third, a set of clutching sequences is developed. Fourth, the gears are sized to provide a set of desired speed ratios. The selection of an optimal clutching sequence and the sizing of gears cannot be solved analytically. Some engineers have formulated the problem as a constraint satisfaction problem [9, 11, 12]. Others use algorithmic techniques [6, 7]. In this section, we are primarily concerned with the enumeration of feasible EGTs.

We start the enumeration by searching for feasible one-dof EGTs. Assume that the minimal number of speed ratios is three forward speeds and one reverse drive, $n_r = 4$. It follows from Equation (8.8) that there should be at least four coaxial links, $n_c = 4$, in the EGT. It becomes obvious that none of the three- and four-link EGTs developed in Chapter 7 satisfies this condition. Examining the labeled graphs listed in Appendix F, we obtain one 5-vertex and six 6-vertex labeled graphs of EGTs. These seven labeled graphs and their corresponding gear trains are sketched, up to mechanism pseudoisomorphism, in Figures 8.14 and 8.15, where the common joint axis of the coaxial links is labeled as “a–a.” For simplicity, only one-half of the gear trains are sketched. Furthermore, a graph having one circuit formed exclusively by geared edges is included. We note that there are six additional six-link chains having four coaxial links. However, they all contain a redundant link and, therefore, are excluded from the list.

A survey of the literature reveals that all known epicyclic transmission gear trains with six or fewer links are developed from the labeled graphs given in Figures 8.14 and 8.15 [16]. For example, the gear set illustrated in Figure 8.8 corresponds to the 6206 graph shown in Figure 8.14. This mechanism was incorporated in the General Motors Corporation’s THM-4T60 and THM-700-R4 transmissions, and Ford Motor Company’s Axod 4-speed transmission. Two other commonly used gear trains are the Simpson and Ravigneaux gear sets as shown in Figures 8.16 and 8.17. The Simpson gear set is, perhaps, the most popular transmission gear set. It has been developed by nearly all automotive manufacturers as three- and four-speed automatic transmissions. The Ravigneaux gear set was developed by Borg Warner, Mitsubishi Corporation, and others.

8.5 Canonical Graph Representation of EGMS

An EGM typically consists of several coaxial links supported by the housing on a common joint axis. Furthermore, only these coaxial links are utilized as the input, output, or reaction member. Such an EGM may have numerous pseudoisomorphic mechanisms. This creates the need for a unique graph representation called the *canonical graph*. In a canonical graph representation, the vertex representing the housing of a transmission mechanism is denoted as the *root*. Recall that those joints connecting the coaxial links of a mechanism can be rearranged in several different ways without affecting the function of the mechanism. Among various arrangements of the coaxial joints, a unique configuration exists in which all the thin-edged paths emanating from the root and terminating at any other vertices have distinct edge levels. Such a unique graph representation is called the *canonical graph representation* [15]. For example, Figure 8.18 illustrates the conventional and canonical graph representations of the Simpson gear set shown in Figure 8.16.

ID No.	Graph	Schematic
3020		
6206		
6503a		
6503b		

FIGURE 8.14
Feasible transmission gear trains having five and six links — part 1.

Using canonical representation, the similarities and differences among various transmission mechanisms can be clearly distinguished. In particular, the vertices of a canonical graph can be divided into several levels. The housing of a transmission is denoted as the *ground level vertex*. A vertex that is connected directly to the root by one thin edge is called the *first level vertex*. A vertex that is connected to the root by two thin edges is called the *second level vertex*, and so on. Each vertex at any particular level is connected to the preceding vertex by precisely one thin edge. All thin edges of the same label are incident to a common lower level vertex. The first level vertices represent those coaxial sun gears, ring gears, or carriers, whereas the second level vertices represent planet gears [1].

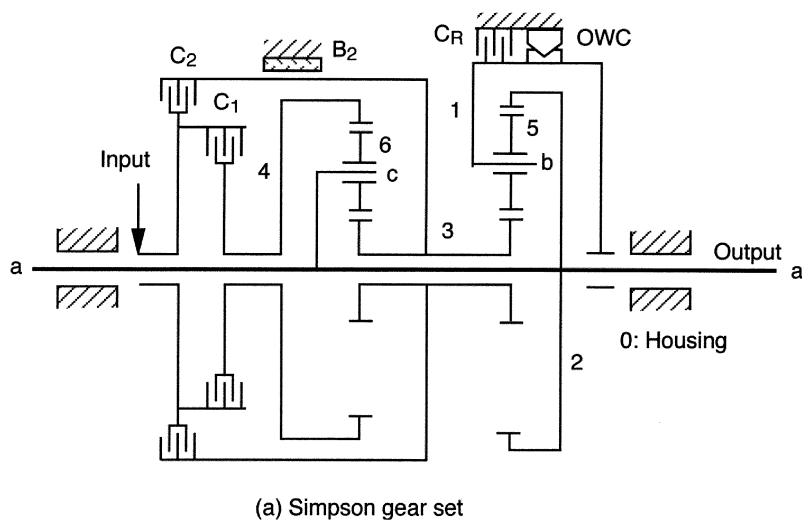
ID No.	Graph	Schematic
6506		
6401		
6601		
6701		

FIGURE 8.15
Feasible transmission gear trains having five and six links — part 2.

EGMs with their links distributed higher than the second level may contain one or more floating carriers. These kinds of EGMs are not practical from the mechanical complexity point of view. In the following, we limit ourselves to those EGMs having their vertices distributed only up to the second level.

8.5.1 Structural Characteristics of Canonical Graphs

Obviously, the canonical graph of an EGM should obey all the structural characteristics, C1 through C3, outlined in the preceding section. In addition, it should also



Range	Activated clutches				
	C ₁	C ₂	C _R	B ₂	OWC
Drive 1	X		⊗		X
Drive 2	X			X	
Drive 3	X	X			
Reverse		X	X		

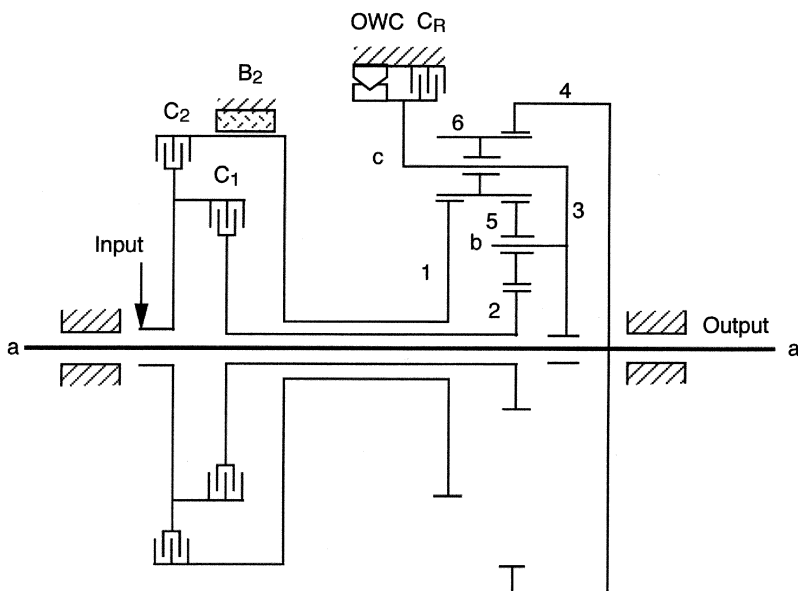
⊗ For downhill braking only

(b) Clutching sequence

FIGURE 8.16
Simpson gear set and its clutching sequence (graph 6506).

possess the following characteristics:

- C4. The first level vertices are connected to the root by thin edges of the same label. No geared edges can be incident to the root.
- C5. All thin edges of the same label are incident to a common lower level vertex. Those second level vertices that are connected to a common first level vertex by thin edges of the same label form a *family*. By definition, vertices of different families are connected to lower level vertices by thin edges of different labels.
- C6. All second level vertices must have at least two geared edges and one turning pair edge incident to it. This prevents formation of a redundant link.



(a) Ravigneaux gear set

Range	Activated clutches				
	C ₁	C ₂	C _R	B ₂	OWC
Drive 1	X		⊗		X
Drive 2	X			X	
Drive 3	X	X			
Reverse		X	X		

⊗ for downhill braking only

(b) Clutching sequence

FIGURE 8.17

Ravigneaux gear set and its clutching sequence (graph 6401).

C7. A geared edge can have one of the following pairs of vertices as its end point:

- Two second level vertices that are connected to a first level vertex by thin edges of different labels.
- One first level vertex and one second level vertex that are not adjacent to one another.

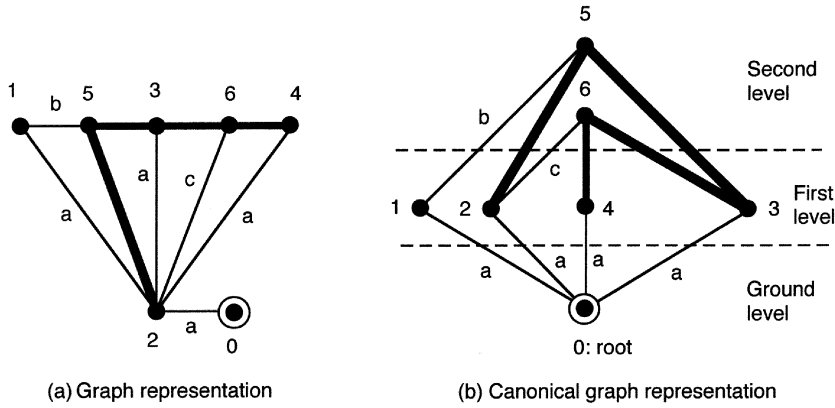


FIGURE 8.18
Graph and canonical graph representation of Simpson gear set.

C8. Although EGMs are fractionated two-dof mechanisms, their canonical graphs contain no articulation points.

8.5.2 Enumeration of Canonical Graphs

Canonical graph representation of EGMs dictates some specific arrangement of the vertices. It also requires the thin edges to be labeled in a particular way that prohibits the generation of pseudoisomorphic graphs. Using the above structural characteristics, an efficient hierarchical algorithm has been developed for enumeration of EGMs [1]. The process is divided into two phases. In the first phase, trees that are suitable for creation of canonical graphs are enumerated. In the second phase, geared edges are added to the trees to form canonical graphs. Each of the two phases is comprised of a few key steps as follows.

Enumeration of Trees

Given the number of links, n (including the base link), the structural characteristics C1, C2, C4, and C5 are used to formulate an algorithm for enumeration of feasible trees.

- S1. Determine the minimum number of coaxial links, n_c , by Equation (8.8). This is the minimum number of vertices that a tree should have at the first level.
- S2. Distribute the remaining $n - n_c - 1$ vertices into the first and second levels in as many combinations as possible. Various distributions of a number of vertices in two levels are given in Table 8.1. We call each distribution a *type*. Since there are already n_c vertices preassigned to the first level from the preceding step, the total number of first level vertices is equal to that given in Table 8.1 plus n_c .

Table 8.1 Distribution of Vertices into Two Levels.

No. of Vertices	Type	Level 1	Level 2
2	1	0	2
	2	1	1
3	1	0	3
	2	1	2
	3	2	1
4	1	0	4
	2	1	3
	3	2	2
	4	3	1

S3. Connect all the first level vertices to the root by thin edges of the same label.

S4. Partition the second level vertices into as many parts as possible. Various partitions of an integer into parts are given in Table 8.2. We call each partition a *kind*, and each part of a partition a *family*.

Table 8.2 Partition of Second Level Vertices into Parts.

Partition of	Kind	Family 1	Family 2	Family 3	Family 4
2	1	2	0	0	0
	2	1	1	0	0
3	1	3	0	0	0
	2	2	1	0	0
	3	1	1	1	0
4	1	4	0	0	0
	2	3	1	0	0
	3	2	2	0	0
	4	2	1	1	0
	5	1	1	1	1

S5. Connect the second level vertices to the first level vertices. According to C5, all members of the same family are connected to a common first level vertex by thin edges of the same label. We add one family at a time, starting from the family with the largest number of members.

Note that in S5, if a family of vertices is to be connected to a first level vertex in all possible ways, a number of isomorphic graphs would be generated. To reduce the number of isomorphic graphs, the concept of *similar vertices* can be employed. All first level vertices are similar before they are connected by one or more second level vertices. When a vertex is to be connected to a first level vertex, choose only one

out of all similar vertices. A large number of isomorphic graphs can be avoided by applying this simple rule of thumb.

Example 8.1 In this example, we enumerate all feasible trees of canonical graphs that are suitable for the creation of 7-link, 4-speed automatic EGMs.

- S1. There are seven links, $n = 7$ (including the housing). Substituting $n_r = 5$ into Equation (8.8), we obtain $n_c = 4$ as the minimum number of coaxial links.
- S2. Referring to Table 8.1, the remaining two vertices can both be located at the second level, or one at the first level and the other at the second level. Figure 8.19a and b provide graphical representations of the two types of distribution. The total number of vertices in each level is given in Table 8.3.

Table 8.3 Partition of Six Vertices into Two Levels.

Classification	Level 1	Level 2
Type 1	4	2
Type 2	5	1

- S3. Connect the first level vertices to the root by thin edges of the same level, a , as shown in Figure 8.19a and b.
- S4. Referring to Table 8.2, the two second level vertices of the first type can be further partitioned into two kinds. The first kind contains a family of two vertices, whereas the second kind contains two families (one vertex per family). The second type contains only one vertex and no further division is necessary.
- S5. For the first kind of the first type, there is only one family and both vertices must be connected to one of the four first level vertices with the same edge label as shown in Figure 8.19c. For the second kind of the first type, there are two families and they can be connected to one or two first level vertices by thin edges of different labels. Since the four first level vertices are similar, we obtain two nonisomorphic trees as shown in Figure 8.19d and e. For the second type, there is only one second level vertex and it can be connected to any one of the first level vertices as shown in Figure 8.19f.

The above procedure can be implemented on a computer using the adjacency matrix and a *nested-do loops* algorithm. For the above example, the corresponding matrix representations are shown in Figure 8.20. The matrix can be divided into nine submatrices. Since the root does not connect to itself, the element of the I-I submatrix is set to zero. Since the first level vertices are connected to the root by thin edges of the same label and not among themselves, all elements of the I-II and II-I submatrices are given by the same edge label “a,” whereas all elements of the II-II submatrix are set to zero. All elements of the I-III and III-I submatrices are also set to zero because

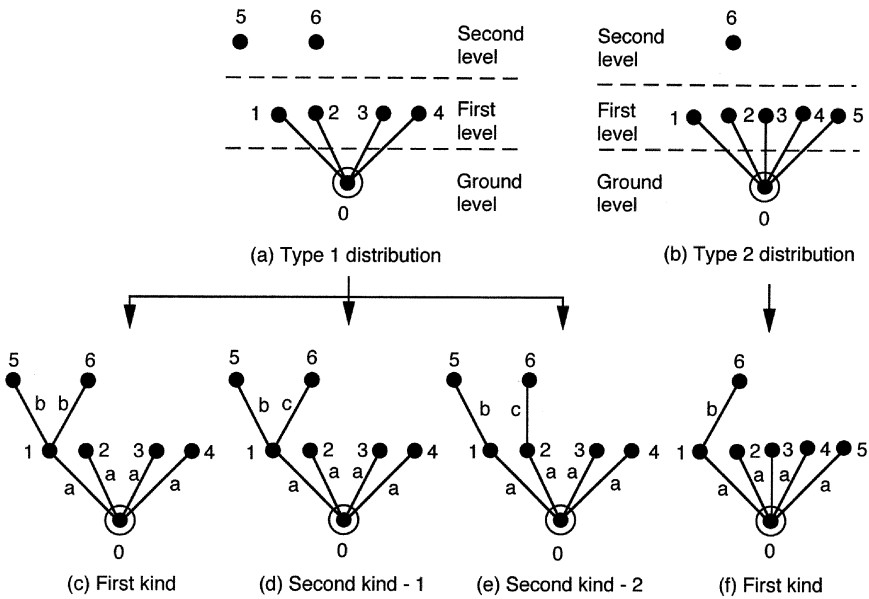


FIGURE 8.19
Enumeration of trees of seven vertices.

the second level vertices cannot be connected directly to the root. Hence, we only need to work on the elements of II-III (and III-II) and III-III submatrices. \square

Addition of Geared Edges

We now apply structural characteristics C3, C6, and C7 for the addition of geared edges.

- S6. We first connect two second level vertices of different families by a geared edge. This means that the III-III submatrix of the adjacency matrix shown in Figure 8.20 is under consideration. There are two provisions, one of adding some geared edges and the other of not adding any.
- S7. Next we connect one second level vertex to one first level vertex by a geared edge. That is, the II-III (and III-II) submatrix of the adjacency matrix shown in Figure 8.20 is under consideration. While adding geared edges, make sure that every second level vertex is incident by at least two geared edges. The total number of geared edges to be added is equal to $n - 3$ where n is the number of links, including the housing.
- S8. For every canonical graph generated, check for the existence of locked sub-chains, redundant links, and possible graph isomorphisms.

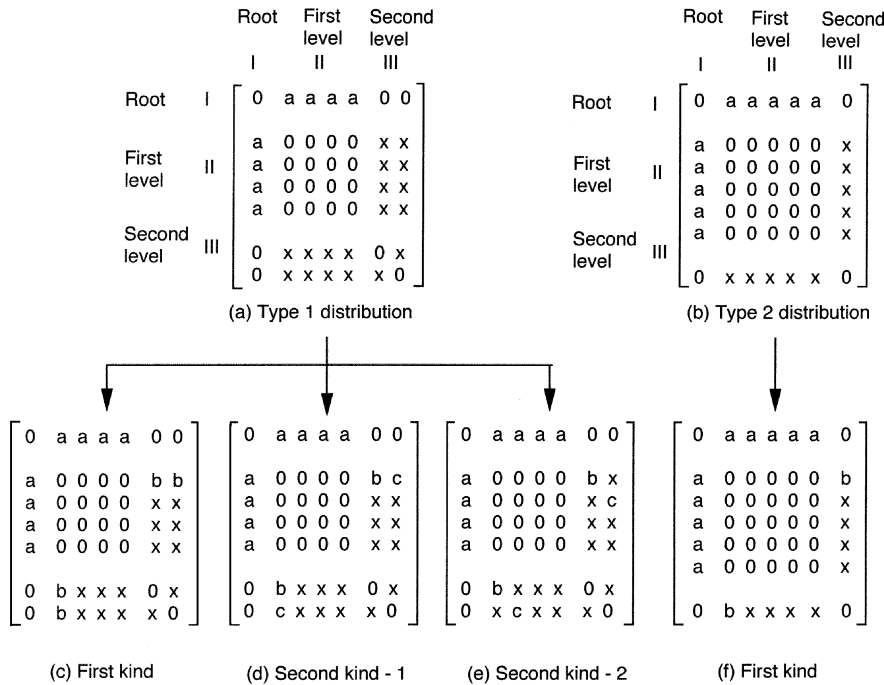


FIGURE 8.20
Matrix representation of trees of seven vertices.

Example 8.2 In this example, we enumerate the canonical graphs of seven-link 4-speed automatic transmission mechanisms by adding four geared edges to the tree shown in Figure 8.19d to illustrate the principle.

Referring to Figure 8.21a, there are two second level vertices. Since these two vertices do not belong to the same family, there are two possible cases:

Case (1): One geared edge connects the two second level vertices to each other. There are three more geared edges to be added. To avoid the creation of articulation points, each of the three first level vertices, vertices 2, 3, and 4, must be incident by one and exactly one geared edge. Hence, there are four different ways of distributing the three geared edges to the two second level vertices: (3 + 0), (2 + 1), (1 + 2), and (0 + 3), where the first number in the parentheses represents the number of geared edges incident to vertex 5, and the second number denotes the number of geared edges incident to vertex 6. The (3 + 0) and (0 + 3) distributions are not feasible because both distributions leave one of the second level vertices with only one incident geared edge. Furthermore, the (1 + 2) and (2 + 1) distributions result in two isomorphic graphs. Hence, we obtain only one nonisomorphic canonical graph as shown in Figure 8.21b.

Case (2): The two second level vertices are not connected to each other by a geared edge. All four geared edges will be used to connect the two second level vertices to the three first level vertices 2, 3, and 4. To avoid the creation of articulation points, two of the three first level vertices should be connected by one geared edge, whereas the third should be connected by two geared edges. Since vertices 2, 3 and 4 are similar, this leads to only one nonisomorphic distribution of the four geared edges to the three first level vertices. Furthermore, there are five different ways of distributing the four geared edges to the second level vertices: $(4 + 0)$, $(3 + 1)$, $(2 + 2)$, $(1 + 3)$, and $(0 + 4)$. The $(4 + 0)$, $(3 + 1)$, $(1 + 3)$, and $(0 + 3)$ distributions are not feasible because they all leave one of the second level vertices with less than two incident geared edges. As a result, we obtain one labeled nonisomorphic canonical graph as shown in Figure 8.21c.

Note that the two canonical graphs shown in Figure 8.21b and c do not contain locked subchain or redundant links. Furthermore, they are not isomorphic. The corresponding matrix representations derived by replacing four “x” with “g” and the remaining “x” with “0” are shown in Figure 8.22. \square

Using canonical graph representation, Chatterjee and Tsai [1] developed an atlas of canonical graphs of EGMs with up to ten links. The number of solutions as a function of the number of links are listed in Table 8.4. Figure 8.23 shows eight labeled canonical graphs of EGMs with six and seven links. Readers should verify that these canonical graphs can be obtained by adding a coaxial fixed link to the graphs of EGTs shown in Figures 8.14 and 8.15. Figure 8.24 shows 20 labeled canonical graphs of EGMs having eight links.

Table 8.4 Canonical Graphs of EGMs.

No. of Links	No. of Geared Edges	No. of Solutions
6	3	1
7	4	7
8	5	20
9	6	128
10	7	620

8.5.3 Identification of Fundamental Circuits

In this section, we introduce an algebraic method for identification of fundamental circuits in an EGM. The method utilizes the graph theory and some related matrices. Specifically, Equation (2.33) will be applied for identification of fundamental circuits.

The Simpson gear set will be used as an example to demonstrate the principle. The canonical graph G of the Simpson gear set and its spanning tree T are shown in Figure 8.25. To facilitate the analysis, we have labeled the arcs of G from e_1 to e_6 , and the chords from e_7 to e_{10} . Obviously, the union of the arcs and chords constitutes the edge set of G .

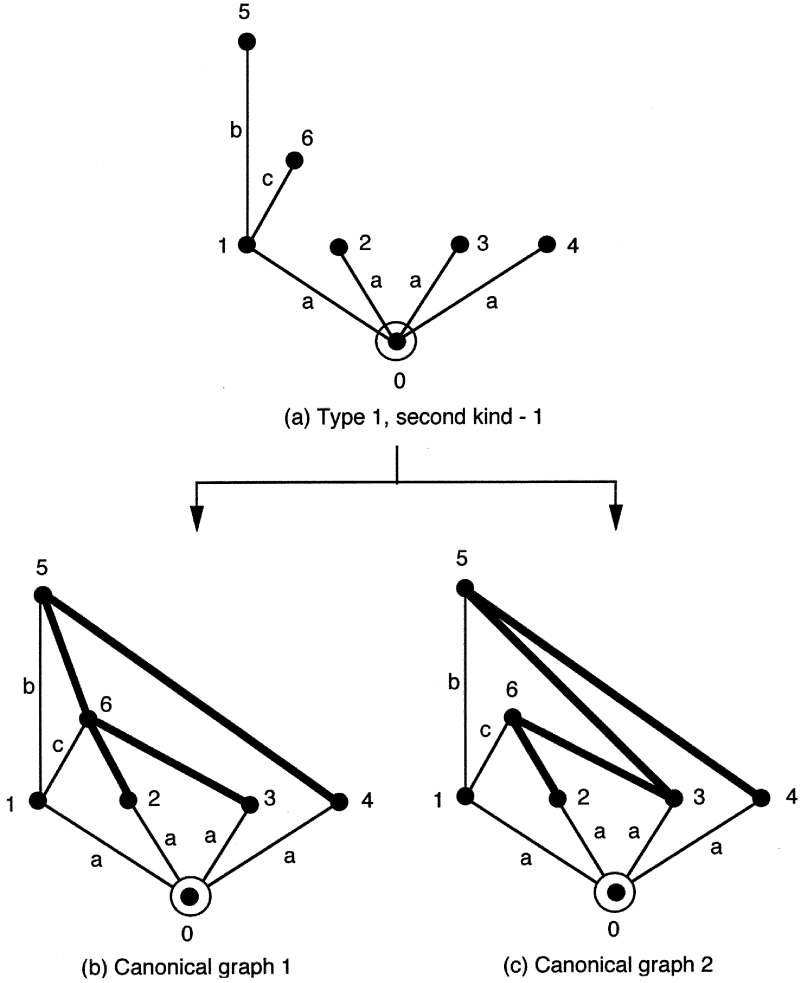
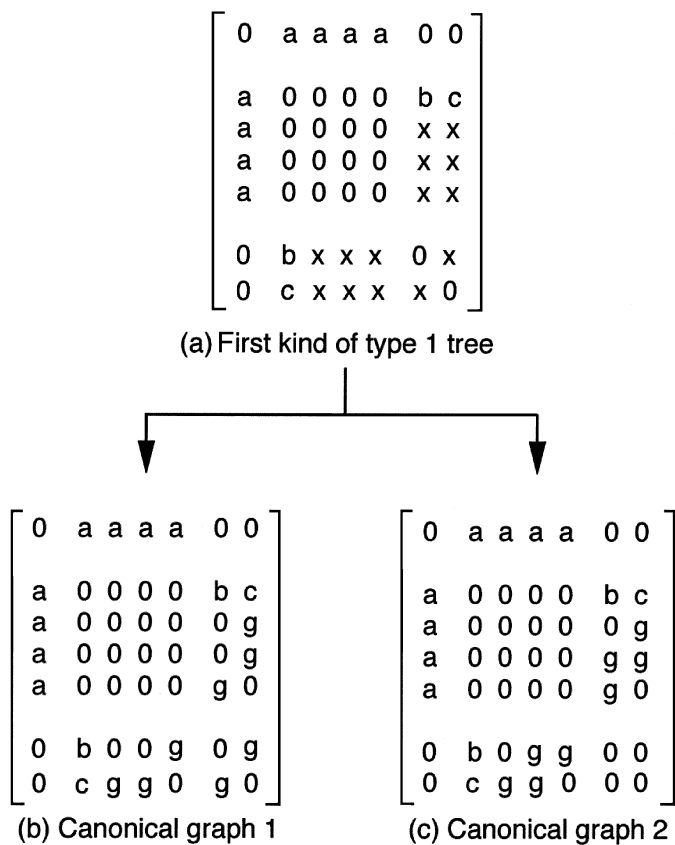


FIGURE 8.21
Addition of geared edges to a tree.

By definition, the incidence matrix for the directed graph is given by

$$B = \begin{bmatrix} 1 & 1 & 1 & 1 & 0 & 0 & 0 & 0 & 0 & 0 \\ 1 & 0 & 0 & 0 & 1 & 0 & 0 & 0 & 0 & 0 \\ 0 & 1 & 0 & 0 & 0 & 1 & 1 & 0 & 0 & 0 \\ 0 & 0 & 0 & 1 & 0 & 0 & 0 & 0 & 1 & 1 \\ 0 & 0 & 1 & 0 & 0 & 0 & 0 & 1 & 0 & 0 \\ 0 & 0 & 0 & 0 & 1 & 0 & 1 & 0 & 0 & 1 \\ 0 & 0 & 0 & 0 & 0 & 1 & 0 & 1 & 1 & 0 \end{bmatrix}. \tag{8.9}$$

**FIGURE 8.22****Matrix representations of canonical graphs.**

The reduced incidence matrix associated with the arcs is

$$\tilde{B}_A = \begin{bmatrix}
 1 & 0 & 0 & 0 & 1 & 0 \\
 0 & 1 & 0 & 0 & 0 & 1 \\
 0 & 0 & 0 & 1 & 0 & 0 \\
 0 & 0 & 1 & 0 & 0 & 0 \\
 0 & 0 & 0 & 0 & 1 & 0 \\
 0 & 0 & 0 & 0 & 0 & 1
 \end{bmatrix}. \quad (8.10)$$

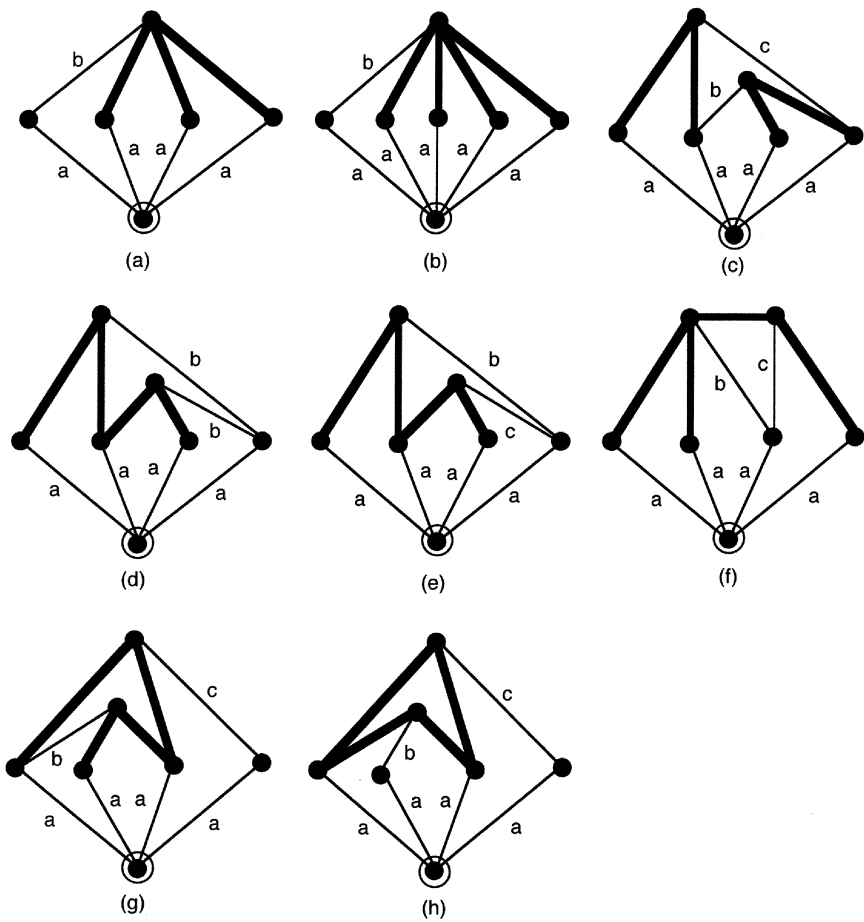


FIGURE 8.23
Canonical graphs of six- and seven-link EGMs.

The reduced incidence matrix associated with the chords is

$$\tilde{B}_C = \begin{bmatrix} 0 & 0 & 0 & 0 \\ 1 & 0 & 0 & 0 \\ 0 & 0 & 1 & 1 \\ 0 & 1 & 0 & 0 \\ 1 & 0 & 0 & 1 \\ 0 & 1 & 1 & 0 \end{bmatrix}. \tag{8.11}$$

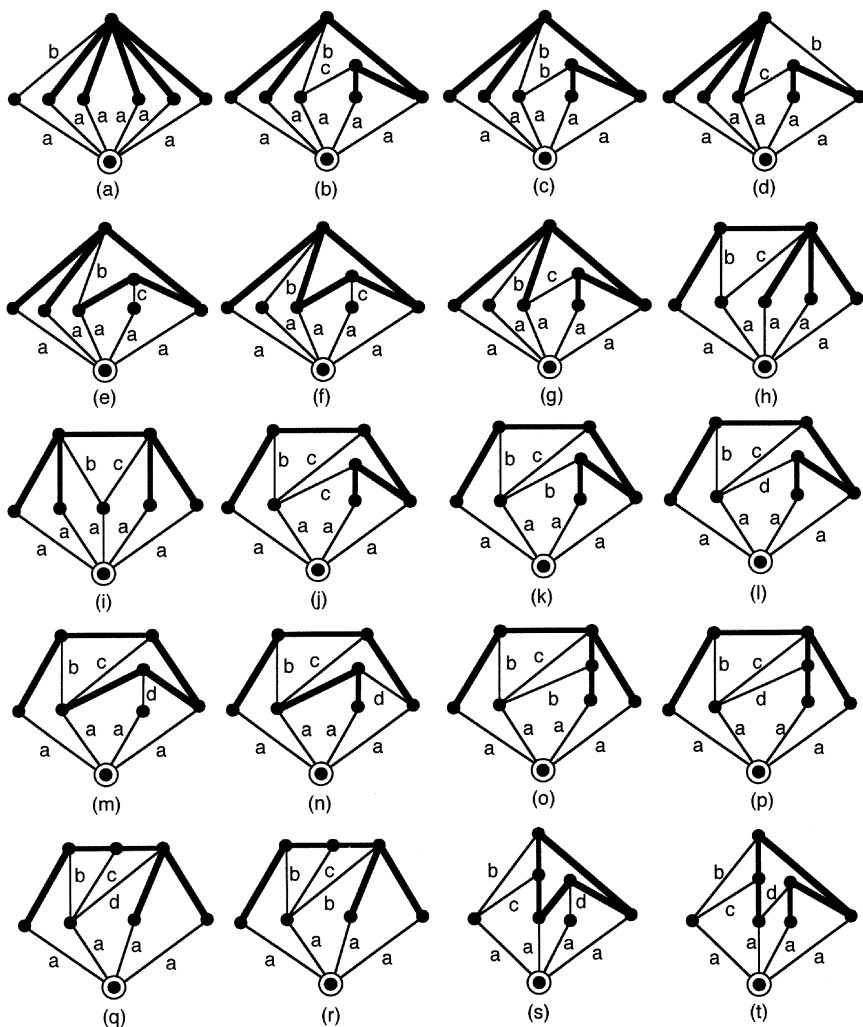
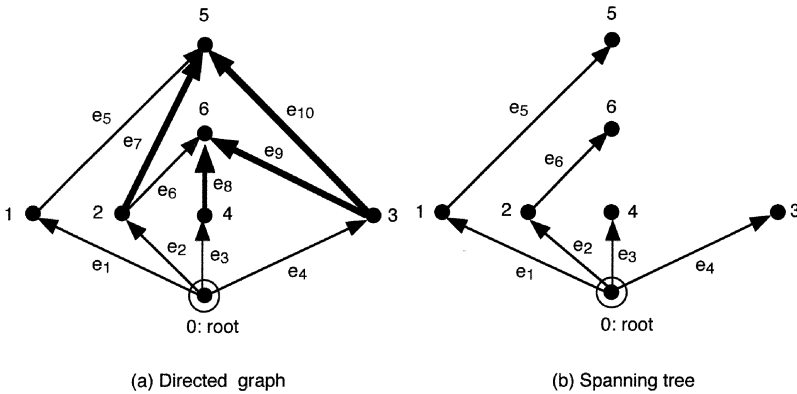


FIGURE 8.24
Canonical graphs of eight-link EGMS.

The path matrix, Equation (2.26), associated with the rooted tree shown in Figure 8.25b is

$$T = \begin{bmatrix} 1 & 0 & 0 & 0 & 1 & 0 \\ 0 & 1 & 0 & 0 & 0 & 1 \\ 0 & 0 & 0 & 1 & 0 & 0 \\ 0 & 0 & 1 & 0 & 0 & 0 \\ 0 & 0 & 0 & 0 & 1 & 0 \\ 0 & 0 & 0 & 0 & 0 & 1 \end{bmatrix}. \quad (8.12)$$

**FIGURE 8.25**

Labeled canonical graph and spanning tree of the Simpson gear set.

Substituting Equations (8.11) and (8.12) into Equation (2.28) yields

$$T\tilde{B}_A = \begin{bmatrix} 1 & 0 & 0 & 0 & 0 & 0 \\ 0 & 1 & 0 & 0 & 0 & 0 \\ 0 & 0 & 1 & 0 & 0 & 0 \\ 0 & 0 & 0 & 1 & 0 & 0 \\ 0 & 0 & 0 & 0 & 1 & 0 \\ 0 & 0 & 0 & 0 & 0 & 1 \end{bmatrix} = I \quad (8.13)$$

as predicted by the theory.

Substituting Equations (8.11) and (8.12) into Equation (2.32) and the resulting expression into Equation (2.33) yields

$$C = \begin{bmatrix} 1 & 1 & 0 & 0 & 1 & 0 & 1 & 0 & 0 & 0 \\ 0 & 1 & 1 & 0 & 0 & 1 & 0 & 1 & 0 & 0 \\ 0 & 1 & 0 & 1 & 0 & 1 & 0 & 0 & 1 & 0 \\ 1 & 0 & 0 & 1 & 1 & 0 & 0 & 0 & 0 & 1 \end{bmatrix}. \quad (8.14)$$

From Equation (8.14), we observe that there are four fundamental circuits. Circuit 1 consists of edges e_1 , e_2 , e_5 , and e_7 ; circuit 2 consists of edges e_2 , e_3 , e_6 , and e_8 ; circuit 3 consists of edges e_2 , e_4 , e_6 , and e_9 ; and circuit 4 consists of edges e_1 , e_4 , e_5 , and e_{10} .

8.5.4 Detection of Transfer Vertices

The transfer vertices in the canonical graph of an EGM can be easily detected. The transfer vertex associated with a gear pair is found by scanning the row of the adjacency matrix corresponding to the higher-level vertex of the gear pair. The column number, where the first nonzero element that is not a “g” occurs, is the link number of

the transfer vertex. If both vertices of the gear pair are located at the same level, then scan across either row of the two vertices. Note that since the links are numbered from zero, the row number in the adjacency matrix is greater than the link number by one.

In the following, we use the Simpson gear set as an example to illustrate the concept. Referring to the canonical graph shown in Figure 8.18b, the link-to-link adjacency matrix is given below.

$$A = \begin{bmatrix} 0 & \vdots & 1 & 1 & 1 & 1 & \vdots & 0 & 0 \\ \cdots & \cdot & \cdots & \cdots & \cdots & \cdots & \cdot & \cdots & \cdots \\ 1 & \vdots & 0 & 0 & 0 & 0 & \vdots & b & 0 \\ 1 & \vdots & 0 & 0 & 0 & 0 & \vdots & g & c \\ 1 & \vdots & 0 & 0 & 0 & 0 & \vdots & g & g \\ 1 & \vdots & 0 & 0 & 0 & 0 & \vdots & 0 & g \\ \cdots & \cdot & \cdots & \cdots & \cdots & \cdots & \cdot & \cdots & \cdots \\ 0 & \vdots & b & g & g & 0 & \vdots & 0 & 0 \\ 0 & \vdots & 0 & c & g & g & \vdots & 0 & 0 \end{bmatrix}. \quad (8.15)$$

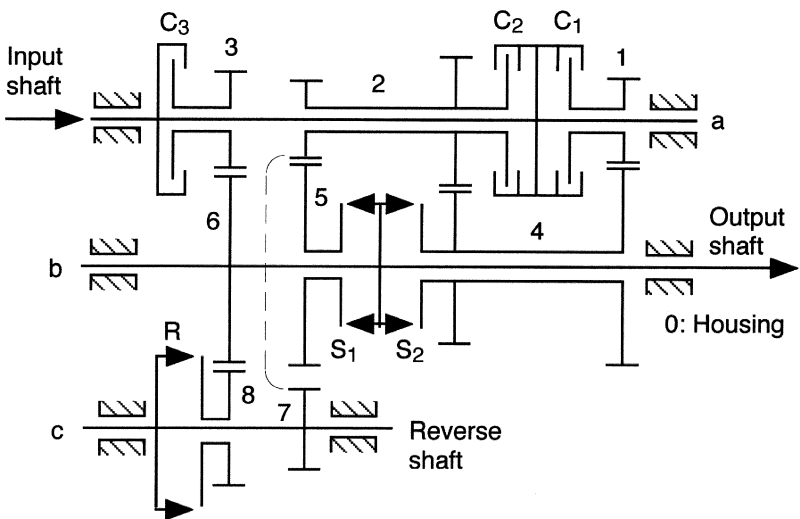
From Equation (8.14), we observe that circuit 1 consists of edges e_1 , e_2 , e_5 , and e_7 in which e_7 is a geared edge. Scanning down the 8th column of the incidence matrix, Equation (8.9), we find that e_7 connects vertices 2 and 5. Since vertex 5 is located at a higher level, we next scan across the 6th row of the adjacency matrix to find the transfer vertex. From Equation (8.15), we observe that the (6, 2) element is nonzero. Hence, link 1 is the transfer vertex. Similarly the transfer vertices of circuits 2, 3, and 4 are found to be vertices 2, 2, and 1, respectively.

8.6 Atlas of Epicyclic Gear Transmission Mechanisms

Appendix G provides an atlas of some commonly used epicyclic gear transmission mechanisms. It should be noted that several clutching sequences can be developed from a given gear set. A computer-aided methodology for the enumeration of clutching sequences can be found in [6]. It should also be noted that transmission mechanisms of higher complexity can be formed by connecting two planetary gear trains by clutches instead of spline shafts. Several transmission gear trains of this type, such as Figures G.10 and G.11 are included in Appendix G to illustrate the concept. See [16] and [5] for more examples.

Finally, we point out an entirely different type of transmission mechanism as shown in Figure 8.26. The mechanism consists of two counter-rotating shafts and an intermediate reverse shaft on which several compound gear pairs, rotating clutches, and

synchronizers are mounted. Unlike the conventional countershaft transmission, this type of transmission allows power to circulate back and forth between the two countershafts. As a result, many speed ratios can be obtained by just a few gear pairs and control clutches.



(a) Schematic diagram

Range	Activated clutches					
	C ₁	C ₂	C ₃	S ₁	S ₂	R
First	X			X		
Second		X		X		
Third			X			
Fourth	X				X	
Fifth		X			X	
Reverse	X					X

(b) Clutching sequence

FIGURE 8.26
Polak's transmission mechanism.

8.7 Summary

In this chapter, we have shown that by using the design methodology outlined in Chapter 1, the kinematic structures of mechanism can be enumerated in a systematic and essentially unbiased manner. The usefulness of the method is demonstrated with the enumeration of variable-stroke engine mechanisms, constant-velocity shaft couplings, and automatic transmission mechanisms. It is hoped that the methodology and the atlas developed in this chapter will be useful for practicing engineers. Furthermore, a simple procedure for identification of fundamental circuits and the corresponding transfer vertices of epicyclic gear trains was described. An atlas of commonly used epicyclic transmission gear trains is provided in Appendix G.

References

- [1] Chatterjee, G. and Tsai, L.W., 1994, Enumeration of Epicyclic-Type Automatic Transmission Gear Trains, *SAE 1994 Transactions, Journal of Passenger Cars*, Sec. 6, 103, 1415–1426.
- [2] Freudenstein, F. and Maki, E.R., 1979, Creation of Mechanisms According to Kinematic Structure and Function, *Journal of Environmental and Planning B*, 6, 375–391.
- [3] Freudenstein, F. and Maki, E.R., 1983, Development of an Optimum Variable-Stroke Internal-Combustion Engine from the Viewpoint of Kinematic Structure, *ASME Journal of Mechanisms, Transmissions, and Automation in Design*, 105, 2, 259–266.
- [4] Freudenstein, F. and Maki, E.R., 1984, Kinematic Structure of Mechanisms for Fixed and Variable-Stroke Axial-Piston Reciprocating Machines, *ASME Journal of Mechanisms, Transmissions, and Automation in Design*, 106, 3, 355–364.
- [5] Gott, P.G., 1991, *Changing Gears*, Society of Automotive Engineers, Inc., Warrendale, Pennsylvania.
- [6] Hsieh, H.I. and Tsai, L.W., 1996, A Methodology for Enumeration of Clutching Sequences Associated with Epicyclic-Type Automatic Transmission Mechanisms, *SAE 1996 Transactions, Journal of Passenger Cars*, Sec. 6, 105, 928–936.

- [7] Hsieh, H.I. and Tsai, L.W., 1998, The Selection of a Most Efficient Clutching Sequence Associated with an Automatic Transmission Mechanism, *ASME Journal of Mechanical Design*, 120, 4, 514–519.
- [8] Hunt, K.H., 1983, Structural Kinematics of In-Parallel-Actuated Robot-Arms, *ASME Journal of Mechanisms, Transmissions, and Automation in Design*, 105, 705–712.
- [9] Mogalapalli, S., Magrab, E.B., and Tsai, L.W., 1993, A CAD System for the Optimization of Gear Ratios for Automotive Automatic Transmissions, SAE International Congress and Exposition, Automotive Transmissions and Drive-lines, SP-965, Paper No. 930675.
- [10] Martin, G.H., 1982, *Kinematics and Dynamics of Machines*, McGraw-Hill Book Co., New York, NY.
- [11] Nadel, B.A. and Lin, J., 1991, Automobile Transmission Design as a Constraint Satisfaction Problem: Modeling the Kinematic Level, *Artificial Intelligence for Engineering Design, Analysis and Manufacturing*, 5, 3, 137–171.
- [12] Nadel, B.A., Wu, X., and Kagan, D., 1993, Multiple Abstraction Levels in Automobile Transmission Design: Constraint Satisfaction Formulations and Implementations, *International Journal of Expert Systems*, 6, 4, 489–559.
- [13] Pouliot, H.N., Delameter, W.R., and Robinson, C.C., 1977, Variable-Displacement Spark-Ignition Engine, *SAE Transactions*, 86, 446–464.
- [14] Siegla, D.C. and Siewert, R.M., 1978, Variable-Stroke Engine — Problems and Promises, *SAE Transactions*, 87, 2726–2736.
- [15] Tsai, L.W., 1988, The Kinematics of Spatial Robotic Bevel-Gear Trains, *IEEE Journal of Robotics and Automation*, 4, 2, 150–156.
- [16] Tsai, L.W., Maki, E.R., Liu, T., and Kapil, N.G., 1988, The Categorization of Planetary Gear Trains For Automatic Transmissions According to Kinematic Topology, in *SAE XXII FISITA '88, Automotive Systems Technology: The Future*, P-211, 1, 1.513–1.521, SAE paper No. 885062.
- [17] Tuttle, E.R., Peterson, S.W., and Titus, J.E., 1989, Enumeration of Basic Kinematic Chains Using the Theory of Finite Groups, *ASME Journal of Mechanisms, Transmissions, and Automation in Design*, 111, 4, 498–503.
- [18] Tuttle, E.R., Peterson, S.W., and Titus, J.E., 1989, Further Application of Group Theory to the Enumeration and Structural Analysis of Basic Kinematic Chains, *ASME Journal of Mechanisms, Transmissions, and Automation in Design*, 111, 4, 494–497.

Exercises

- 8.1 Enumerate all the feasible eight-link variable-stroke engine mechanisms with only one prismatic joint and ground-connected control pivot.
- 8.2 Study the structural characteristics of an automobile suspension mechanism, and enumerate feasible alternative suspension mechanisms.
- 8.3 Study the structural characteristics of an airplane landing wheel mechanism, and enumerate feasible mechanisms of the same type.
- 8.4 Study the structural characteristics associated with wobble-plate axial mechanisms and enumerate feasible variable-stroke axial-piston reciprocating machines using this type of construction. (Hint: See [4].)
- 8.5 Study the structural characteristics associated with variable-valve-timing mechanisms, and enumerate potential new mechanisms. (Hint: an ideal variable-valve-timing mechanism should have the capability of changing the valve lift and the valve opening duration with respect to the engine crankshaft angle.)
- 8.6 Sketch a transmission mechanism by incorporating two sun and two ring gears into the graph shown in Figure 8.24i.
- 8.7 Sketch a transmission mechanism by incorporating two sun and one ring gears into the graph shown in Figure 8.24m. How many potentially feasible clutching sequences can we obtain from this mechanism?

Chapter 9

Robotic Mechanisms

9.1 Introduction

During the last few decades, robot manipulators have been used primarily for repetitive operations and in hazardous environments. Typical applications include parts loading and unloading, radioactive material handling, space and undersea exploration, spot welding, spray painting, sealant application, and some simple component assembly. Recently, there is an increasing interest in making robots more intelligent and more user friendly. Thus, medical-surgery robots, household service robots, micro-robots, and others are becoming available. Although much effort has been spent on the development of robot manipulators, the ultimate goal of developing user-friendly, intelligent robots that can emulate human functions is still in its infancy. Major obstacles are some of the key technologies have not been fully developed. In this chapter, structural characteristics and structural enumeration of some robotic mechanisms are presented.

9.2 Parallel Manipulators

The development of *parallel manipulators* can be dated back to the early 1960s when Gough and Whitehall [6] first devised a six-linear jack system for use as a universal tire testing machine. Later, Stewart [17] developed a platform manipulator for use as a flight simulator. Since 1980, there has been an increasing interest in the development of parallel manipulators. Potential applications of parallel manipulators include mining machines [3], pointing devices [5], and walking machines [26].

Although parallel manipulators have been studied extensively, most of the studies have concentrated on the *Stewart-Gough manipulator*. The Stewart-Gough manipulator, however, has a relatively small workspace and its direct kinematics are extremely difficult to solve. Hence, it may be advantageous to explore other types of parallel manipulators with the aim of reducing the mechanical complexity and simplifying

the kinematics and dynamics [10, 14, 16, 25]. A structural classification of parallel manipulators has been made by Hunt [8].

In this section, parallel manipulators are classified into planar, spherical, and spatial mechanisms. The kinematic structures of parallel manipulators are enumerated according to their degrees of freedom and connectivity listing [22].

9.2.1 Functional Requirements

As shown in Figure 9.1, a parallel manipulator typically consists of a moving platform that is connected to a fixed base by several limbs. The number of limbs is preferably equal to the number of degrees of freedom of the moving platform such that each limb is controlled by one actuator and all actuators can be mounted on or near the fixed base. As a result of this structural arrangement, parallel manipulators possess the advantages of low inertia, high stiffness, and large payload capacity. These advantages continue to motivate the development of parallel kinematic machines, such as Ingersoll's milling machine shown in Figure 9.2 [2], Giddings and Lewis's machining center shown in Figure 1.7, Toyoda's milling machine shown in Figure 9.3 [13], and the Hexaglide and Triaglide [7].

From the above discussion, we summarize the functional requirements of parallel manipulators as follows:

- F1. The mechanism possesses multiple degrees of freedom. The number of degrees of freedom required depends on the intended application.
- F2. The manipulator consists of a moving platform that is connected to a fixed base by several limbs; that is, it possesses a parallel kinematic architecture.
- F3. The number of limbs is preferably equal to the number of degrees of freedom such that each limb is controlled by one actuator, and external loads on the moving platform are shared by all actuators.
- F4. The actuators are preferably mounted on or near the fixed base.

9.2.2 Structural Characteristics

We now translate as many functional requirements into structural characteristics as possible. Obviously, the manipulator should satisfy the general structural characteristics of a mechanism. For example, the number of degrees of freedom is governed by Equation (4.3); the number of independent loops, number of links, and number of joints are related by Euler's equation, Equation (4.5); and the loop mobility criterion is given by Equation (4.7). In addition, the following manipulator-specific characteristics should also be satisfied.

We assume that each limb is made up of an open-loop chain and the number of limbs, m , is equal to the number of degrees of freedom of the moving platform. It follows that

$$m = F = L + 1. \quad (9.1)$$

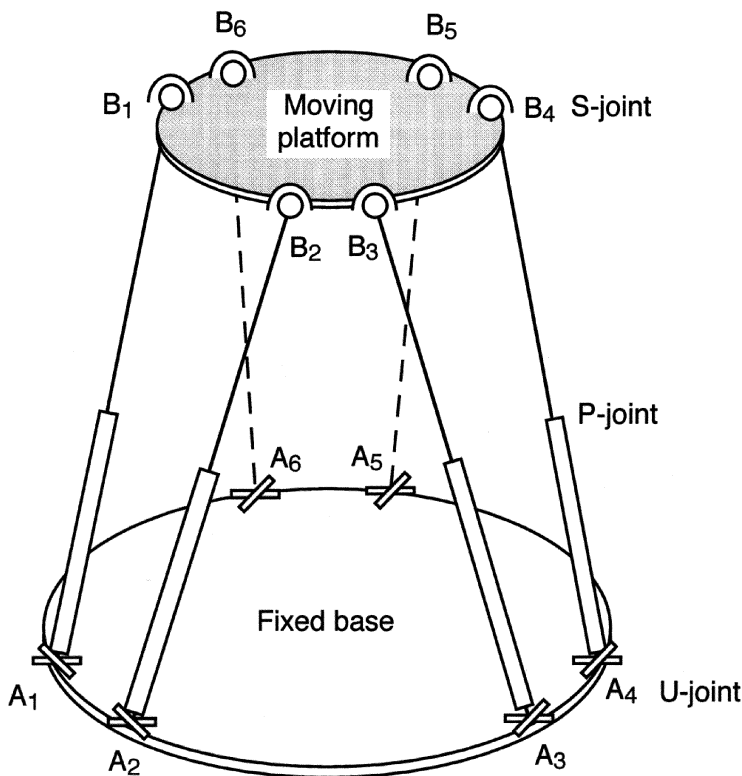


FIGURE 9.1
A typical parallel manipulator.

Let the *connectivity* of a limb, C_k , be defined as the number of degrees of freedom associated with all the joints, including the terminal joints, in that limb. Then,

$$\sum_{k=1}^m C_k = \sum_{i=1}^j f_i . \quad (9.2)$$

Substituting Equation (9.2) into Equation (4.7) and making use of Equation (9.1), we obtain

$$\sum_{k=1}^m C_k = (\lambda + 1)F - \lambda . \quad (9.3)$$

To ensure proper mobility and controllability of the moving platform, the connectivity of each limb should not be greater than the motion parameter or be less than the number of degrees of freedom of the moving platform; that is,

$$\lambda \geq C_k \geq F . \quad (9.4)$$



FIGURE 9.2
Hexapod. (Courtesy of NIST, Gaithersburg, MD, photographed by K.K. Simon.)

Equations (4.3), (9.1), (9.3), and (9.4) completely characterize the structural topology of parallel manipulators.

As mentioned in Chapter 1, the systematic design methodology consists of two engines: a *generator* and an *evaluator*. By incorporating Equations (9.1), (9.3), and (9.4) in the generator, functional requirements F1, F2, and F3 are automatically satisfied. Functional requirement F4 implies that there should be a base-connected revolute or prismatic joint in each limb, or a prismatic joint that is immediately adjacent to a base-connected joint. This condition and other requirements, if any, are more suitable for use as evaluation criteria. In what follows, we enumerate the

**FIGURE 9.3**

Hexam. (Courtesy of Toyota Machine Works Ltd., Aichi-Pref., Japan.)

kinematic structures of parallel manipulators according to their nature of motion and degrees of freedom.

9.2.3 Enumeration of Planar Parallel Manipulators

For planar manipulators, $\lambda = 3$. Furthermore, we assume that revolute and prismatic joints are the desired joint types. All revolute joint axes must be perpendicular to the plane of motion and prismatic joint axes must lie on the plane of motion.

Planar Two-dof Manipulators

For two-dof manipulators, Equation (9.1) yields $m = 2$ and $L = 1$, whereas Equation (9.3) reduces to $\sum_{k=1}^2 C_k = 5$. Thus, planar two-dof manipulators are single-loop mechanisms. The number of degrees of freedom associated with all the joints is equal to five. Furthermore, Equation (9.4) states that the connectivity in each limb is limited to no more than three and no less than two. Hence, one of the limbs

is a single-link and the other is a two-link chain. These two limbs, together with the end-effector and the base link, form a planar five-bar linkage.

A simple combinatorial analysis yields the following possible planar five-bar chains: *RRRRR*, *RRRRP*, *RRRPP*, and *RRPRP*. Any of the five links can be chosen as the fixed link. Once the fixed link is chosen, either of the two links that is not adjacent to the fixed link can be chosen as the end-effector. For example, Figure 9.4 shows a planar *RR–RRR* parallel manipulator with links 1 and 2 serving as the input links and link 4 as the output link. Figure 9.5 shows a planar *RR–RPR* parallel manipulator.

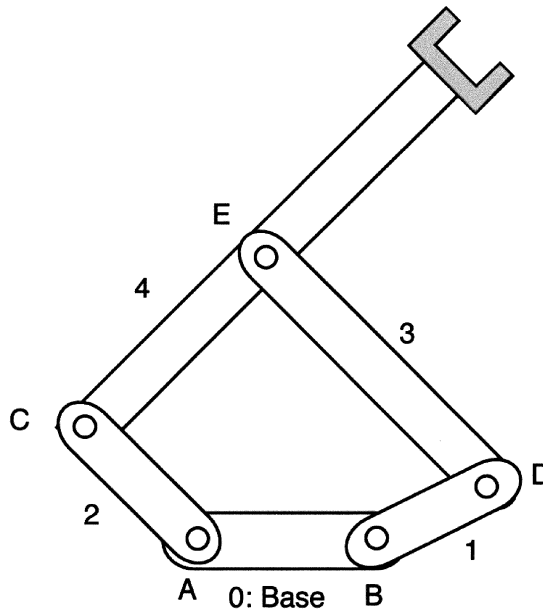


FIGURE 9.4
Planar *RR–RRR* manipulator.

Planar Three-dof Manipulators

For planar three-dof parallel manipulators, Equation (9.1) yields $m = 3$ and $L = 2$. Substituting $\lambda = 3$ and $F = 3$ into Equation (9.3), we obtain

$$\sum_{k=1}^3 C_k = (3 + 1)F - 3 = 9. \quad (9.5)$$

Furthermore, Equation (9.4) reduces to

$$3 \geq C_k \geq 3. \quad (9.6)$$

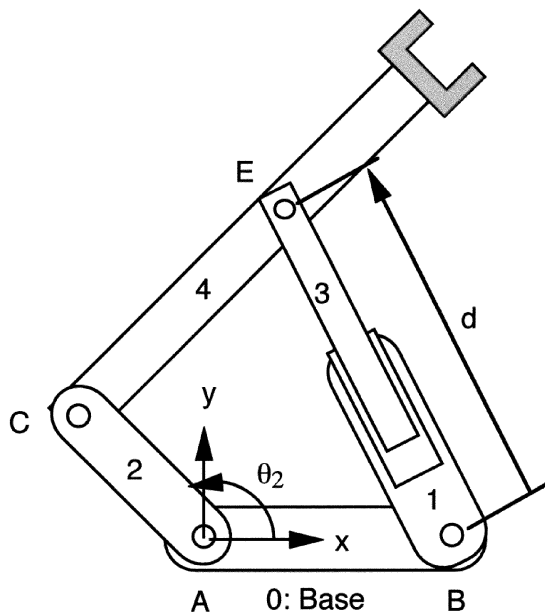


FIGURE 9.5
Planar RR - RPR manipulator.

Hence, the connectivity of each limb should be equal to three; that is, each limb has three degrees of freedom in its joints. Using revolute and prismatic joints as the allowable kinematic pairs, we obtain seven possible limb configurations: RRR , RRP , RPR , PRR , RPP , PRP , and PPR , where the first symbol denotes a base-connected joint and the last symbol represents a platform-connected joint. The PPP combination is rejected due to the fact that it cannot provide rotational degrees of freedom of the end-effector. Theoretically, any of the above configurations can be used as a limb. Hence, there are potentially $7^3 = 343$ possible planar three-dof parallel manipulators. However, if we limit ourselves to those manipulators with identical limb structures, then the number of feasible solutions reduces to seven.

For example, a planar three-dof parallel manipulator using the RRR limb configuration has already been shown in Figure 6.9. Figure 9.6 shows another manipulator using the RPR limb configuration [12].

9.2.4 Enumeration of Spherical Parallel Manipulators

The motion parameter for spherical mechanisms is also equal to three, $\lambda = 3$. Hence, the connectivity requirement for spherical parallel manipulators is identical to that of planar parallel manipulators. However, the revolute joint is the only permissible joint type for construction of spherical linkages. In addition, all the joint axes must intersect at a common point, called the *spherical center*. In this regard, geared

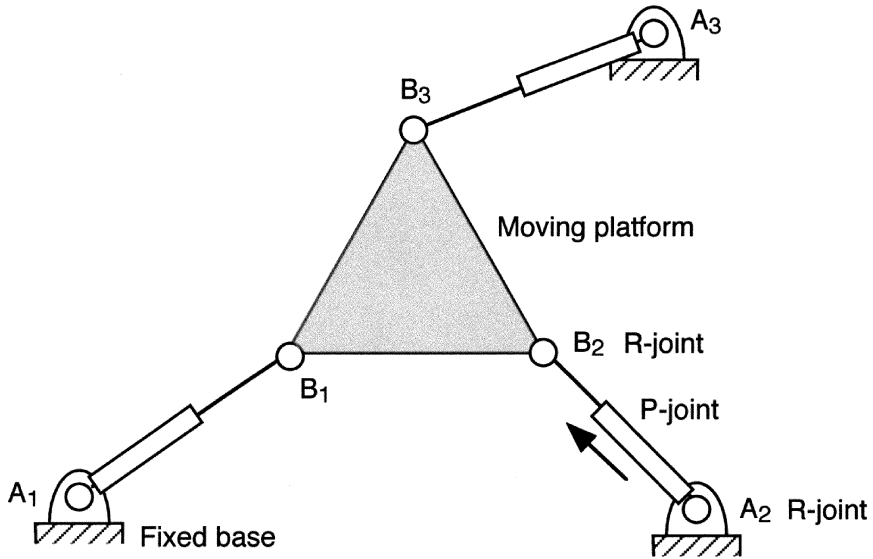


FIGURE 9.6
Planar 3-RPR parallel manipulator.

spherical mechanisms are not included. Therefore, the only feasible two-dof spherical manipulator is the five-bar *RR–RRR* manipulator. Similarly, the only feasible three-dof spherical manipulator is the 3-*RRR* manipulator as shown in Figure 6.14. Several articles related to kinematic analysis, dimensional synthesis, and design optimization of spherical parallel manipulators can be found in [4, 5, 9, 27].

9.2.5 Enumeration of Spatial Parallel Manipulators

For spatial manipulators, $\lambda = 6$. Thus, Equations (9.3) and (9.4) reduce to

$$\sum_k^m C_k = 7F - 6, \quad (9.7)$$

$$6 \geq C_k \geq F. \quad (9.8)$$

Solving Equation (9.7) for positive integers of C_k in terms of the number of degrees of freedom, subject to the constraint imposed by Equation (9.8), we obtain all feasible limb connectivity listings as shown in Table 9.1. Each connectivity listing given in Table 9.1 represents a family of parallel manipulators for which the number of limbs is equal to the number of degrees of freedom of the manipulator, and the total number of joint degrees of freedom in each limb is equal to the value of C_k .

The number of links (and joints) to be incorporated in each limb can be any number, as long as the total number of degrees of freedom in the joints is equal to the required

Table 9.1 Classification of Spatial Parallel Manipulators.

Number of Degrees of Freedom F	Total Joint Degrees of Freedom $\sum_i f_i$	Limb Connectivity Listing C_1, C_2, \dots, C_m
2	8	4, 4 5, 3 6, 2
3	15	5, 5, 5 6, 5, 4 6, 6, 3
4	22	6, 6, 5, 5 6, 6, 6, 4
5	29	6, 6, 6, 6, 5
6	36	6, 6, 6, 6, 6, 6

connectivity, C_k . The maximum number of links occurs when all the joints are one-dof joints. In practice, however, the number of links incorporated in a limb should be kept to a minimum. This necessitates the use of spherical and universal joints. In what follows, we enumerate three- and six-dof manipulators to illustrate the methodology.

Three-dof Translational Platforms

We first enumerate three-dof parallel manipulators with pure translational motion characteristics. To reduce the search domain, we limit our search to those manipulators having three identical limb structures. In this way, the $(5, 5, 5)$ connectivity listing becomes the only feasible limb configuration. Hence, the joint degrees of freedom associated with each limb is equal to five. Furthermore, we assume that revolute (R), prismatic (P), universal (U), and spherical (S) joints are the applicable joint types. A simple combinatorial analysis yields four types of limb configurations as listed in Table 9.2.

Table 9.2 Feasible Limb Configurations for Three-dof Manipulators.

Type	Limb Configuration
120	PUU, UPU, RUU
201	$RRS, RSR, RPS, PRS, RSP, PSR, SPR, PPS, PSP, SPP$
310	$RRRU, RRPV, RPRU, PRRU, RPPU, PRPU, PPRU, RRUR, RRUP, RPUR, PRUR, RPUP, PRUP, PPUR, RURR, RURP, RUPR, PURR, RUPP, PURP, PUPR, UPRR, UPRP, UPPR$
500	$RRRRR, RRRRP, RRRPR, RRPRR, RPRRR, PRRRR, RRRPP, RRPPR, RPPRR, PPRRR, PRPRR, PRRPR, PRRRP, RPRPR, RPRRP, RRPRP$

For each type of limb configuration listed in Table 9.2, the first digit denotes the number of one-dof joints, the second represents the number of two-dof joints, and the third indicates the number of three-dof joints. For example, type 201 limb has two one-dof, zero two-dof, and one three-dof joints, whereas type 120 limb consists of one one-dof, two two-dof, and zero three-dof joints. The joint symbols listed, from left to right, correspond to a base-connected joint, one or more intermediate joints, and lastly a platform-connected joint. Since it is preferable to have a base-connected revolute or prismatic joint, or an intermediate prismatic joint for actuation purposes, *SRR*, *SRP*, *URU*, *UUR*, *UUP*, *URRR*, *URRP*, *URPR*, and *URPP* configurations are excluded from the solution list.

Next, we consider a condition that leads to translational motion of the moving platform. Theoretically, each limb should provide one rotational constraint to the moving platform to completely immobilize the rotational degrees of freedom. Furthermore, the constraints imposed by the three limbs should be independent of one another. Since the spherical joint cannot provide any constraint on the rotation of a rigid body, the entire type-201 configurations are excluded from further consideration. Considering a universal joint as two intersecting revolute joints, the remaining limb configurations contain three to five revolute joints. Let these revolute joints be arranged such that their joint axes are parallel to a plane. Then instantaneous rotation of the moving platform about an axis perpendicular to the common plane is not possible. For example, Figure 9.7 shows four limb arrangements that satisfy this condition.

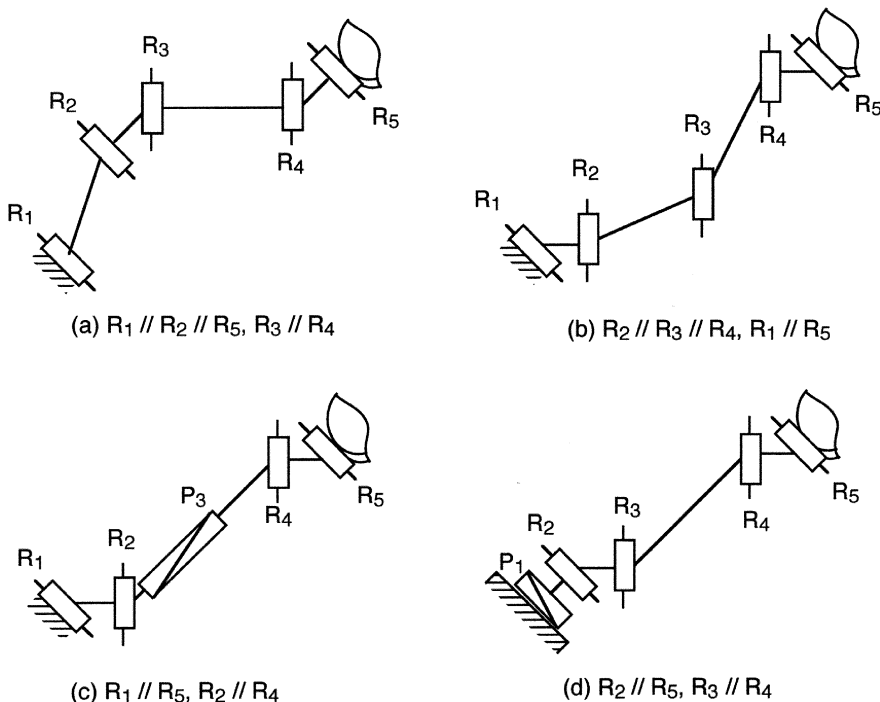
Figures 9.8, 9.9, and 9.10 show the schematic diagrams of three parallel manipulators that are constructed by using the 3-*UPU*, 3-*PUU*, and 3-*RUU* limb configurations, respectively. The kinematics of the 3-*UPU* manipulator was studied in detail by Tsai [21]. The 3-*RUU* manipulator was evolved into a mechanism with two additional short links and a planar parallelogram in each limb as shown in Figure 9.11 [16].

Six-dof Parallel Manipulators

In this section, we briefly discuss the enumeration of six-dof parallel manipulators. To simplify the problem, we limit ourselves to those manipulators with six identical limb structures. Furthermore, we assume that each limb consists of two links and three joints.

Referring to Table 9.1, we observe that the (6, 6, 6, 6, 6, 6) connectivity listing is the only solution. Thus, the degrees of freedom associated with all the joints of a limb should be equal to six. Since there are two links and three joints, the only possible solution is the type 111 limb, which means that each limb consists of one one-dof, one two-dof, and one three-dof joints. Let revolute, prismatic, universal, and spherical joints be the applicable joint types. Six feasible limb configurations exist: *RUS*, *RSU*, *PUS*, *PSU*, *SPU*, and *UPS* as shown in Figure 9.12. Configurations *SRU*, *SUR*, *URS*, *USR*, *SUP*, and *USP* are excluded because they do not contain a base-connected revolute or prismatic joint, or an intermediate prismatic joint.

Note that the universal joints shown in Figure 9.12 can be replaced by a spherical joint. This results in a passive degree of freedom, allowing the intermediate link(s) to spin freely about a line passing through the centers of the two spheres. Thus, *RSS*,

**FIGURE 9.7**

Feasible limb configurations for translational platforms.

PSS, and *SPS* are also feasible limb configurations. Furthermore, if a cylindric joint is allowed, then *UCU* and *SCS* limbs with the cylindric joint axes passing through the centers of the universal and spherical joints, respectively, are also feasible configurations. The *SCS* limb configuration possesses two passive degrees of freedom. Figure 9.13 shows these five additional six-dof limbs.

9.3 Robotic Wrist Mechanisms

A robot manipulator requires at least six degrees of freedom to manipulate an object freely in space. As shown in Figure 9.14, a serial manipulator typically utilizes its first three degrees of freedom for manipulating the position, and the last three degrees of freedom for changing the orientation of its end-effector. For this reason, the first three links are called the *major links* or *arm*, and the last three links the *minor links* or *wrist*. Furthermore, the last three joint axes often intersect at a point called the *wrist center*. This section introduces some frequently used robotic wrist mechanisms, investigates

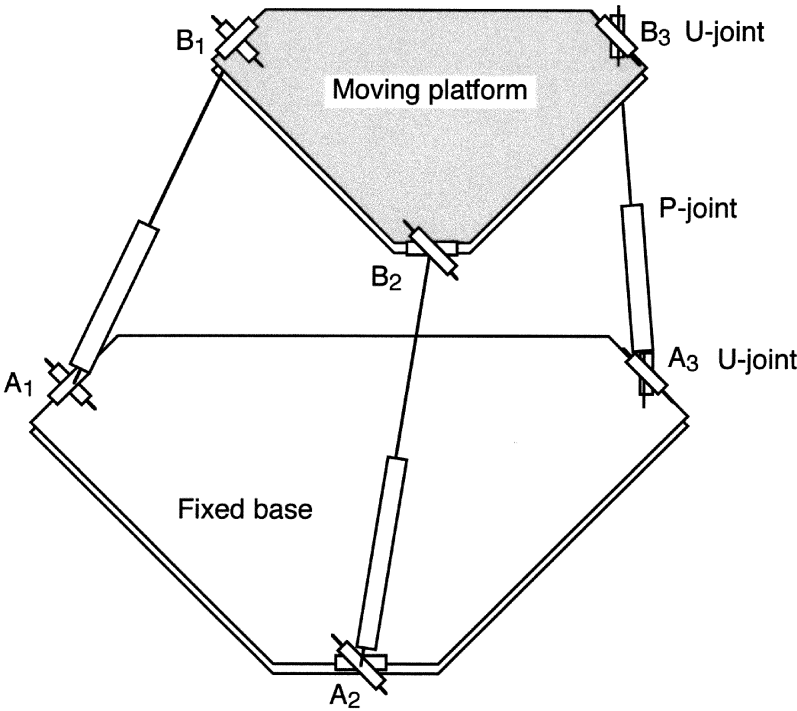


FIGURE 9.8
Spatial 3-UPU translational platform.

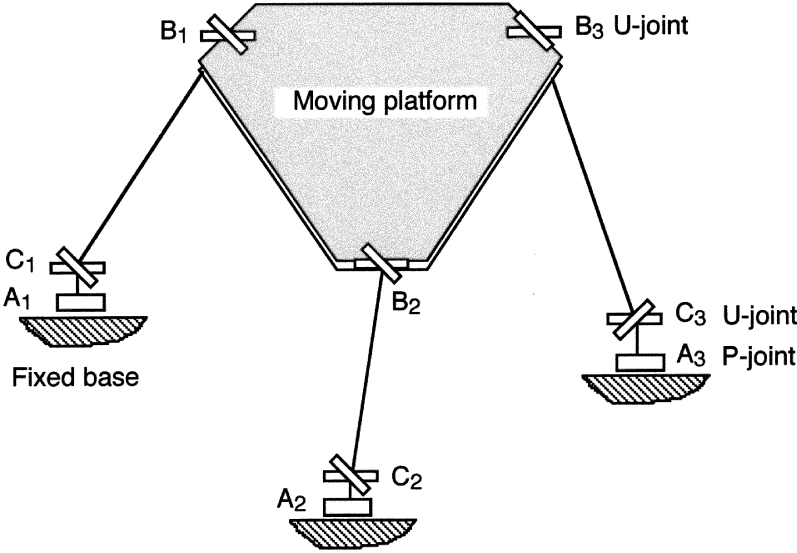


FIGURE 9.9
Spatial 3-PUU translational platform.

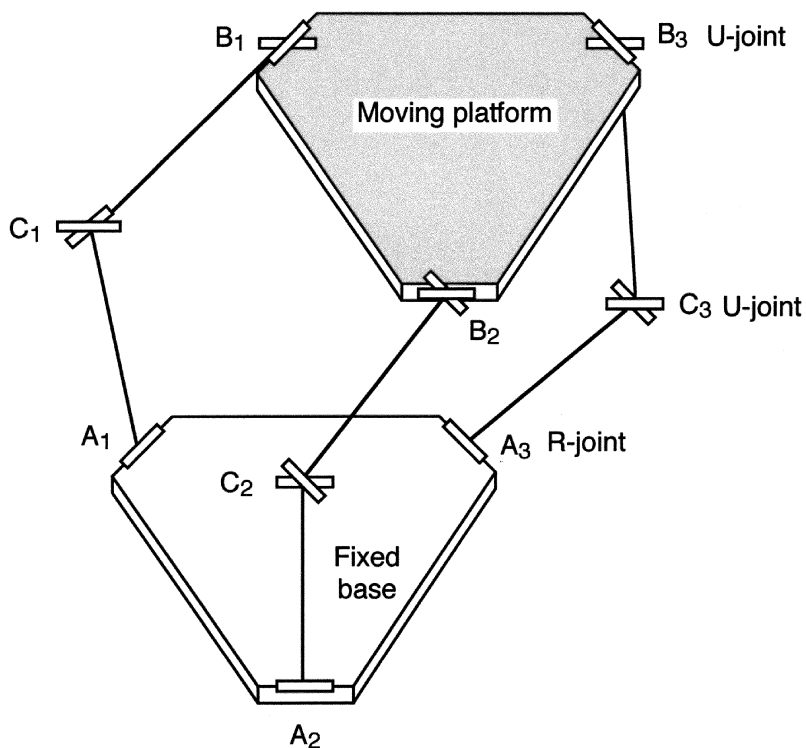


FIGURE 9.10
Spatial 3-RUU translational platform.

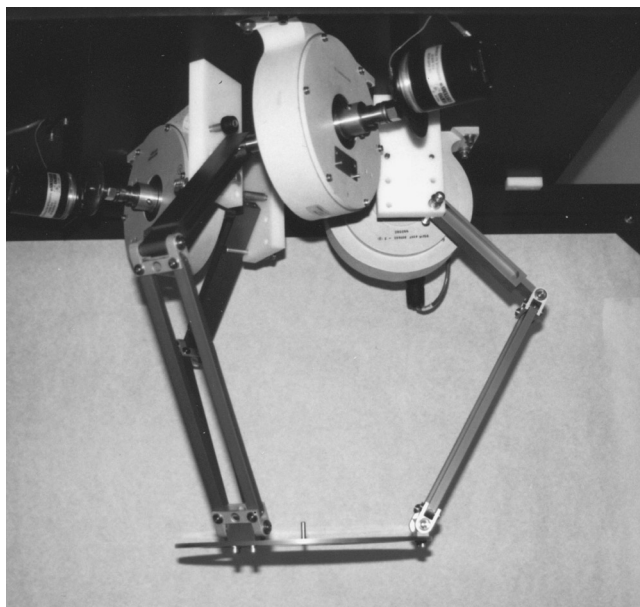


FIGURE 9.11
Prototype translational platform.

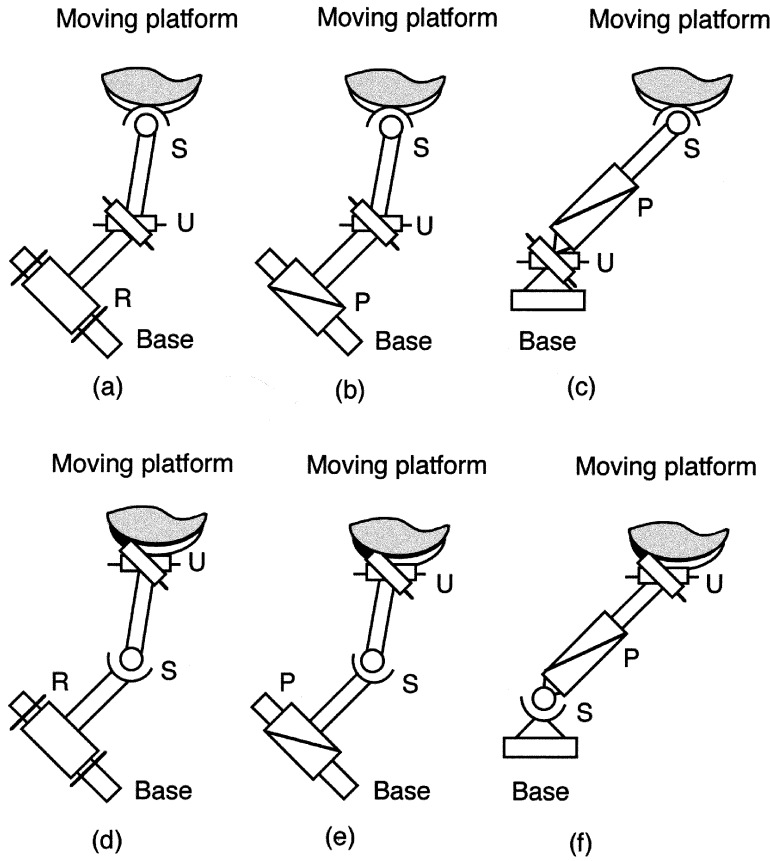


FIGURE 9.12
Six limb configurations.

their structural characteristics, and then presents a methodology for enumeration of a class of such mechanisms.

9.3.1 Functional Requirements

Since the wrist mechanism is located at the distal end of a serial manipulator, it should be compact, light weight, and dextrous. To achieve these goals, gear trains, belts-and-pulley drives, and other mechanical transmissions are often used to permit actuators to be installed away from the wrist center. This section is concerned with the enumeration of wrist mechanisms using gear trains as the power transmission mechanism.

The schematic diagram of a wrist mechanism developed by Bendix Corporation is shown Figure 9.15a [1]. Three coaxial members, links 2, 5, and 6, serve as the inputs to the mechanism. Bevel gear pairs 5–7, 7–4, 6–8, and 8–4 transmit rotations

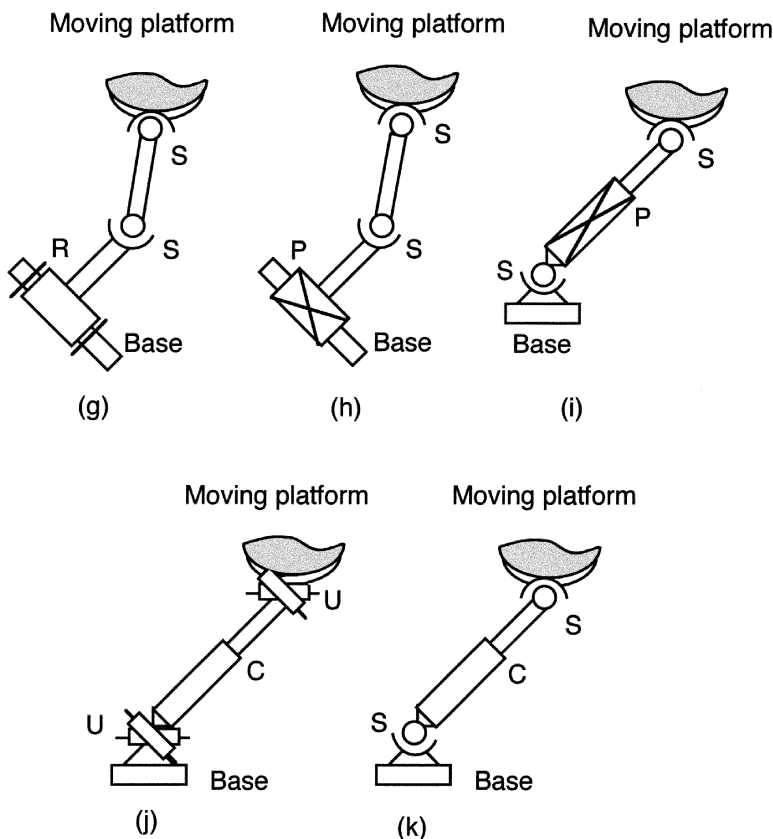
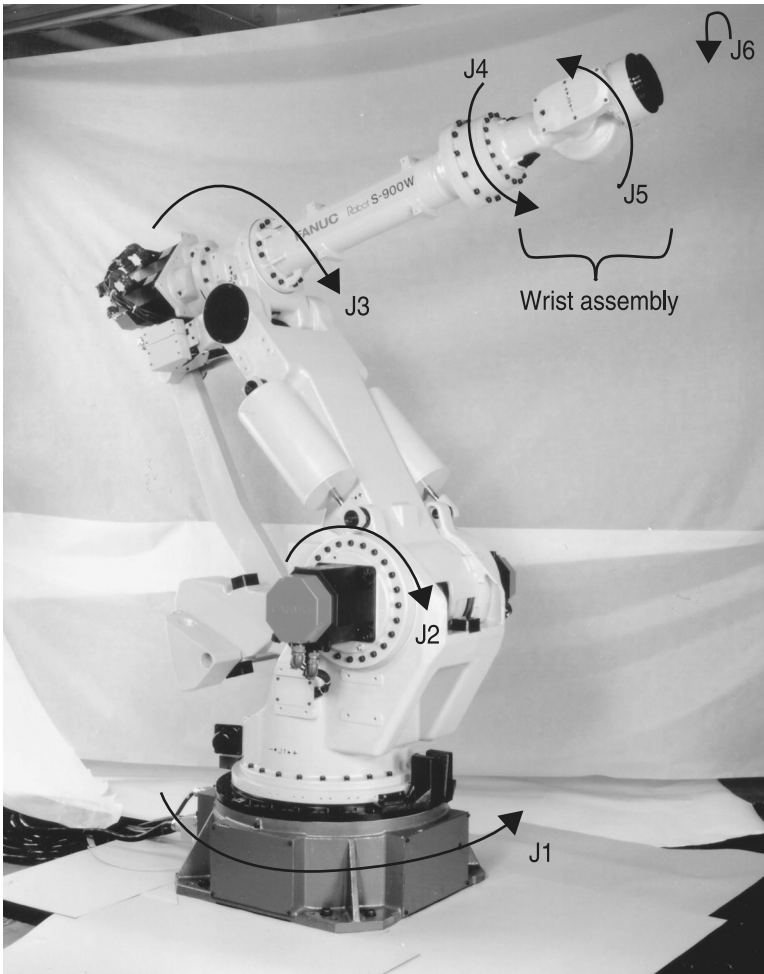


FIGURE 9.13
Five alternative limb configurations.

of the input links to the end-effector, link 4, which is housed in the carrier, link 3. The three joint axes, z_1 , z_2 , and z_3 , intersect at the wrist center O . Including the base link, the mechanism consists of eight links, seven turning pairs, and four gear pairs. The conventional graph representation of the mechanism is shown in Figure 9.15b. Applying the vertex selection technique, the graph can be reconfigured into one with a bridge and one articulation point as shown in Figure 9.15c. Hence, the mechanism is a fractionated, three-dof spherical wrist mechanism.

Figure 9.16a shows the schematic diagram of another wrist mechanism developed by Cinnati Milacron [15]. The conventional and canonical graph representations of the mechanism are shown in Figures 9.16b and c. The mechanism consists of seven links, six turning pairs, and three bevel gear pairs. Bevel gear pairs 5–3, 6–7, and 7–4 transmit rotations of the three coaxial input links 2, 5, and 6 to the end-effector, link 4. The three joint axes, z_1 , z_2 , and z_3 , intersect at the wrist center, O . We observe that the conventional graph contains a bridge and an articulation point. Hence, the

**FIGURE 9.14**

Fanuc robot. (Courtesy of Fanuc Robotics North America, Inc., Rochester Hills, MI.)

mechanism is a fractionated three-dof spherical mechanism. Unlike the Bendix wrist, the twist angles between the three joint axes are no longer equal to 90 degrees. One advantage of using this arrangement is that it allows unlimited rotations of the links about the three joint axes. This is, perhaps, the simplest design among all three-dof geared wrist mechanisms.

In general, the joint axes of a wrist mechanism do not have to intersect at a common point. Further, the twist angles between adjacent joint axes are not necessarily equal to 90 degrees. Figure 9.17 shows a Fanuc wrist for which the three joint axes do not

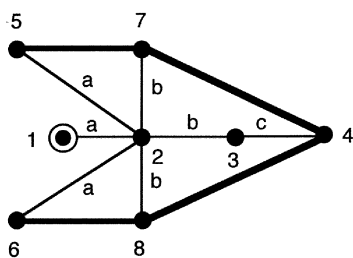
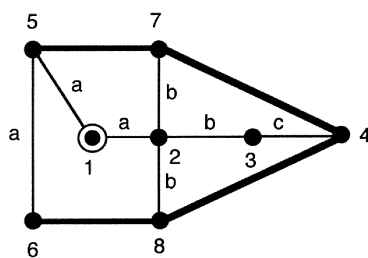
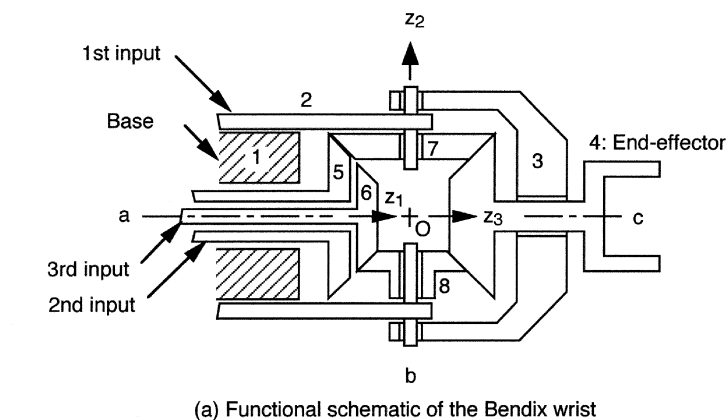


FIGURE 9.15

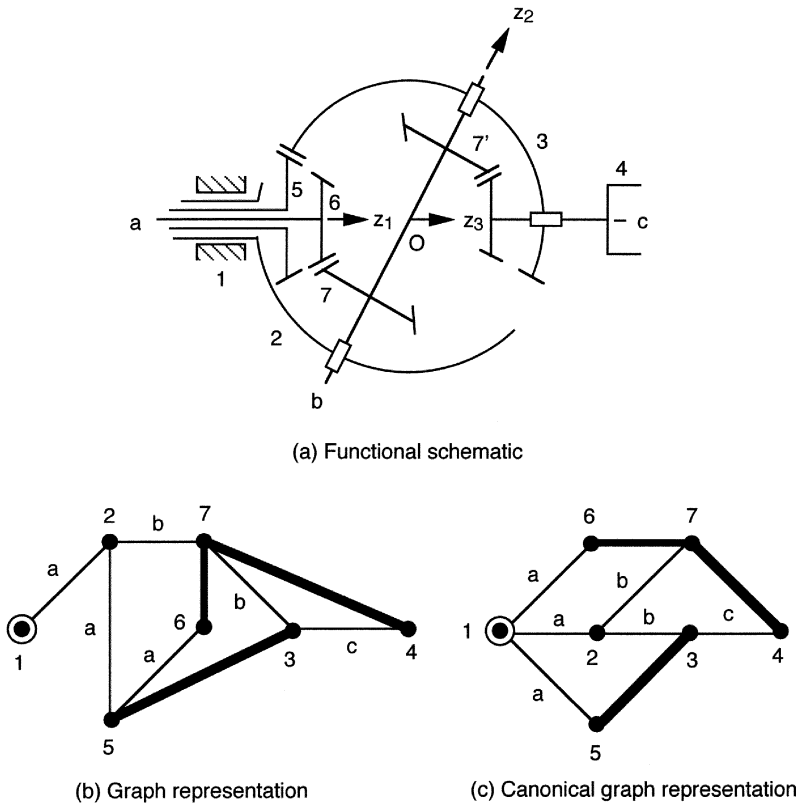
Bendix wrist mechanism and its graph representations.

intersect at a point. In this section we concentrate on spherical wrist mechanisms. Nonspherical wrist mechanisms can be constructed in a similar manner.

A wrist is said to be a *simple wrist* if the twist angles are all equal to 90 degrees, and an *oblique wrist* if any of the twist angles is not equal to 90 degrees. A joint axis is called a *roll axis* if its rotation angle is mechanically unlimited, otherwise it is called a *bend axis*. In this regard, the Bendix wrist is a simple roll-bend-roll wrist, whereas the Cincinnati Milacron wrist is an oblique three-roll wrist.

In summary, a good wrist design should possess the following functional requirements:

- F1. Three degrees of freedom.
- F2. Spherical motion characteristics.
- F3. Remote actuation capability.
- F4. Large rotational workspace.
- F5. Compact size, light weight, and mechanically stiff.

**FIGURE 9.16**

Cincinnati Milacron wrist mechanism and its graph representations.

9.3.2 Structural Characteristics

In the preceding chapter it was shown that the graph of a geared mechanism can be reconfigured into a canonical form, and that removal of all geared edges from the graph results in a tree. The tree represents an open-loop kinematic chain that is made up of links connected together by revolute joints. For wrist mechanisms, we call the serial chain, which corresponds to the thin-edged path emanating from the root and terminating at the end-effector vertex, the *equivalent open-loop chain* [20]. For example, Figure 9.18 demonstrates the equivalent open-loop chain of the Cincinnati Milacron wrist shown in Figure 9.16. For a wrist mechanism to possess three degrees of freedom, the open-loop chain should contain three moving links connected in series to a base link by revolute joints.

From the above discussion, we summarize the structural characteristics of robotic wrists as follows:

**FIGURE 9.17**

Fanuc wrist. (Courtesy of Fanuc Robotics North America, Inc., Rochester Hills, MI.)

- C1. Most wrist mechanisms are fractionated three-dof geared mechanisms; that is, they are made up of a two-dof gear train in series with a base link.
- C2. There are at least three coaxial members that serve as the input links to permit remote actuation of the wrist.
- C3. When all gear meshes are removed, the resulting mechanism contains a three-dof open-loop chain. The joint axes of the open-loop chain preferably intersect at a common point.

In terms of a graph, the conventional graph of a three-dof wrist mechanism contains a bridge. One side of the bridge is a base link, whereas the other side represents a nonfractionated two-dof EGT. The graph of such a two-dof EGT contains at least three vertices that are connected by thin edges of the same label. These vertices are the potential candidates for use as coaxial input links. Starting from one of the coaxial vertices, there exists a thin-edged path having at least three edge levels. In the canonical graph representation, the vertices can be divided into four levels, including the root, and there are at least three vertices located at the first level.

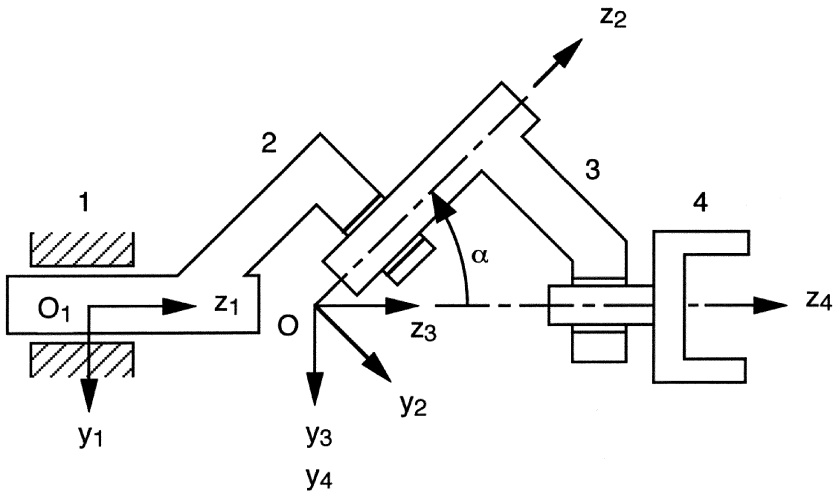


FIGURE 9.18
Equivalent open-loop chain.

9.3.3 Enumeration of Three-dof Wrist Mechanisms

Using the structural characteristics described in the preceding section, a systematic methodology can be developed for enumeration of wrist mechanisms. Since an atlas of EGTs having up to three degrees of freedom has already been developed, a straightforward approach can be developed as follows.

First, nonfractionated two-dof EGTs that satisfy structural characteristic C2 are identified. Then, a base link is added to these gear trains to form fractionated three-dof mechanisms, satisfying structural characteristics C1 and C3. Finally, the resulting mechanisms are qualitatively evaluated against the remaining functional requirements. Lin and Tsai [11] used this approach to enumerate a class of three-dof wrist mechanisms having up to eight links. Wrist mechanisms of higher complexity have also been studied.

A wrist mechanism is called a *basic mechanism* if rotations of the input links are transmitted to the joints by gears mounted only on the three axes of rotation of the equivalent open-loop chain. It is called a *derived mechanism* if additional idler gears are used to transmit the motion. Figure 9.19 shows an atlas of five basic three-dof spherical wrist mechanisms having seven, eight, and nine links. Figure 9.20 shows three wrist mechanisms derived from the seven-link wrist shown in Figure 9.19. In all mechanisms, link 1 denotes the base link and link 4 represents the end-effector. Links 2, 5, and 6 are the coaxial input links for all mechanisms except for that shown in Figures 9.19c through e for which links 5, 6, and 7 are the input links. Other choices of input links will either lead to a redundant link or render a nonfunctional mechanism. The base link is to be attached to the forearm of a manipulator. Although the canonical graph of Figure 9.19e is not planar, it can be reconfigured into a pseudoisomorphic

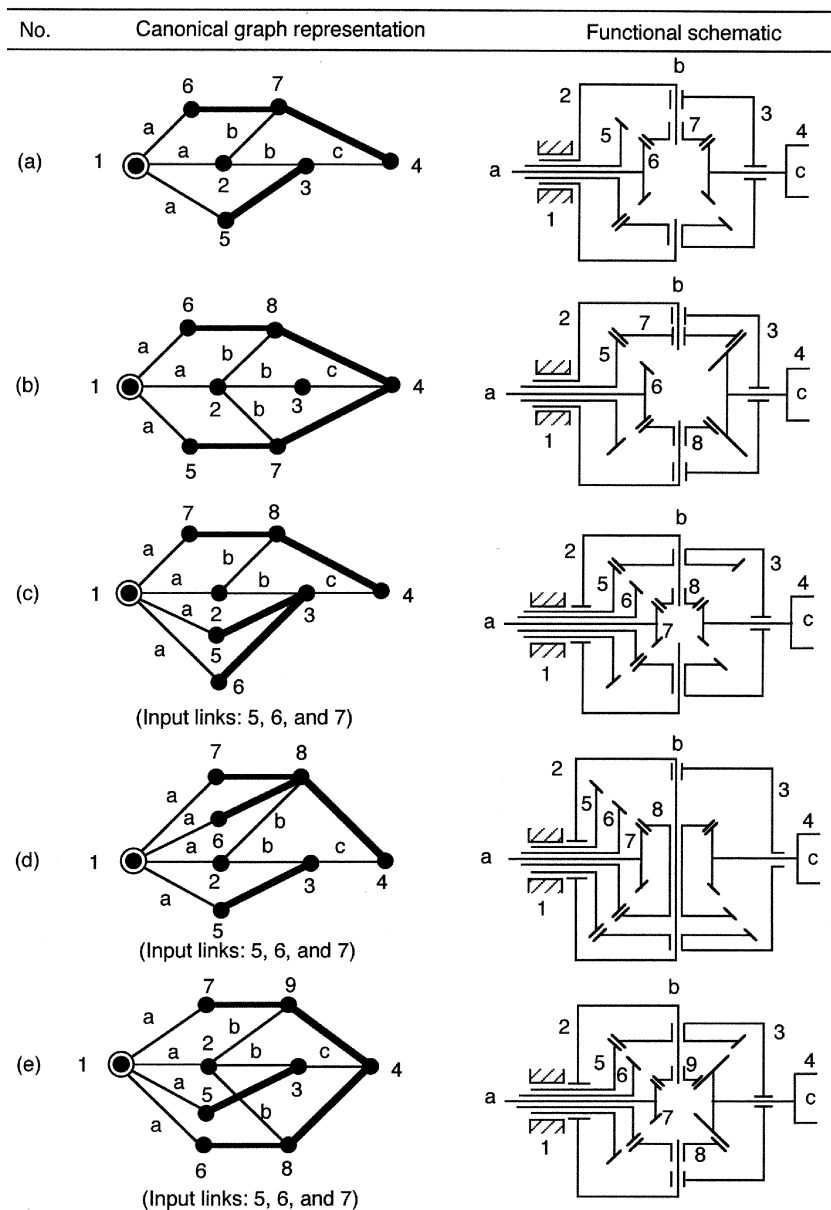


FIGURE 9.19

Basic three-dof wrist mechanisms having up to nine links.

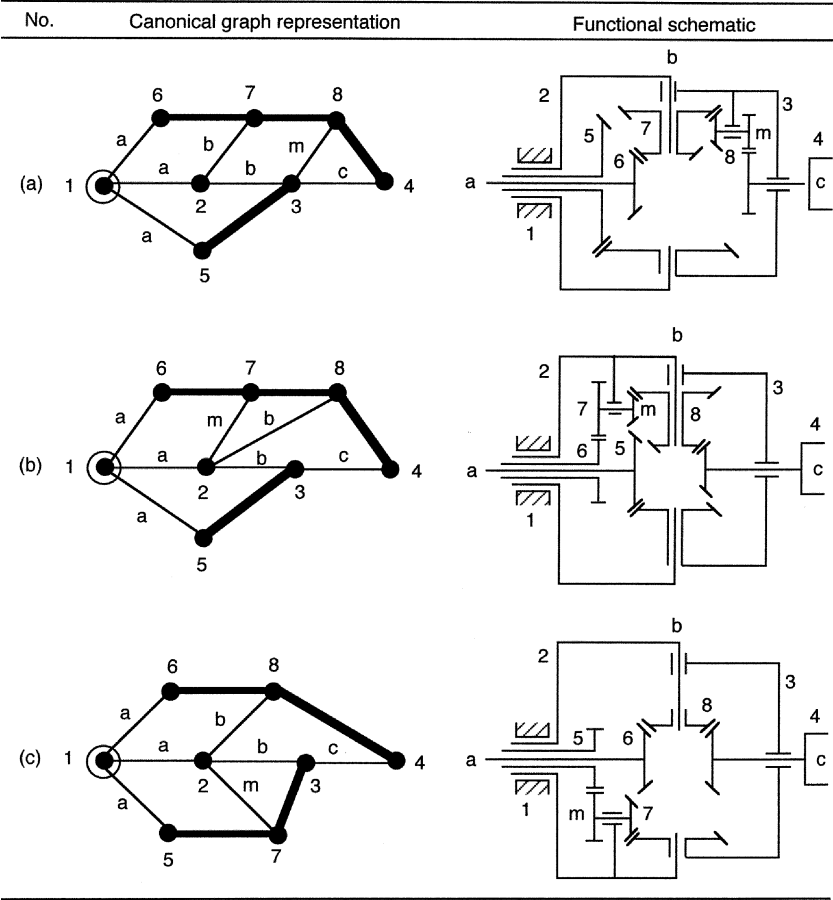


FIGURE 9.20
Eight-link wrist mechanisms derived from the seven-link basic wrist.

planar graph. Obviously, many more wrist mechanisms can be derived from the five basic mechanisms shown in Figure 9.19 by adding idler gears.

Note that all the mechanisms shown in Figures 9.19 and 9.20 are sketched in a roll-bend-roll spherical wrist configuration. These mechanisms can also be configured into oblique three-roll wrists. Except for the twist angles, the Cincinnati Milacron and Bendix wrists correspond to the basic wrists shown in Figures 9.19a and b, respectively, and the PUMA wrist belongs to the derived wrist shown in Figure 9.20a. The advantages of using one mechanism configuration as opposed to the others have yet to be explored from the kinematics and dynamics points of view.

We note that it is entirely possible for a three-dof wrist mechanism to be made up of more than three joint axes in the equivalent open-loop chain. For such a mechanism to function as a three-dof wrist, the joint angles in the open-loop chain must be me-

chanically constrained. Hence, the joint motions are no longer independent [19]. For example, Figure 9.21 shows a wrist mechanism with four joint axes, where rotations of the end-effector about the third and fourth joint axes are coupled by a gear pair attached to links 3 and 4.

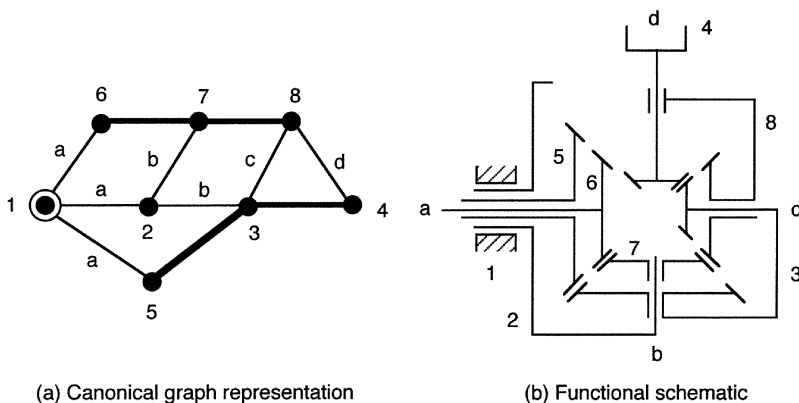


FIGURE 9.21

A three-dof wrist with four articulation points.

9.4 Summary

Parallel manipulators were classified into planar, spherical, and spatial mechanisms. The structural characteristics associated with parallel manipulators were identified and employed for the enumeration of the kinematic structures of parallel manipulators. Note that we have limited ourselves to those manipulators with the number of limbs equal to the number of degrees of freedom and with each limb being made up of an open-loop chain. Obviously, if these limitations are removed, the number of feasible solutions will grow exponentially.

It is conceivable for a parallel manipulator to have fewer number of limbs than the number of degrees of freedom. For such a manipulator, more than one actuator will be needed for each limb. For example, Tahmasebi and Tsai [18, 25] developed a six-dof parallel manipulator with three supporting limbs as shown in Figure 9.22, where each limb connects the moving platform to a planar bidirectional motor by a revolute joint at the upper end and a spherical joint at the lower end. The limbs are not extensible. The planar motor can move freely on a plane in any direction.

It is also conceivable to construct a parallel manipulator with more number of limbs than the number of degrees of freedom. In this case, the connectivity of some of the limbs should be equal to the motion parameter, λ , such that they do not impose any constraint on the moving platform. Figure 9.23 shows a three-dof manipulator with

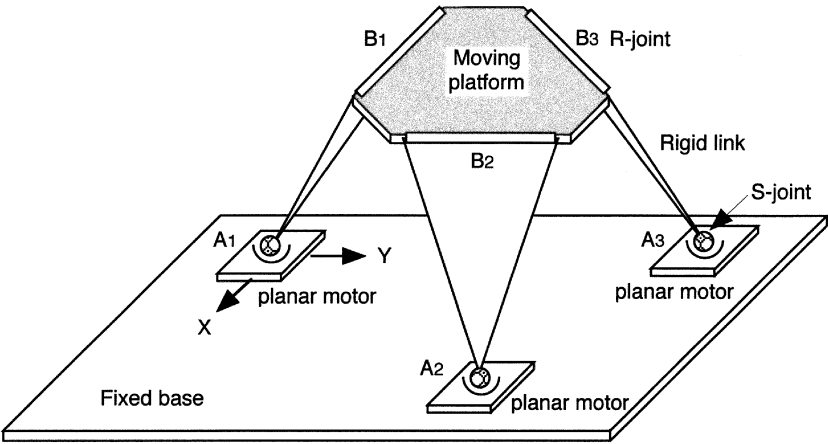


FIGURE 9.22
A six-dof parallel manipulator with three supporting limbs.

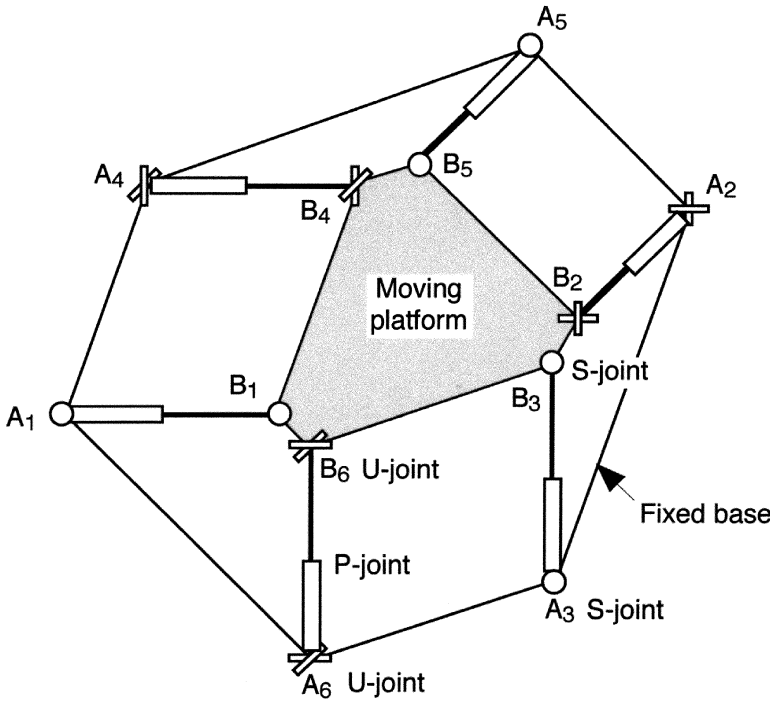


FIGURE 9.23
A three-dof platform with six supporting limbs.

six limbs. The three *UPU* limbs, A_2B_2 , A_4B_4 , and A_6B_6 , provide three constraints to the moving platform, whereas the prismatic joints in the three *SPS* limbs, A_1B_1 , A_3B_3 , and A_5B_5 , are driven by three linear actuators. This arrangement has the advantage of separating the function of constraint from that of actuation.

Finally, the structural characteristics of geared robotic wrist mechanisms were investigated from which an atlas of three-dof wrist mechanisms was developed.

References

- [1] Anonymous, 1982, Bevel Gears Makes Robot's Wrist More Flexible, *Machine Design*, 54, 18, 55.
- [2] Aronson, R.B., 1996, A Bright Horizon for Machine Tool Technology, *Manufacturing Engineering*, 116, 57–70.
- [3] Clearly, K. and Arai, T., 1991, A Prototype Parallel Manipulator: Kinematics, Construction, Software, Workspace Results, and Singularity Analysis, in *Proceedings of the IEEE International Conference on Robotics and Automation*, Sacramento, CA, 1, 561–571.
- [4] Gosselin, C. and Angeles, J., 1989, The Optimum Kinematic Design of a Spherical Three-Degree-of-Freedom Parallel Manipulator, *ASME Journal of Mechanisms, Transmissions, and Automation in Design*, 111, 202–207.
- [5] Gosselin, C. and Hamel, J., 1994, The Agile Eye: A High-Performance Three-Degree-of-Freedom Camera-Orienting Device, in *Proceedings of the IEEE International Conference on Robotics and Automation*, San Diego, CA, 781–786.
- [6] Gough, V.E. and Whitehall, S.G., 1962, Universal Tyre Test Machine, in *Proceedings of the 9th International Technical Congress*, F.I.S.I.T.A., Institution of Mechanical Engineers, London, 177.
- [7] Hebsacker, M., Treib, T., Zirn, O., and Honegger, M., 1999, Hexaglide 6 DOF and Triaglide 3 DOF Parallel Manipulators, in *Parallel Kinematic Machines*, Boër, C.R., Molinari-Tosatti, L., and Smith, K.S., eds., Springer-Verlag, London, 345–355.
- [8] Hunt, K.H., 1983, Structural Kinematics of In-Parallel-Actuated Robot-Arms, *ASME Journal of Mechanisms, Transmissions, and Automation in Design*, 105, 705–712.
- [9] Innocenti, C. and Parenti-Castelli, V., 1993, Echelon Form Solution of Direct Kinematics for the General Fully Parallel Spherical Wrist, *Mechanism and Machine Theory*, 28, 4, 553–561.

- [10] Lee, K. and Shah, D.K., 1987, Kinematic Analysis of a Three Degrees of Freedom In-Parallel Actuated Manipulator, in *Proceedings of the IEEE International Conference on Robotics and Automation*, San Diego, CA, 1, 345–350.
- [11] Lin, C.C. and Tsai, L.W., 1989, The Development of an Atlas of Bevel-Gear Type Spherical Wrist Mechanisms, in *Proceedings of the First National Conference on Applied Mechanisms and Robotics*, Paper No. 89-AMR-2A-3.
- [12] Mohammadi, H.R., Daniali, P.J., Zsombor-Murray, P.J., and Angeles, J., 1993, The Kinematics of 3-DOF Planar and Spherical Double-triangular Parallel Manipulator, in *Computational Kinematics*, Kluwer Academic Publishers, Dordrecht, 153–164.
- [13] Pierrot, F. and Shibukawa, T., 1999, From Hexa to Hexam, in *Parallel Kinematic Machines: Theoretical Aspects and Industrial Requirements*, Böer, C.R., Molinari-Tosatti, L., and Smith, K.S., eds., Springer-Verlag, London, 357–364.
- [14] Pierrot, F., Reynaud, C., and Fournier, A., 1990, DELTA: A Simple and Efficient Parallel Robot, *Robotica*, 8, 105–109.
- [15] Stackhouse, T., 1979, A New Concept in Wrist Flexibility, in *Proceedings of the 9th International Symposium on Industrial Robots*, Washington, DC, 589–599.
- [16] Stamper, R.E., Tsai, L.W., and Walsh, G.C., 1997, Optimization of a Three DOF Translational Platform for Well-Conditioned Workspace, in *Proceedings of the IEEE International Conference on Robotics and Automation*, Raleigh, NC, Paper No. A1-MF-0025.
- [17] Stewart, D., 1965, A Platform with Six Degrees of Freedom, Institution of Mechanical Engineers, London, 180, 371–386.
- [18] Tahmasebi, F. and Tsai, L.W., 1995, On the Stiffness of a Novel Six-DOF Parallel Mini-manipulator, *Journal of Robotic Systems*, 12, 12, 845–856.
- [19] Trevelyan, J.P., Kovesi, P.D., Ong, M., and Elford, D., 1986, ET: A Wrist Mechanism without Singular Positions, *The International Journal of Robotics Research*, 4, 4, 71–85.
- [20] Tsai, L.W., 1988, The Kinematics of Spatial Robotic Bevel-Gear Trains, *IEEE Journal of Robotics and Automation*, 4, 2, 150–156.
- [21] Tsai, L.W., 1996, Kinematics of a Three-DOF Platform with Three Extensible Limbs, in *Recent Advances in Robot Kinematics*, Lenarčić, J. and Parenti-Castelli, V., eds., Kluwer Academic Publishers, Dordrecht, 401–410.
- [22] Tsai, L.W., 1999, Systematic Enumeration of Parallel Manipulators, in *Parallel Kinematic Machines: Theoretical Aspects and Industrial Requirements*, Böer, C.R., Molinari-Tosatti, L., and Smith, K.S., eds., Springer-Verlag, London, 33–49.
- [23] Tsai, L.W., 1999, *Robot Analysis: The Mechanics of Serial and Parallel Manipulators*, John Wiley & Sons, New York, NY.

- [24] Tsai, L.W. and Stamper, R., 1996, A Parallel Manipulator with Only Translational Degrees of Freedom, in CD-ROM *Proceedings of the ASME 1996 Design Engineering Technical Conferences*, Irvine, CA, 96-DETC-MECH-1152.
- [25] Tsai, L.W. and Tahmasebi, F., 1993, Synthesis and Analysis of a New Class of Six-DOF Parallel Mini-manipulators, *Journal of Robotic Systems*, 10, 5, 561–580.
- [26] Waldron, K.J., Vohnout, V.J., Pery, A., and McGhee, R.B., 1984, Configuration Design of the Adaptive Suspension Vehicle, *International Journal of Robotic Research*, 3, 37–48.
- [27] Wohlhart, K., 1994, Displacement analysis of the General Spherical Stewart Platform, *Mechanism and Machine Theory*, 29, 4, 581–589.

Exercises

- 9.1 Enumerate all feasible parallel three-dof spatial manipulators with the connectivity listing of (6,6,3), assuming that each limb is made of two links. Sketch the mechanism schematics and their corresponding graphs.
- 9.2 Enumerate all feasible parallel three-dof spatial manipulators with the connectivity listing of (6,5,4), assuming that each limb is made of two links. Sketch the mechanism schematics and their corresponding graphs.
- 9.3 Enumerate feasible three-dof parallel manipulators having four supporting limbs.
- 9.4 Enumerate all feasible parallel six-dof spatial manipulators with three limbs, assuming that each limb is made of three links. Sketch the mechanism schematics and their corresponding graphs. Discuss possible ways of assigning the actuated joints.
- 9.5 Study the structural characteristics associated with the bevel-gear differential shown in Figure 7.2. Enumerate alternative feasible seven-link differential mechanisms.
- 9.6 Enumerate all feasible three-dof geared spherical mechanisms having eight links.

Appendix A

Solving m Linear Equations in n Unknowns

In this appendix, we develop a procedure for solving a system of m linear equations in n variables subject to a constraint that all the variables are nonnegative integers. We first discuss a method for solving one equation in n unknowns. Then, we extend the method to solving a system of m equations in n unknowns.

A.1 Solving One Equation in n Unknowns

Consider the following linear equation:

$$c_1x_1 + c_2x_2 + c_3x_3 + \cdots + c_nx_n = k , \quad (\text{A.1})$$

where x_i s are the variables and c_i s are the coefficients. The c_i s are nonnegative integers and k is a positive integer. We wish to solve for x_i , for $i = 1, 2, \dots, n$ subject to a constraint that all x_i s must be nonnegative integers. In addition, the following constraint may be imposed:

$$x_i \leq q_i \text{ (constant)} . \quad (\text{A.2})$$

Since there are n unknowns in one equation, we may choose $n - 1$ number of unknowns arbitrarily and solve Equation (A.1) for the remaining unknown, provided that all the solutions are nonnegative integers. This can be accomplished by a computer program using a *nested-do loops* algorithm to vary the value of each x_i and check for the validity of the solutions. A more rigorous procedure for solving one linear equation in two unknowns can be found in [1].

Table A.1 A Nested-do Loops Algorithm for Solving One Linear Equation in n Unknowns.

```

FOR  $I_1 = 0$  TO  $q_1$ 
 $x(1) = I_1$ 
  FOR  $I_2 = 0$  TO  $q_2$ 
     $x(2) = I_2$ 
      FOR  $I_3 = 0$  TO  $q_3$ 
         $x(3) = I_3$ 
           $\vdots$ 
          FOR  $I_{n-1} = 0$  TO  $q_{n-1}$ 
             $x(n-1) = I_{n-1}$ 
             $x(n) = (k - c(1) * x(1) - \dots$ 
               $- c(n-1) * x(n-1)) / c(n).$ 
            IF  $x(n) < 0$ , DISCARD THE SOLUTION.
            IF  $x(n) \geq 0$ , SAVE THE SOLUTION.
          NEXT  $I_{n-1}$ 
         $\vdots$ 
      NEXT  $I_3$ 
    NEXT  $I_2$ 
  NEXT  $I_1$ 

```

A.2 Solving m Equations in n Unknowns

Next, we consider a system of m linear equations in n unknowns:

$$\begin{aligned}
 c_{11}x_1 + c_{12}x_2 + \dots + c_{1n}x_n &= k_1, \\
 c_{21}x_1 + c_{22}x_2 + \dots + c_{2n}x_n &= k_2, \\
 &\vdots \\
 c_{m1}x_1 + c_{m2}x_2 + \dots + c_{mn}x_n &= k_m,
 \end{aligned} \tag{A.3}$$

where the coefficients c_{ij} s are nonnegative integers, the constants k_i s are positive integers, and $n > m$. Furthermore, the solutions to the system of equations are subject to a constraint that all the variables x_i , for $i = 1, 2, \dots, n$, must be nonnegative integers. Writing Equation (A.3) in matrix form yields

$$C \mathbf{x} = \mathbf{0}, \tag{A.4}$$

where

$$C = \begin{bmatrix} c_{11} & c_{12} & c_{13} & \dots & c_{1n} & -k_1 \\ c_{21} & c_{22} & c_{23} & \dots & c_{2n} & -k_2 \\ \vdots & \vdots & \vdots & \ddots & \vdots & \vdots \\ c_{m1} & c_{m2} & c_{m3} & \dots & c_{mn} & -k_m \end{bmatrix},$$

$$\mathbf{x} = [x_1, x_2, \dots, x_n, 1]^T.$$

Applying Gauss elimination, Equation (A.4) can be reduced to an upper triangular form:

$$G\mathbf{x} = \mathbf{0}, \quad (\text{A.5})$$

where

$$G = \begin{bmatrix} g_{11} & g_{12} & g_{13} & \dots & \dots & g_{1n} & p_1 \\ 0 & g_{22} & g_{23} & \dots & \dots & g_{2n} & p_2 \\ 0 & 0 & \ddots & \vdots & \dots & \vdots & \vdots \\ 0 & 0 & 0 & g_{m,m} & \dots & g_{mn} & p_m \end{bmatrix}.$$

The last row in Equation (A.5) contains $n - m + 1$ unknowns which can be solved by the procedure outlined in the preceding section. Once x_m, \dots, x_n are known, the remaining unknowns are found by back substitution.

Example A.1 We wish to solve the following two equations for all possible nonnegative integers of x_i s

$$x_1 + x_2 + x_3 = 6, \quad (\text{A.6})$$

$$2x_1 + 3x_2 + 4x_3 = 16. \quad (\text{A.7})$$

Subtracting Equation (A.6) $\times 2$ from Equation (A.7), we obtain

$$x_2 + 2x_3 = 4. \quad (\text{A.8})$$

Equation (A.8) contains two unknowns. Since both $2x_3$ and 4 are even numbers, x_2 must be an even number. Let x_2 assume the values of 0, 2, and 4, one at a time, and solve Equation (A.8) for x_3 . Once x_3 is found, we solve Equation (A.6) for x_1 . As a result, we obtain the three solutions:

Solution	x_1	x_2	x_3
1	4	0	2
2	3	2	1
3	2	4	0

□

References

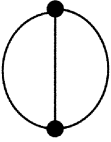
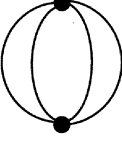
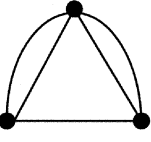
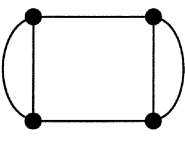
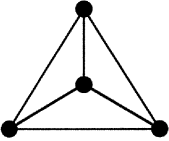
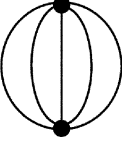
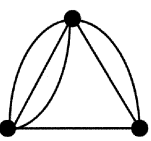
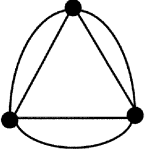
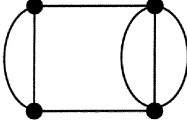
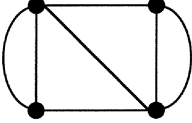
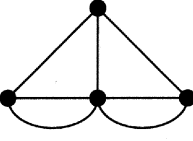
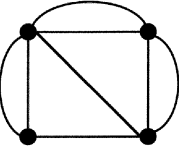
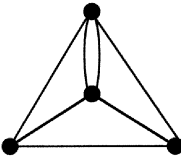
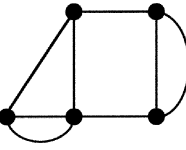
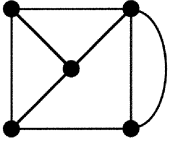
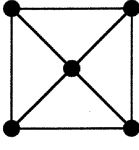
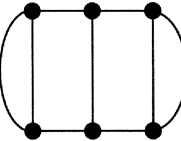
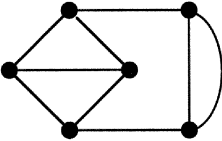
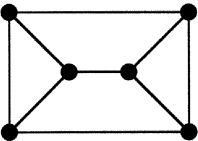
- [1] Gelfond, A.O., 1981, *Solving Equations in Integers*, Translated by Sheinin, O.B., Mir Publisher, Moscow.

Appendix B

Atlas of Contracted Graphs

This appendix provides an atlas of contracted graphs having two to four independent loops.

Table B.1 Contracted Graphs Having Two to Four Independent Loops.

			
23-1	24-1	35-1	46-1
			
46-2	25-1	36-1	36-2
			
47-1	47-2	47-3	47-4
			
47-5	58-1	58-2	58-3
			
69-1	69-2	69-3	

Appendix C

Atlas of Graphs of Kinematic Chains

This appendix provides an atlas of graphs of kinematic chains having up to three independent loops and eight links.

Table C.1 Graphs Having One Independent Loop: Three to Eight Vertices.

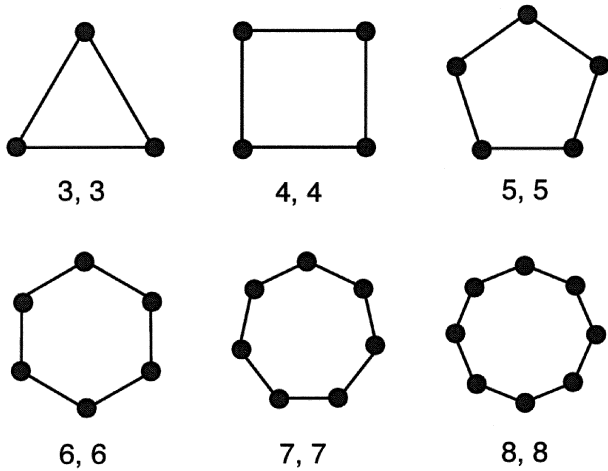


Table C.2 Graphs Having Two Independent Loops: Four to Eight Vertices.

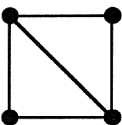
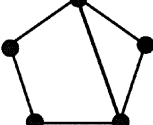
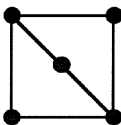
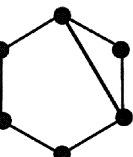
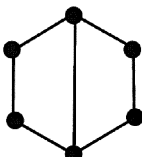
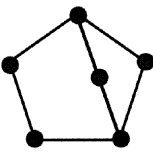
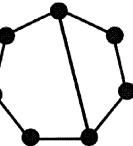
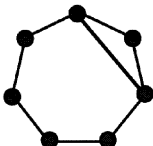
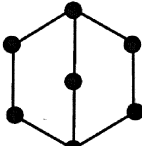
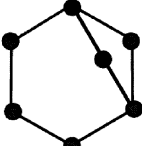
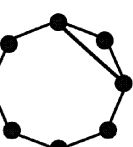
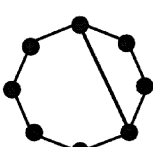
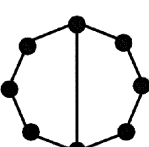
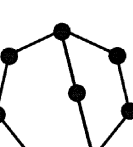
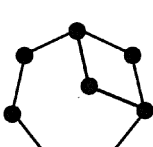
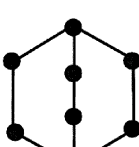
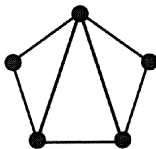
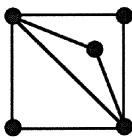
			
4, 5	5, 6 (a)	5, 6 (b)	
			
6, 7 (a)	6, 7 (b)	6, 7 (c)	
			
7, 8 (a)	7, 8 (b)	7, 8 (c)	7, 8 (d)
			
8, 9 (a)	8, 9 (b)	8, 9 (c)	
			
8, 9 (d)	8, 9 (e)	8, 9 (f)	

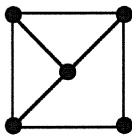
Table C.3 Graphs Having Three Independent Loops: Five to Six Vertices.



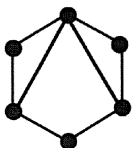
5, 7 (a)



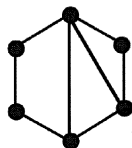
5, 7 (b)



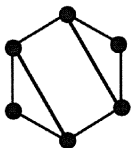
5, 7 (c)



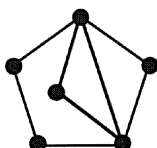
6, 8 (a)



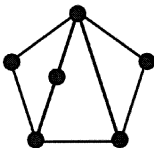
6, 8 (b)



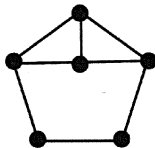
6, 8 (c)



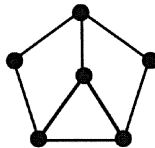
6, 8 (d)



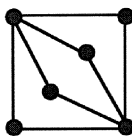
6, 8 (e)



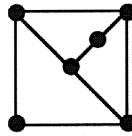
6, 8 (f)



6, 8 (g)



6, 8 (h)



6, 8 (i)

Table C.4 Graphs Having Three Independent Loops: Seven Vertices.

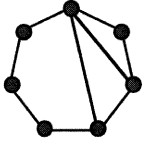
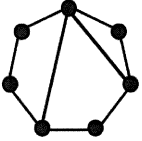
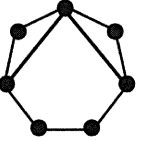
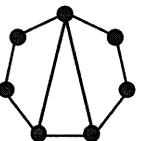
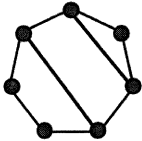
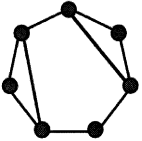
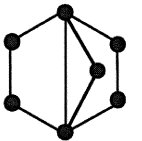
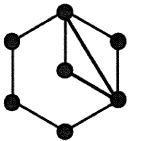
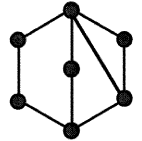
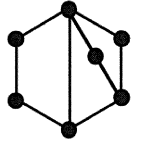
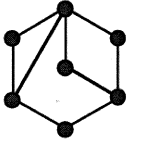
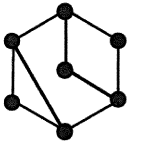
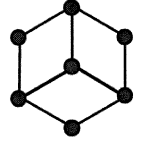
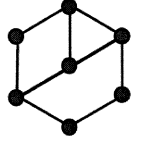
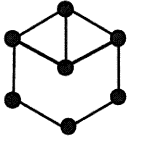
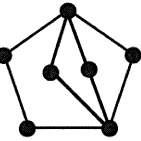
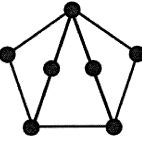
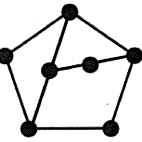
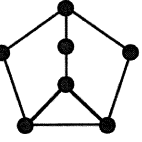
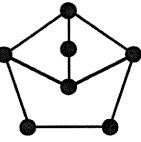
			
7, 9 (a)	7, 9 (b)	7, 9 (c)	7, 9 (d)
			
7, 9 (e)	7, 9 (f)	7, 9 (g)	7, 9 (h)
			
7, 9 (i)	7, 9 (j)	7, 9 (k)	7, 9 (l)
			
7, 9 (m)	7, 9 (n)	7, 9 (o)	7, 9 (p)
			
7, 9 (q)	7, 9 (r)	7, 9 (s)	7, 9 (t)

Table C.5 Graphs Having Three Independent Loops: Eight Vertices — Part 1.

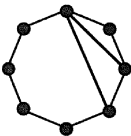
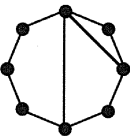
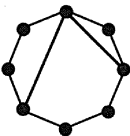
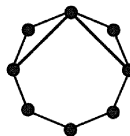
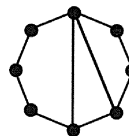
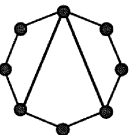
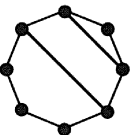
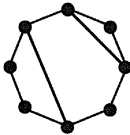
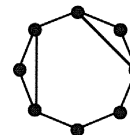
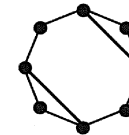
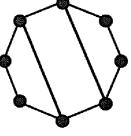
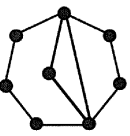
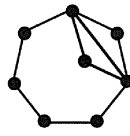
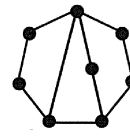
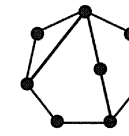
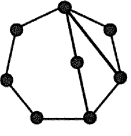
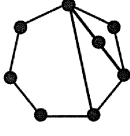
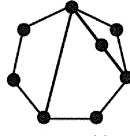
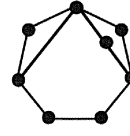
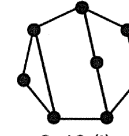
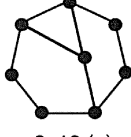
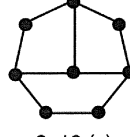

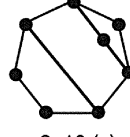
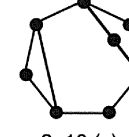

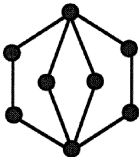
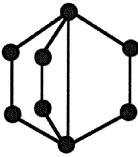
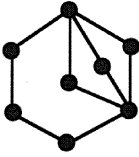
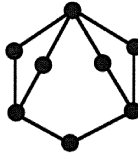
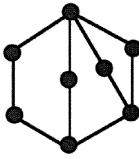
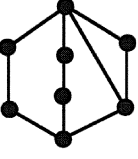
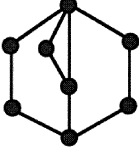
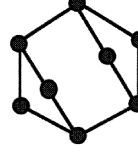
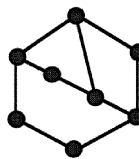
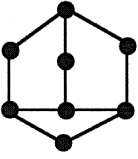


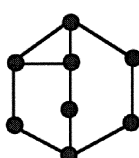
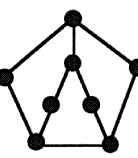
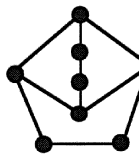
				
8, 10 (a)	8, 10 (b)	8, 10 (c)	8, 10 (d)	8, 10 (e)
				
8, 10 (f)	8, 10 (g)	8, 10 (h)	8, 10 (i)	8, 10 (j)
				
8, 10 (k)	8, 10 (l)	8, 10 (m)	8, 10 (n)	8, 10 (o)
				
8, 10 (p)	8, 10 (q)	8, 10 (r)	8, 10 (s)	8, 10 (t)
				
8, 10 (u)	8, 10 (v)	8, 10 (w)	8, 10 (x)	8, 10 (y)
				
8, 10 (z)				

Table C.6 Graphs Having Three Independent Loops: Eight Vertices — Part 2.

			
8, 10 (a)	8, 10 (b)	8, 10 (c)	8, 10 (d)
			
8, 10 (e)	8, 10 (f)	8, 10 (g)	8, 10 (h)
			
8, 10 (i)	8, 10 (j)	8, 10 (k)	8, 10 (l)
			
8, 10 (m)	8, 10 (n)	8, 10 (o)	

Appendix D

Atlas of Planar Bar Linkages

This appendix provides an atlas of planar linkages classified according to the number of degrees of freedom, the number of independent loops, the vertex degree listings, and the corresponding contract graphs.

Table D.1 Planar One-dof Four-Bar Linkage.

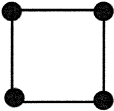
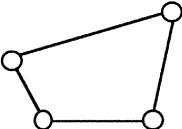
No. of Loops	Vertex Degree	Contracted Graph	Conventional Graph	Kinematic Chain
1	4000	Not applicable		

Table D.2 Planar One-dof Six-Bar Linkages.

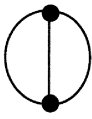
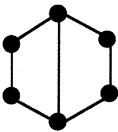
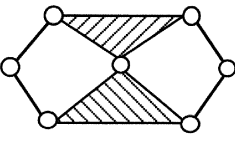
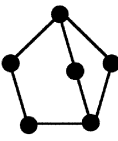
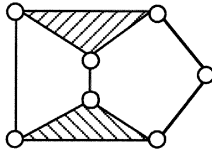
No. of Loops	Vertex Degree	Contracted Graph	Conventional Graph	Kinematic Chain
2	4200			
				

Table D.3 Planar One-dof Eight-Bar Linkages: Part 1.

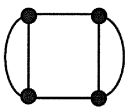
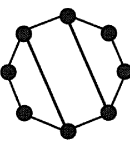
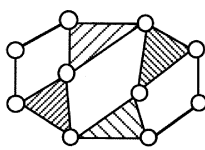
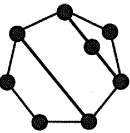
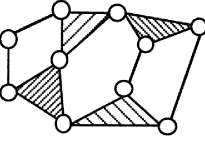
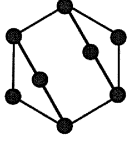
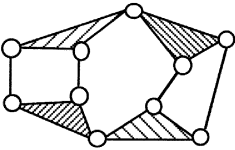
No. of Loops	Vertex Degree	Contracted Graph	Conventional Graph	Kinematic Chain
3	4400			
				
				

Table D.4 Planar One-dof Eight-Bar Linkages: Part 2.

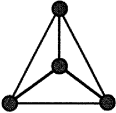
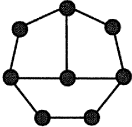
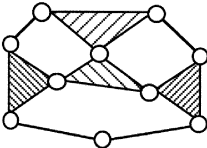
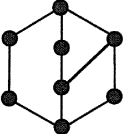
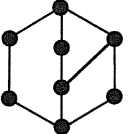
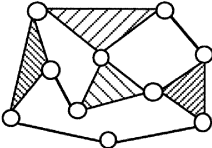
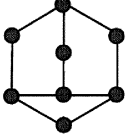
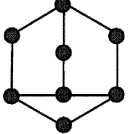
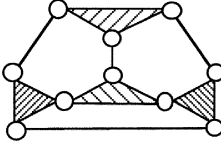
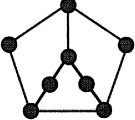
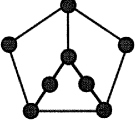
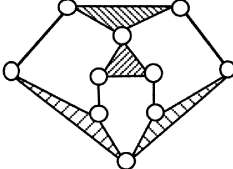
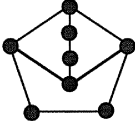
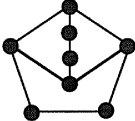
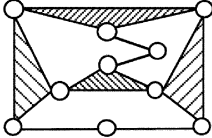
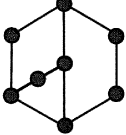
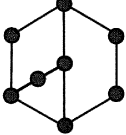
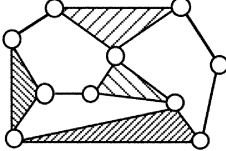
No. of Loops	Vertex Degree	Contracted Graph	Conventional Graph	Kinematic Chain
3	4400			
				
				
				
				
				

Table D.5 Planar One-dof Eight-Bar Linkages: Part 3.

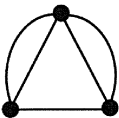
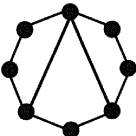
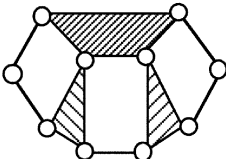
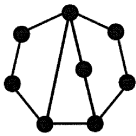
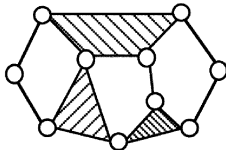
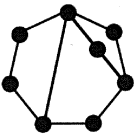
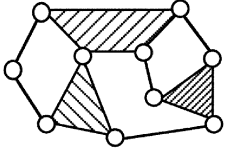
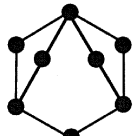
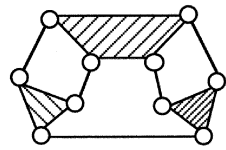
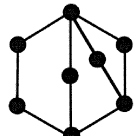
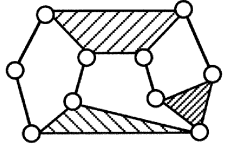
No. of Loops	Vertex Degree	Contracted Graph	Conventional Graph	Kinematic Chain
3	5210			
				
				
				
				

Table D.6 Planar One-dof Eight-Bar Linkages: Part 4.

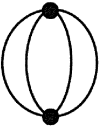
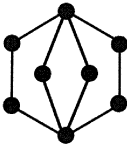
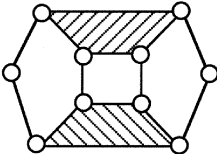
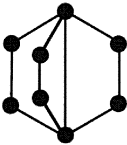
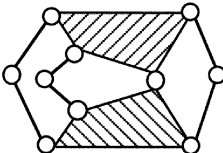
No. of Loops	Vertex Degree	Contracted Graph	Conventional Graph	Kinematic Chain
3	6020			
				

Table D.7 Planar Two-dof Five-Bar Linkage.

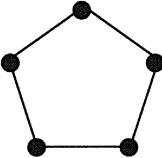
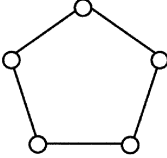
No. of Loops	Vertex Degree	Contracted Graph	Conventional Graph	Kinematic Chain
1	5000	Not applicable		

Table D.8 Planar Two-dof Seven-Bar Linkages.

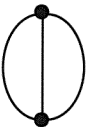
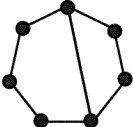
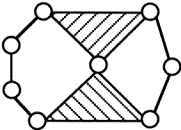
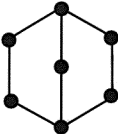
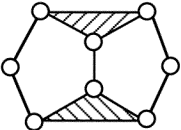
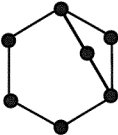
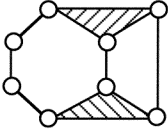
No. of Loops	Vertex Degree	Contracted Graph	Conventional Graph	Kinematic Chain
2	5200			
				
				

Table D.9 Planar Two-dof Nine-Bar Linkages: Part 1.

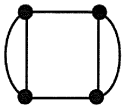
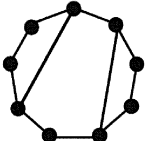
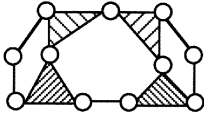
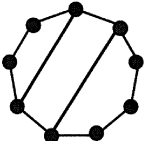
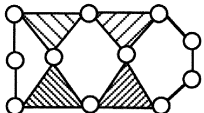
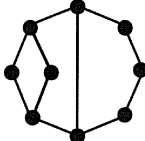
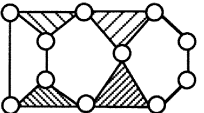
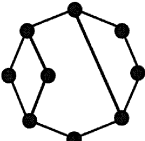
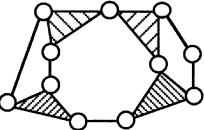
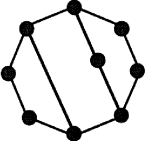
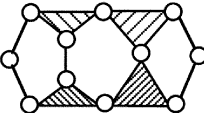
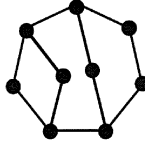
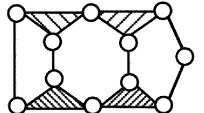
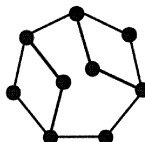
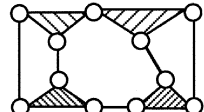
No. of Loops	Vertex Degree	Contracted Graph	Conventional Graph	Kinematic Chain
3	5400			
				
				
				
				
				
				

Table D.10 Planar Two-dof Nine-Bar Linkages: Part 2.

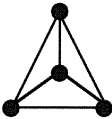
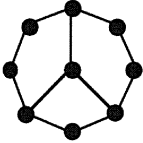
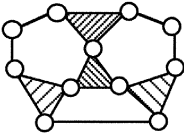
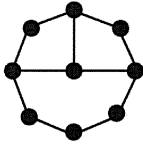
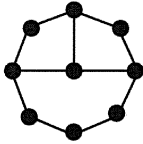
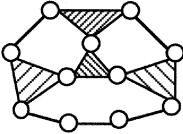
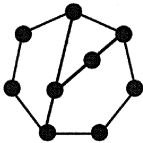
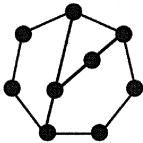
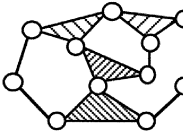
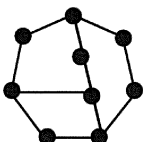
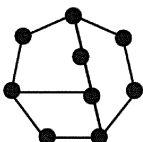
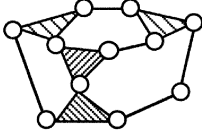
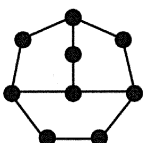
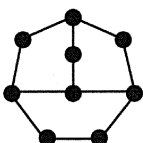
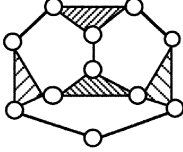
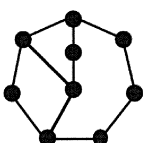
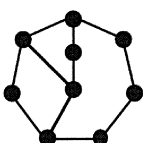
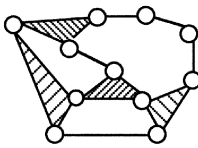
No. of Loops	Vertex Degree	Contracted Graph	Conventional Graph	Kinematic Chain
3	5400			
				
				
				
				
				

Table D.11 Planar Two-dof Nine-Bar Linkages: Part 3.

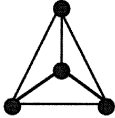
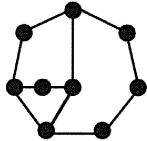
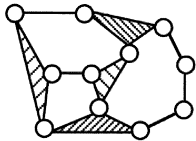
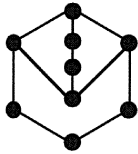
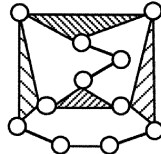
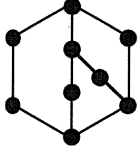
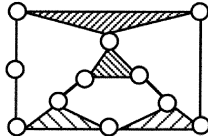
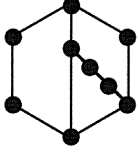
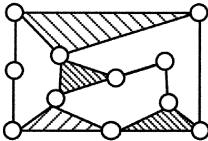
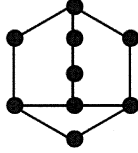
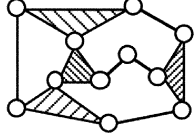
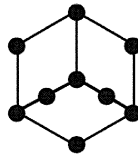
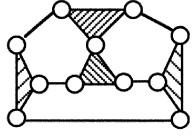
No. of Loops	Vertex Degree	Contracted Graph	Conventional Graph	Kinematic Chain
3	5400			
				
				
				
				
				

Table D.12 Planar Two-dof Nine-Bar Linkages: Part 4.

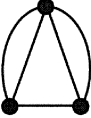
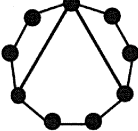
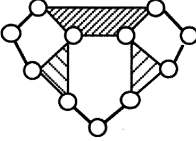
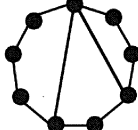
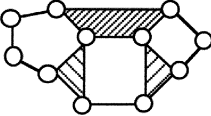
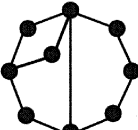
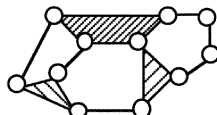
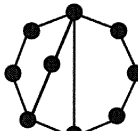
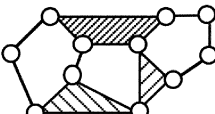
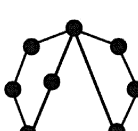
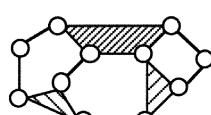
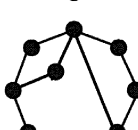
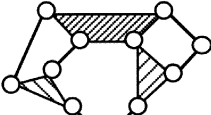
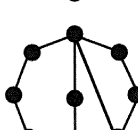
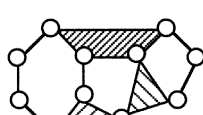
No. of Loops	Vertex Degree	Contracted Graph	Conventional Graph	Kinematic Chain
3	6210			
				
				
				
				
				
				

Table D.13 Planar Two-dof Nine-Bar Linkages: Part 5.

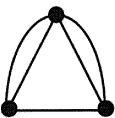
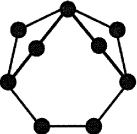
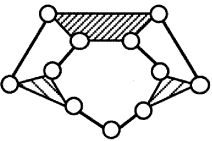
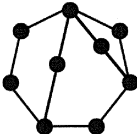
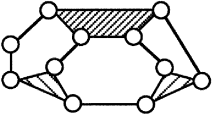
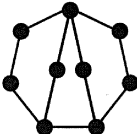
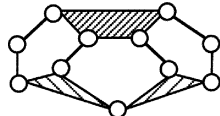
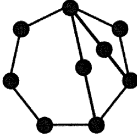
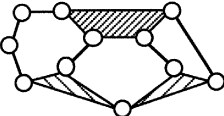
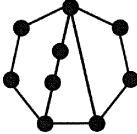
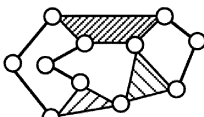
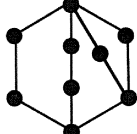
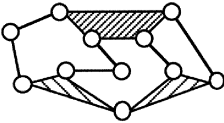
No. of Loops	Vertex Degree	Contracted Graph	Conventional Graph	Kinematic Chain
3	6210			
				
				
				
				
				

Table D.14 Planar Two-dof Nine-Bar Linkages: Part 6.

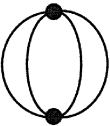
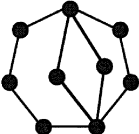
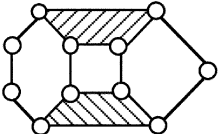
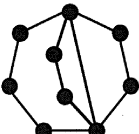
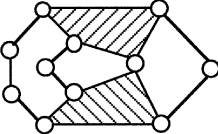
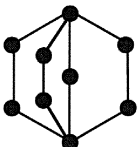
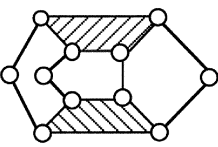
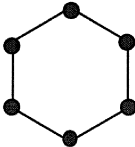
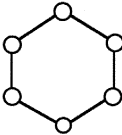
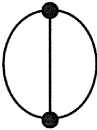
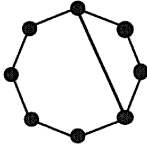
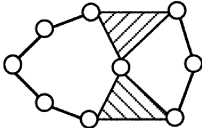
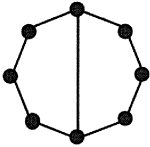
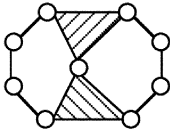
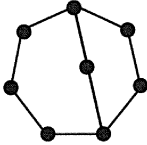
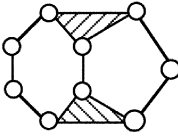
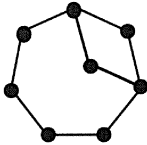
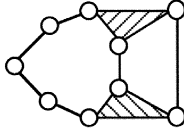
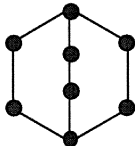
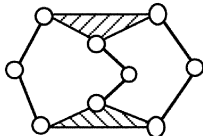
No. of Loops	Vertex Degree	Contracted Graph	Conventional Graph	Kinematic Chain
3	7020			
				
				

Table D.15 Planar Three-dof Linkages: One and Two Independent Loops.

No. of Loops	Vertex Degree	Contracted Graph	Conventional Graph	Kinematic Chain
1	6000	None		
2	6200			
				
				
				
				

Appendix E

Atlas of Spatial One-dof Kinematic Chains

This appendix provides an atlas of spatial one-dof, single-loop kinematic chains having four to seven links.

Table E.1 Spatial One-dof Four-Link Chains.

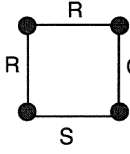
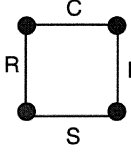
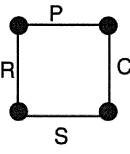
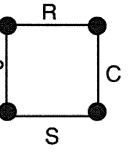
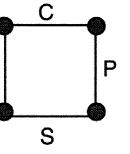
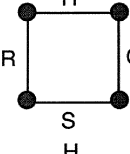
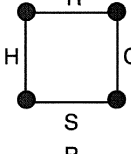
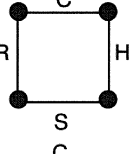
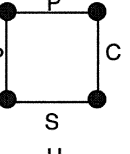
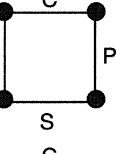
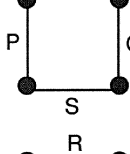
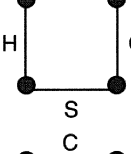
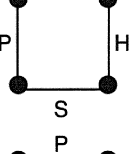
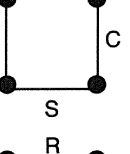
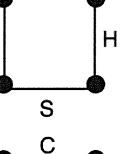
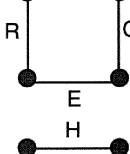
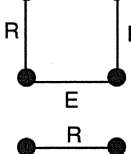
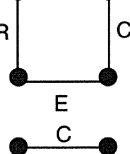
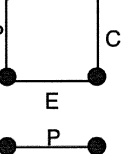
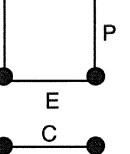
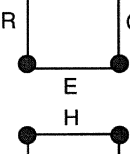
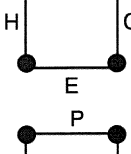
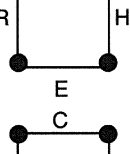
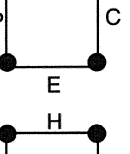
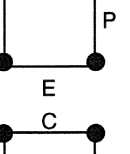
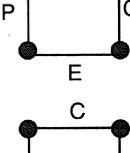
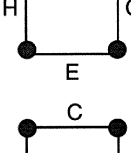
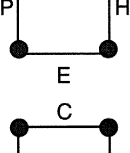
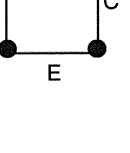
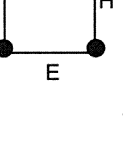
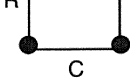
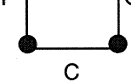
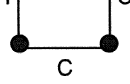
				
				
				
				
				
				
				

Table E.2 Spatial One-dof Five-Link Chains.

Table E.3 Spatial One-dof Six-Link Chains.

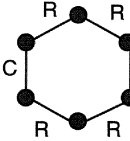
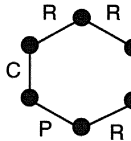
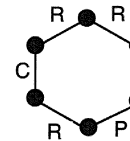
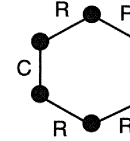
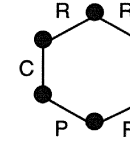
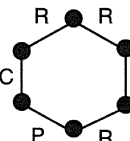
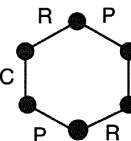
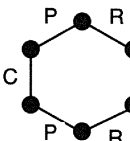
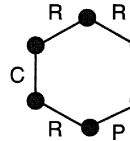
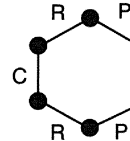
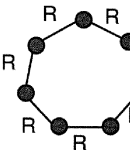
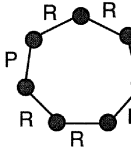
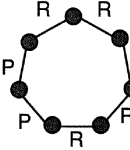
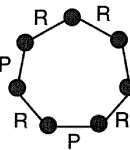
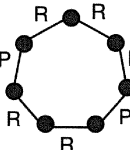
				
				

Table E.4 Spatial One-dof Seven-Link Chains.

				
---	---	---	---	--

Appendix F

Atlas of Epicyclic Gear Trains

This appendix provides an atlas of epicyclic gear trains classified according to the number of degrees of freedom, the number of independent loops, and the vertex degree listings. Both labeled graphs and typical functional schematic diagrams are sketched.

Table F.1 One-dof Epicyclic Gear Trains: One and Two Independent Loops.

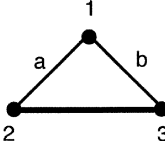
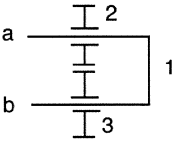
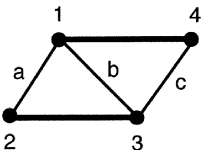
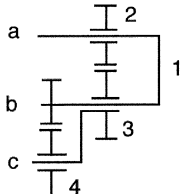
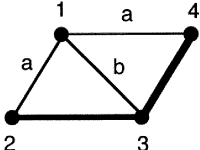
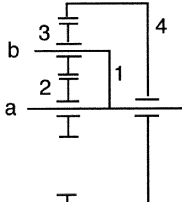
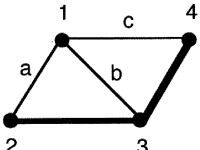
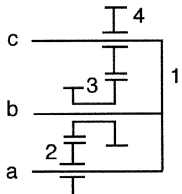
No. of Loops	Vertex-degree Listing	Conventional Graph	Functional Schematic
1	3000		
2	2200-1		
	2200-2a		
	2200-2b		

Table F.2 One-dof Epicyclic Gear Trains: Three Independent Loops — Part 1.

No. of Loops	Vertex-degree Listing	Conventional Graph	Functional Schematic
3	1400		

Table F.3 One-dof Epicyclic Gear Trains: Three Independent Loops — Part 2.

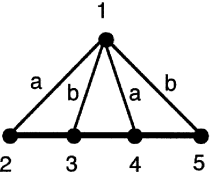
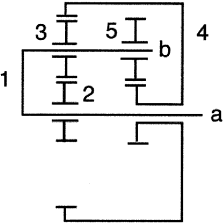
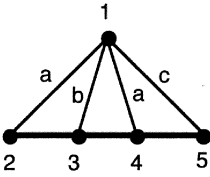
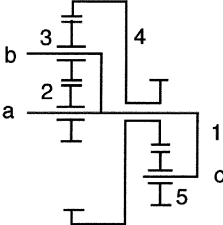
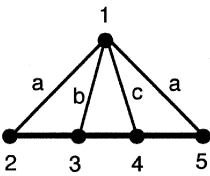
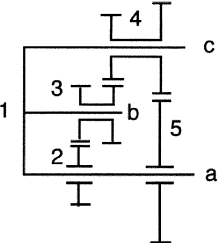
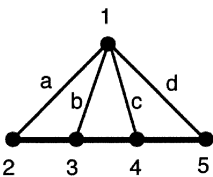
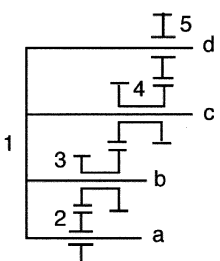
No. of Loops	Vertex-degree Listing	Conventional Graph	Functional Schematic
3	2210-3a		
	2210-3b		
	2210-3c		
	2210-3d		

Table F.4 One-dof Epicyclic Gear Trains: Three Independent Loops — Part 3.

No. of Loops	Vertex-degree Listing	Conventional Graph	Functional Schematic
3	3020-1a		
	3020-1b		
	3020-2a		
	3020-2b		
	3020-2c		

Table F.5 One-dof Epicyclic Gear Trains: Four Independent Loops — Part 1.

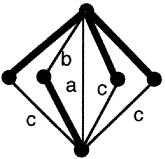
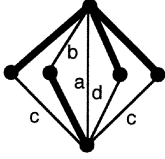
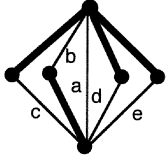
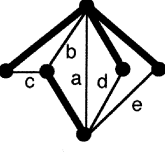
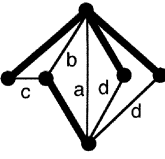
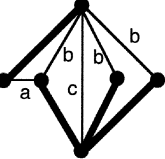
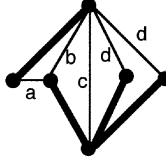
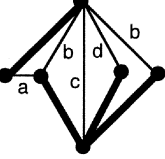
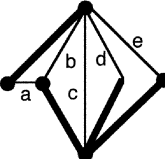
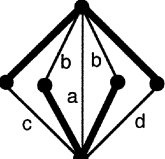
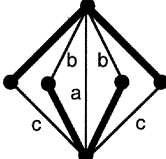
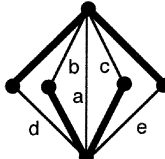
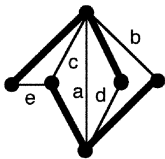
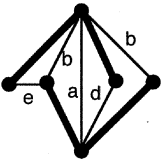
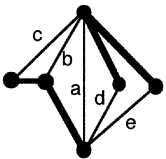
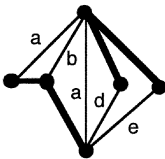
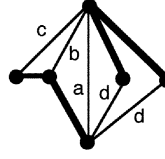
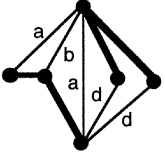
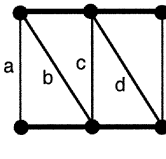
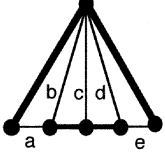
 6101-1	 6101-2	 6101-3	 6102-1
 6102-2	 6103-1	 6103-2	 6103-3
 6103-4	 6201-1	 6201-2	 6201-3
 6202-1	 6202-2	 6203-1	 6203-2
 6203-3	 6203-4	 6204-1	 6205-1

Table F.6 One-dof Epicyclic Gear Trains: Four Independent Loops — Part 2.

<p>6205-2</p>	<p>6206-1</p>	<p>6206-2</p>	<p>6206-2</p>
<p>6301-1</p>	<p>6301-2</p>	<p>6301-3</p>	<p>6301-4</p>
<p>6301-5</p>	<p>6302-1</p>	<p>6303-1</p>	<p>6303-2</p>
<p>6304-1</p>	<p>6305-1</p>	<p>6305-2</p>	<p>6305-3</p>
<p>6305-4</p>	<p>6305-5</p>	<p>6306-1</p>	<p>6306-2</p>

Table F.7 One-dof Epicyclic Gear Trains: Four Independent Loops — Part 3.

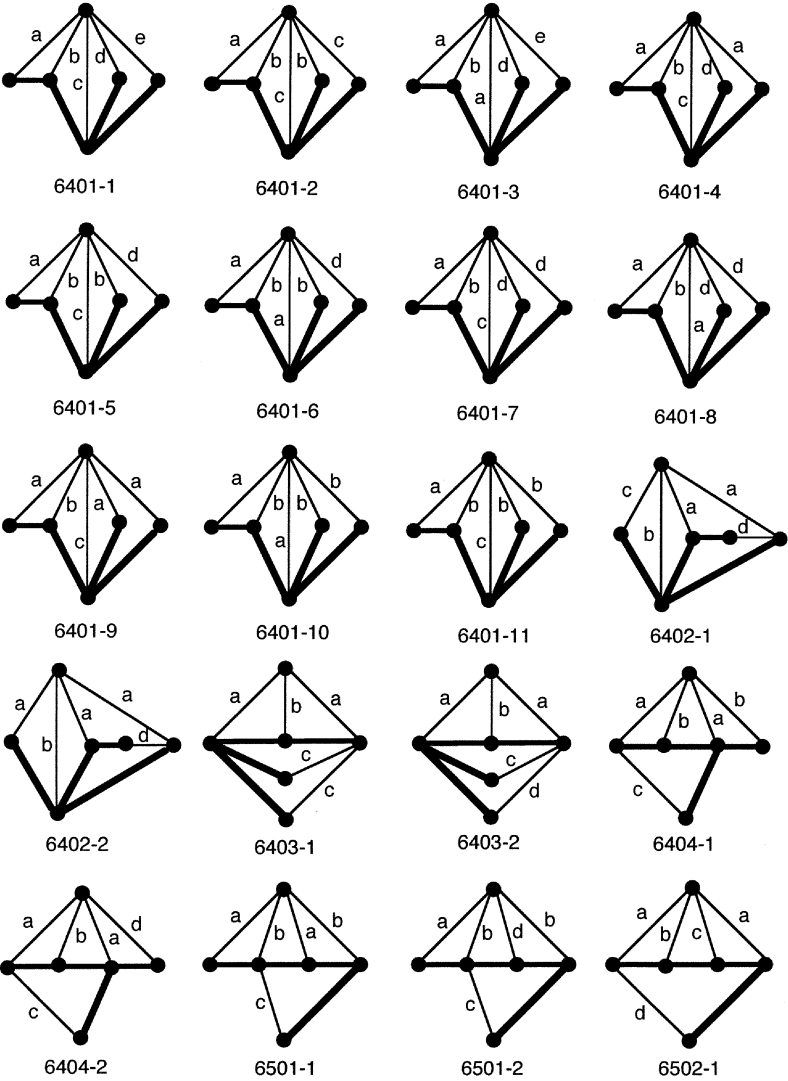


Table F.8 One-dof Epicyclic Gear Trains: Four Independent Loops — Part 4.

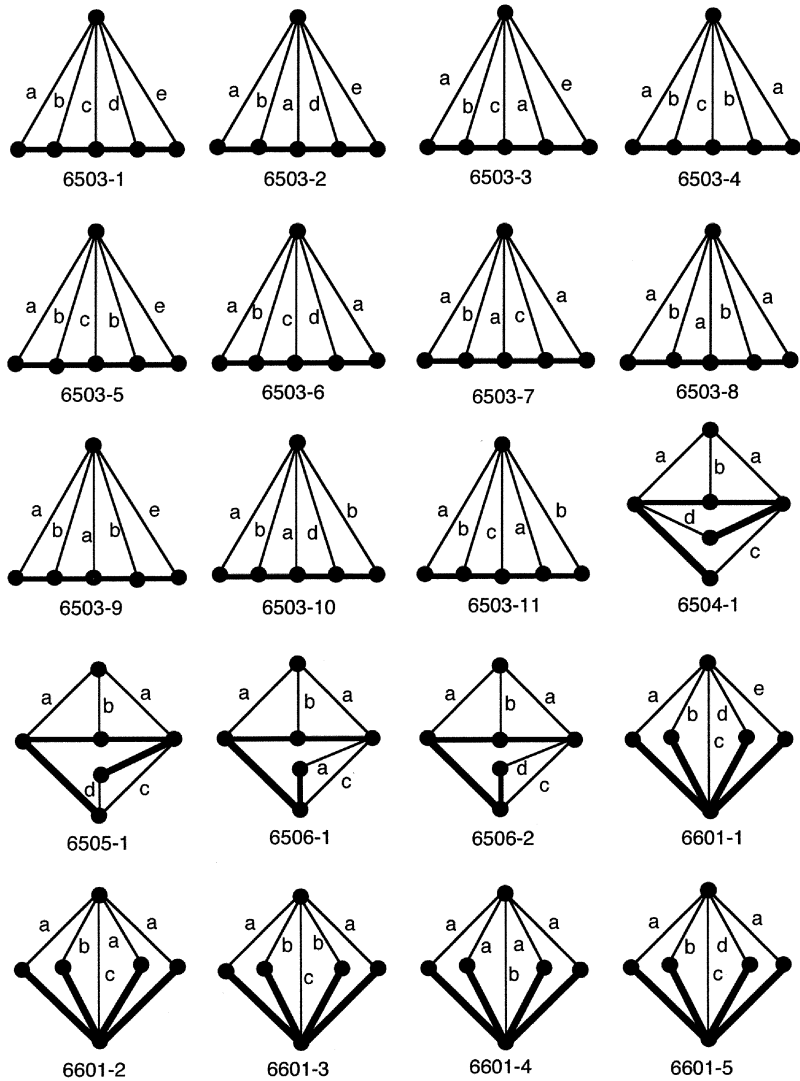
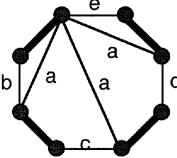
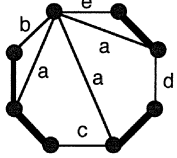
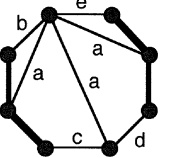
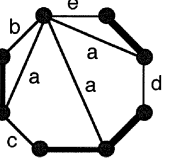
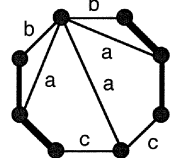
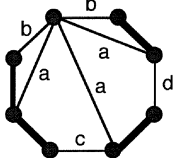
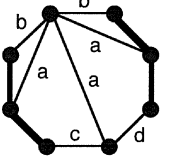
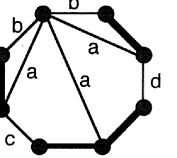


Table F.9 Two-dof Epicyclic Gear Trains: Three Independent Loops.

No.	Graph	Functional Schematic
1		
2		
3		

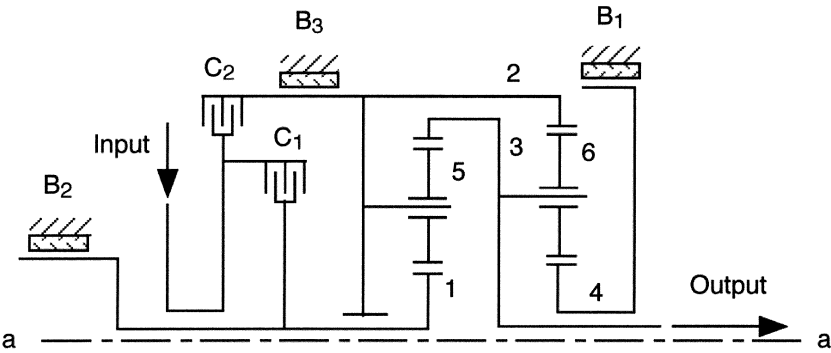
Table F.10 Three-dof Epicyclic Gear Trains.

 <p>(1)</p>	 <p>(2)</p>	 <p>(3)</p>	 <p>(4)</p>
 <p>(5)</p>	 <p>(6)</p>	 <p>(7)</p>	 <p>(8)</p>

Appendix G

Atlas of Epicyclic Gear Transmission Mechanisms

This appendix provides the schematic diagrams and clutching sequences of some commonly used epicyclic transmission gear trains.

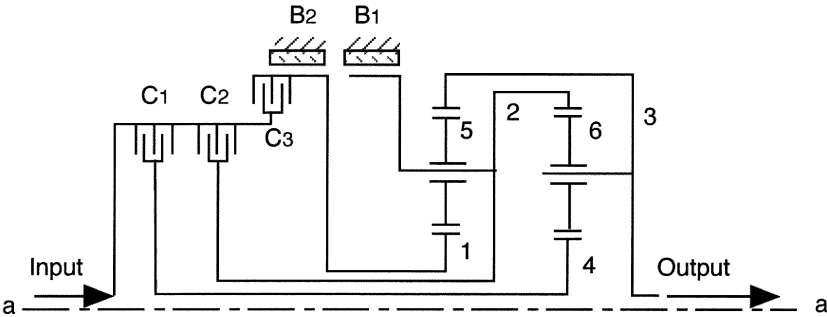


(a) Schematic diagram

Range	C ₁	C ₂	B ₁	B ₂	B ₃
Drive 1	X		X		
Drive 2		X	X		
Drive 3	X	X			
Drive 4		X		X	
Reverse	X				X

(b) Clutching sequence

FIGURE G.1
Type 6206 transmission mechanism: version 1.

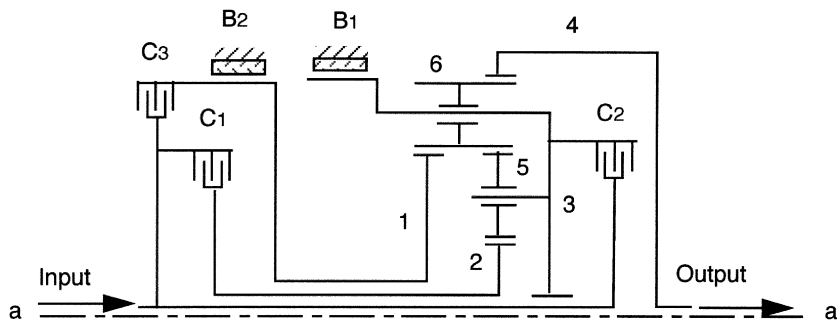


(a) Schematic diagram

Range	C1	C2	C3	B1	B2
Drive 1	X			X	
Drive 2	X				X
Drive 3	X	X			
Drive 4		X			X
Reverse			X	X	

(b) Clutching sequence

FIGURE G.2
Type 6206 transmission mechanism: version 2.

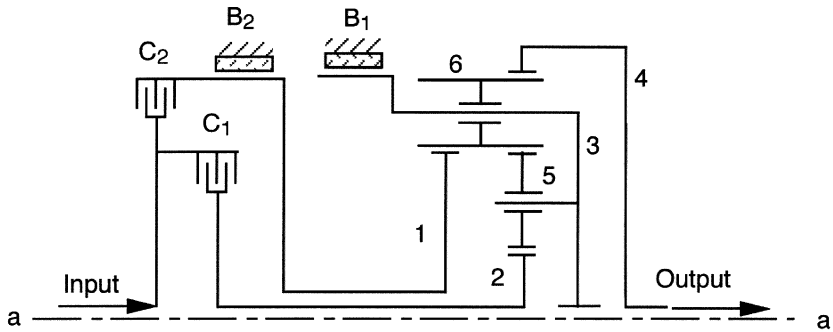


(a) Schematic diagram

Range	C1	C2	C3	B1	B2
Drive 1	X			X	
Drive 2	X				X
Drive 3	X	X			
Drive 4		X			X
Reverse			X	X	

(b) Clutching sequence

FIGURE G.3
Type 6401 transmission mechanism (Ravigneaux): version 1.



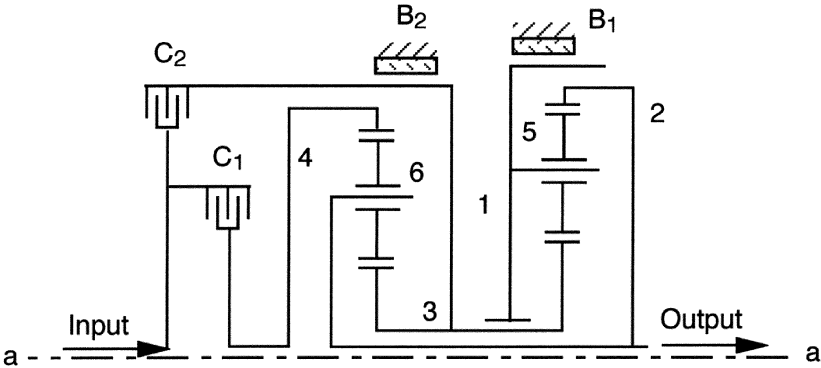
(a) Schematic diagram

Range	C ₁	C ₂	B ₁	B ₂
Drive 1	X		X	
Drive 2	X			X
Drive 3	X	X		
Reverse		X	X	

(b) Clutching sequence

FIGURE G.4

Type 6401 transmission mechanism (Ravigneaux): version 2.

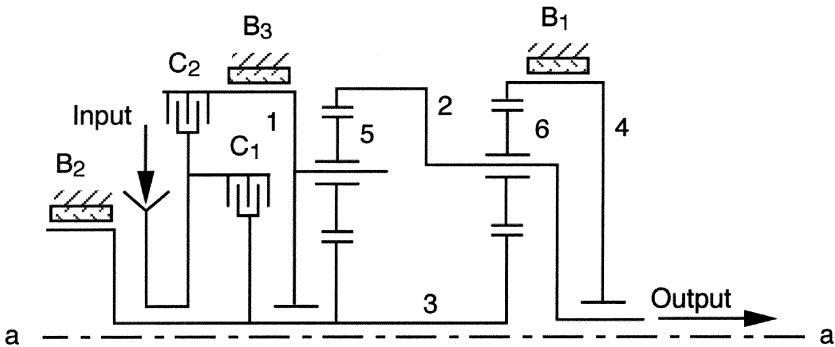


(a) Schematic diagram

Range	C ₁	C ₂	B ₁	B ₂
Drive 1	X		X	
Drive 2	X			X
Drive 3	X	X		
Reverse		X	X	

(b) Clutching sequence

FIGURE G.5
Type 6506 transmission mechanism (Simpson): version 1.

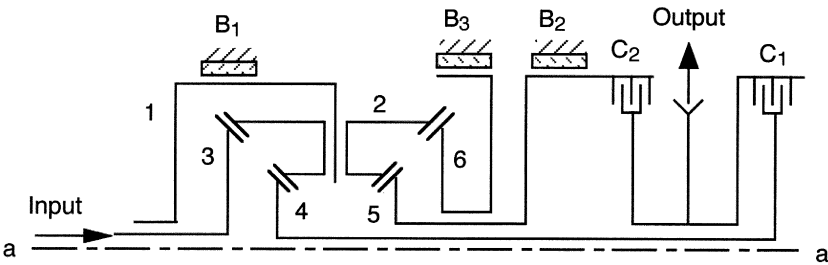


(a) Schematic diagram

Range	C ₁	C ₂	B ₁	B ₂	B ₃
Drive 1	X		X		
Drive 2		X	X		
Drive 3	X	X			
Drive 4		X		X	
Reverse	X				X

(b) Clutching sequence

FIGURE G.6
Type 6506 transmission mechanism (Simpson): version 2.

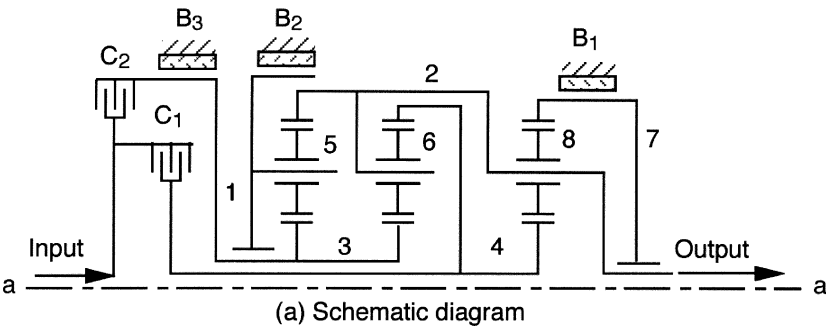


(a) Schematic diagram

Range	C ₁	C ₂	B ₁	B ₂	B ₃
Drive 1	X		X		
Drive 2	X			X	
Drive 3	X				X
Drive 4	X	X			
Reverse		X	X		

(b) Clutching sequence

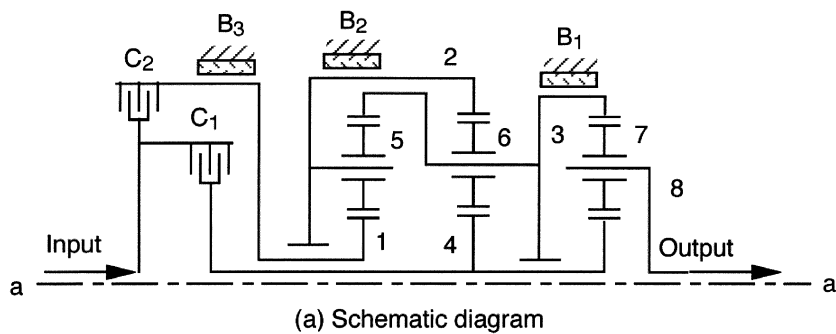
FIGURE G.7
Type 6601 transmission mechanism.



Range	C ₁	C ₂	B ₁	B ₂	B ₃
Drive 1	X		X		
Drive 2	X			X	
Drive 3	X				X
Drive 4	X	X			
Reverse		X	X		

(b) Clutching sequence

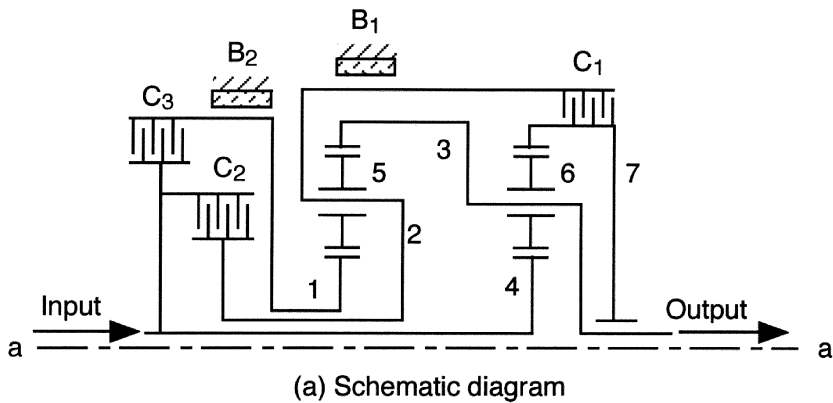
FIGURE G.8
Type 8001 transmission mechanism.



Range	C ₁	C ₂	B ₁	B ₂	B ₃
Drive 1	X		X		
Drive 2	X			X	
Drive 3	X				X
Drive 4	X	X			
Reverse		X	X		

(b) Clutching sequence

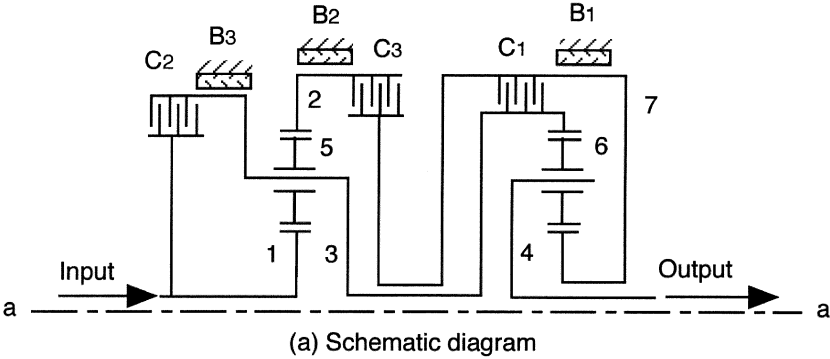
FIGURE G.9
Type 8002 transmission mechanism.



Range	Activated clutches				
	C ₁	C ₂	C ₃	B ₁	B ₂
Drive 1	X			X	
Drive 2	X				X
Drive 3	X	X			
Drive 4		X			X
Reverse			X	X	

(b) Clutching sequence

FIGURE G.10
Transmission mechanism consisting of two type-4200 gear trains: version 1.

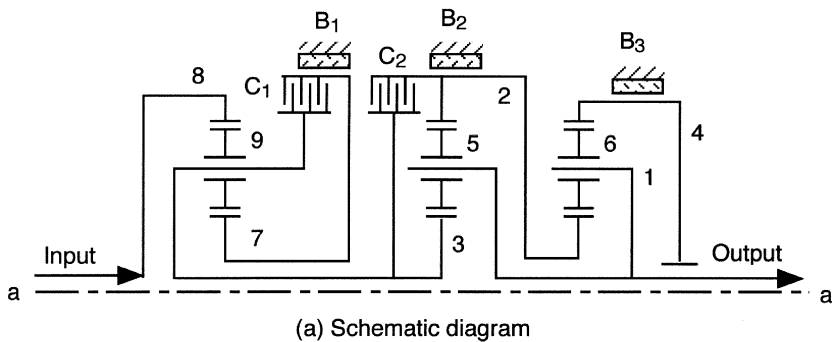


(a) Schematic diagram

Range	Activated clutches					
	C1	C2	C3	B1	B2	B3
Drive 1				X	X	
Drive 2	X				X	
Drive 3		X		X		
Drive 4	X	X				
Reverse			X			X

(b) Clutching sequence

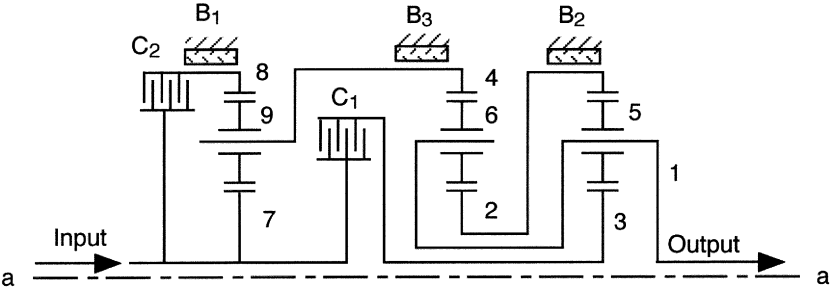
FIGURE G.11
Transmission mechanism consisting of two type-4200 gear trains: version 2.



Range	Activated clutches				
	C ₁	C ₂	B ₁	B ₂	B ₃
Drive 1			X	X	
Drive 2	X			X	
Drive 3		X	X		
Drive 4	X	X			
Reverse			X		X

(b) Clutching sequence

FIGURE G.12
Transmission mechanism consisting of type-4200 and type-6503 gear trains: version 1.

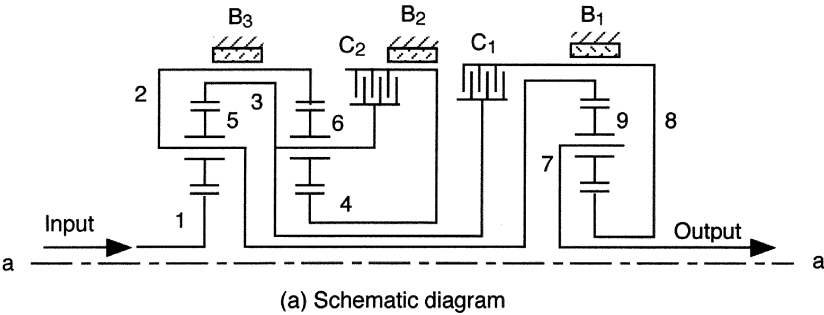


(a) Schematic diagram

Range	Activated clutches				
	C ₁	C ₂	B ₁	B ₂	B ₃
Drive 1			X	X	
Drive 2	X			X	
Drive 3		X		X	
Drive 4	X	X			
Reverse	X				X

(b) Clutching sequence

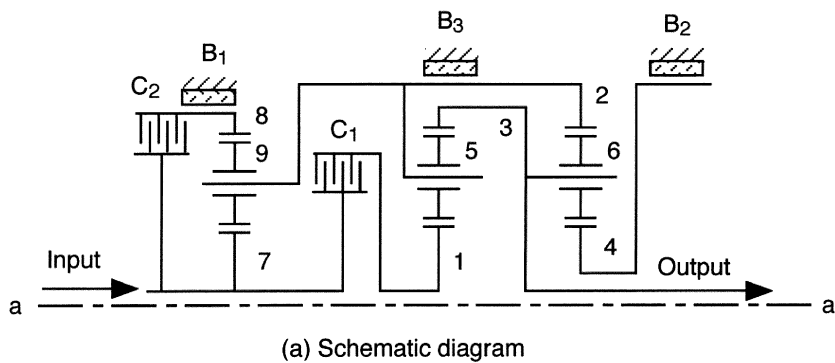
FIGURE G.13
Transmission mechanism consisting of type-4200 and type-6503 gear trains: version 2.



Range	Activated clutches				
	C ₁	C ₂	B ₁	B ₂	B ₃
Drive 1	X		X		
Drive 2			X	X	
Drive 3		X	X		
Drive 4	X	X			
Reverse	X				X

(b) Clutching sequence

FIGURE G.14
Transmission mechanism consisting of type-4200 and type-6206 gear trains: version 1.



Range	Activated clutches				
	C ₁	C ₂	B ₁	B ₂	B ₃
Drive 1			X	X	
Drive 2	X			X	
Drive 3		X		X	
Drive 4	X	X			
Reverse	X				X

(b) Clutching sequence

FIGURE G.15
Transmission mechanism consisting of type-4200 and type-6206 gear trains: version 2.

Index

- adjacency matrix, 32, 57, 102
- adjacent, 21, 22
- arcs, 28, 38, 45, 209, 211
- arm, 145, 149, 231
- articulation point(s), 23, 65, 101, 115, 204, 235
- automatic transmission(s), 145, 171, 179, 189, 192, 193, 195, 199, 208, 217
- automorphic graph(s), 81
- automorphism(s), 81, 83
- axial configuration, 180

- ball type, 186
- band clutch(es), 190, 191, 194
- base, 9, 23, 135, 204, 222
- basic mechanism, 240, 242
- bend axis, 237
- bend-shaft coupling, 185, 186
- Bendix, 234, 237, 242
- binary joint(s), 8, 47, 161
- binary link chain(s), 76, 77
- binary link(s), 8, 51
- binary string(s), 38, 39, 89, 91
- bipartite, 24
- block, 23
- branch(es), 78, 79, 107–111
- bridge(s), 23, 65, 101, 115, 235

- cam, 7, 11
- cam mechanism(s), 133, 134
- cam pair, 6–8
- canonical graph(s), 161, 199–204, 207–215, 235, 238–243

- Cardan joint, 7
- carrier(s), 50, 130, 145, 149
- chord(s), 28, 38, 45, 209, 212
- Cincinnati Milacron, 235, 238, 242
- circuit matrix, 35, 38, 57
- circuit(s), 22, 26, 147, 148, 155
- closed-loop chain(s), 9, 72
- closed-loop mechanism(s), 115
- clutch-to-clutch shift, 195, 197
- clutching sequence, 192, 194, 202, 203
- complete bipartite, 24, 26
- complete graph, 24, 26
- component(s), 22, 23
- conceptual design phase, 1, 2
- connected graph(s), 22
- connectivity, 223
- connectivity listing(s), 228, 229
- contracted graph(s), 38–40, 102–107, 253
- contraction, 39, 102
- countershaft transmission, 193, 196, 216
- Crossley's operator, 75, 76, 108
- customer's requirements, 1, 2
- cut point(s), 23
- cycle, 22, 81, 84
- cylindric joint, 5

- decodability, 85, 89
- degree code, 90, 91
- degree of a vertex, 21
- degrees of freedom, 3, 65–69
- derived mechanism, 240
- design process, 1, 12
- differential, 14, 148, 189, 191, 197
- differential gear train(s), 145, 148, 164, 171

- dimensional synthesis, 2, 3, 12, 179, 181, 228
- direct drive, 195, 197
- directed graph, 23, 24, 210
- dof, 3
- dual graph, 40–42
- edge-induced, 83, 85
- edge(s), 21–34, 79
- efficiency, 85, 158, 179
- EGM, 197–198, 201–203, 209, 212–214
- EGT(s), 145, 147–153, 158–161, 163–165, 197–199, 209
- eight-bar linkage(s), 124, 127, 262–265
- element(s), 81, 82
- embedded, 26, 27
- end point(s), 21, 23, 203
- end-effector, 136, 226, 227, 231, 235, 237, 240, 243
- epicyclic gear train(s), 145, 146, 162–165, 193, 279–289
- epicyclic gear transmission, 192, 194, 215, 291
- epicyclic gear type, 192, 194
- equivalent, 115, 138
- equivalent open-loop chain, 238, 240, 242
- Euler's equation, 30, 36, 72
- evaluator, 3, 181, 224
- expansion, 39, 102, 107, 112
- external loop, 27, 28, 121, 125
- family, 75, 107, 202, 205
- Fanuc Robot, 236
- Fanuc wrist, 239
- feasible mechanisms, 2, 3, 179, 181
- feasible solutions, 1, 101
- final reduction unit, 189, 190, 197
- first level vertex(ices), 200, 202, 203, 205
- five-bar linkage(s), 124, 265
- five-link chain(s), 277
- fixed link, 9, 23
- four-bar linkage(s), 13, 118, 119, 261
- four-link chain(s), 276
- fractionated mechanism, 101, 148
- functional requirements, 1, 179–182, 184, 194–195, 222, 224, 234, 237
- functional schematic, 48
- fundamental circuit equation(s), 167–169
- fundamental circuit(s), 28, 36, 149, 151, 167, 209
- gear-cam mechanism, 116
- gear pair, 6, 52, 57
- gear train(s), 129, 145
- geared edge(s), 147, 149, 207
- geared mechanism(s), 116, 129, 130, 133
- General Motors, 185, 191, 193–195
- generator, 3, 224
- genetic graph, 158
- Giddings and Lewis, 9, 10, 222
- graph, 2, 21
- graph automorphism(s), 90
- graph isomorphism(s), 25, 32, 34, 103, 107, 207
- graph representation, 52
- graph theory, 2, 3, 21
- graph(s), 255–260
- ground level vertex, 200
- group, 81–85
- group of automorphism(s), 81, 83–85, 90
- group operation, 82
- Grübler criterion, 67, 69
- helical joint, 5, 6
- Hexaglide, 222
- Hexam, 225
- Hexapod, 224
- higher pair(s), 5, 7, 8, 185
- hinge, 5
- homeomorphic, 28
- homokinetic plane, 185, 186
- Hooke joint, 7, 12
- Humpage reduction gear, 61
- hybrid kinematic chain, 9
- identity permutation, 81, 89
- in-line configuration, 180
- incidence matrix, 33, 34, 57, 58, 210
- independent loops, 28, 30, 67
- inverse(s), 82, 83
- isolated vertex, 21
- isomorphic, 16, 25, 79
- isomorphic graphs, 25, 81

- joint(s), 2, 3, 5
- kind, 138, 205
- kinematic analysis, 11, 53, 165, 228
- kinematic chain(s), 9, 15
- kinematic inversion, 15, 16, 118, 129, 130
- kinematic pair(s), 5, 6, 8, 51
- kinematic structure(s), 2, 11, 43, 47, 81
- kinematic synthesis, 11
- Kuratowski's theorem, 28
- Kutzbach criterion, 67
- labeled graph(s), 32, 83, 162, 199
- law of gearing, 6
- layshaft transmission, 193
- length, 22, 32, 76, 78, 81, 159
- letter(s), 57, 149
- level(s), 149, 151, 200, 239
- link(s), 3, 4, 51, 52
- link assortment(s), 52, 54, 74, 75, 107
- linkage type, 186
- linkage(s), 11, 116–128, 261–273
- loop mobility criterion, 53, 71, 72, 115
- loop(s), 26–30, 66, 67, 71–72
- lower pair(s), 5, 7, 8, 92, 116
- machine(s), 9, 10
- major links, 231
- manual transmissions, 189
- Mathematica, 87
- Matlab, 87
- Matrix-Tree Theorem, 35
- MAX code, 89, 90, 92, 94
- mechanism(s), 2, 9, 10
- member(s), 4, 5
- MIN code, 90, 94
- minor links, 231
- modulo 2, 29, 36, 37
- motion parameter, 67
- multigraph, 23
- multiple joint(s), 8, 161
- nested-do loops, 75, 78, 103, 249, 250
- nine-bar linkage(s), 126, 267–272
- number synthesis, 11
- numeral(s), 57
- object(s), 81
- objects, 103, 118
- oblique wrist, 237
- one-dof epicyclic gear train(s), 280–287
- one-way clutch(es), 191, 195
- open-loop chain, 9, 71, 222
- optimum code, 89–91
- ordinary gear train(s), 129, 145
- overconstrained mechanisms, 69
- OWC, 191
- pair element(s), 5
- parallel edges, 23, 39–41
- parallel kinematics machine(s), 126, 141, 222
- parallel manipulator(s), 128, 141, 221, 222, 225, 230
- parent bar linkage, 159, 161
- passive degrees of freedom, 68
- path, 22, 26
- path matrix, 36, 57, 213
- peripheral loop, 27, 112
- permutation group, 81, 82
- PGT(s), 145
- physical embodiment, 1
- pin-in-slot, 116
- pin joint, 5
- plain vertices, 51
- planar graph, 26–30, 41
- planar linkage(s), 12, 116
- planar mechanism(s), 12, 15
- planar motion, 12
- planar three-dof linkages, 126, 128, 273
- planar two-dof linkages, 124, 125
- plane pair, 5
- planet gears, 145, 200
- planetary gear train(s), 129, 145
- Polak's transmission mechanism, 216
- prismatic joint, 5
- product design phase, 1
- pseudoisomorphic graphs, 161
- pseudoisomorphic mechanisms, 161
- pseudoisomorphisms, 161
- PUMA wrist, 242
- quaternary link, 8, 51, 74

- ratio range, 195
- Ravigneaux, 294, 295
- Ravigneaux gear set, 199, 203
- reduced incidence matrix, 35, 37, 211, 212
- redundant link, 148, 197, 198, 202, 240
- redundant paths, 47
- revolute joint, 5
- ring gear, 145
- roll axis, 237
- roll-bend-roll wrist, 237
- root, 23, 161, 199
- rooted graph, 23, 38
- rotary configuration, 180
- rotating clutch(es), 190, 191, 193

- Sandia Laboratories, 182
- screw pair, 5
- second level vertex(ices), 200, 203
- self-loop, 23
- seven-bar linkage(s), 125, 266
- seven-link chain(s), 278
- shaft coupling(s), 140, 179, 184, 186, 188
- shaper mechanism, 121, 123
- similar edges, 85, 107, 108, 110
- similar vertices, 84, 205
- simple graph, 23, 41
- simple wrist, 237
- Simpson, 296, 297
- Simpson gear set, 145, 199, 202, 204, 209, 215
- six-bar linkage(s), 121, 127, 262
- six-link chain(s), 278
- sliding pair, 5
- sling, 23
- solid vertices, 51
- South Pointing Chariot, 145
- spanning tree(s), 28, 29, 35, 36, 150, 209, 214
- spatial mechanism(s), 12, 15, 136
- spatial motion, 15
- spatial parallel manipulator(s), 228
- speed ratio(s), 191, 194
- spherical center, 12, 135, 227
- spherical four-bar linkage(s), 14
- spherical joint, 5
- spherical mechanism(s), 12, 15, 135, 236
- spherical motion, 12
- spherical parallel manipulator(s), 135, 227

- step ratio, 195
- Stephenson, 73, 83, 89, 121, 181
- stereographic projection, 27
- Stewart-Gough manipulator, 10, 221
- structural analysis, 59, 65
- structural isomorphism, 57, 58, 79, 81, 85
- structural representation, 47, 51
- structure synthesis, 3, 11
- subgraph(s), 22, 23
- sun gear, 145
- swash-plate, 15, 70, 180

- terminal edges, 149, 157
- ternary link(s), 8, 74, 75
- theory of fundamental circuits, 53, 165, 172
- thick edge(s), 52, 147
- thin edge(s), 52, 147
- THM-440, 191
- three-dof epicyclic gear train(s), 289
- three-dof linkage(s), 273
- three-roll wrist, 237, 242
- top-dead-center, 179, 180
- topological analysis, 59
- topological synthesis, 11
- Toyoda, 222, 225
- trail, 22
- transfer vertex(ices), 149, 151, 214
- translational platform(s), 229, 231–233
- transmission mechanism(s), 291–306
- tree(s), 26, 27, 151
- turning pair, 5, 57, 147
- two-dof epicyclic gear train(s), 288
- type synthesis, 11

- uniqueness, 85
- universal joint, 7, 12, 229, 230

- variable-stroke engine mechanism(s), 179–182
- VARIAX[®], 10
- vertex degree listing, 75, 85, 115, 121, 163
- vertex-induced, 83
- vertex selection, 161, 235
- vertex(ices), 21
- VS-engine mechanism(s), 181, 183–185

walk, 22, 33

Wankel engine, 181

Watt, 57, 99, 121, 123, 181

wobble-plate, 62, 180

wrist, 231

wrist center, 231

wrist mechanism(s), 136, 231, 234, 236,
237, 239–242

Z-crank mechanism, 62, 140

